

**Development and Evaluation of Multidimensional Gas
Chromatographic and Mass Spectrometric Techniques for the Analysis
of Highly Complex Chemical Mixtures**

Werner Welthagen

**Development and Evaluation of Multidimensional Gas
Chromatographic and Mass Spectrometric Techniques for the Analysis
of Highly Complex Chemical Mixtures**

Dissertation

zur

Erlangung des akademischen Grades

doctor rerum naturalium (Dr.rer.nat.)

der Mathematisch-Naturwissenschaftlichen Fakultät

der Universität Rostock

vorgelegt von

Welthagen, Werner, geb. am 1979.03.25 in Pretoria, Süd Afrika

aus Parys, Süd Africa

Rostock, 2010.03.18

Univ.-Prof. Dr. rer. nat. Ralf Zimmermann (Universität Rostock)

Univ.-Prof. Egmont Rohwer (Universität Pretoria, Süd Afrika)

Datum der Einreichung: 2010.03.18

Datum der Verteidigung: 2010.06.08

CONTENTS

1. INTRODUCTION	
1.1 General introduction	2
1.2 Approach	4
1.3 Presentation and arrangement	5
2. BACKGROUND	
2.1 Multidimensional separation techniques	8
<i>2.1.1 Orthogonality of multidimensional techniques</i>	11
2.2 Comprehensive two-dimensional gas chromatography (GC x GC)	12
<i>2.2.1 GC x GC principles</i>	12
<i>2.2.2 GC x GC modulator</i>	15
<i>2.2.3 GC x GC column selection</i>	21
2.3 Time-of-flight mass spectrometry (TOFMS)	23
<i>2.3.1 TOFMS principles</i>	23
<i>2.3.2 Orthogonal accelerated TOF</i>	25
2.4 Comprehensive two-dimensional coupling of gas chromatography and mass spectrometry (GC x MS)	26
<i>2.3.1 GC x MS principles</i>	26
<i>2.3.2 Resonance enhance multiphoton ionization (REMPI)</i>	30
<i>2.3.3 Single photon ionization (SPI)</i>	33
<i>2.3.4 Lamp based SPI</i>	34
2.5 References	36
3. NEW DEVELOPMENTS IN GC x GC-TOFMS DATA ANALYSIS	
3.1 Introduction	40

3.2	Method for chemical classification and the application on urban aerosol and diesel samples	41
3.2.1	<i>Rule based approach for chemical classification of PM 2.5 Aerosols</i>	58
3.2.2	<i>Experimental</i>	60
3.2.3	<i>Results and discussion</i>	63
3.2.4	<i>Conclusions</i>	83
3.3	Methods for comparison of sample classes and the application on metabolomic profiles	84
3.3.1	<i>Biomarker identification in mouse spleen extracts</i>	85
3.3.2	<i>Experimental</i>	88
3.3.3	<i>Results and discussion</i>	90
3.3.3.1	<i>Comparison of chromatograms</i>	99
3.3.3.2	<i>Chromatogram averaging</i>	100
3.3.3.3	<i>Bubble plot representation of GC x GC–TOFMS data</i>	102
3.3.3.4	<i>Difference chromatograms</i>	104
3.3.3.5	<i>Normalizing peak surfaces for generation of difference chromatograms</i>	106
3.3.3.6	<i>t-Test comparison</i>	108
3.3.3.7	<i>Fisher values</i>	110
3.3.3.8	<i>Principle component analysis</i>	112
3.3.4	<i>Conclusions</i>	113
3.4	References	114
4.	PHOTO IONIZATION MASS SPECTROMETRY COUPLED TO GC AND GC x GC	
4.1	Introduction	118
4.1.1	<i>Comprehensive coupling of GC and MS: Separation enhancement</i>	118
4.1.2	<i>Coupling of GC with selective detectors: Selectivity enhancement</i>	120
4.2	Laser photo ionization (REMPI / SPI) for GC x MS	122
4.2.2	<i>Experimental</i>	122
4.2.3	<i>Results and discussion</i>	124
4.3	Laser photo ionization (SPI) for GC x GC x MS	146
4.3.2	<i>Experimental</i>	146
4.3.3	<i>Results and discussion</i>	147
4.4	VUV-lamp photo ionization (SPI) for GC x MS	152
4.4.1	<i>Experimental</i>	152
4.4.2	<i>Results and discussion</i>	154
4.5	VUV-lamp photo ionization (SPI) for GC x GC x MS	162

4.5.1	<i>Experimental</i>	162
4.5.2	<i>Results and discussion</i>	163
4.6	Conclusions	173
4.7	References	173
Appendices		177

Chapter 1

INTRODUCTION

1.1	General introduction	2
1.2	Approach	4
1.3	Presentation and arrangement	5

Chapter 1

INTRODUCTION

1.1 General introduction

In modern day analytical chemistry, existing techniques of separation science and targeted analysis are being pushed to their limits. These limits include the cost of analysis, analysis time, and physical constraints of the techniques. For health and other control organizations it is, however, quite important to push the analytical techniques even further. The physical constraints of the techniques especially need to be improved in terms of detection limits and separation capacity. These organizations are thus increasing pressure on industries and even governments to provide more and more detailed analysis of their products and wastes. Many of the compounds that need to be detected and quantified are typically in trace or ultra-trace amounts and comprise a wide range of chemical compound classes. Moreover, these compounds may be contained within extremely complex sample matrices that require extensive sample preparations. With the increase of separation and lowering of detection limits compounds are detected that were previously not known to exist in the sample matrices. The detection of these compounds could improve the understanding of various chemical or biochemical mechanisms. The samples of choice in this thesis exert most of the characteristics given above and include urban aerosol particulate matter, metabolite extracts from animal tissues and diesel petroleum samples.

Aerosol particulate matter is implicated in various health effects for toxic, genotoxic and carcinogenic mechanisms when inhaled. These particulates contain various chemical compounds from equally diverse sources, for example automobile exhausts, biomaterial burning and natural sources. To trace the harmful effects of these particulates it is necessary to analyze them in great detail to determine the contribution of different sources and to link those with epidemiological studies.

Metabolomic extracts from animal tissue samples can provide interesting results for metabolic pathway studies and the detection of genetic diseases. These samples are however, extremely complex and variations in samples are influenced by many factors, including time of the day when extracted, food consumed etc. These samples thus not

only require high separation capabilities but also statistical methods to correct for diversity within same sample variations and to detect biomarkers for the diagnosis of diseases.

The detailed analysis of petroleum fuels can be used in various studies to combine physical properties of the diesel with its chemical composition. These studies could include a chemical prediction of the Research Octane Number (RON) in gasoline sample or the Cetane number for diesel samples.

Capillary gas chromatography has become the first choice in many applications in modern day organic analysis, due to its excellent separation capabilities, speed of analysis and ability to be combined with a variety of selective detectors. The most commonly used gas chromatographic detector when samples of high complexity need to be analyzed is mass spectrometry. The excellent separation power of gas chromatography combined with the spectroscopic information of mass spectrometry where compounds can be identified through fragmentation patterns is highly desirable in many applications including the ones investigated in this thesis.

To further the separation capabilities of gas chromatographic techniques, the analysis of complex samples can be carried out on different chromatographic columns, which could then possibly separate compounds using different chemical or physical properties to reveal compounds that previously overlapped. In multidimensional gas chromatography (MDGC) or as more commonly used two-dimensional gas chromatography (GC-GC or 2DGC) selected fractions of the first column are injected into a second column for analysis on a different stationary phase. GC-GC provides great detail of specific targeted analysis sections and can be extended to for other chromatographic techniques for example liquid chromatography coupled to gas chromatography (LC-GC). The analysis of complete samples with two-dimensional chromatography is however a lengthy procedure and new methods like comprehensive two-dimensional gas chromatography (GC x GC) were introduced. In GC x GC the entire sample from the first dimension column is subjected to analysis on a second-dimension column and thus enhance the separation capabilities of GC.

Separation enhancement is also demonstrated through the use of GC coupled to soft ionization mass spectrometry (GC x MS). The use of mass spectrometry as a separation dimension, where compounds are separated according to their molecular mass is a new way of looking at GC-MS data and allow for fast screening of samples of high complexity. The possibility of connecting another GC to the GC x MS (GC x GC x MS) in a three-dimensional separation approach opens quite a few new possibilities but also introduce some new limitations in data interpretation, such as how to visualize three or four dimensions on a two-dimensional surface.

1.2 Approach

Gas chromatography is a well-used technique for various applications. In many of these applications a level of sophistication has been reached that makes any further improvements on the respective systems too expensive to consider. With the development of two-dimensional gas chromatograph (GC x GC) some of these existing applications can be revisited and improvements can be done at little extra costs. In some cases even a reduction in cost of the current analytical systems can be anticipated.

The focus of this study was to improve techniques used for the analysis of urban aerosol particulate matter, metabolomic extracts from animal tissues and diesel petrochemical samples. Some of the present techniques in industry, like GC-TOFMS analysis, are already well established and used on a routine basis in many laboratories. GC x GC-TOFMS can be introduced in these fields as a complimentary technique when the current methods fail to reach the detection limits or separation required to identify target compounds. It will also be shown that because of significantly higher spectral purities obtained using GC x GC-TOFMS, due to improved separation compounds can be assigned with improved library matches.

In the current work the inherent properties of GC x GC to separate compounds into ordered bands of species with similar chemical or physical properties is investigated, and combined with the unique fragmentation information of compound classes from mass spectrometry detection. This was used to facilitate a new compound classification approach whereby compounds could be grouped into chemical classes through basic classification rules and used in statistical evaluation of samples. These compound class groups were introduced for the statistical evaluation of the organic content of urban aerosol samples as complimentary technique for the ongoing daily monitoring of the organic content of urban aerosol particulate matter (PM_{2.5}) in Augsburg, Germany.

GC x GC-TOFMS is also introduced for the first time to the analysis of metabolic extracts from mammalian tissue samples (mice spleen extracts). In a proof of concept study it is shown that tentative biomarker detection is possible using GC x GC-TOFMS. For the biomarker detection new statistical methods were developed and compared to existing methods. When compared to GC-TOFMS which is currently used in the analysis of metabolomic extracts, GC x GC-TOFMS is able to detect more peaks (compounds) in a shorter time frame. This is particularly important where high sample throughput is required for a comprehensive statistical study.

A new method for the enhancement of separation is introduced in gas chromatography coupled to selective soft photo ionization time-of-flight mass spectrometry (GC x PI TOFMS). In this approach the existing soft ionization techniques of resonance enhanced multiphoton ionization (REMPI) and single photon ionization (SPI) were used as

selective detectors to detect various different compound class groups within a diesel petroleum sample and present them in a two-dimensional plane of GC separation *vs.* molecular mass. These two-dimensional representations of GC-separation *vs.* molecular mass are compared to GC x GC separation. The two-dimensional separation approach with GC x MS is further extended to include an additional GC dimension for a comprehensive three-dimensional separation approach (GC x GC x MS). Finally a VUV lamp is introduced instead of the pulsed laser to produce a continuous source of SPI photons. The continuous source of photons obtained is used to increase the frequency of the detector from 10 Hz to 20 Hz, providing improved coupling to GC x GC. The frequency could be further improved with faster data recording.

1.3 Presentation and arrangement

The first section of this chapter provides a brief general introduction and the general approach of the thesis. In Chapter 2 a literature overview is given of the multi dimensional gas chromatographic and spectroscopic techniques under investigation. The next section focuses more on GC x GC, introducing the instrumentation setup and basic principles. Finally the photo ionization techniques are introduced as well as a summary of the initial work done on GC x MS.

In Chapter 3 the use of GC x GC-TOFMS for the analysis of the organic content of urban aerosol particulate matter is investigated and a classification rule set based on two-dimensional retention time and mass spectral fragmentation is developed. Chapter 3 also introduces GC x GC-TOFMS for the first time for the analysis of metabolomic profiles of mammalian tissue extracts. In this section a proof-of-concept investigation is done to determine if GC x GC could detect possible biomarkers to distinguish between genetic diseased mice and control mice. New statistical methods are introduced for the comparison of GC x GC-TOFMS samples.

In Chapter 4 soft photo ionization mass spectrometry is introduced as an additional separation dimension combined with GC for a two- and three-dimensional separation approach. The selectivity obtained using REMPI at different laser wavelengths is demonstrated. SPI, using laser and a novel VUV lamp, is applied as a universal soft ionization technique for a full overview of the analysis of a diesel petroleum sample in a two- and three-dimensional separation.

Chapter 2

BACKGROUND

2.1	Multidimensional separation techniques	8
	<i>2.1.1 Orthogonality of multidimensional techniques</i>	11
2.2	Comprehensive two-dimensional gas chromatography (GC x GC)	12
	<i>2.2.1 GC x GC principles</i>	12
	<i>2.2.2 GC x GC modulator</i>	15
	<i>2.2.3 GC x GC column selection</i>	21
2.3	Time-of-flight mass spectrometry (TOFMS)	23
	<i>2.3.1 TOFMS principles</i>	23
	<i>2.3.2 Orthogonal accelerated TOF</i>	25
2.4	Comprehensive two-dimensional coupling of gas chromatography and mass spectrometry (GC x MS)	26
	<i>2.3.1 GC x MS principles</i>	26
	<i>2.3.2 Resonance enhance multiphoton ionization (REMPI)</i>	30
	<i>2.3.3 Single photon ionization (SPI)</i>	33
	<i>2.3.4 Lamp based SPI</i>	34
2.5	References	36

Chapter 2

BACKGROUND

2.1 Multidimensional separation techniques

In order to increase the number of detectable peaks in complex samples it is possible to improve current one dimensional separation techniques but only until limitations of costs, time or physical constraints inhibit further improvements. By hyphenating or coupling of different one dimensional separation techniques the resulting multidimensional technique may have significant separation improvement.

Typically two or more independent separation techniques are coupled to give improved separation of an extremely complex mixture. The separation parameters are based on characteristic properties of compounds, such as their partition coefficients or density. There are numerous separation systems, each using a different property to control separation. A short selection of the most common separation types is listed in table 2.1 [1]. The coupling of any two of these separation techniques results in a theoretical 225 possible two-dimensional techniques [1].

Furthermore, within any single type of separation, such as chromatography, several independent, techniques can exist, yielding more coupling options. Table 2.2 lists the main chromatographic separation techniques available today. Any two of the chromatographic techniques in Table 2.2 can in turn be coupled to provide some 81 additional two-dimensional separation systems [1, 2]. By adding more parameters to an existing two-dimensional system, separation could be further enhanced, but it would also increase the complexity of the system.

Table 2.1 One-dimensional separations which might serve as building blocks for comprehensive multidimensional separation techniques [1, 2].

Type of separation	Abbreviation	Property controlling separation	
Bulk displacement	BLK	Nonselective	N
Flow	FLO	Nonselective	N
Chromatographic	CHR	Partition coefficient	K
Field flow fractionation	FFF	Field interaction parameter	ϕ
Electrophoretic	ELP	Electrical mobility	μ
Isoelectric	IEL	Isoelectric point	I
Isotachophoretic	ITP	Electrical mobility	μ
Dielectrophoretic	DEL	Dielectric constant	K
Sedimentation	SED	Sedimentation coefficient	s
Isopycnic sedimentation	IPY	Density	ρ
Magnetic gradient	MAG	Magnetic susceptibility	Ψ
Thermal diffusion	THD	Thermal diffusion coefficient	D'
Thermogravitational	THG	Thermal diffusion factor	α
Diffusophoretic	DIF	Interfacial energy	γ
Photophoretic	PHO	Photophoretic mobility	σ
Molecular mass*	MS	Mass to charge ratio	m/z

* Molecular mass was added as a type of separation since under special conditions Mass spectrometry using soft ionization compounds can be separated according to their molecular mass (2.3.1 GC x MS principles).

Table 2.2 Different chromatographic techniques that could be combined to form comprehensive separation methods [1, 2].

Chromatographic method	Abbreviation	Property controlling separation
Gas liquid chromatography	GLC	Partition coefficient
Gas solid chromatography	GSC	Solute distribution
Supercritical fluid chromatography	SFC	Partition coefficient
Reverse phase liquid chromatography	RP LC	Partition coefficient
Normal phase liquid chromatography	NP LC	Adsorption-desorption kinetics
Size exclusion liquid chromatography	SE LC	Hydrodynamic volume
Gradient elution liquid chromatography	GE LC	Partition coefficient
Thin layer liquid chromatography	TLC	Partition coefficient

Two modes of coupling are commonly used today (Figure 2.1); two-dimensional coupling and comprehensive two-dimensional coupling. In two-dimensional coupling a portion of the separated compounds of the first dimension is subjected to a second independent separation dimension. Thus a two-dimensional (x,y) plane results when the first separation parameter separates compounds in a linear axis and the second parameter separates the compounds in an independent second axis (Figure 2.1A). In the special case of comprehensive two-dimensional separation it will be considered that multiple second dimensions is combined such that there is no loss in the separation obtained in the first dimension (Figure 2.1B).

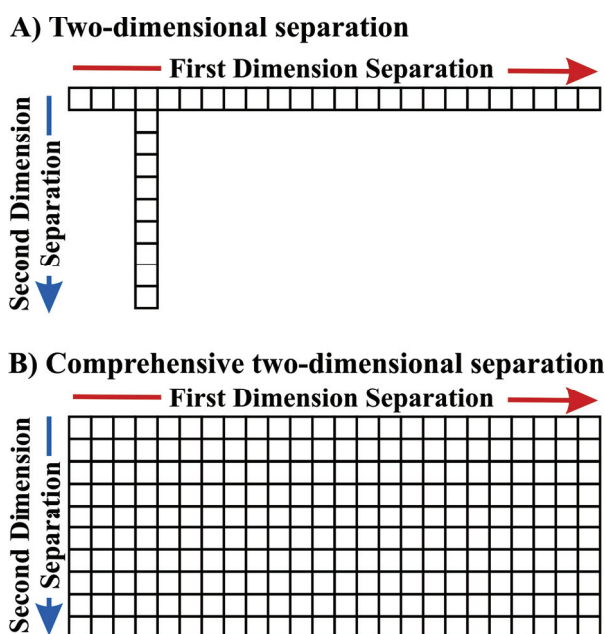


Figure 2.1 A) Representation of a two-dimensional separation where part of the first-dimension separation is subjected to a second separation dimension. B) Comprehensive two-dimensional separation where the complete first-dimension is subjected to separation on a second-dimension without the loss of the separation on either dimension

In the scope of this thesis gas chromatography is coupled to gas chromatography, where both GC systems use column combinations such that the separation in each column is independent of the other (GC x GC). The application of two-dimensional separation and comprehensive two-dimensional separation in chromatography are explained in detail later (2.2.1 GC x GC Principles).

Mass spectrometry will be introduced as a new separation dimension whereby with soft ionization the spectroscopic properties of fragmentation mass spectra (electron impact at 70 eV) are dominated by the separation of molecular ions.

2.1.1 Orthogonality of multidimensional techniques

In order to obtain separation in a two-dimensional system, two separation parameters are required. The parameters should be mutually independent to separate compounds over the full separation plane created by the coupled technique. One such a system is the GC x GC, discussed in section 2.2 in detail, where the first dimension separates components on a volatility basis according to “boiling point”, while the second dimension separates the components further on a “polarity” basis, giving a two-dimensional chromatogram with independent axes. Orthogonality thus simply indicates that the two separation systems are totally independent of each another. For closely related separation mechanisms, the components of a mixture will tend to elute on the diagonal between the two separation axes, i.e. again in a single dimension.

Other hyphenated techniques such as chromatography and mass spectrometry are typically not orthogonal, although the techniques are completely different. This due to the correlation of molecular mass and volatility, which is compounds with lower volatility typically also have smaller masses. However, as will be demonstrated later, gas chromatography can be coupled orthogonally to mass spectrometry when the boiling point dependency is factored out from chromatography.

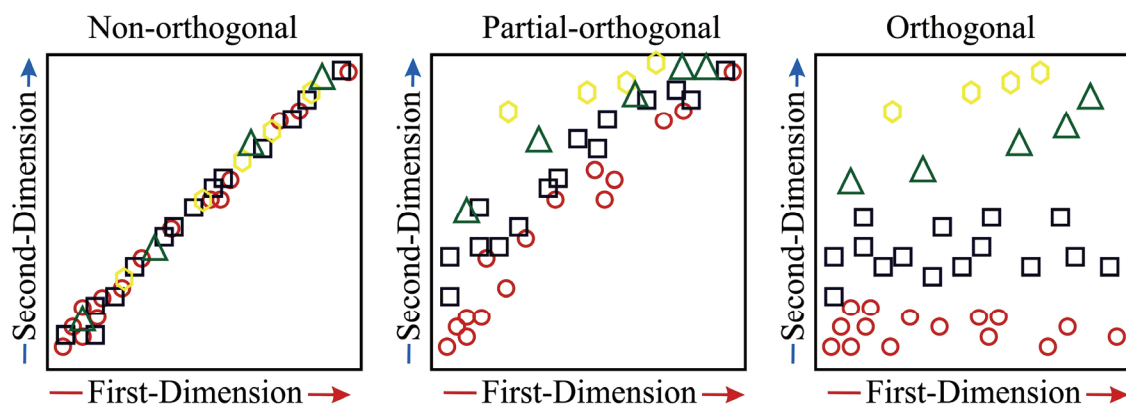


Figure 2.2 Representation of orthogonality in two-dimensional separation systems.

2.2 Comprehensive two-dimensional gas chromatography (GC x GC)

2.2.1 GC x GC Principles

As indicated before the separation of a sample can be enhanced by subjecting the sample to different separation criteria. In normal one-dimensional gas chromatography (GC) a sample is typically run on differently coated capillary columns to separate compounds that co-elute on one column. The introduction of heart-cut two dimensional systems enhanced the separation possibilities of gas chromatographic systems to a large extent. In a heart-cut two-dimensional GC system (GC-GC), selected fractions of the first-dimension column are subjected to further analysis on a second chromatographic column. The successful application of GC-GC is reported in numerous publications [3, 4]. The application of GC-GC is, however limited, as only a small fraction of the first dimension eluent is subjected to a second dimension separation. If an entire sample were subjected to a *comprehensive* two-dimensional separation on a GC-GC system analysis times would become impractical, due to the large number of chromatographic runs.

If however the eluent from the first dimension column could be repeatedly injected into the second-dimension column, an entire sample could be analyzed in two-dimensions, in the time taken for a single one dimensional analysis. For the technique to be truly *comprehensive* the fractions cut from the first-dimension columns should be small enough so that the separation obtained in the first dimension is not lost. Comprehensive two-dimensional gas chromatography (GC x GC) thus is a two-dimensional gas chromatographic system where an entire sample is subjected to two-dimensions of separation without the loss of the separation obtained in either dimension.

In terms of the theoretical *peak capacity* (n) or maximum number of chromatographic peaks that can be fitted into available separation space [1, 5], the peak capacity of a two-dimensional separation method (such as GC-GC) would have a total peak capacity based on the peak capacity of the first dimension (n_1) added to the peak capacity of the second-dimension separation (n_2) or ($n_1 + n_2$). In a comprehensive two-dimensional separation the total peak capacity of the separation system follow a multiplicative law as described by Guiochon *et al.* [6]

$$n_{2D} = n_{Dy} \times n_{Dz}$$

Where n_{2D} represents the peak capacity of the two-dimensional system, obtained by comprehensively coupling the two distinct one-dimensional separations with peak capacity n_{Dy} and n_{Dz} .

The process of collecting narrow elution fractions from the first separation system and transferring them to the second is called *modulation* (section 2.2.2). This modulation requires that separation on the second column is complete in the same time that the

following fraction is collected on the first column, thus the second separation must be very fast. The time constraint placed on the second-dimension column is overcome by the use of capillary columns of different dimensions (*Section 2.2.3*).

The outcome of a GC x GC run is usually a large number of fast second-dimension chromatograms. These Chromatograms are stacked next to one another to produce a three-dimensional image of first-dimension retention time vs. second-dimension retention time vs. signal intensity. Figure 2.3 shows how this three dimensional image can be transformed into a two dimensional contour and color plot.

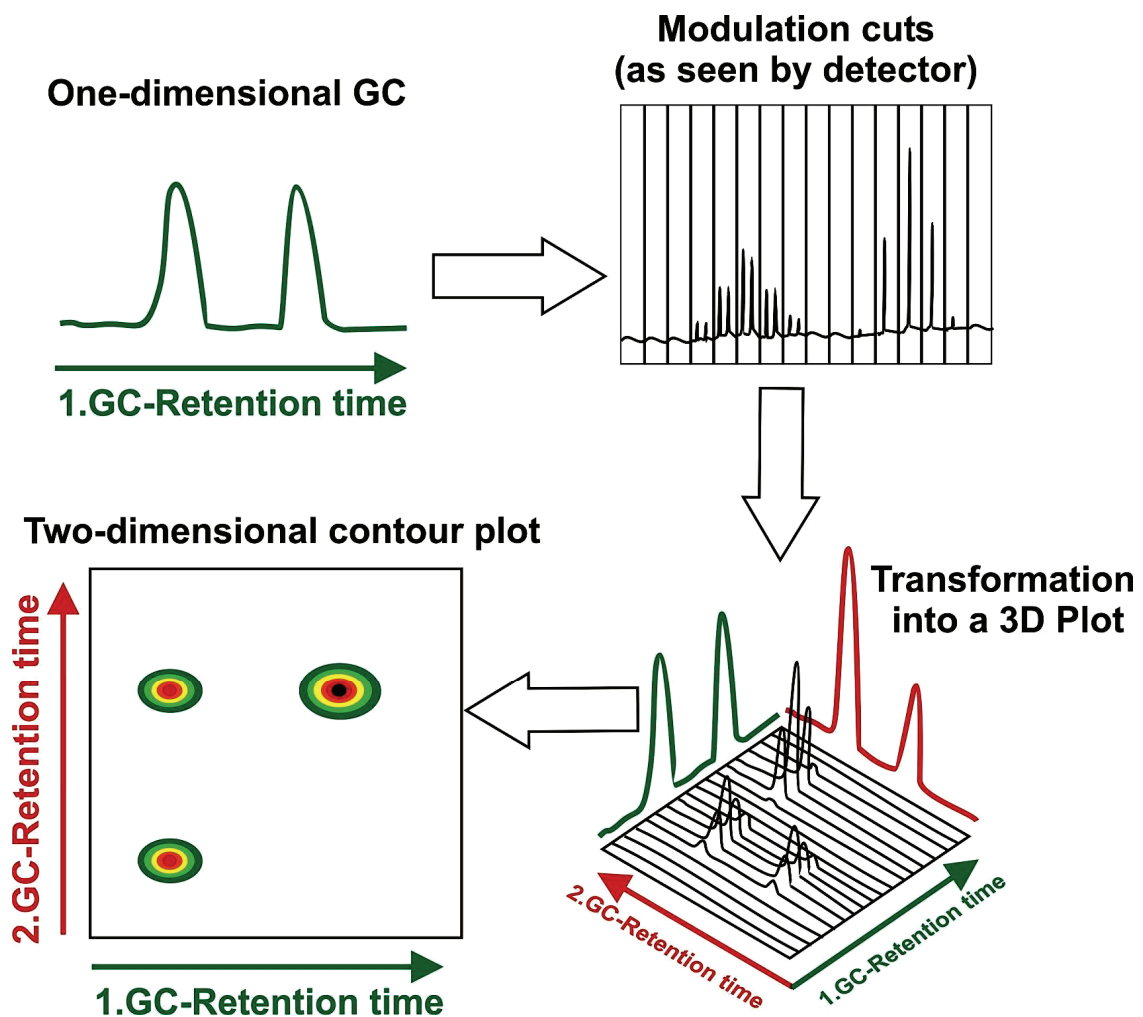


Figure 2.3 The transformation of a one dimensional separation into a two-dimensional separation [7]

The most important advantages of GC x GC over 1D-GC and GC-GC as discussed in the literature [[7-11] are: increased peak capacity; increase of detection limits due to the

refocusing of analytes in cryogenic modulated systems; and arrangement of compounds of similar chemical or physical properties in distinct bands or group on the two-dimensional separation plane when orthogonal column sets are used.

To interpret a GC x GC chromatogram, it is essential to understand the separation of compounds in different dimensions. The assumption of random distributions in one-dimensional chromatography [12, 13] provided valuable information in the understanding of peak distributions in a chromatographic axis. However, peak distribution is not truly random: All the components in the mixture have definite structures and must be directed to definite locations in retention space based on these structures [14].

Giddings [5] showed theoretically that the key property of a separation method, which determines whether or not it can show the inherent structure of a mixture being separated, is the method's *dimensionality* and that this should match the *dimensionality* of the mixture. The *dimensionality* of a mixture is the number of independent variables in which the members of the mixture can be separated. When a mixture is then separated according to these independent variables (by a system of matching dimensionality), each type of compound will separate to a unique location on the separation plane (chromatogram). However, as indicated above, the compounds are composed of molecules with discrete structures that are related, the compounds must thus distribute over the dimensional separation space (chromatogram) to discrete locations which are also related to each other [2, 5].

To explain the Giddings theory, separation in GC x GC is used as an example [2]: If a mixture is separated into one dimension, such as the boiling point fractions in petroleum samples, the alkanes and the aromatics with similar boiling points will overlap and thus insignificant ordering of compounds occurs. If the variable "boiling point" is changed to "polarity" the same overlap does not occur but a new overlap is created by different "boiling point" fractions, thus the separation or ordering is still insignificant. The mixture is simply not sufficiently well ordered in any one dimension, it requires at least two matching independent variables to uniquely separate the compounds of the mixture.

GC x GC chromatograms (volatility x polarity separation, method dimensionality of two) of petroleum fractions are highly ordered, indicating that these samples have a *dimensionality* of two (can be classified by either volatility or polarity), for most of their components [13]. Ordered chromatograms have the potential advantage of being more interpretable than disordered ones. The pattern of peak placement is highly informative by itself and may make it possible to classify most or all of the components of a given mixture into chemical classes.

2.2.2 *GC x GC modulator*

The process of collecting narrow elution fractions from the first separation system and transferring them to the second is called modulation. To achieve comprehensive coupling of two techniques, the modulation frequency has to be high enough to prevent loss of first dimension separation. This in turn, limits the time available to the second dimension separation, as successive separations have to be performed at the same frequency.

The modulator can thus be viewed as the heart of the GC x GC system and is situated between the two serially coupled columns. The eluents from the first column are captured, refocused and re-injected into the second column where further separation takes place. The basic stages of modulation in a cryogenic jet cooled modulator are demonstrated in Figure 2.4. The stages are highlighted by a trapping stage a focussing stage and an injecting stage.

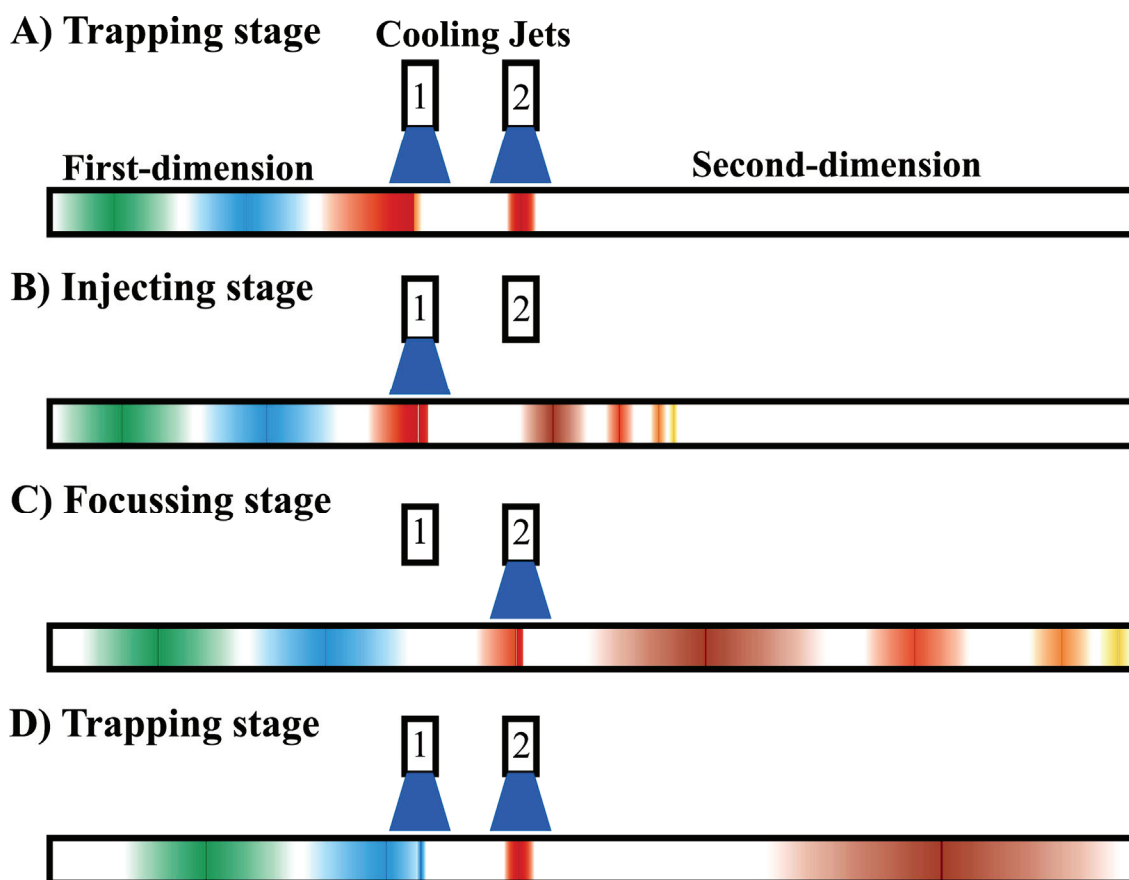


Figure 2.4 Demonstration of the basic working of modulation based on a cryogenic jet modulator. A) Trapping stage, where the eluent from the first dimension is trapped in the modulator, both cold jets are on, B) Injecting stage, where the trapped and focussed eluent from the first-dimension is injected into the second-dimension by switching off the second cold jet, C) Focussing stage, the cold jet 1 is switched off and the eluent is focussed under jet 2 which is switched on, D) Trapping stage, cold jet 1 is switched on again and trapping of the first dimension eluent resumes.

The period between the re-injected samples, is constant and is known as the modulation period. Statistically, in order to preserve the separation of the first dimension, each first-dimension peak needs to be analysed as several segments. It was demonstrated that the modulation period should be no faster than a quarter of the first dimension peak widths to maintain the first dimension resolution [7, 15, 16]. Thus, to obtain a comprehensive separation, the modulation period must be as short as possible. The modulator therefore needs to perform on a rapid, repeatable basis. The typical modulation period is in the order of two to ten seconds, providing four to six secondary analyses per first dimension peak.

The second dimension thus has a very short time period to separate components further and is therefore run under fast gas chromatographic conditions under isothermal conditions. One of the prerequisites of fast gas chromatographic separation is a narrow sample injection, in order to obtain well separated chromatograms with the best possible peak capacity.

A number of modulators have been developed that satisfy the requirements discussed above. These modulators can be grouped into two major categories, those based on thermal modulation and those based on mechanical (valves and diaphragms) modulators [2, 7, 11].

Thermal modulators

The thermal modulators consist of a variety of elegant and simple basic concepts. The ability of a column with a thicker stationary phase to slow down the movement of chromatographic peaks was the basis of most of the early modulators. The first modulator was reported in 1991 by Phillips and Liu [17]. This novel GC x GC system had a thermal desorption modulator in-between the two gas chromatographic columns. The modulation was achieved by means of a resistively heated trap that repetitively heats a segment of column with a thicker stationary phase (Figure 2.5C). The modulator was able to separate complex samples but it was rather unstable [17]. This led to the design of other modulation systems, which utilizes the same phase ratio effect. The most notable of these are the slotted heater (sweeper) modulator [8] (Figure 2.5A) where by a rotating heater is swiped over the column section with the thicker stationary phase, resulting in a focussing and sharper injection bandwidth of the retained compounds. The resistively heated modulator was also adapted to make use of the sweeping effect by using several resistively heated segments and heating them as to emulate the sweeping effect, as demonstrated by Burger *et al* [18] (Figure 2.5D).

The next evolution in modulator development occurred when, instead of using the phase ratio to slow down the movement of the sample, the researchers switched to cryogenics to condense or "freeze out" the sample. This has lead to the current generation of modulators [2, 7, 11] and the modulators that were used in the current work.

Longitudinal cryogenic modulator [19] (Figure 2.5B)

This modulator, the first generation of cryogenic trap modulators, works on the principle of trapping eluents from the first column by cooling down the column, thereby slowing down the movement of compounds in the column. Upon reheating, the eluent is remobilised and starts to move through the second column. The modulator operates in the following way: When the modulator is at the top position, a narrow zone containing the eluents from the first column is cold-trapped and focussed in the inlet of the second column. When the modulator moves to the bottom position the cold spot in the second

column is rapidly heated by the oven and the eluents are remobilised for separation in the second column. The modulation chamber is cooled down to 100°C below the oven temperature by evaporative cooling of liquid CO₂ expanding at the orifice at the end of the supply tubing. The temperature is controlled by activating and deactivating the carbon dioxide solenoid valve. This modulator has proved to be very simple and robust, producing narrow peaks (100 ms, peak base width) and can be operated at high oven temperatures.

Nitrogen jet-cooled thermal modulator [20] (Figure 2.5 E)

This jet-cooled modulator, developed by Ledford and co-workers, operates in a simple fashion, making it an ideal modulator for precision work. The modulator has two cooled jets for trapping and two warm jets for remobilisation. The nitrogen in the cooled jets is cooled in a nitrogen exchanger, while the nitrogen for the heated jets is heated through a cartridge-heated block in front of the modulator.

Carbon dioxide jet-cooled thermal modulator [21] (Figure 2.5 F)

The concept of Ledford was pursued by Beens and co workers [21], and to use two CO₂ jets to cool down the modulation tube. The arrangement of the jets is in such a way that no heat pulses are required, instead it uses the temperature of the oven to remobilise the sample.

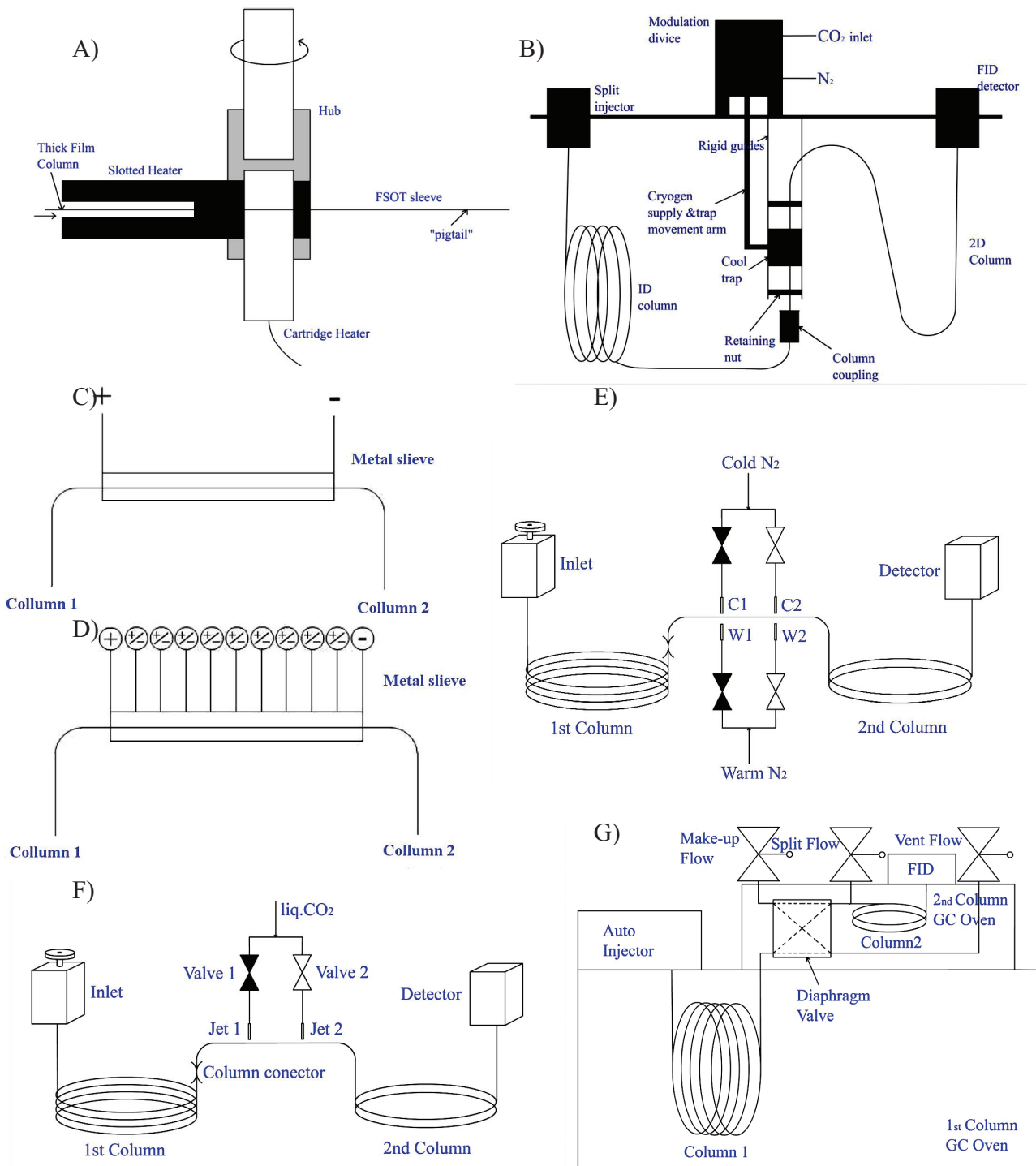


Figure 2.5 Different GC x GC modulators used [2]. A) Slotted heater thermal modulator. B) Longitudinally modulated thermal modulator. C) Resistively heated modulator D) Multi segment resistively heated modulator. E) Dual stage cryogenically modulated modulator “nitrogen” F) Dual-stage cryogenically modulated modulator “carbon dioxide” G) Valve operated modulator

Mechanical modulators.

The development of the use of valves and diaphragms in GC x GC modulation, occurred in parallel to thermal modulators. These modulators are based on GC-GC re-injections where only up to 70% of the sample is re-injected giving an almost comprehensive separation [2, 7, 11]. The modulator by Synovlec *et al* [19] (Figure 2.5G) works with a fast switching six port valve. The fast switching creates pulses of the sample to be analysed on a separate GC column. Only 10 to 20% of the sample injected reaches the detector, thus reducing the sensitivity. The modulator cannot operate at temperatures above 200 °C thus the use of the valve is limited to samples of medium volatility.

Comparison of Modulators

The different modulators are compared by Beens *et al* [7, 22] in Table 2.3 according to the following parameters:

- Focussing effect; the method employed for trapping the eluents from the first column before remobilisation or reinjection.
- Bandwidth; this parameter indicates the width of the remobilised peak. To obtain better chromatographic separation and peak capacities the reinjected band of peaks should be as narrow as possible.
- Sensitivity enhancement; this occurs due to refocusing of the eluents from the first column. The compounds eluting during the modulation period (2 to 10 s) are trapped in the modulator, causing a concentration effect. These concentrated eluents are then remobilised in the second dimension as a narrow band (10 to 300 ms).
- Comprehensiveness of the modulator indicates whether the whole sample is subjected to both dimensions of separation and whether the separation of both columns is preserved.

Type	Focussing effect	Bandwidth Injection pulse (ms)	Sensitivity enhancement percentage %	Comprehensive
Duel-stage heated	Phase ratio	16-20	10-20	yes
multi-stage heated	Phase ratio	300	1-2	yes
Sweeper	Phase ratio	60	5-15	yes
LMCS	Cryo CO ₂	20-50	5-15	yes
Moving direct spray	Cryo CO ₂	20-50	5-15	yes
Four jets cryo	Cryo N ₂	<10	10-40	yes
Two jets cryo	Cryo CO ₂	<10	10-40	yes
Single jet cryo	Cryo CO ₂ /N ₂	<10	10-40	yes
Rotating cryo	Cryo CO ₂	50	5-15	yes
Diaphragm valve	Valve	50	1	no
Differential flow	Valve	50	20	almost

The cryogenic jet modulators have the narrowest injection pulses and the larger peak enhancement of all the modulators currently available. The cryogenic jet modulators thus outperform the other designs and are a popular choice where the cost of gas and liquid nitrogen can be ignored.

2.2.3 GC x GC column selection

The type of column used is a very important parameter in the design of a GC x GC system. In GC x GC, two capillary columns with different selectivities are used [7, 8, 11]. For example, it is assumed that if two solutes co-elute on a non-polar column they will have the same or similar boiling points. This forces their separation to be a function of their specific interaction with the stationary phase, e.g. polarizability or dipole-dipole interaction [23, 24]. The choice of a stationary phase thus depends on the selectivity and separation property required for the separation problem. For practical reasons the first-dimension stationary phase is generally chosen to perform a volatility separation. The most common of these stationary phases are the 100 % dimethyl polysiloxane and the 5 % diphenyl 95 % dimethyl polysiloxane coatings. Even though volatility or boiling point separation is a commonly used term, the separation is based on the interactions of the

molecules with the stationary phase. Typically aliphatic compounds would react more with these types of columns while more polar compounds would be less retained. The more polar compounds thus would typically be moving unretained through the column depending on the column temperature.

The selection of a second-dimension column is more critical. Separation on the second column is dictated by the selective interaction of the sample with the stationary phase. Therefore, the choice of second dimension column will be based on the sample and what selectivity is required [23, 24]. Typically the separation in GC x GC second-dimension is based on either polarity or size selection. Polarity separations are also used in this work and refer to the solute interactions with the stationary phase, determined by dispersion, dipole-dipole and hydrogen bonding interactions [23, 24].

Dispersion interaction is determined by differences in solute heat of vaporization ΔH_{vap} . The value can be approximated from vapor pressure of the solute.

Dipole-dipole interaction is determined by dipole moment of the molecule. Smaller differences require a stronger dipole phase.

Hydrogen bonding interactions. Strong: alcohols, carboxylic acids, primary and secondary amines. Moderate: aldehyde, ketones, esters. Weak: hydrocarbons, halocarbons, ethers.

Some commonly used columns and their selective interaction are given in Table 2.4.

In this study, two “polar” second dimension columns were used. The first column had a poly-ethylene glycol stationary phase, $\text{HO}(\text{CH}_2\text{CH}_2\text{O})_n\text{CH}_2\text{CH}_2\text{OH}$. This stationary phase contains hydroxyl groups that can undergo hydrogen bonding with oxygenated compounds, making it an ideal column for the resolution of oxygenated compounds (particularly alcohols) and other polar solutes.

The second column, a methyl phenyl polysiloxane column, contains phenyl groups that also take part in hydrogen bonding, but to a more moderate extent. The weaker hydrogen bonding of this column makes it ideal for the separation of mixtures with a wider polarity range. This is due to the isothermal properties of the second dimension column, which may result in compounds being retained longer in the column than the allocated time for the second dimension separation. This phenomenon is also referred to as “wrap-around”.

Although a number of different column lengths and sizes have been used and discussed in GC x GC literature [7, 11, 14, 25, 26], the underlying principle governing the selection is constant. For the two columns to work in a comprehensive way, without losing efficiency in either of the two dimensions, the second column must run at speeds much faster than that of the first column. In general, this speeding up of separation (in fast GC) is obtained by increased linear flow rates [2, 22, 27]. Unfortunately, since the columns are connected in series, without additional carrier gas sources, the linear flow rate is governed by the first column’s requirements. However, by coupling a column with a smaller inner diameter to the first column a faster linear flow rate of the second column and thus faster

separation speed is achieved. The most common choice of columns is a 250 μm inner diameter first-dimension column coupled to a 100 μm inner diameter second-dimension column.

Stationary phase	Separation
100% dimethyl polysiloxane	Dispersion interaction
95% dimethyl/ 5% diphenyl polysiloxane	Dispersion interaction and some Dipole-dipole interaction
14% cyanopropylphenyl/ 86% dimethyl polysiloxane	Dipole-dipole interaction Polarizability
50% dimethyl /50% diphenyl polysiloxane	Dipole-dipole interaction Hydrogen bonding
Polyethelene glycol (PEG)	Hydrogen bonding

2.3 Time-of-flight mass spectrometry (TOFMS)

2.3.1 TOFMS principles.

Time-of-flight mass spectrometry construction was first described by Stephens *et al* [28] in 1946. The ions are accelerated in an electrostatic field and subsequently separated over time, according to their mass to charge ratio (m/z), in a field-free path of known length. It is thus obvious that the ions need to start at the same time or in a sufficiently short time. Typically ions would be pulsed into the flight path through pulsed extraction, but it is also possible to use pulsed ionization methods in a constant extraction field. The early TOFMS systems were designed for the use for gas chromatographic coupling due to their higher rate of spectral acquisition over the magnetic sector mass spectrometers. However, the introduction of the linear quadrupole mass spectrometers [29] has halted the development till the 1980s when TOFMS was revived, due to the success of pulsed ion sources [30]. The most notable of these pulsed ion sources were matrix assisted laser desorption ionization (MALDI) that required the detection of extremely high masses [31]. The reintroduction of TOFMS has after that advanced development by a huge margin and TOFMS was adapted for various ion sources [30].

Advantages of TOFMS:

- i) Mass to charge range (m/z) is in principle unlimited (detector dependant)
- ii) A full mass spectrum can be obtained from single ionization events (laser pulse in laser ionization methods)
- iii) The transmission of TOFMS is quite high, giving rise to high sensitivities

- iv) Design is simple compared to other mass spectrometric designs and it is inexpensive to construct
- v) Recent developments allow for accurate mass spectrometry and even tandem mass spectrometry.

Time-of-flight data acquisition

The performance of a TOF spectrometer depends strongly on the electronic data acquisition used. In principle TOF spectrometers allow the measurement of the complete mass distribution with one single shot i.e. huge amounts of data are created within a very short time interval. The challenge in TOF data acquisition is to design a system which combines extreme velocity (time resolution < 1 ns), zero inter-bin dead time and high data throughput rates. Depending on the ionization scheme TOF spectra are either measured using very fast AD converters (digital storage scopes, transient recorders) or fast ion counting techniques (TOF/multi-channel analyzer, time-to-digital converters).

In the case of laser ionization one laser pulse can create hundreds of ions which arrive in a pulse a few nanoseconds wide at the detector. As counting is quite difficult analog registration is normally employed. To reduce statistical uncertainties hundreds to thousands of TOF spectra have to be averaged. Typically a spectrum consists of 32k time channels with a vertical resolution of 8 bit i.e. after every laser pulse 32 kbyte of data has to be transferred and summed. The data transfer rate limits the spectrometer repetition frequency to less than 100 Hz which is compatible with conventional pulsed high power lasers.

In this thesis four types of TOFMS systems were used, each with its own distinct advantages.

The first TOFMS was a system designed by Leco corporation, St. Josephs, USA, using electron impact ionization with a pulsed extraction of the ions into the TOF. This TOFMS has a unique data acquisition system whereby the collected mass spectra are dynamically binned into mass bins to reduce the amount of data to be stored. This mass-binning technology allows for very fast data acquisition rates of up to 500 recorded spectra per second. This high data acquisition in turn is ideal for fast chromatographic applications and thus also for GC x GC.

The second TOFMS, Kaesdorf, Munich, Germany, were implemented together with the laser ionization systems. This TOFMS uses a combination of a constant extraction field and a pulsed extraction field to accelerate the ions into the TOF. The TOFMS can be switched to pulsed mode for electron impact ionization, but in the scope of this thesis the extraction was in continuous mode in conjunction with the pulsed photo ionization laser.

The third TOFMS system, also from Kaesdorf, Munich, Germany, implemented for the GC x GC x SPI TOFMS again has a constant extraction field for use with pulsed laser photo ionization.

The fourth TOFMS system was an orthogonal accelerated TOFMS (oa-TOFMS) from Tofwerk, Switzerland. The system was implemented for continuous photo ionization from a VUV-lamp source (discussed later). This TOFMS system is significantly different from the more conventional TOFMS systems described above, and will thus be discussed in more detail in the next section.

2.3.2 Orthogonal acceleration time-of-flight mass spectrometer (Figure 2.6) [32]

The most notable feature of oa-TOFMS is the orthogonal extraction TOF axis relative to the ion beam from the ion source. Ions are accelerated into the TOF through a 10-100 ns electrostatic field, creating a force on the ions in the field. The direction of the force is strictly orthogonal to the ion beam axis. The resulting orthogonal acceleration imparts a new component of velocity to the sampled ions and this component is vectorially independent of the axial velocity of the ion beam. Vectorial decoupling of the velocity of ions in the ion beam and TOF directions is an important feature of oa-TOFMS resulting in greater sensitivity. Ions sampled for TOF analysis retain the velocity gained in the ion beam. Thus their spontaneous drift trajectories will be inclined from the TOF direction according to the ratio of their components of drift-velocity in the ion beam and TOF directions [32].

The orthogonal accelerator (oa) is a highly efficient device for sampling ions from an ion beam into a TOF mass analyzer. Most orthogonal accelerators are (in fact) Wiley and McLaren “ion accelerators” consisting of two stages of acceleration (different electric field strengths defined by conducting electrode and grids) [33]. Sometimes, the first stage is divided into two regions to reduce the amplitude of the push-out pulse. The ion beam enters the oa at right angles to the TOF direction and, at regular intervals of time, ions in a section of the beam in the oa are orthogonally accelerated and they are thus raised to a much higher kinetic energy.

Some authors refer to the oa as an ion storage device [34, 35]. This can be misleading as it implies some sort of trapping of the ions in the oa. The beam simply fills the oa in about the same time as it takes for the ion with the largest m/z to pass through the TOFMS stage after orthogonal acceleration. In the penetration or “fill-up mode”, the first stage of the accelerator is set to be field free. Once the ion beam has “filled the oa”, a field is rapidly generated in the first stage to accelerate the ions orthogonally relative to their velocity in the beam. The pulse, or one that is synchronous with it, is also used to

start the timing electronics. This method of gating ions into a TOFMS introduces relatively little peak width from temporal spread in the time of ion acceleration [36-38].

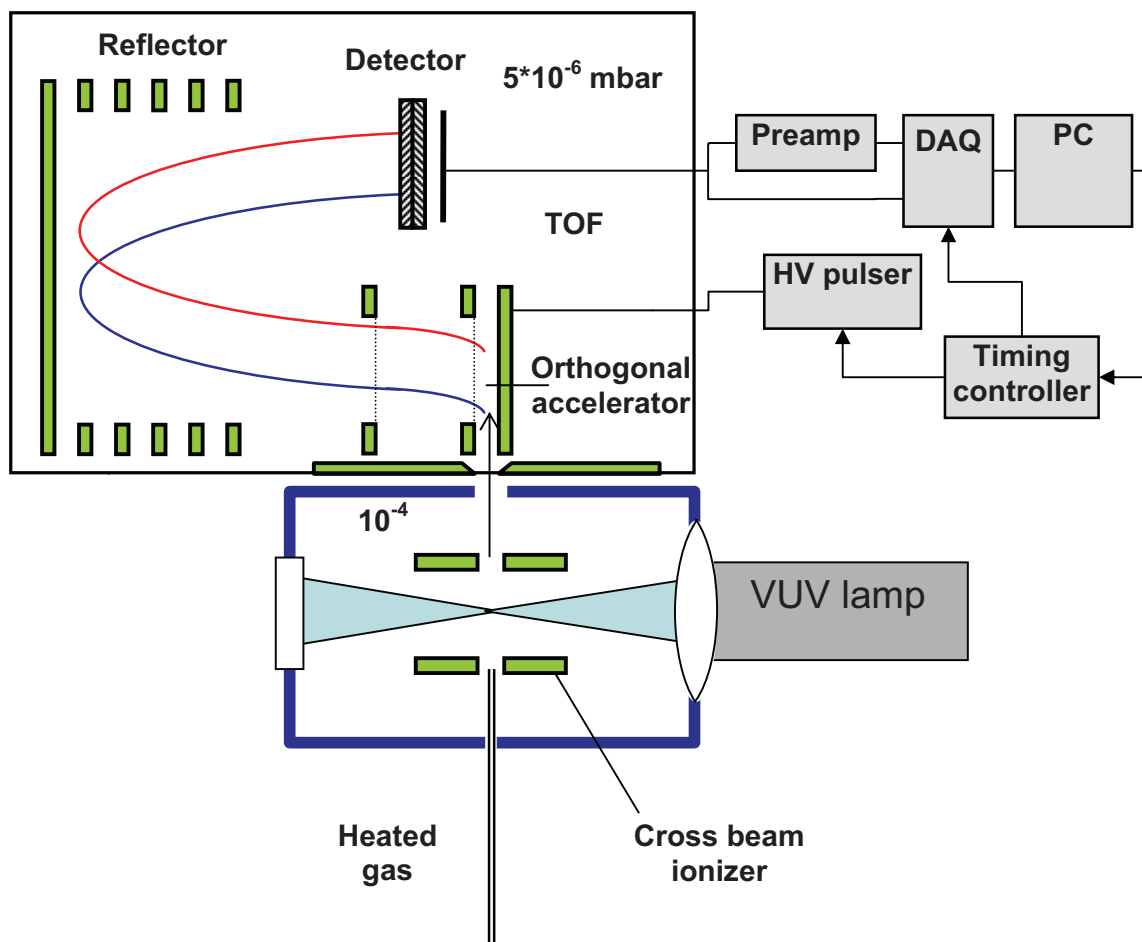


Figure 2.6 Orthogonal accelerated time-of-flight mass spectrometer (oa-TOFMS), coupled to the continuous ion stream from single photo ionization through the use of a VUV lamp [32].

2.3 Comprehensive two-dimensional coupling of gas chromatography and mass spectrometry (GC x MS)

2.3.1 GC x MS principle

In contrast to comprehensively coupled separation techniques (e.g. GC x GC), the second-dimension in hyphenated two-dimensional technologies (e.g. GC-MS) often represents a spectroscopic identification technology. As separation in this dimension is

only possible through deconvolution of the spectral information, two-dimensional data representation does not result in ordered groups of signals representing different compounds with similar chemical/physical properties. In this context MS exhibits interesting properties.

On the one hand MS can be applied as a spectrometric technique, whereby the fragmentation fingerprint pattern of a molecule is used to determine its identity.

On the other hand MS separates molecular ions and fragments according to their mass, thus representing literally a separation technique.

The separation aspect of MS is, however, in the most typical case (i.e. electron impact ionization, EI with 70eV kinetic energy) dominated by the spectrometric aspect due to the fragmentation of the molecules. Venkatramani *et al* [39] proposed that systems such as coupled gas chromatography and mass spectrometry can also be regarded as comprehensive two-dimensional systems (GC x MS). This is particularly true, however, if soft ionization methods such as photo ionization (PI), chemical ionization (CI) or field ionization (FI) are used for the ion generation in MS. Soft ionization avoids the formation of fragments and therefore fully reveals the “separation character” of mass spectrometry (i.e. molecular ions are separated by their mass). Thus, in principle, the comprehensive coupling of chromatographic and mass spectrometric separation is possible (GC x MS). Wang *et al* [40] have recently demonstrated that with appropriate gas chromatography separation parameters, i.e. a polarity separation (column), coupled to mass spectrometry with soft ionization, the hyphenated system is independent enough to allow a comprehensive GC x MS approach.

Figure 2.7 schematically illustrates the result of the separation that can be achieved when combining MS with GC.

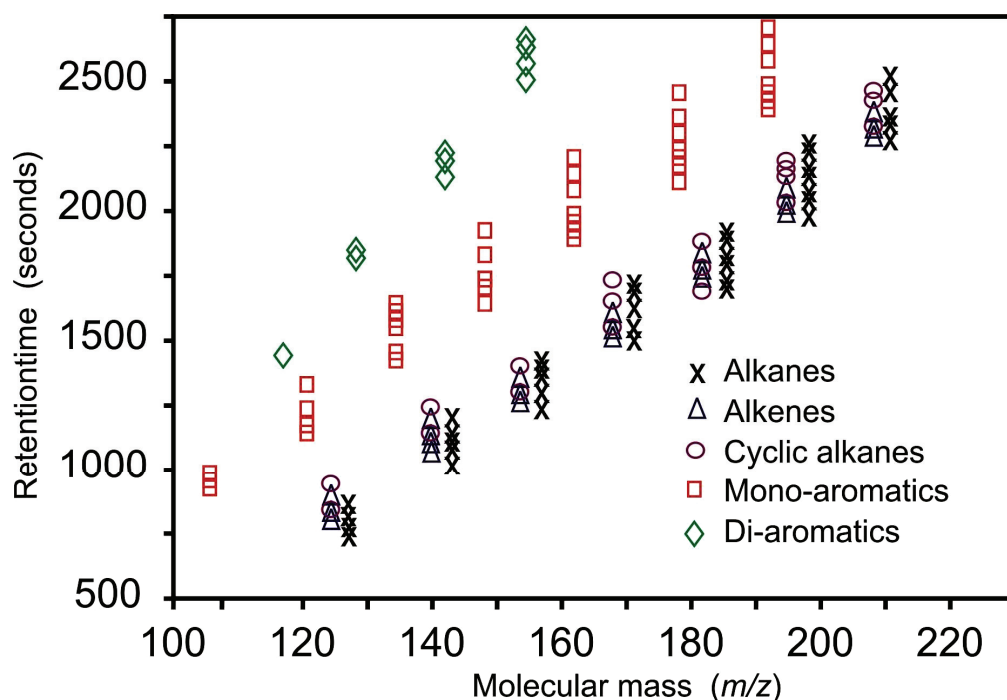


Figure 2.7 Illustrated representation of the obtainable separation of GC combined with soft ionization mass spectrometry.

Molecules with different molecular mass are clearly separated from one another in the MS dimension. Molecules with the same molecular mass (isobaric and isomeric compounds) require separation in the GC dimension. Isobaric molecules like alkenes and cyclic alkanes are not easily separated by chromatography and are thus still undistinguishable. This is even more problematic for isomeric compounds. However the separation achieved in GC x MS is easily obtained and easy to interpret. MS can also be considered a comprehensive technique as long as the acquisition rate of the MS is fast enough to retain the separation achieved in the chromatographic dimension.

Orthogonality in GC x MS is however more difficult to achieve. Molecular size is often related to the volatility of the compounds thus separating compounds on a volatility basis using GC would result in two dependant separation dimensions. Even chromatographic columns that separate compounds on their chemical or physical interactions with the stationary phase have a temperature dependency. The temperature dependency can be eliminated by rearranging the GC x MS plots so that the n-alkanes form a straight line. This type of adjustment is similar to a Kovats index adjustment.

Figure 2.8 shows the schematically illustrated adjustment of the two-dimensional plot seen in Figure 2.8. Mass spectrometry coupled to gas chromatography, thus can be viewed as an orthogonal two-dimensional separation system. Another benefit of the

rearrangement of the GC x MS plot is that the separation space can be more effectively used, since the empty space below the alkanes where no compounds elute is removed from the plot.

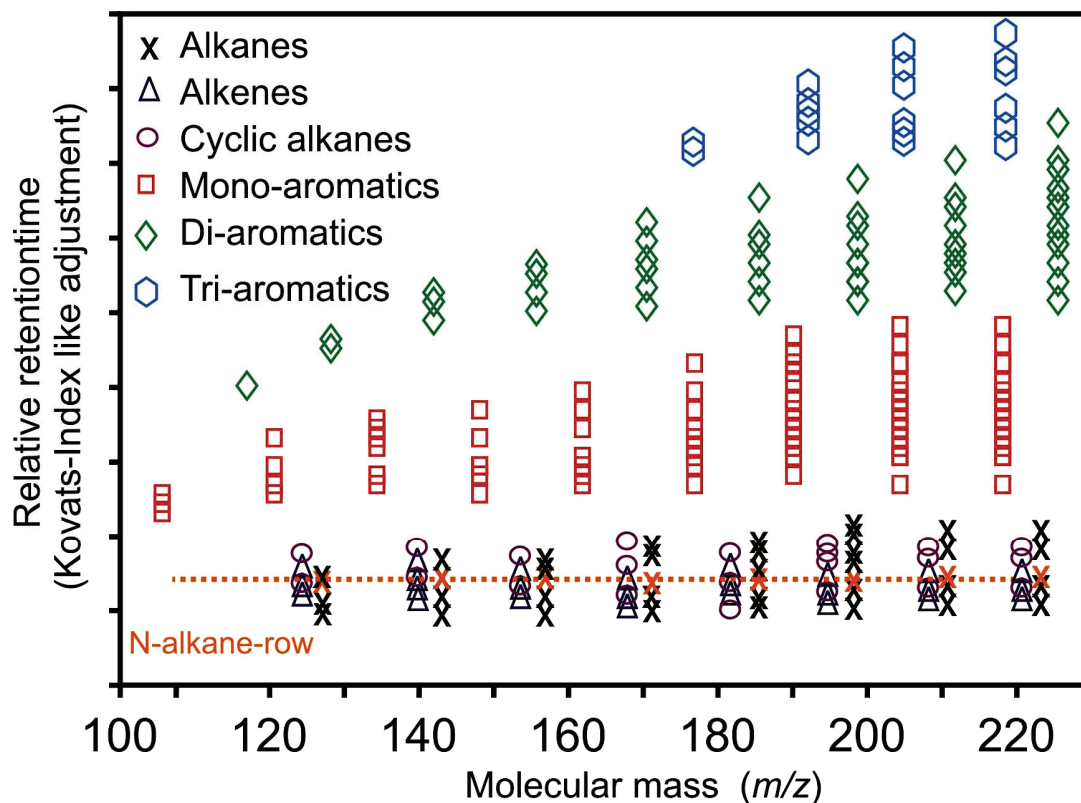


Figure 2.8 Illustrated representation of the obtainable separation of GC combined with soft ionization mass spectrometry. Retention times are now adjusted to eliminate the temperature dependency in a Kovats-index like adjustment (*n*-alkanes are now in a straight line).

This representation of GC x MS closely resembles the type of plot expected from GC x GC separation obtained using a non-polar first dimension and polar second dimension column. The unique distribution bands of chemically or physically related compounds make it a technique ideal for fast sample screening.

Soft ionization is unfortunately not as common and readily available as other ionization techniques. A universal soft ionization technique is even more difficult to obtain. Field ionization is one universal soft ionization technique that was introduced by Wang *et al* [40] as an ion source for GC x MS.

In this thesis photo ionization is investigated as a soft ionization source, with single photon ionization as a universal soft ionization source and resonance enhanced multi-photon ionization as a highly selective soft ionization source.

2.3.2 Resonance enhanced multi-photon ionization (REMPI)

Resonance enhanced multi-photon ionization (REMPI) is a highly selective and sensitive ionization method. Essentially REMPI TOFMS can be viewed as a two dimensional detector with the combination of two powerful detection techniques: ultraviolet (UV) laser spectroscopy and mass spectroscopy. Two photons are required for REMPI ionization the first is in the selective absorption step that is either followed by the observation of fluorescence (Laser Induced Fluorescence, LIF) or by the subsequent absorption of a second laser photon resulting in the ionization of the molecule (REMPI). The ionization scheme of REMPI is shown in Figure 2.9, and it is obvious that the selection of the photon energies are crucial to obtain ionization. The first photon's energy is resulting in excitation of the target molecule while the second photon must have sufficient energy to ionize the excited molecule.

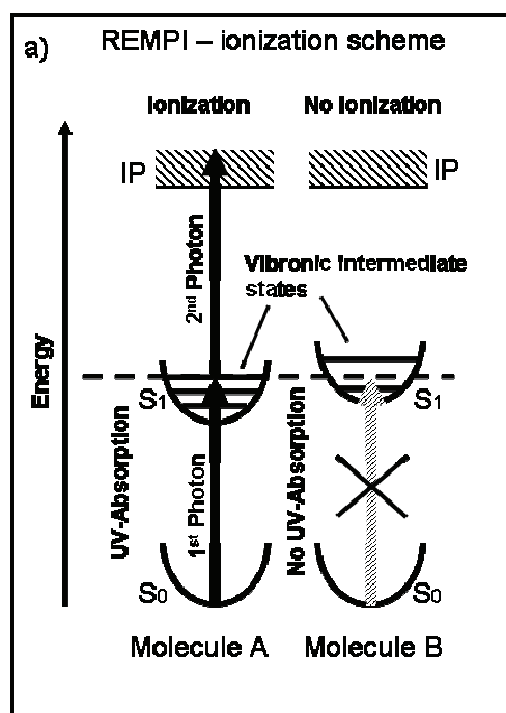


Figure 2.9 The ionization scheme of REMPI, two photons is needed to ionize the target molecule.

The use of REMPI-TOFMS coupled to gas chromatography is well known in the literature [41-44]. The selective ionization of REMPI-TOFMS allows for the detection of co-eluting compounds or for the differentiation between isomers.

Aromatic compounds have strong absorption bands in the UV region, while most aliphatic compounds have no absorption in the UV region. A GC-REMPI TOFMS

chromatogram of a petroleum sample, using a wavelength of 266 nm, would thus only show the aromatic content of the sample (Figure 2.10). This type of selectivity in the analysis of petroleum samples is ideal for the analysis of the aromatic fraction, since the aliphatic component of the sample usually greatly overshadows the smaller aromatic content. Obtaining an aromatic profile of the sample analyzed is beneficial for many applications: a) in environmental aerosol organic content monitoring, the aromatic fraction is related to toxic effects, b) in gasification processes the aromatic compounds are typically the precursors for soot formation, c) in the petroleum industry aromatic species are associated with lubrication properties, etc. The use of GC-REMPI-TOFMS is thus beneficial for processes where different compound classes need to be monitored.

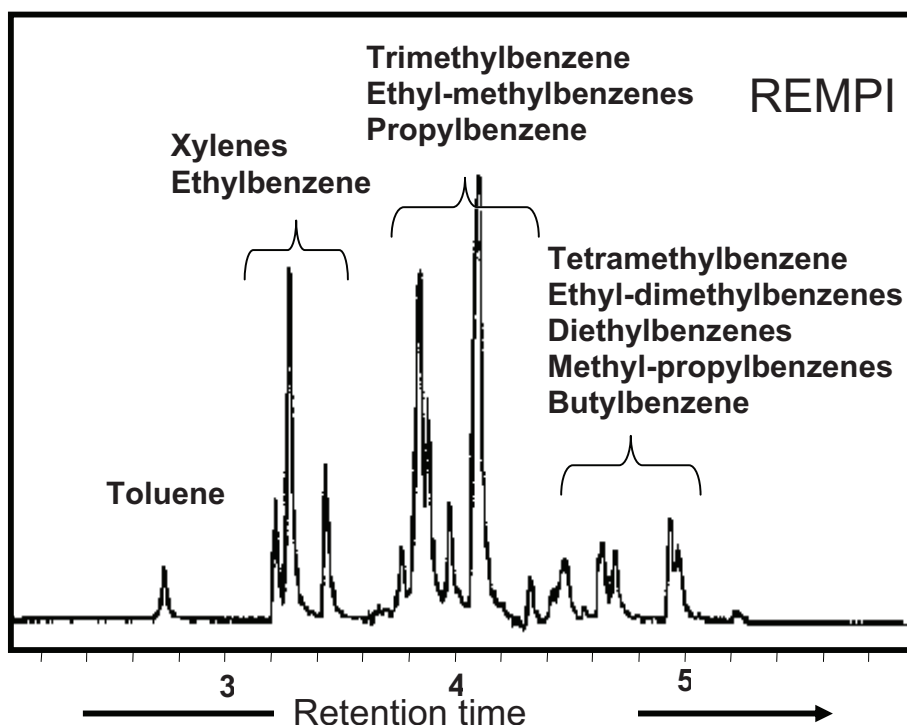


Figure 2.10 The selective ionization of aromatic compounds in a petroleum sample. [44]

Different mass spectrometric inlets (GC to MS interface) can be used in the coupling of gas chromatography and photo ionization mass spectrometry [44]. The most noted of these inlets and also used later on in this thesis is the use of supersonic jet cooled inlets. The supersonic jet inlet cools the effluent from the GC column to very low temperatures, which considerably reduces any fragmentation [45] in the MS source and increases the REMPI selectivity. REMPI selectivity for cooled molecules is increased due to thermal

de-excitation of vibrational and rotational intramolecular motions [46, 47] and the associated narrowing of the UV absorption bands.

Figure 2.11a-d shows the REMPI-ionization as a function of the laser wavelength for jet-cooled *o*-xylene, *m*-xylene, *p*-xylene [48], and ethylbenzene. From the REMPI spectra it can be observed that the individual molecules have unique REMPI bands (i.e. UV absorption bands) at different wavelengths (see Figure 2.11a-d). It is thus possible to selectively ionize the different isomers by selecting the appropriate wavelength. In Figure 2.11e and f the result of a GC-EI-TOFMS and GC-REMPI-TOFMS separation of a gasoline sample is shown. In the depicted section of the chromatogram it is shown that by using the specific column combination it is impossible to distinguish between *m*-xylene and *p*-xylene using EI, but by selecting a REMPI wavelength of 272.325 nm the *p*-xylene can be selectively ionized without interference from the other compounds [49] (Figure 2.11f).

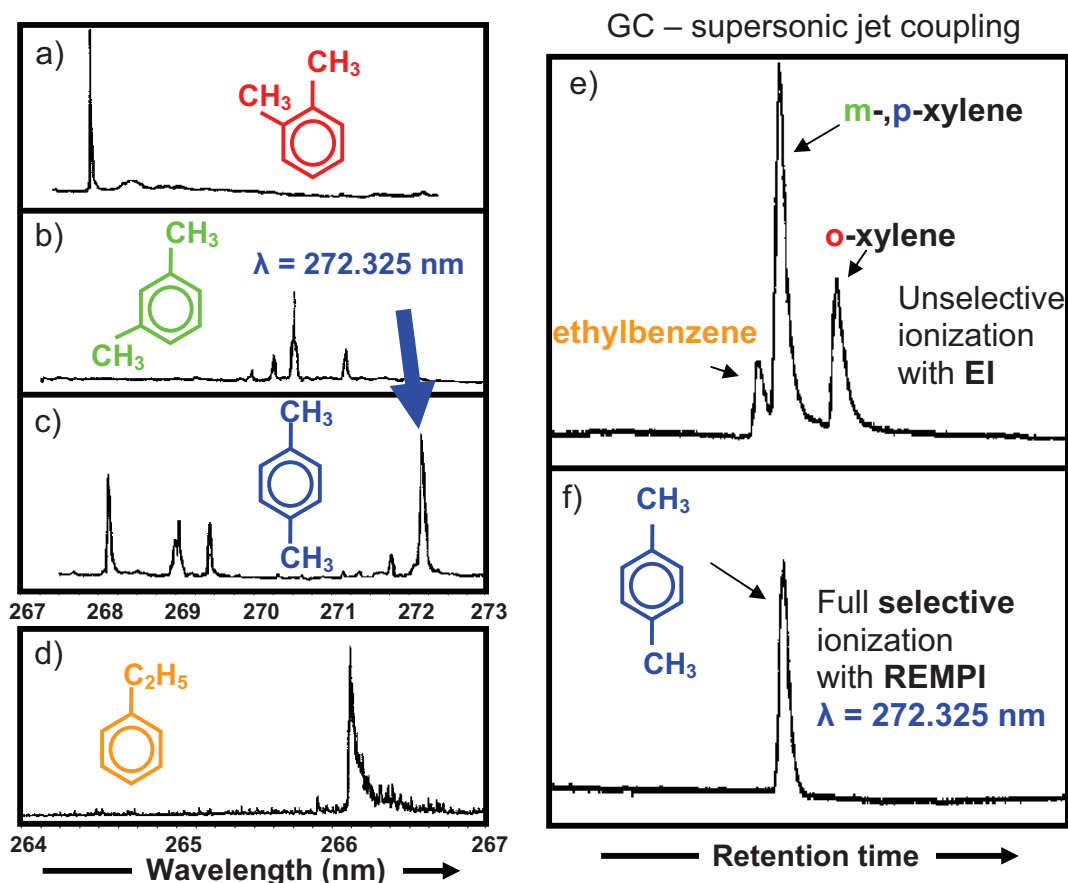


Figure 2.11 Selective ionization of REMPI, to selectively detect *para*-xylene in the presence of *ortho*-xylene, *meta*-xylene and ethyl benzene. a-d) Ionization spectra of *ortho*-, *meta*-, *para*-xylene and ethyl benzene. e) Chromatograms obtained using EI, f) Selective detection of *para*-xylene

[44]

To date, most GC-REMPI-TOFMS work was focused on increasing the selectivity for specific target analyte applications, rather than on the analysis of an entire sample. In the context of this work REMPI at different wave lengths is used to investigate compound classes with similar REMPI absorption bands.

2.3.3 Single photon ionization (SPI)

Single photon ionization is a universal ionization method that ionizes molecules based on their ionization potential. In SPI (Figure 2.12) vacuum ultraviolet (VUV) photons with sufficient energy to ionize the target molecules in a single absorption step are used. Some selectivity in SPI can be obtained by adjusting the energy of the photons to either exceed or fall short of the ionization potential (IP) of target molecules.

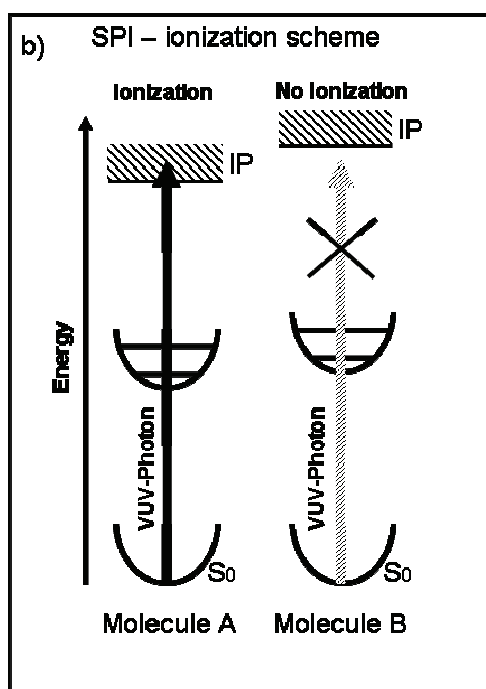


Figure 2.12 The ionization scheme of SPI, the energy of the photon should be sufficient to excite the target molecule to its ionized state.

2.3.4 Lamp based SPI [32, 50, 51]

The use of laser photo ionization is a costly procedure and a high level of experience is required to maintain these systems. Another disadvantage of laser sources is the laser repetition rate. The 10 Hz laser systems are sufficient for online applications and to some extent for normal gas chromatography, but for fast GC applications and for applications where high averaging is required the cost of higher repetition rate lasers becomes impractical.

To overcome these disadvantages VUV lamps have been applied as a photon source. However, conventional VUV lamps often suffer from low spectral resolution in the required frequency range. In addition, for intensive VUV generation these lamps need water cooling. The VUV emission of rare gas excimers is known [52] including both excimer laser and lamp. A very efficient method of excimer light generation is via electron beam excitation of dense rare gases. This requires acceleration of electrons in an evacuated chamber with subsequent guiding of the electron beam through a thin foil into a gas cell. This method has significant advantages such as a high efficiency of the light sources. 35 % conversion of electron energy to light was reported for argon [53]. Very clean excimer emission spectra have been shown due to an extremely low level of impurities in the gas and the low gas temperature during operation [53]. The gas purity is achieved by avoiding debris production, which is a problem in discharge driven excimer lamps due to electrode erosion. The compact electron beam pumped excimer lamps (EBEL) can be operated continuously and in pulsed mode. Running the EBEL continuously a maximum of 2.6×10^{14} VUV photons per second can be generated compared to the 7.9×10^8 photons per laser pulse generated by the excimer laser system.

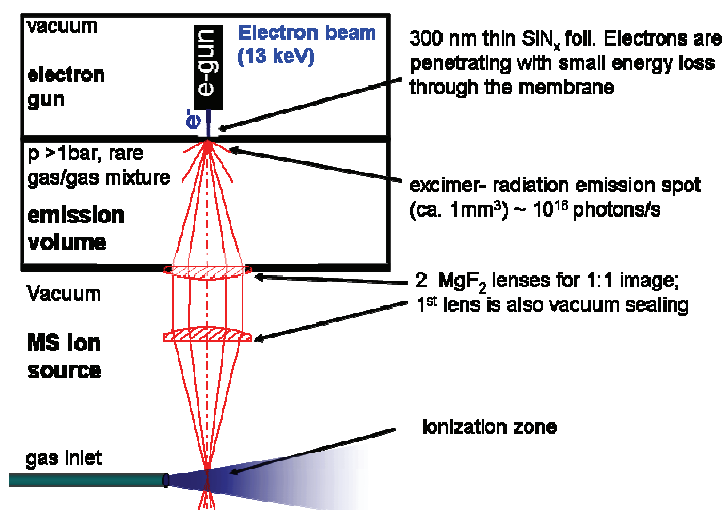


Figure 2.13 Illustration of the EBEL [32, 50, 51]

Different rare gasses or gas mixtures can be used for the excimer radiation using the EBEL lamp. Figure 2.14 shows the photon wavelengths that can be obtained by using Xe, Kr, Ar, Ne and He.

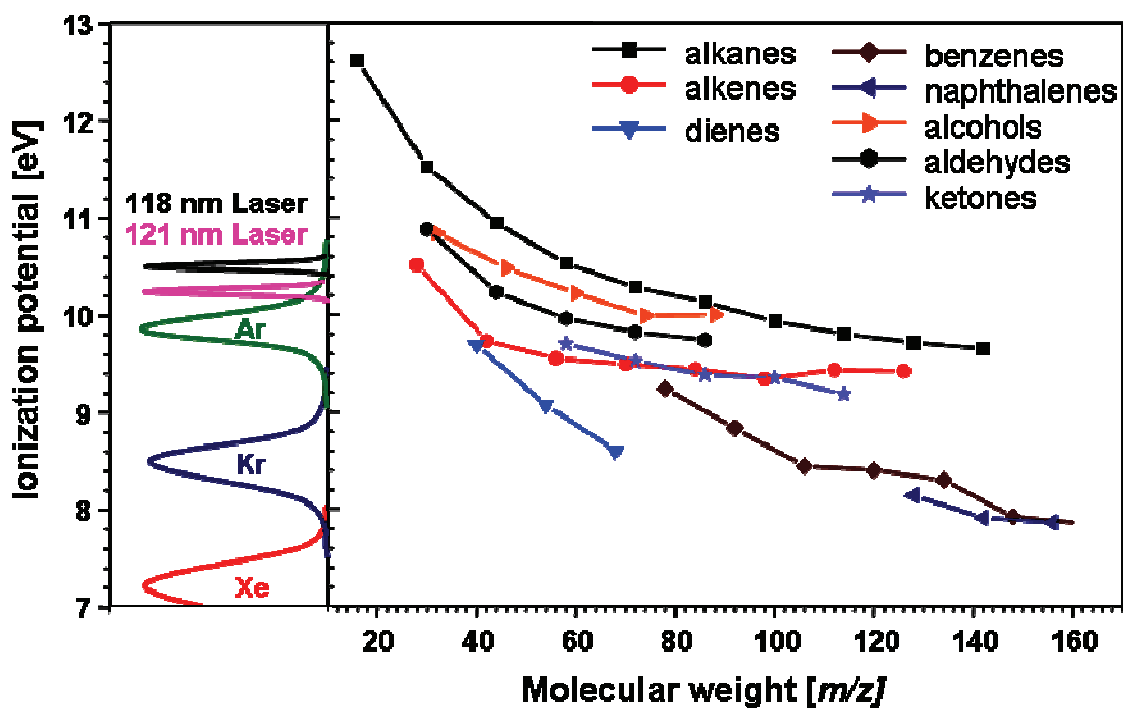


Figure 2.14 the use of different excimer gasses to obtain selective photon energies.[54]

The different wavelengths obtained are related to the energy of the generated photon and correspond to the ionization potentials of the target molecules to be ionized. The argon excimer gas used in the EBEL presented later in this thesis gives a 126 nm photon, which correspond to 10.8 eV. Molecules with an ionization potential greater than 10.8 eV would thus not be ionized.

2.6 References

- [1] Giddings JC (1984) *Anal. Chem.* 56:1258-1270
- [2] Welthagen W (2004) The optimisation of GC x GC and the analysis of diesel petrochemical samples. In: Chemistry Department University of Pretoria, Pretoria
- [3] Schomburg G (1995) *Journal of Chromatography A J. Chromatogr. A* 703:309
- [4] Bertsch W (1999) *J. High Resolut. Chromatogr.* 22
- [5] Giddings JC (1995) *J. Chromatogr. A* 703:3-15
- [6] Guiochon G, Beaver LA, Gonnord MF, Siouffi AM, Zakaria MJ (1983) *J. Chromatogr.* 255:415
- [7] Dallüge J, Beens J, Brinkman UAT (2003) *J. Chromatogr. A* 1000:69
- [8] Phillips JB, Xu J (1995) *J. Chromatogr. A* 703:327-334
- [9] de Geus HJ, Brinkman UAT (1996) *Trends Anal. Chem.* 15:168-178
- [10] Bertsch W (2000) *J. High Resol. Chromatogr.* 23:167
- [11] Marriott PJ, Shellie R (2002) *Trends Anal. Chem.* 21:573-581
- [12] Davis JM, Giddings JC (1983) *Anal. Chem.* 55:418
- [13] Davis JM, Giddings JC (1985) *Anal. Chem.* 57:2168
- [14] Phillips JB, Beens J (1999) *J. Chromatogr. A* 856:331-347
- [15] Murphy RE, Schure MR, Foley JP (1998) *Anal. Chem.* 70:1585
- [16] Seeley JV (2002) *J. Chromatogr. A* 962:21
- [17] Liu Z, Phillips JB (1991) *J. Chromatogr. Sci.* 29:227-231
- [18] Burger BV, Snyman T, Burger WJG, Van Rooyen WF (2003) *J. Sep. Sci.* 26:123-128
- [19] Marriott P, Kinghorn R (1999) *Trends anal. chem.* 18:114-125
- [20] Ledford EB, Billesbach CA, Zhu QY (2000) *J. High Resol. Chromatogr.* 23:205
- [21] Beens J, Adahchour M, Vreuls RJJ, van Altena K, Brinkman UAT (2001) *J. Chromatogr. A* 919:127-132
- [22] Beens J (2003) In: First International Symposium on Comprehensive Multidimensional Gas Chromatography, Volendam, The Netherlands
- [23] Poole CF, Poole SK (1991) *Chromatography Today*. Elsevier, Amsterdam
- [24] Skoog DA, Holler FJ, Nieman TA (1998) *Principles of instrumental analysis*. Brooks/Cole Thomson learning. United States of America
- [25] Dallüge J, Van Stee LLP, Williams J, Beens J, Vreuls RJJ, Brinkman UAT (2002) *J. Chromatogr. A* 974:169-184
- [26] Welthagen W, Schnelle-Kreis J, Zimmermann R (2003) *J. Chromatogr. A* 1019:233-249
- [27] Cramers CA, Leclercq PA (1999) *J. Chromatogr. A* 842:3-13
- [28] Stephens WE (1946) *Phys. Rev.* 69:674

- [29] de Hoffmann E, Stroobant V (2003) *Mass Spectrometry: Principles and Applications*. Wiley
- [30] Wolf B (1995) *Handbook of ion sources*. CRC Press
- [31] Hillenkamp F, J P-K (2007) *MALDI MS: a practical guide to instrumentation, methods and applications*. Wiley-VCH
- [32] Muhlberger F, Saraji-Bozorgzad M, Gonin M, Fuhrer K, Zimmermann R (2007) *Anal. Chem.* 79:8118-8124
- [33] Wiley WC, McLaren IH (1955) *Rev. Sci. Instrum.* 26:1150-1157
- [34] Boyle JG, Whitehouse CM (1992) *Anal. Chem.* 64:2084-2089
- [35] Laiko VV, Dodonov AF (1994) *Rapid Commun. Mass Sp.* 8:720-726
- [36] Coles J, Guilhaus M (1992) *Orthogonal Acceleration TOF-MS - Making TOF Work with Continuous Ion Sources*. In: *The Ion Trap Storage/Reflectron Time-of-Flight Mass Spectrometer*, Blunar GJ, Cotter RJ (eds) Le Croy Corporation, New York
- [37] Coles JN, Guilhaus MJ (1994) *J. Am. Soc. Mass Spectr.* 5:772-778
- [38] Guilhaus M, Mlynski V, Selby D (1997) *Rapid Commun. Mass Sp.* 11:951-962
- [39] Venkatramani CJ, Xu J, J.B. P (1996) *Anal. Chem.* 68:1486-1492
- [40] Wang FCY, Qian K, Green LA (2005) *Anal. Chem.* 77:2777-2785
- [41] Opsal RB, Reilly JP (1988) *Anal. Chem.* 58:1060
- [42] Dobson RLM, D'Silva AP, Weeks SJ, Fassel VA (1986) *Anal. Chem.* 58:2129-2137
- [43] Imasaka T, Okamura T, Ishibashi N (1986) *Anal. Chem.* 58:2152-2155
- [44] Zimmermann R, Lerner C, Schramm K-W, Kettrup A, Boesl U (1995) *Eur. Mass Spectrom.* 1:341-351
- [45] Amirav A, Danon A (1990) *Int. J. Mass Spectrom and Ion Proc* 97:107-113
- [46] Stiller SW, Johnston MV (1987) *Anal. Chem.* 59:567-572
- [47] Hayes JM (1987) *Chem. Rev.* 87:745
- [48] Zimmermann R (1995) *Anwendung isomerenselektiver Lasermassenspektrometrie (LAMS) in der Analytik: Entwicklung einer Gaschromatographie-LAMS Kopplung sowie spektroskopische Untersuchungen zur on-line Emissionsüberwachung technischer Verbrennungsanlagen*. In: *Fakultät für Landwirtschaft und Gartenbau Technische Universität München, München*, p. 254
- [49] Zimmermann R, Boesl U, Heger HJ, Rohwer ER, Ortner EK, Schlag EW, Kettrup A (1997) *J. High Resol. Chromatogr.* 20:461-470
- [50] Muhlberger F, Wieser J, Ulrich A, Zimmermann R (2002) *Anal. Chem.* 74:3790-3801
- [51] Mühlberger F, Wieser J, Ulrich A, Zimmermann R (2002) *Anal. Chem.* 74:3790-3801
- [52] Tanaka Y, Jursa AS, Blanc FJ (1958) *J. Opt. Soc. Am. B* 48:304

- [53] Wieser J, Murnick DE, Ulrich A, Huggins HA, Liddle A, Brown WL (1997) *Rev. Sci. Instrum.* 68:1360-1364
- [54] Adam T, Mitschke S, Streibel T, Baker RR, Zimmermann R (2006) *Chem. Res. Toxicol.* 19:511

Chapter 3

**NEW DEVELOPMENTS IN GC x GC-TOFMS
DATA ANALYSIS**

3.1	Introduction	40
3.2	Method for chemical classification and the application on urban aerosol and diesel samples	41
3.2.1	<i>Rule based approach for chemical classification of PM 2.5 Aerosols</i>	58
3.2.2	<i>Experimental</i>	60
3.2.3	<i>Results and discussion</i>	63
3.2.4	<i>Conclusions</i>	83
3.3	Methods for comparison of sample classes and the application on metabolomic profiles	84
3.3.1	<i>Biomarker identification in mouse spleen extracts</i>	85
3.3.2	<i>Experimental</i>	88
3.3.3	<i>Results and discussion</i>	90
3.3.3.1	<i>Comparison of chromatograms</i>	99
3.3.3.2	<i>Chromatogram averaging</i>	100
3.3.3.3	<i>Bubble plot representation of GC x GC-TOFMS data</i>	102
3.3.3.4	<i>Difference chromatograms</i>	104
3.3.3.5	<i>Normalizing peak surfaces for generation of difference chromatograms</i>	106
3.3.3.6	<i>t-Test comparison</i>	108
3.3.3.7	<i>Fisher values</i>	110
3.3.3.8	<i>Principle component analysis</i>	112
3.3.4	<i>Conclusions</i>	113
3.4	References	114

Chapter 3

NEW DEVELOPMENTS IN GC x GC-TOFMS DATA ANALYSIS

3.1 Introduction

The development of techniques to analyze and resolve complex mixtures is needed to understand the underlying chemical or physical properties or to adhere to control regulations. GC x GC-TOFMS can resolve extremely complex mixtures, but a major draw back of the technique to date is the lack of powerful data analysis computational tools to interpret the obtained GC x GC-TOFMS data. Depending on the sample being analyzed several thousands of compounds could be separated in a single analysis, for example 2 000 compounds separated in cigarette smoke by Dallüge *et al.* [1], over 5 000 volatile organics in the atmosphere by Dallüge *et al.* [2] or more than 10 000 compounds by Welthagen *et al.* [3]. The huge amount of separated peaks makes it difficult to extract chemical information when large sample throughput is required. A typical GC x GC-TOFMS chromatographic run takes in the order of 1 to 2 hours to complete, however, depending on the level of data analysis thereafter, it could take between 5 and 24 hours to allocate chromatographic peaks and to perform mass spectral library searches on the separated chromatographic peaks. The quality of these library matches is often poor and the identification needs to be corrected afterwards by the operator according to known retention time positions and experience on the type of sample, or through the use of data banks. After this initial phase of identifying compounds it is then possible for an operator to select single compounds for further analysis, however it could take several weeks to analyze the entire sample.

New developments in data analysis are thus needed to help in the interpretation of the GC x GC-TOFMS data. In the current work a method is introduced that uses the unique properties of GC x GC and TOFMS to group compounds into compound classes. This classification method is demonstrated on a diesel petroleum sample and on urban aerosol samples.

The second data analysis method introduced is the implementation of statistical methods and subtraction or averaging methods for visual pattern recognition to screen samples timely for differences. This method is demonstrated on the detection of possible biomarkers in mouse spleen extracts.

3.2 Method for chemical classification and the application on diesel and urban aerosol samples [3]

One route for the rapid computation of samples is to classify chemically related compounds into groups. The GC x GC-technique itself is rather well suited for group separations. The use of the two-dimensional (2D) retention data for this purpose is already described by a number of publications [4, 5], and is therefore a useful parameter to include in this study. This relates to Giddings theory published on the concepts of two-dimensional systems [6, 7]. Giddings showed theoretically that the key property of a separation method, which determines whether it can show the inherent structure of a mixture being separated or not is the method's dimensionality. The dimensionality of a mixture is the number of independent variables of every member of the mixture. Mixtures with only one variable differentiating between the members within, for example boiling point, could thus be separated using a separation dimension based on this variable. For mixtures containing more than one independent variable more than one independent separation would be needed to separate the members of the sample. When a mixture is then separated based on these independent variables, each compound will separate to a unique location on a separation space (two-dimensional plane in a GC x GC chromatogram). However, as the compounds are composed of molecules with discrete structures that are related, the compounds must distribute over the dimensional separation space (chromatogram) to discrete locations, which are also related to each other. Explaining Giddings' theory in GC x GC separation [5]: if a mixture is separated in one dimension, such as the boiling point fractions in petroleum samples, the alkanes and aromatics with similar boiling points overlap and thus insignificant ordering of compounds occurs. If the variable "boiling point" is changed to "polarity", the same overlap does not occur but new overlaps are created by different "boiling point" fractions, thus the separation or ordering is still insignificant. The mixture is simply not sufficiently well ordered in any one dimension, it requires at least two independent variables to uniquely speciate the compounds of the mixture. This theory applied to two-dimensional gas chromatography thus provides the basis on which compounds are separated in a two-dimensional plane. It should however be noted that all GC separations are dependant on the "boiling point" variable, and thus the two separation systems in GC x GC cannot strictly be considered as independent of one another. GC x MS is another two-dimensional system where mixtures are separated according to the variables of chromatographic "polarity" and molecular mass obtained through soft ionization (discussed in more detail in Chapter 4)

Compounds belonging to the same chemical group in a chemical mixture are related to one another in some chemical or physical way, thus separating them according to these physical and chemical properties will result in compounds being separated into chemical groups, providing structured distribution patterns of the chemical groups. This is in particular true for homologues series of compounds for example the increasing carbon number in organic species so that the chemical properties of the

species don't change that fast. Petrochemical samples contain thousands of compounds but the small number of chemical classes, make it ideal for a two-dimensional system like GC x GC. Aerosol samples also contain thousands of compounds but they belong to many different compound classes. The two dimensions of GC x GC are simply not enough, therefore at least another dimension (MS) needs to be added.

The use of fragmentation patterns in mass spectral data to identify compounds and to classify compounds is a well established technique [8] and was long used before mass spectral libraries became available.

Several chemical compounds classes show a unique distribution of ions (fragmentation patterns) in the mass spectrum. These fragmentation patterns depend on the structures of the molecules ionized and the stability of the fragment ions. This includes the stable neutral ions of carboxyl ($-\text{CO}_2$) species or the stability of the troponium ion (91 m/z) in aromatic species. It is clear that the complexity of these fragmentation patterns often increases with molecule size and number of functional groups, but it still gives valuable interpretable results.

The purpose of the current study therefore is to improve on an already well-established GC x GC-based concept for group type separation by additionally using the mass spectral information. The deconvoluted mass spectra and the retention time of both dimensions are the basis of sorting these peaks into chemically related groups. Compounds are separated on a volatility basis (non-polar column, dimethyl polysiloxane stationaryphase) in the first dimension and on a polarity basis (medium-polar column, methyl phenyl polysiloxane stationaryphase) in the second dimension.

Figure 3.1A shows a typical two-dimensional contour-plot of an Augsburg PM2.5 aerosol sample. The peak finding routine (based on deconvolution techniques, Chroma-TOF software, version 2.01, Leco Inc., USA) detected about 15,000 peaks. A library search (NIST) resulted in the majority of the peaks not being identified (library matches below 700). In order to efficiently develop and test concepts for automated peak classification, we decided to use a smaller part (Figure 3.1B) of the two-dimensional plot located in a less crowded region of the chromatogram. In this region only 1060 peaks were found. The chromatographic peak data consists of:

- first dimension retention times;
- second dimension retention times;
- peak area (analytical ion current (AIC)); and
- mass spectrometric peak list.

The chromatographic peak data was exported and further analyzed with external software programs (e.g. EXEL 2000 software, Microsoft Inc., USA). The peak data (*i*) to (*iii*) could be represented as a so-called bubble-plot. Each bubble represents a chromatographic peak. The bubble position is given by the retention time co-ordinates of the peak (i.e. by: (*i*) first retention time; and (*ii*) second dimension retention time).

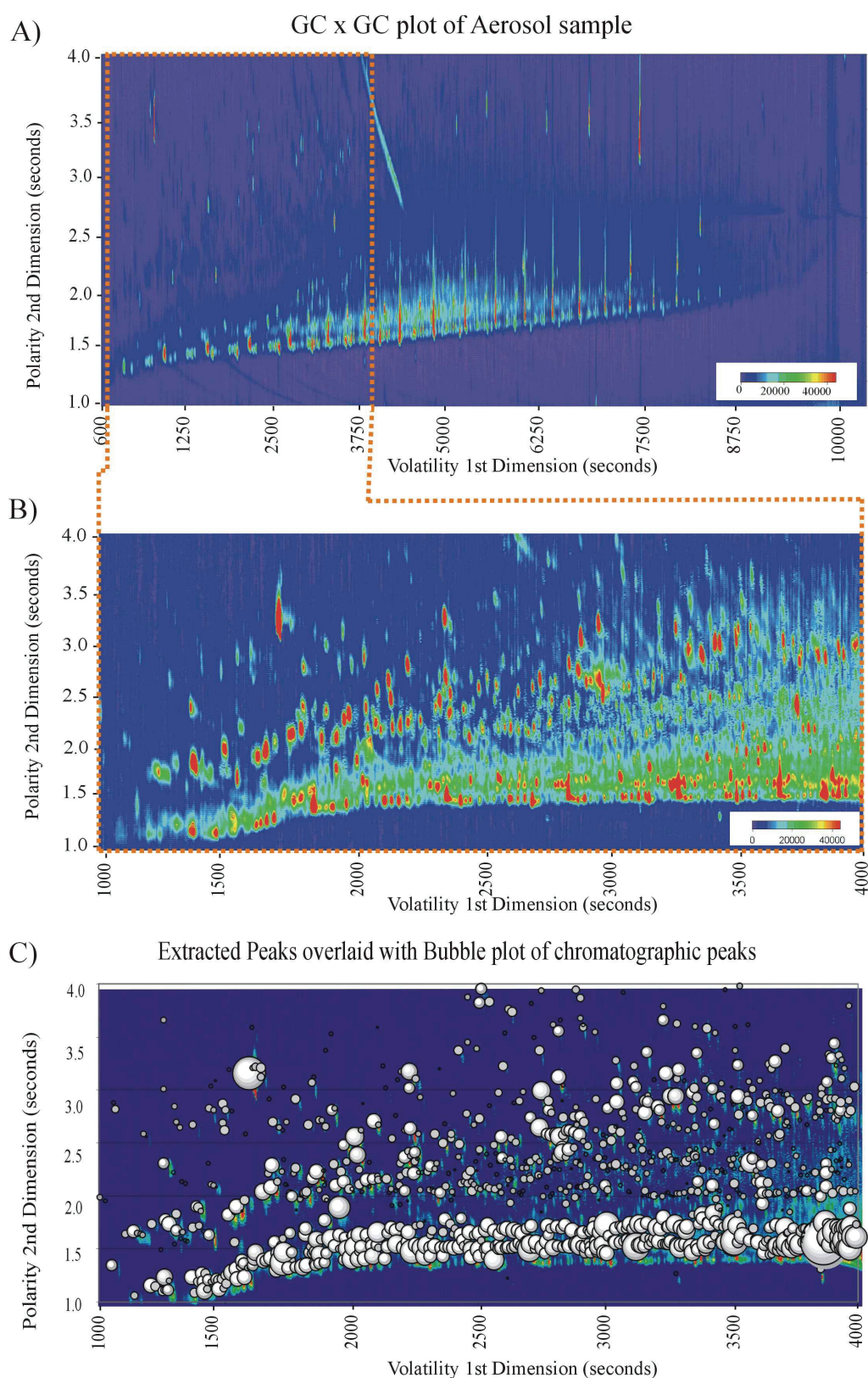


Figure 3.1 Two-dimensional GC x GC-TOFMS total ion current (TIC)-plot of an aerosol sample in 2D contour-plot representation: (A) Full GC x GC-TOFMS chromatogram of the analyzed aerosol (B) Extraction of the selected section for the data analysis; (C) Extracted section overlaid with a bubble-plot generated from the peak apexes of the same selection[3].

The area of the bubble corresponds to the peak area; *(iii)* calculated from the deconvoluted chromatographic peak. Figure 3.1C shows the contour-plot of the extracted section with overlaid bubble-plot regression.

In order to evaluate the concept of substance class assignment based on fragmentation patterns, the exported mass spectrometric fragmentation pattern information was screened for characteristic ion pattern information, using classical mass spectroscopic fragmentation analysis knowledge [8]. The rules applied in this preliminary investigation were based on ion abundances and first and second dimension retention times. The peak lists were thus sorted in the exported spreadsheet to match the selected retention time criteria and then sorted according to their mass spectral features.

The mass spectral peak selection criteria (ion abundance rules) and the retention time criteria are given in Table 3.1.

Table 3.1: Selection Rules (<i>ion abundance rules</i>) for compound class identification [3]		
Compound class/group	Compound class/group identification rules	
	Mass pattern selection rules	Retention time selection Rules
Alkanes	Base Peak 57 or 71 with second largest peak 71 or 57	<u>No time Rule needed</u> (Must be within 1s and 1.5s of second dimension)
Alkenes and Cycloalkanes	Base peak 55 or 69 with both present and with three of following peak in more than 15% relative intensity 97,83,70,57,56	Must be within 1s and 2s of second dimension
n-Alkane acids	Peaks with base mass 60 and second highest mass 73	<u>No time Rule</u>
Alkyl substituted Benzenes	1. Peaks with mass 91 above 15% relative intensity and greater than mass 77 present above 5% relative intensity 2. Compounds with mass 77 above 25% relative intensity.	<u>No time Rule needed</u> 1. (Generally above 2s second dimension time with exceptions at first dimension time below 1700s) 2. For mass selection point 2 only those compounds below 2s second dimension and below 1700s first dimension.
Benzenes with Polar and with or without Alkyl groups	Peaks with mass 77 above 25% relative intensity	Above 2s second dimension time
Partly Hydrated Naphthalenes and alkenyl substituted Benzenes	Peaks with mass 91 above 15% relative intensity mass 77 above 5% relative intensity and mass 128 above 10% relative intensity	<u>No time Rule needed</u> (Generally above 2s second dimension time)
Naphthalene and alkyl substituted Naphthalenes	1. Peaks with mass 128 above 15% relative intensity and mass 77 above 5% relative intensity 2. Also peaks with base peak or in higher relative intensity than 50% masses 141, 155, 169	<u>No time Rule needed</u> (Generally above 2s second dimension time)

All of the components identified by these rules were then compared to the results of the NIST library search (similarity search) as shown in Table 3.2. The unknowns listed in Table 3.2 are the components with a similarity match below 600. Mismatched components listed in Table 3.2 are those components that are typically misidentified by the NIST library or in some cases incorrectly identified compounds that fit the same rules applied to identify the group.

Table 3.2 Confirmation by NIST library of compounds find in each group [3]					
Compound class/group	Peaks identified by mass and retention time rules	NIST			
		Confirmed	Unknown library match below 600	Mismatch	Not identified by rule approach*
Alkanes	104	100	4	0	5
Alkenes and cycloalkanes	184	44 alkenes 90 cycloalkanes	31	19	10 14
<i>n</i> -Alkanoic acids	4	4	0	0	0
Alkyl-substituted benzenes	229	98	114	17	2
Polar benzenes with or without alkyl groups	41	11	28	2	1
Partly hydrated naphthalenes and alkenyl-substituted benzenes	145	59	61	25	2
Naphthalene and alkyl-substituted naphthalenes	70	36	20	14	5

* Compounds assigned to respective compound classes through NIST library matches but not identified through the rule approach.

An example of a mismatched component is E-2-octadecadecen-1-ol which is identified within the alkene and cycloalkane group, the mass spectra of this compound fits the group perfectly and it falls within the retention time window specified. Future work will hopefully eliminate these exceptions. The various groups/rules (see Table 3.1) are described in more detail below. Typical examples of each group are depicted in Figure 3.2 indicating the masses used for classification in Table 3.1.

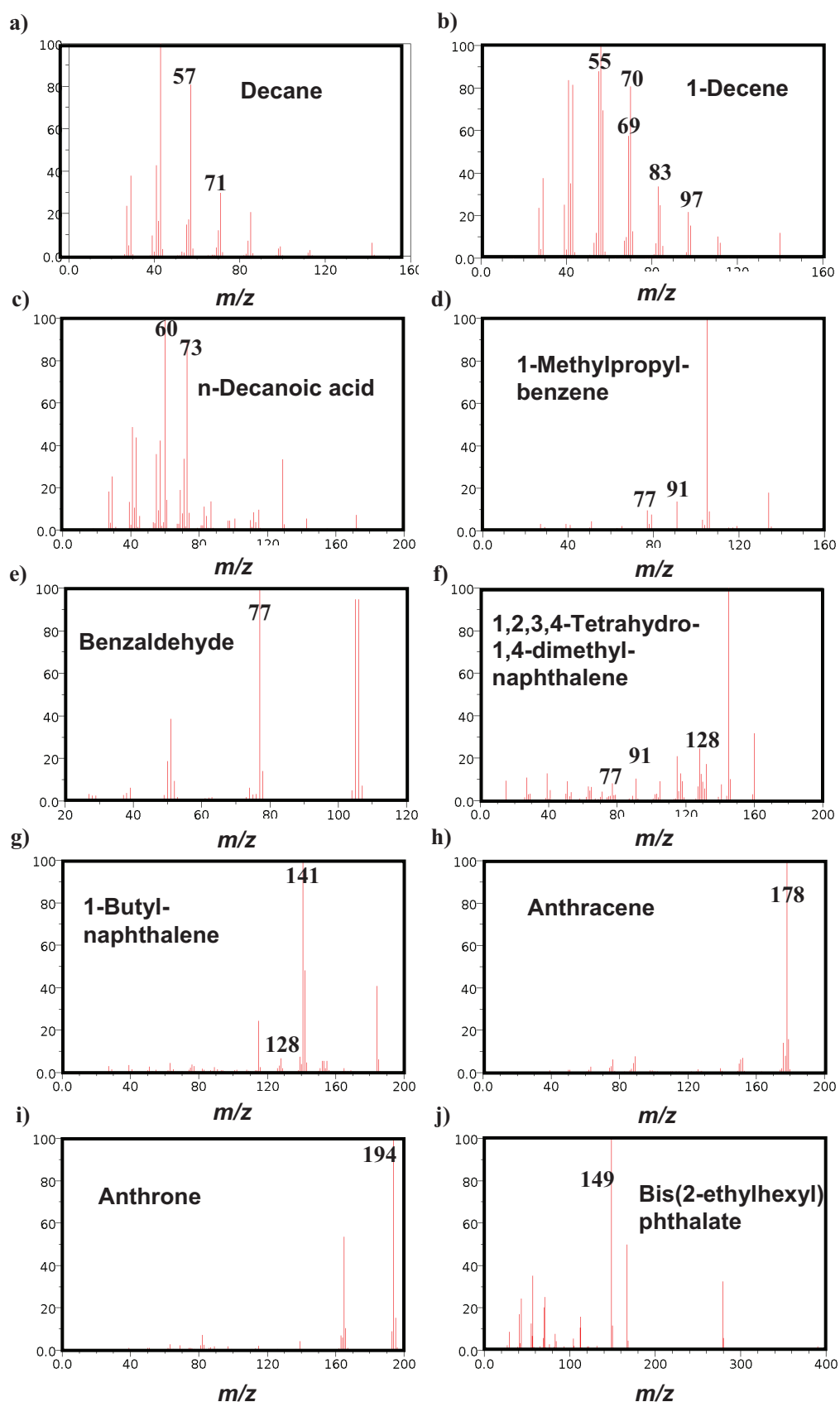


Figure 3.2 Mass spectra [NIST-data base] of typical examples from the different compound classes used in the classification rules (Table 3.1 and 3.4). The masses indicated correspond with those listed in Table 3.1 and 3.4 and are discussed in the following sections.

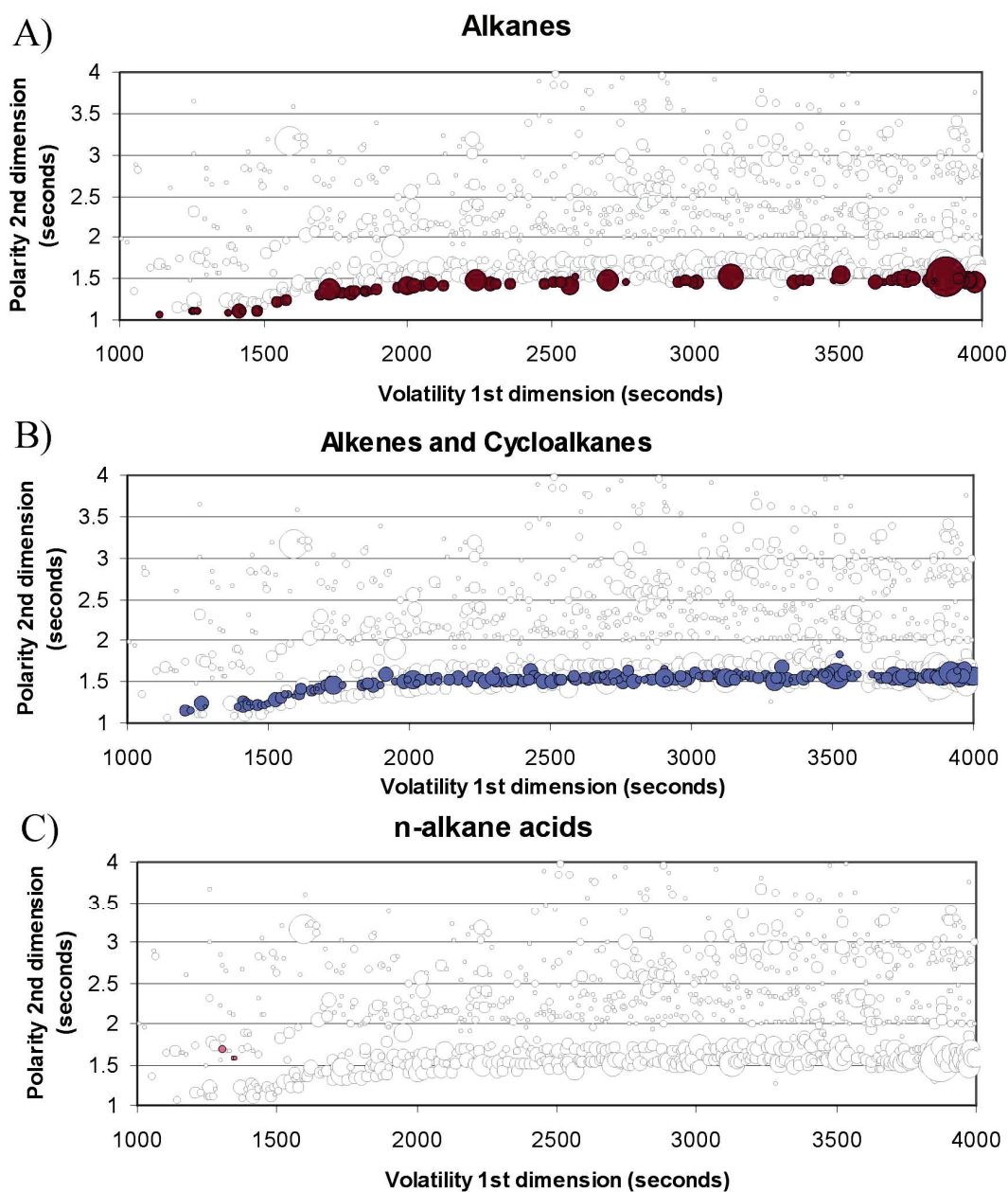


Figure 3.3 The three bubble-plots of the aliphatic groups assigned by the criteria in Table 3.1 with: (A) the alkanes; (B) the alkenes and cycloalkanes; and (C) the n-alkanoic acids.[3]

Aliphatic compounds (Figure 3.3)

Alkanes (Figure 3.3A). The fragmentation patterns in alkanes or saturated aliphatic hydrocarbons indicate a typical ion series of $C_nH_{2n+1}^+$ for straight chain and branched alkanes [8]. For the section of the two-dimensional plot examined, it was found that when searching for alkanes at higher than 50 m/z most alkanes have characteristic peaks at 57 and 71 m/z . The mass spectrum of decane in Figure 3.2a shows peak 57 m/z as base peak when only looking at masses above 50 and peak 71 m/z as second

highest peak. 98% of all alkanes identified by the NIST library fitted this fragmentation criterion. From the two-dimensional chromatogram, it was also easy to confirm the MS assignment of alkanes, due to the fact that they are almost unretained in the polar second column separation.

Alkenes and cycloalkanes (Figure 3.3B). For unsaturated aliphatic hydrocarbons and saturated alicyclic hydrocarbons, the identification process is more complex. The fragmentation in alkenes due to the double bond shows increasing patterns of the $C_nH_{2n-1}^+$ and $C_nH_{2n}^+$ ion series [8]. The cyclic alkanes also show a strong fragmentation pattern of $C_nH_{2n}^+$ [8]. Thus, differentiating between the two is a difficult task for search algorithms. In the approach used in this study, we focused again on masses higher than 50 m/z and were able to classify a large proportion of the combined two compound groups with the fragmentation criteria in Table 3.1. A typical example of a compound in this group is 1-decene and is shown in Figure 3.2b. Alkenes and cycloalkanes have similar retention indexes in both dimensions and it is thus still not possible to separate the two, but using a retentiontime window it is possible to exclude mismatched components. Mismatched components included compounds like cyclohexanone, which fitted the same mass rules but not the retention time rules. The retention window used also contained the unretained components at 1 s up to the more polar aromatics at 2 s second-dimension retention time.

n-Alkanoic acids (Figure 3.3C). The third group investigated in this preliminary study was the acids of the unbranched alkanes. The most prominent mass in the aliphatic acids is 60 m/z , due to the γ -hydrogen rearrangement peak [8], $CRR'C(OH)_2^+$. From the spectra obtained, it was further recognized that to identify this group more accurately the second most abundant mass 73 m/z was also needed. Figure 3.2c show the mass spectrum of n-decanoic acid which matches the above criteria. Four acids are listed in Table 3.2, where only two acids were present. This is due to an error in the analysis software where second-dimension peaks are combined to produce the total area of a compound. The reconstruction is complicated when there is tailing in the first dimension. The problems with reconstruction lie with the peak detection algorithms of the software, in that as the peak tails in the first dimension it is subjected to increasing higher temperatures in the second dimension. Thus, the tail of a first-dimension peak will elute earlier in subsequent second dimension chromatograms and the shift of peak apexes does not allow for accurate recombination of the peak. Peak tailing often occurs with acids on non-polar stationary phases.

Aromatic compounds (Figure 3.4)

The aromatic groups identified in this study can be divided into four sections. When containing electro-negative substituents the dominating series are [8] $C_nH_{0.5n}^+$ - $C_nH_{0.8n}^+$ ($n = 3-6$), and in the presence of electron-donating substituents or heterocyclic compounds the series $C_nH_{0.9n}^+$ - $C_nH_{1.2n}^+$ is more predominant [8]. Using these characteristic fragmentation patterns, four aromatic groups were assigned.

Alkyl-substituted benzenes (Figure 3.4A). The first of this group were the alkyl-substituted benzenes, this group is characterized by abundance of mass 91 m/z above 15% and also present in above 5% relative abundance mass 77 m/z . For example the mass spectrum of 1-methylpropyl benzene is shown in Figure 3.2d. The retention window of these compounds was limited to those eluting after 2 s in the second dimension. The group was expanded by adding some aromatic compounds with different retention and mass criteria, these were the alkylated benzenes with mass 77 m/z above 30% and retention time below 2 s second dimension and below 1700 s first dimension.

Polar benzene derivatives with or without alkyl-substituents (Figure 3.4B). This group containing the aromatic benzenes with polar-substituents was identified using mass 77 m/z in higher than 25% relative abundance using the mass spectrum of benzaldehyde as shown in Figure 3.2e. The retention window in this extraction becomes more critical, and only compounds in the more polar region (above 2 s) of the second dimension qualify.

Partly hydrated naphthalenes and alkenyl substituted benzenes (Figure 3.4C). This class contains benzene derivatives with alkenyl-substituents as well as partly hydrated naphthalene derivatives (one benzene ring remaining). The class is characterized by the masses 77 (above 5%), 91 (above 15%) and 128 m/z (above 10%) in relative abundances. For example the mass spectrum of 1,2,3,4-tetrahydro-1,4-dimethylnaphthalene is shown in Figure 3.2f. The compounds of this group elute like the other aromatic groups after 2 s on the second dimension.

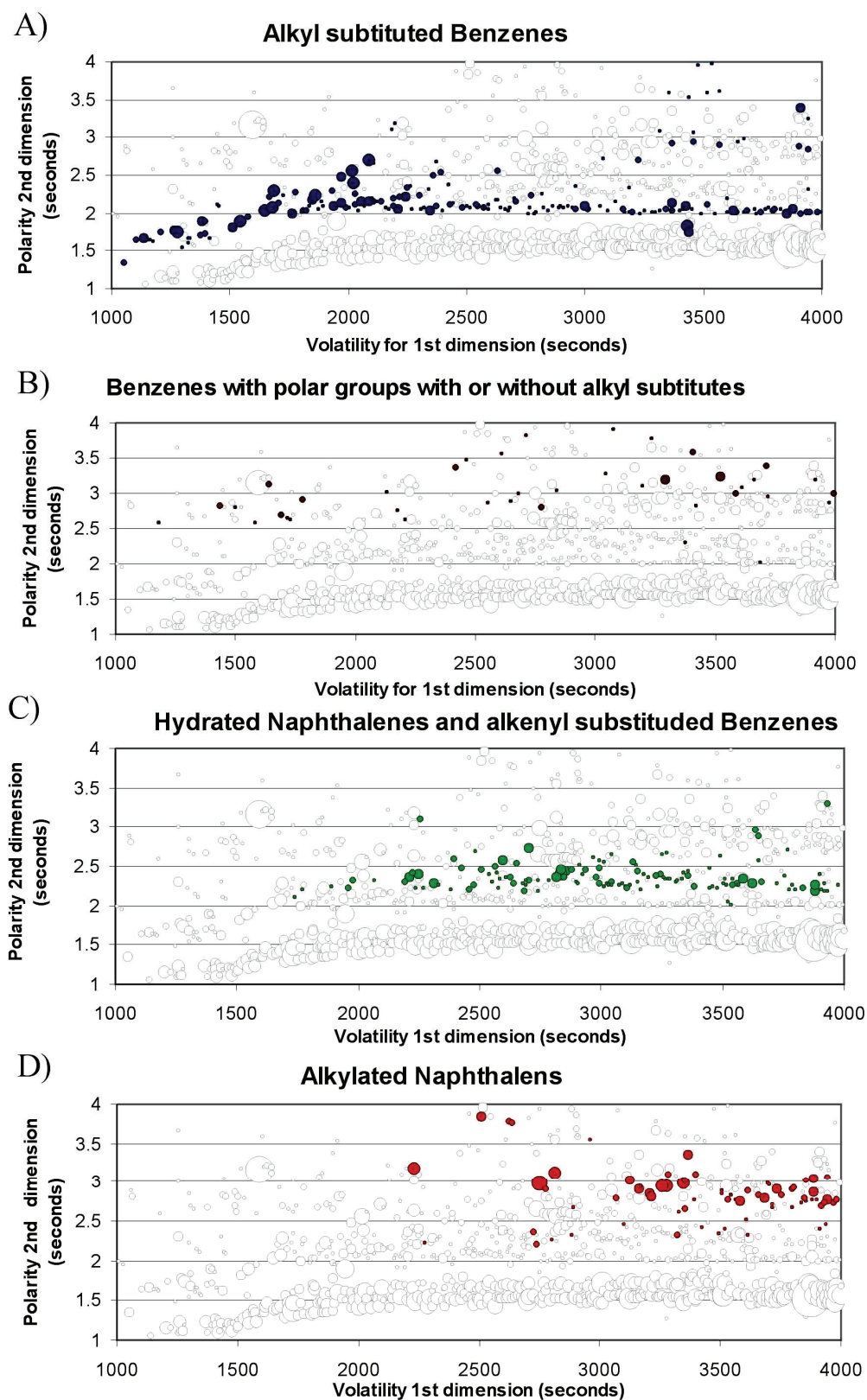


Figure 3.3 The four bubble-plots created from the criteria in Table 3.1 for the aromatic groups: (A) the benzenes with alkyl-substitutions; (B) the polar benzene derivatives with or without alkyl-substitutions; (C) the partly hydrated naphthalenes with one benzene ring still intact and the alkenyl-substituted benzenes; and with (D) the alkylated naphthalenes [3]

Naphthalene and alkyl-substituted naphthalenes (Figure 3.3D). Relative intense peaks at mass 128 m/z (above 15%) characterize the naphthalene derivatives. The alkylated naphthalenes often contain base peaks or relatively high abundances (above 50%) at masses 141, 155 and 169 m/z , etc. The mass 91 m/z , which is characteristic for alkylated benzene derivatives, is missing. For example the mass spectrum of 1-butyl-naphthalene is shown in Figure 3.2g. The alkylated naphthalenes elute, like the other aromatic groups, after 2 s on the second dimension.

From these group assignments, the obtained bubble-plot from the chromatographic peak information (Figures. 3.1 and 3.5A) could now be more easily interpreted by coloring the identified peak groups (Figure 3.5B). This color coded bubble plot can be used in a visual recognition of pattern changes at a glance. For statistical evaluations, the remaining ungrouped compounds (about 35% of the total) could then be further divided into different groups, depending on their retention time in the two dimensions as measures for their volatility and polarity. In Figure 3.5C, a potential differentiation scheme for the ungrouped compounds is given. Part 1 of these groups would then be the polar more volatile components, part 2 the non-polar more volatile components, part 3 the polar less volatile components, and part 4 the non-polar less volatile components.

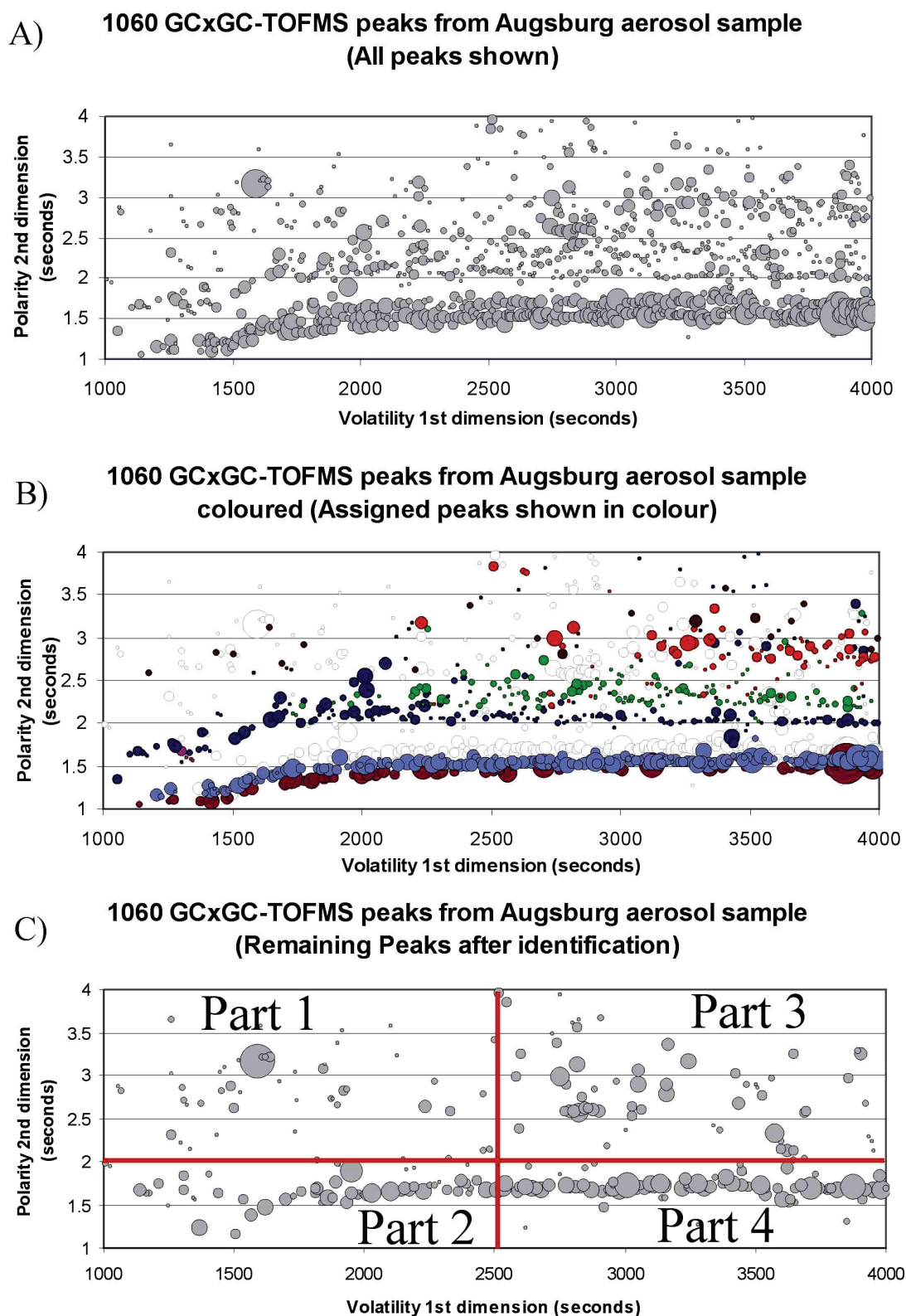


Figure 3.5 (A) shows the bubble-plot of the entire peak apices used in this preliminary study for grouping; (B) indicates the different groups identified on (A); the final plot (C) shows the remaining peak apices not identified in the search criteria, and indicates the four possible groups in which these apices could be divided for identification.[3]

With the developed search parameters, it is possible to group peaks in the 2D chromatogram into distinct chemical classes using TOF mass spectrometric information. These search routines, although in a preliminary development stage, already show significant improvements on previously used methods in the classification of compounds. More than 60% (by peak area) and 65% (by number compounds “697 compounds out of the 1060 present”) of the organic inventory of the aerosol sample in the investigated region of the chromatogram could be effectively assigned to groups allowing a straight forward characterization of the constituents of ambient particulate matter (Figure. 3.6) or other complex samples.

Figure 3.6 shows a pie-chart diagram of the chemical class groups identified in the aerosol sample by applying the rules given in Table 3.1. It is of note that this initial analysis was not focused on quantitative analysis, but rather on finding possible solutions for future applications in grouping different components. The area representation in Figure 3.6 should therefore be viewed in this perspective. With respect to concept of epidemiological evaluation of the health effects of the ambient particulate matter, the assigned chemical-class groups are particularly helpful. Furthermore, the groups could possibly aid the development of statistical models for the chemical variability in aerosols. Note that it is likely that within the ensemble of the unidentified compounds of a chemical-class group, the majority will also belong to the same chemical class.

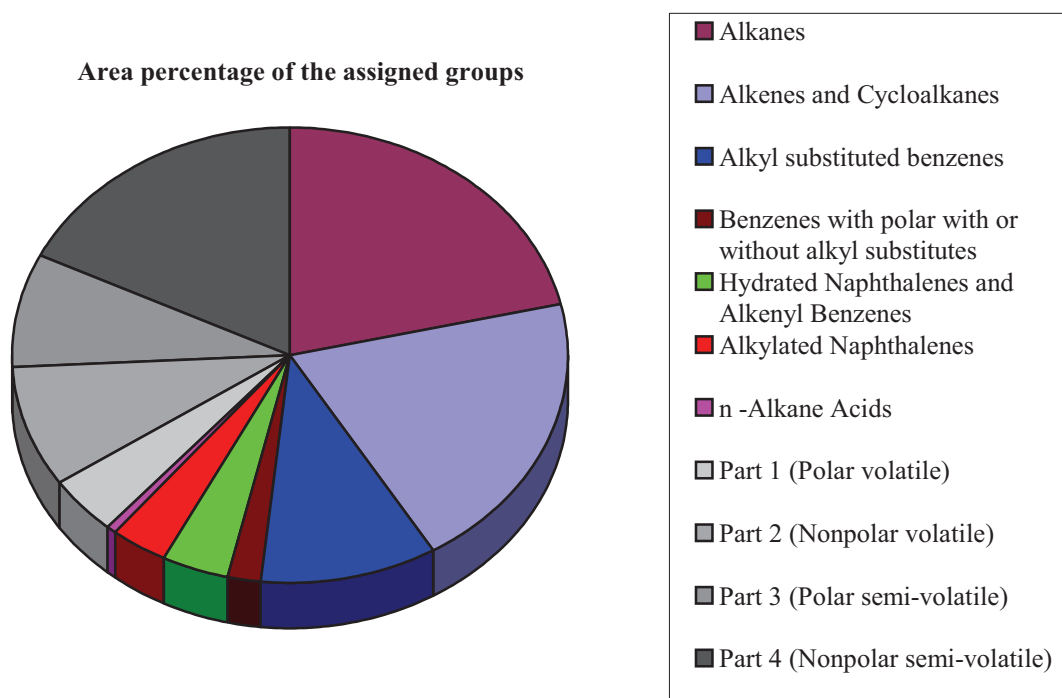


Figure 3.6 Pie-graph representation of the identified groups. The different groups are evaluated according to the area of the combined peak apices in each group.[3]

The chromatographic region (relatively low boiling C8-C16) selected in the aerosol PM sample is characteristic of fossil fuel sources. This is also demonstrated through the type of compounds identified in this range, homologue rows of saturated and non-saturated hydrocarbons and one-, two- and three-ring aromatic species. The analysis of a diesel petroleum sample should thus reveal similar groups and could therefore be directly be analyzed using the group classification rules. Figure 3.7 shows the analysis of a typical diesel sample analyzed through GC x GC-TOFMS. The deconvoluted peaks were thus similarly represented in a bubble plot as shown in Figure 3.8.

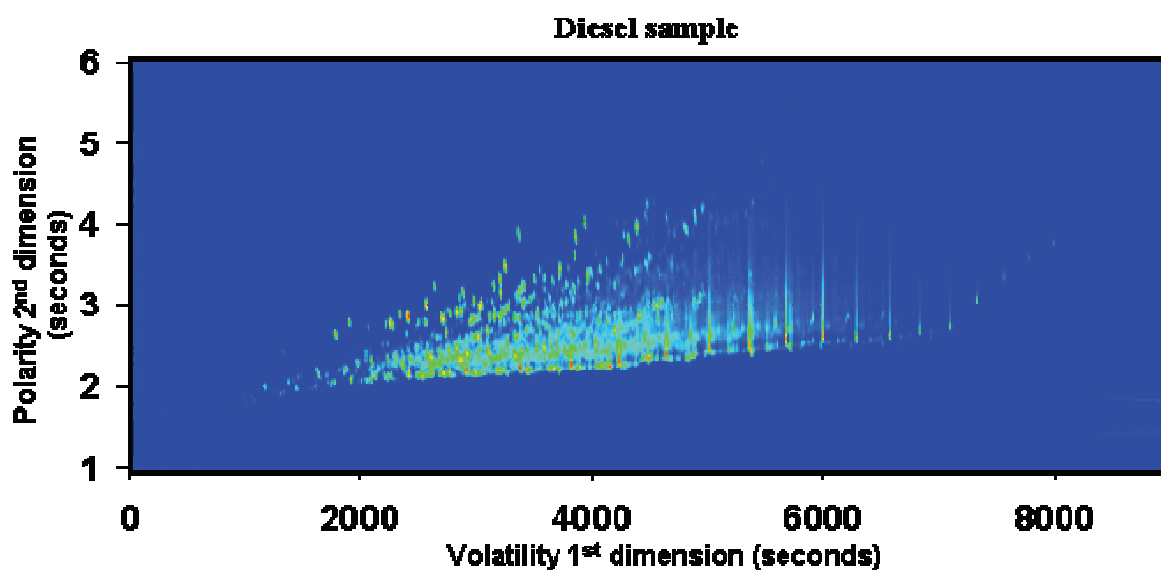


Figure 3.7 Two dimensional contour plot of a diesel petroleum sample

The majority of the compounds present in the diesel sample fit to the classification rules proposed (Figure 3.8 A). If all classified peaks are removed only a small number (less than 20% by area) of bubbles (compound peaks) remain (Figure 3.8 C). The unclassified peaks in the diesel sample are typically unsaturated compounds like dienes and cyclic-alkanes, for which no rules have been implemented at this stage. A total amount of 1984 compounds were detected and of these 1284 (65%) compounds were classified into the proposed groups (ion abundance rules, Table 3.1).

The alkanes, similar to the aerosol samples provides the best performance when compared to NIST results. 213 compounds were identified through the proposed rules of which 204 can be confirmed by NIST, 8 incorrect and 1 unknown (similarity below 500 in NIST library). The alkenes and cyclic alkanes resulted in 271 peaks fitting into the selection rules of which 197 were NIST confirmed and 74 incorrectly assigned. The incorrectly assigned peaks included bicyclic alkanes, dienes, cyclic alkenes and even alkynes. At this stage it was not possible to create rules for these groups to eliminate them.

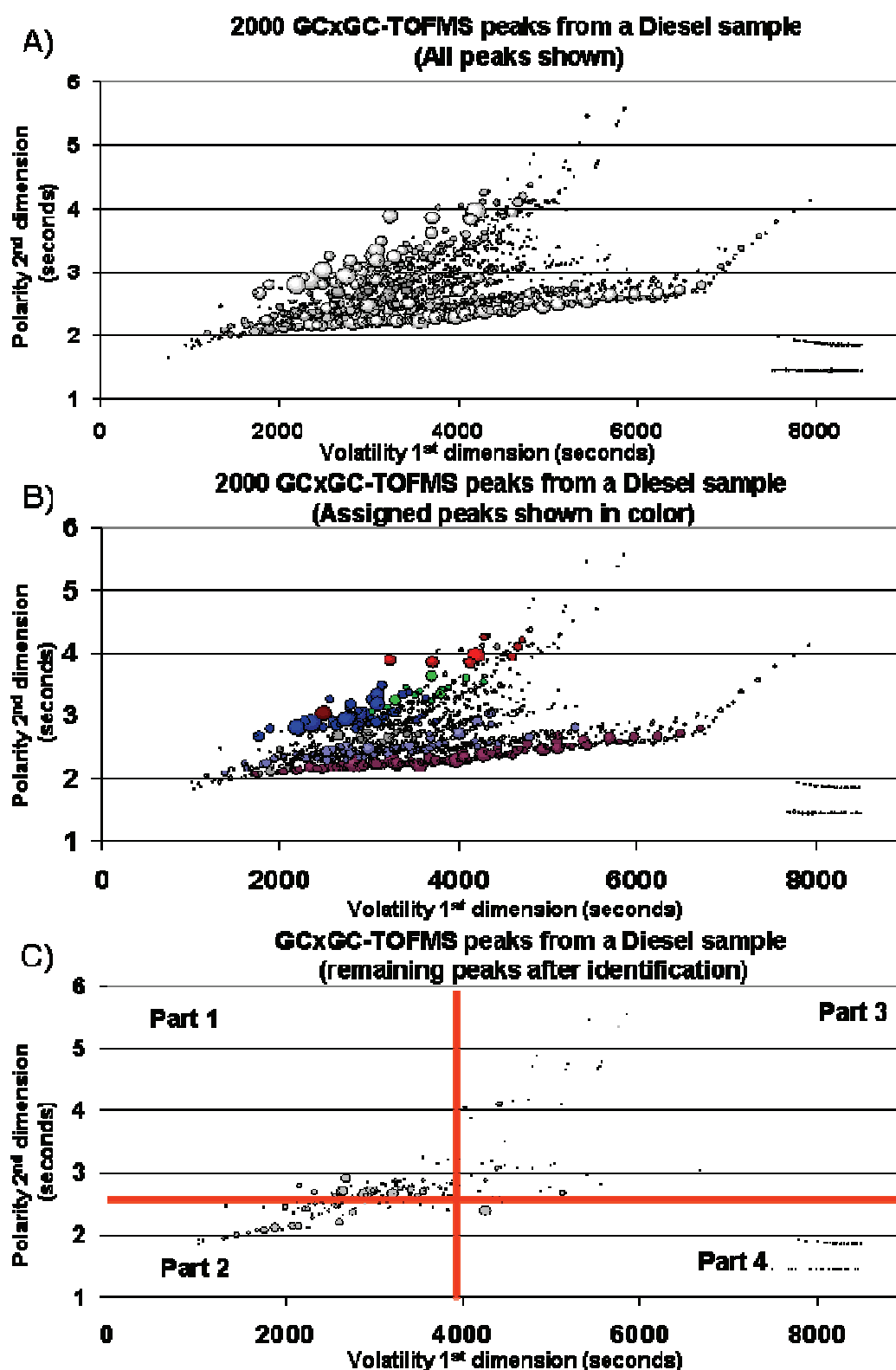


Figure 3.8 Bubble plot representation of a diesel petroleum sample. A) All peaks identified are shown as bubbles, where the size of the bubble the area of the chromatographic peak represents. B) The peaks identified through the rules set out in Table 3.1 are depicted in color. C) The remaining peaks after the identified peaks are removed, the plot is divided in four sections according to volatility and polarity.

Alkyl substituted benzenes showed 290 classified compounds of which 134 were correct (NIST) 145 incorrect (NIST) and 11 unknowns (NIST similarity match below 500).

Benzenes with polar, with or without alkyl substitutions had only 7 classified peaks of which 3 were confirmed through NIST and 4 unknowns (NIST similarity match below 500).

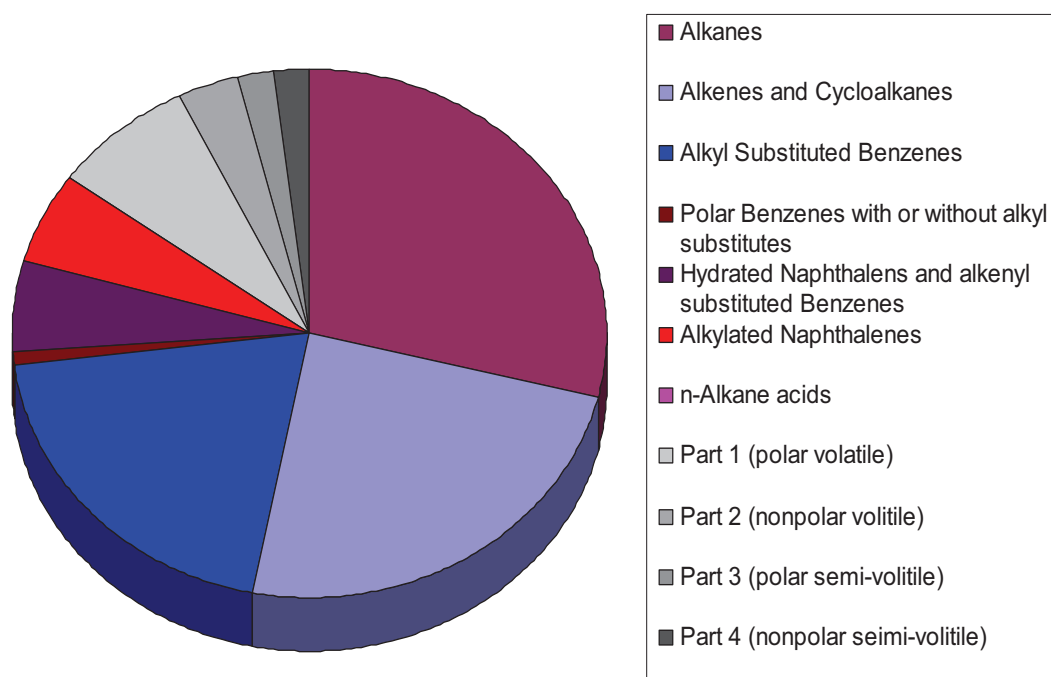


Figure 3.9 Pie-graph representation of the identified peak in a diesel petroleum sample.

140 peaks were classified as partly hydrated naphthalenes or alkanyl substituted benzenes, with 59 correct (NIST), 76 incorrect (NIST) and 5 unknowns (NIST similarity match below 500).

139 peaks were classified as naphthalene and alkyl substituted naphthalenes of which 73 were correct (NIST), 51 were incorrect (NIST) and 15 were unknown (NIST similarity match below 500).

The group classification rules proposed here can provide a fast analytical tool whereby compounds in highly complex samples can be grouped in compound classes. The different compound classes introduced so far are suited for the analysis of diesel petroleum samples, but also provide useful results for ambient aerosol particular matter. The rules provided here could also be adapted to other applications and it is also possible to introduce new rules.

3.2.1 Rule based approach for chemical classification of PM 2.5 Aerosols [3]

Several epidemiological studies have demonstrated the relevance of ambient particles in health effects. The results of these studies together with animal toxicology and in vitro experimental studies support the hypothesis that both physical (particle size, shape, surface) and chemical (dissolved and adsorbed chemicals, surface catalytic reactions) properties of the particles are involved in toxic, genotoxic and carcinogenic mechanisms of inhaled particulates.

It was recently recognized that inhaled ultra fine particles ($D_p < 100$ nm) are more toxic than PM10 particles [9]. Their relatively large surface area and the ability to be absorbed into tissues might be important factors in cardiopulmonary toxicity. However, the number of ultra fine particles in the air is often poorly correlated with PM2.5 mass and even less with PM10 mass. Thus, ultra fine particles are unlikely to explain much of the association between particulate mass and health conditions.

Also the impact of surface absorbed compounds on health outcomes is not well understood yet. Specific compounds related to traffic exhaust like from diesel vehicles [10] or even diesel locomotives [11] are possibly important.

Epidemiological investigations of the influence of individual, particle bound chemical pollutants were done only for few inorganic species [12]. However, little is known on the influence of the organic chemicals present in ambient particulate matter (PM) on the health outcomes. The influence of organic substances was evaluated by measurement of the concentration of elemental and organic carbon (EC/OC) [13]. But so far, the association of individual specific organic pollutants or groups of pollutants with health effects, occurring in the fine dust, was not examined in epidemiological studies.

For a time-series study, on the influence of organic aerosol compounds, it is necessary to have data of several compounds or groups of compounds at least with a daily resolution. Because most of the organic compounds occur in low concentrations in ambient aerosol, time-consuming analytical methods are required for their analysis. Several studies address the organic composition of ambient PM, using gas chromatography-mass spectrometry (GC-MS) [14, 15] for separation and identification of semi volatile organic chemicals (SVOC).

Recently, direct thermal desorption (DTD) was employed for extracting semi-volatile species from ambient particulate matter [16, 17]. During 2003 a project for sampling and analysis of semi-volatile organic compounds associated with ambient PM2.5 on a daily basis by direct thermal desorption – gas chromatography – time-of-flight mass spectrometry (DTD-GC-TOFMS) was started by Dr. J. Schnelle-Kreis¹. The data of this project together with data of particle mass (PM2.5) and number-concentrations will be analyzed in an epidemiological study². In the epidemiological study relative abundance data of compound classes (summarized concentrations of e.g. n-alkanes,

¹ Cooperation with BIfA - Bavarian Institute of Applied Environmental Research and Technology.

² Cooperation with Institute of Epidemiology, GSF-Research Centre, A. Peters and H.E. Wichman.

fatty acids, PAH, PAH-quinones etc.) will be statistically correlated with health data of the population of Augsburg. The health data (myocardial infarction and sudden cardiac deaths, and survival of myocardial infarction survivors) are acquired in the framework of the KORA project (Co-operative Health Research in the Region of Augsburg [3]). One drawback of the approach is, however, that only a small fraction of the SVOC compounds present in ambient particulate matter samples can be identified and assigned to compound classes. This is due to the fact that one-dimensional (1D) gas chromatography cannot provide sufficient chromatographic resolution for the separation of the large numbers of organic compounds present in ambient PM. Typical gas chromatograms of SVOC from PM exhibit broad unresolved bands (unresolved carbonaceous matter (UCM)), including the majority of the SVOC compounds. For better understanding of the nature of the organic chemical inventory hidden in the UCM-bands, it is required to apply novel analytical techniques with considerably increased resolving power.

Comprehensive two-dimensional (2D) gas chromatography (GC x GC) represents a new approach to enhance the GC resolution [18, 19].

3.2.2 Experimental

Sampling



Figure 3.10 Aerosol monitoring station in Augsburg, Germany

Within the project particles (PM 2.5) are sampled on a daily time basis at a central monitoring station in Augsburg, Germany, on quartz fiber filters (Munktell T293, Grycksbo, SE). Daily sampling started in spring 2002 and is still ongoing. Ambient urban air particulate matter is sampled with a PM2.5 sequential sampler (Partisol-Plus 2025, Rupprecht & Pataschnik Albany, NY, USA) at a flow rate of 1 m³/h. Separators are used to isolate the cassettes with filters (eight in each cassette) in the filter magazine. Each filter magazine contains seven filters for daily sampling and one filter as field blank. The filter cassettes are exchanged once a week. In the laboratory, the filters are cut into 13 pieces. Each piece represents a PM 2.5 aliquot of 1 m³ sampled air. These pieces are stored deep-frozen at -18 °C until analysis.

Direct thermal desorption – gas chromatography – time-of-flight mass spectrometry (DTD–GC–TOFMS)

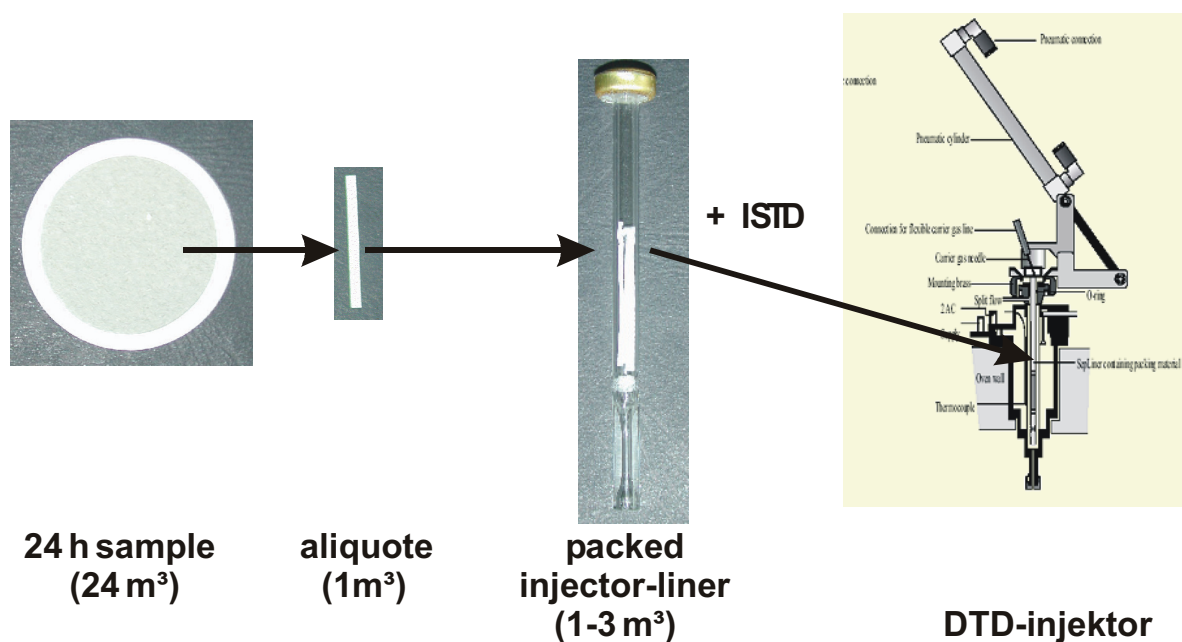


Figure 3.11 Aerosol PM 2.5 sample collected on filter, cut and inserted into the Direct Thermal Desorption injector. [20]

The samples were analyzed for SVOC by direct thermal desorption – gas chromatography – time-of-flight mass spectrometry using a novel DTD interface. The methodology for aerosol monitoring was developed by Schnelle-Kreis *et al* [20], in detail, the liner of the GC injection interface (DTD-liner) was used as sample container for one to three filter pieces. Isotope labeled reference compounds were added for quantification. After automated insertion of the DTD-liner and closing of the cold injector port the liner was purged with helium for 2 min. After this, the injector port was heated to 350 °C and the analytes were thermally desorbed from the DTD-liner directly onto the capillary GC column. During desorption time, the SVOC were focused on a retention gap at an oven temperature of 50 °C. The analytical DTD–GC–TOFMS parameters (instrumentation: Injection port Optic III, ATAS-GL, Veldhoven, NL; GC: Agilent 6890, USA; TOFMS: Pegasus III, LECO Ltd., St. Joseph, MI, USA) were as follows:

Retention gap: deactivated fused silica, 2 m, 0.22 mm i.d. (SGE, Ringwood, AUS)

Column: BPX5, 50 m, 0.22 mm i.d., 0.25 μm d_f (SGE), flow: 1.0 ml/min helium, Thermal desorption: filter purge at 50 °C, split 50 ml/min (2 min hold),

Temperature ramp to 350 °C (15 min hold) at 60 °C/min—split 5 ml/min,

Oven parameters: 50 °C (22 min hold) to 150 °C at 100 °C/min; to 330 °C (30 min hold) at 20 °C/min.

The TOFMS was operated with a data acquisition frequency of 20 Hz. For each analysis, three filter pieces are placed into a DTD-liner. For statistical evaluation, the concentrations of single compounds (e.g. source specific tracer substances) were summarized concentrations of compound groups (e.g. *n*-alkanes, fatty acids, PAH, PAH-quinones) and concentration of the unresolved carbonaceous matter (integral over the UCM-band) were adopted.

Two-dimensional comprehensive gas chromatography – flame ionization detection (GC x GC-FID)

A comprehensive two-dimensional gas chromatography– time-of-flight mass spectrometer was used in this study (instrumentation: Injection port Optic III, ATAS-GL, Veldhoven, NL; GC: Agilent 6890, USA; TOFMS: Pegasus III, LECO Ltd., St. Joseph, MI, USA, GC x GC system: Pegasus 4D option, LECO Ltd., MI, USA). The instrument was retrofitted with a FID system with a detection frequency of 200 Hz. Column parameters of the sets used in this study was a 30 m x 0.25 mm i.d. x 0.25 μm d_f BPX5 from SGE as first dimension column and a 1.5 m x 0.10 mm i.d. x 0.10 μm d_f SGWax from SGE as second dimension column. Samples collected on the quartz fiber filters were extracted with first hexane and then dichloromethane, the extraction aliquots were then combined and evaporated to 100 μl . The hexane-dichloromethane extracts were then injected into the GC x GC under large volume conditions (3 μl at 50 °C with a split flow of 100:1, then heated up to 300 °C at 10 °C/s with a split flow of 25:1). Hydrogen was used as carrier gas at 1.5 ml/min column flow rate. The first dimension oven was held at 60 °C for 10 min then heated to 300 °C at 1.5 °C/min while the second oven was kept at 5 °C above first oven temperature. The modulator containing the heating jets was heated to 100 °C above oven temperatures and the pulse duration of the heated pulses was set to 300 ms. A modulation period of 8 s was used.

Direct thermal desorption – two-dimensional comprehensive gas chromatography – time-of-flight mass spectrometry (DTD-GC x GC-TOFMS)

The same GC x GC setup was used as with the GC x GC-FID, but run in TOFMS mode. Two cut filter stripes representing 1 m^3 each was placed directly into the inlet liner and thermal desorbed similar to the *DTD-GC-TOFMS* approach. Additional instrumentation parameters were as follows: 1.5 ml/min column flow rate, helium carrier gas, and data acquisition rate of 100 Hz. The first dimension oven was held at 60 °C for 10 min then heated to 300 °C at 1.5 °C/min while the second oven was kept at 5 °C above first oven temperature. The modulator conditions were the same as in the GC x GC-FID approach but with a modulation period of 6 s.

3.2.3 Results and discussion

Direct thermal desorption – gas chromatography – time-of-flight mass spectrometry [3]

In the PM_{2.5} samples, among other compounds, *n*-alkanes, long chain carboxylic acids, long chain alkyl nitriles, esters, terpenes, steranes, hopanes, substituted aromatics, PAH, oxygenated-PAH (oxy-PAH), heterocyclic aromatic compounds have been identified and partly quantified. The question, to which degree the detected long chain alkyl nitriles are created from the analog acids in presence of an ammonium source (e.g. NH₄NO₃) or from the amides during the thermal desorption [21] or the use of it as tracers for biomass burning [22] has yet to be investigated in detail.

As shown in Figure 3.12A and B, the differences in the total ion current (TIC) chromatograms are substantial and mainly visible in the unresolved carbonaceous matter region. The relative changes over a 2-week period in May 2002 are depicted. A steady but relative small increase in UCM concentration from 14th to 17th is followed by a steep decrease to the 19th (Figure 3.12A). In Figure 3.12B, the strong changes in concentrations of the organic compounds on a daily basis within a 5-day period are highlighted. Whereas the maximum in UCM concentration in the whole period is at about 46–47 min in the chromatograms, on the middle day of this period, the 22nd, this maximum is shifted to 50–51 min. In addition, the concentration of several individual compounds is strongly increased on this particular day.

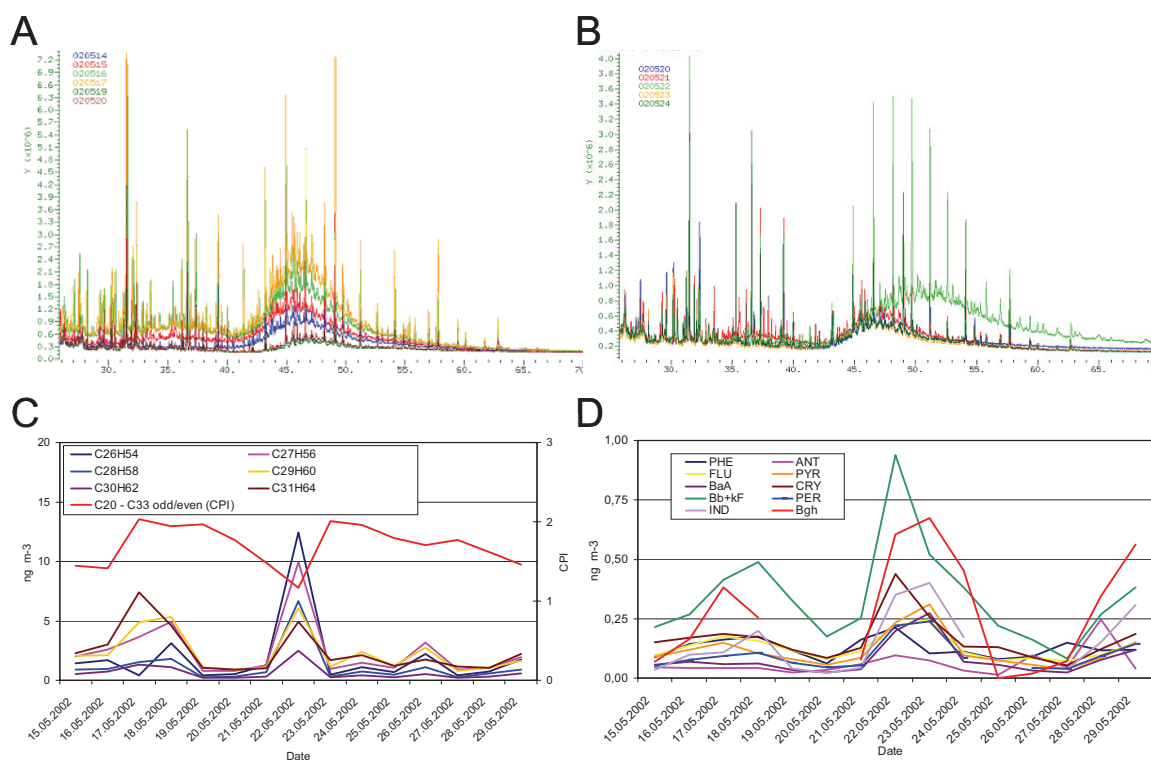


Figure 3.12 Day-to-day changes in the organic inventory of urban PM: (A) concentration increase and decrease in the period 14th to 20th May; (B) strong concentration increase on a single day within a 5-day period 20th to 24th May; (C) concentrations of some *n*-alkanes and carbon preference index (CPI) in the period 15th–29th May; (D) concentrations of some PAH (PHE: phenanthrene; ANT: anthracene; FLU: fluoranthene; PYR: pyrene; BaA: benzo[*a*]anthracene; CRY: chrysene; Bb+kF: sum of benzo[*b*]- and [*k*]fluoranthene; PER: perylene; IND: indeno[1,2,3-*cd*]pyrene; Bgh: benzo[*ghi*]perylene) in the period 15th–29th May. [3]

In Figure 3.12C and D, examples for day-to-day fluctuations of the concentrations of some *n*-alkanes (Figure 3.9C) and PAH (Figure 3.12D) in the same time period are shown. The carbon preference index indicates a slight increased contribution of anthropogenic emissions on the 22nd May only. Although the concentrations of all alkanes were increased on this particular day the increase of the concentrations of the odd-numbered alkanes was higher than of the even-numbered alkanes. Some PAH's (e.g. chrysene <CRY> and benzo[*b+k*]fluoranthene <Bb+kF>) show increased concentrations on the same day, whereas most of the other PAH's (e.g. benzo[*a*]anthracene <BaA>, pyrene <PYR>, indeno[1,2,3-*cd*]pyrene <IND>, benzo[*ghi*]perylene) show a maximum in concentration on two consecutive days. Long-term monitoring and data analysis will give information about the variability of the organic chemical inventory of urban ambient fine particles (PM 2.5). In this study about 250 individual compounds are identified. Most of them are quantified for the statistical evaluation. This is however only a very small fraction of the total number of SVOC associated with ambient PM. The majority of the organic compounds present

in ambient PM, primarily characterised by the UCM-band in the one-dimensional chromatograms are not identified yet.

In summary, Figure 3.12 clearly shows that the SVOC fraction in ambient particulate matter exhibit a rather drastic day-to-day variability. Note that the method was evaluated for reproducibility, which was calculated to be better than 10% for most of the target compounds. The large fluctuations of the SVOC inventory in the ambient aerosol implicate that a large day-by-day variability of the exposure of the Augsburg population to particle-bound SVOC is present. Valid data on the temporal variation of the relative abundances of the compound classes, the concentration of the unresolved carbonaceous matter and the concentrations of the molecular tracers are prerequisites for epidemiological studies on short-term effects of particle associated SVOC. Unfortunately, in this study quantified compounds represent only about 15% of the total SVOC. Therefore, it is likely, that compounds that are involved in the health effects are hidden in the UCM-bands. The determined large variability in the UCM-band therefore is only a poor surrogate for these compounds. The GC x GC-TOFMS can amplify our knowledge on the compounds and compound classes present in aerosol samples. But for use in epidemiological studies the enormous amount of single compound data generated by this technique has to be reduced to reasonable sets of combined data.

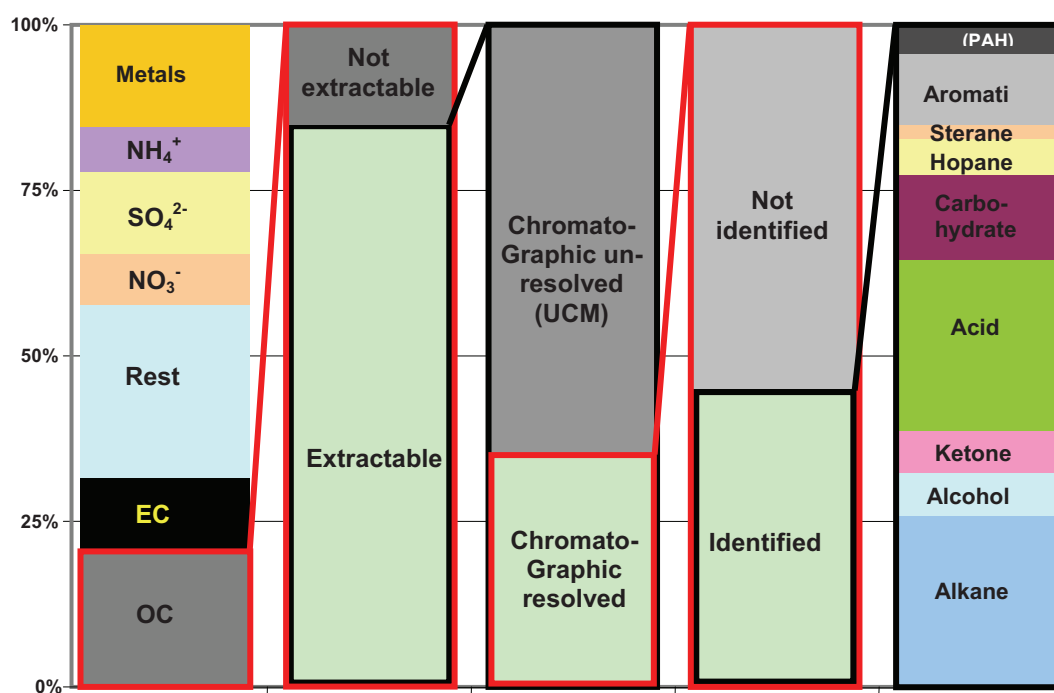


Figure 3.13 Representation of the content of ambient aerosol particulate matter. [23]

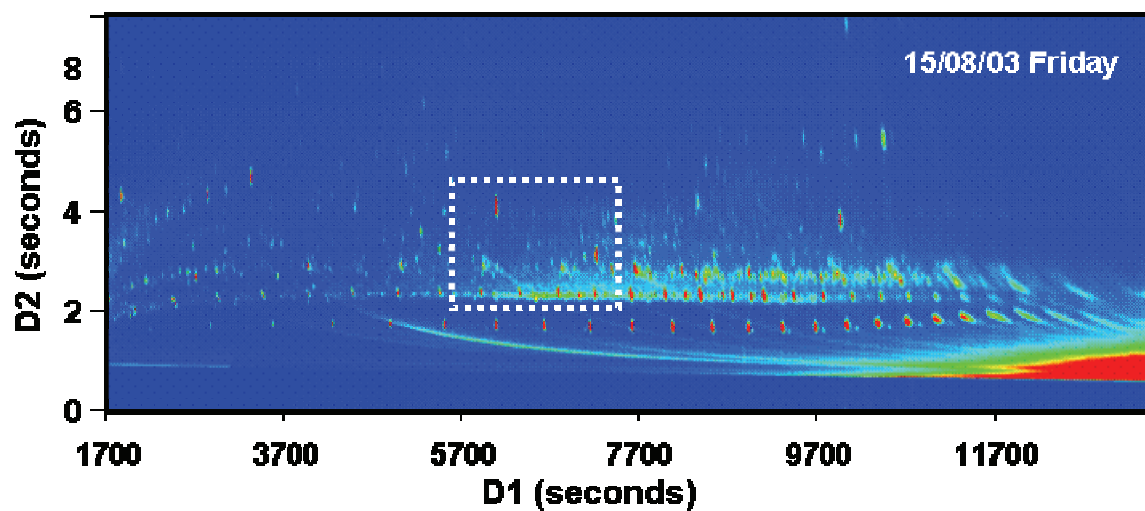
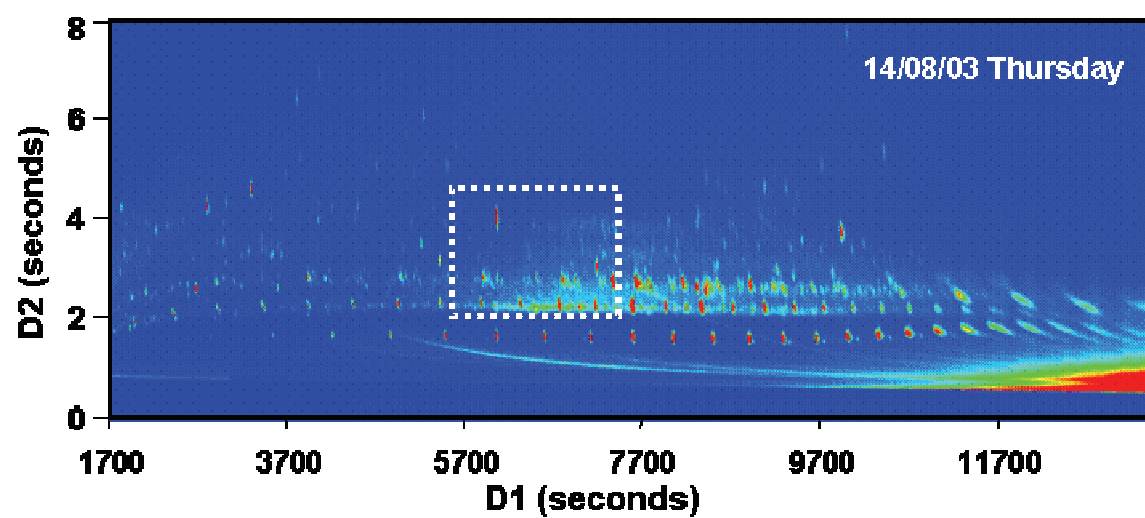
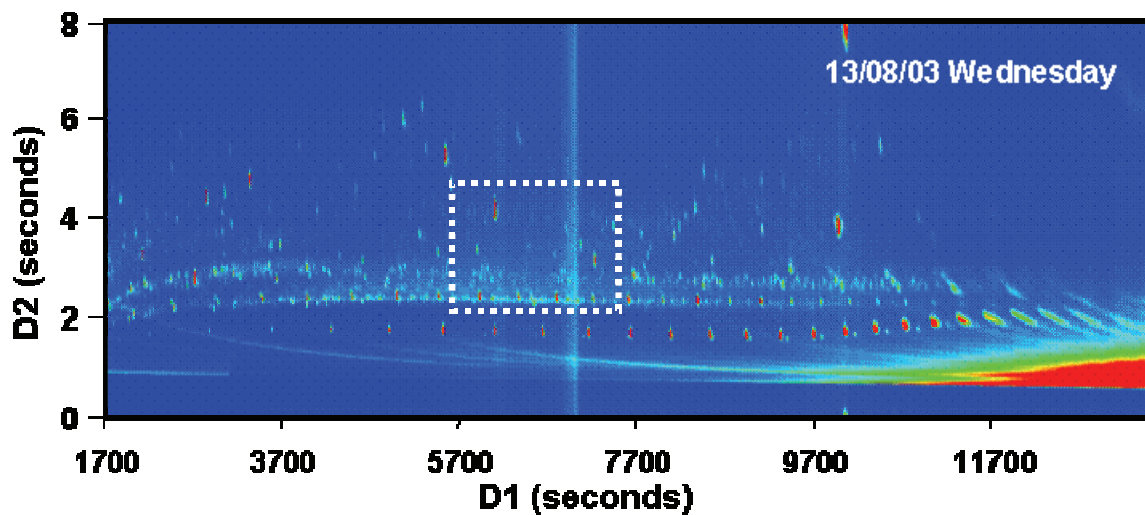
Two-dimensional comprehensive gas chromatography – flame ionization detection (GC x GC–FID)

GC x GC provides a high resolution method by which samples can be screened quickly and effectively to identify differences in concentration and composition. Due to the high resolving power of GC x GC compounds are typically well separated from each other and visual inspection of the two-dimensional chromatograms is possible. For demonstration six PM_{2.5} ambient aerosol samples collected on a daily basis over a week period is presented in Figure 3.14. The chromatograms were normalized according to the total FID signal and subsequently plotted so that the relative concentration of the peaks present in the samples can be compared. Through direct comparison it is possible to notice that there seem to be general differences in compound concentration levels. The Wednesday sample seems to have a much higher concentration of volatile compounds (compounds eluting before 5700 s first dimension time, n-C16) while the Monday sample shows a huge increase of compounds of middle volatility range (5700 s to 9700 s first dimension time, between n-C16 and n-C26). This method of attempting to compare samples looking at in its entirety is too complex to draw any meaningful results. It is therefore necessary to look at smaller sections where a manageable amount of peaks can be compared at a time.

In Figure 3.15 some smaller extracts are shown. From the extracted contour plots it is now possible to see relative concentration differences by looking at the color intensities and it is possible to see compositional differences quite early. In the Wednesday sample for example compound D is absent while it is present in the Thursday sample.

Although concentration differences can be seen through the color scale used, plotting the chromatograms in a three-dimensional representation make these observations easier. In figure 3.16 the concentration differences in the ratio between compounds C and D in the Thursday sample and the Saturday sample are quite obvious.

It should be noted that the concentration differences in this direct comparison were done on a relative basis. No calibration was done for the concentrations and no internal standards were used. It is also of note that due to the dependency of sampling conditions (temperatures and humidity) only compounds with a boiling point above that of hexadecane can be used for any reasonable semi-quantitative work.



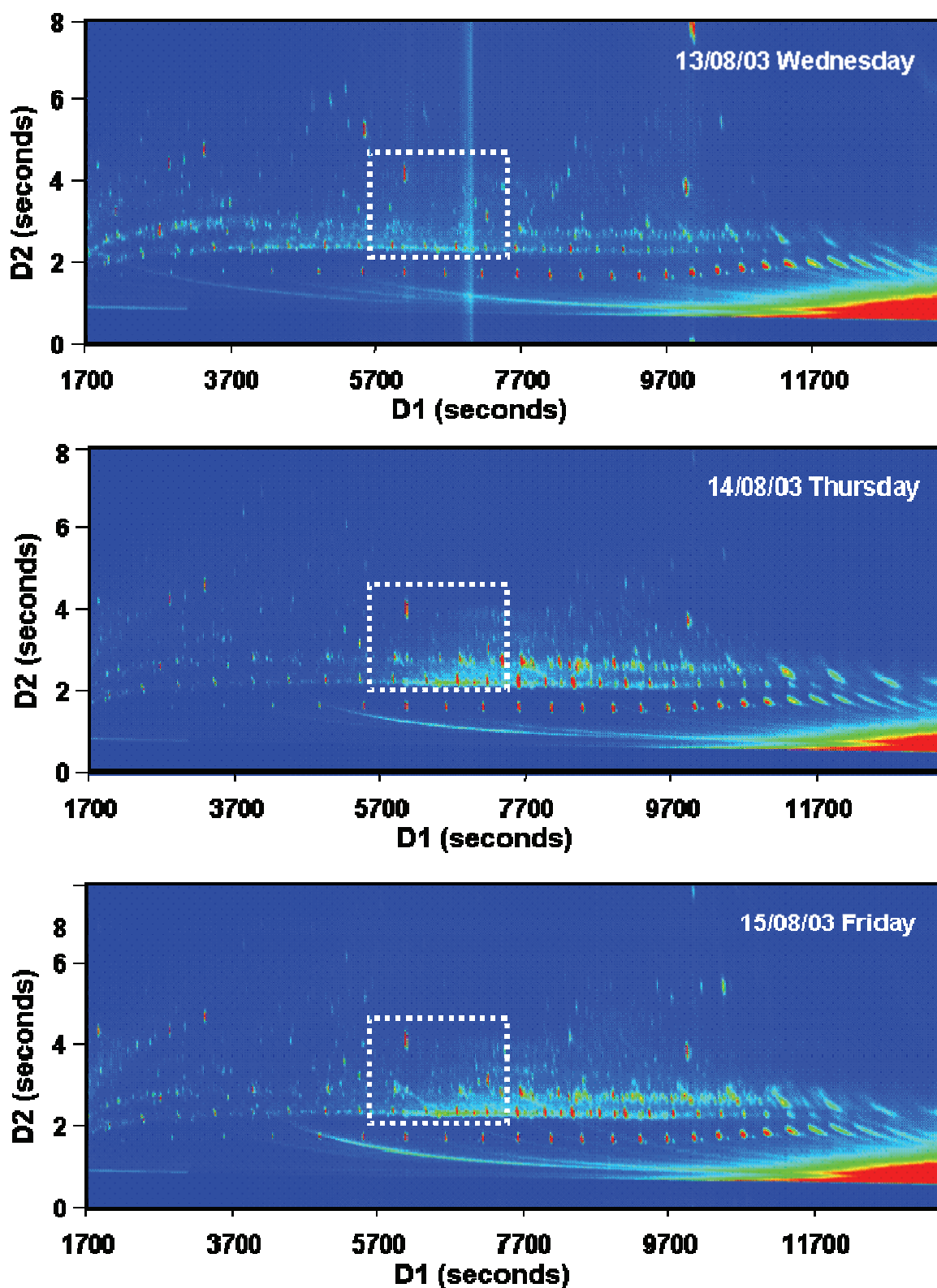


Figure 3.14 GC x GC-FID contour plots of aerosol PM_{2.5} collected on a daily basis over a week period

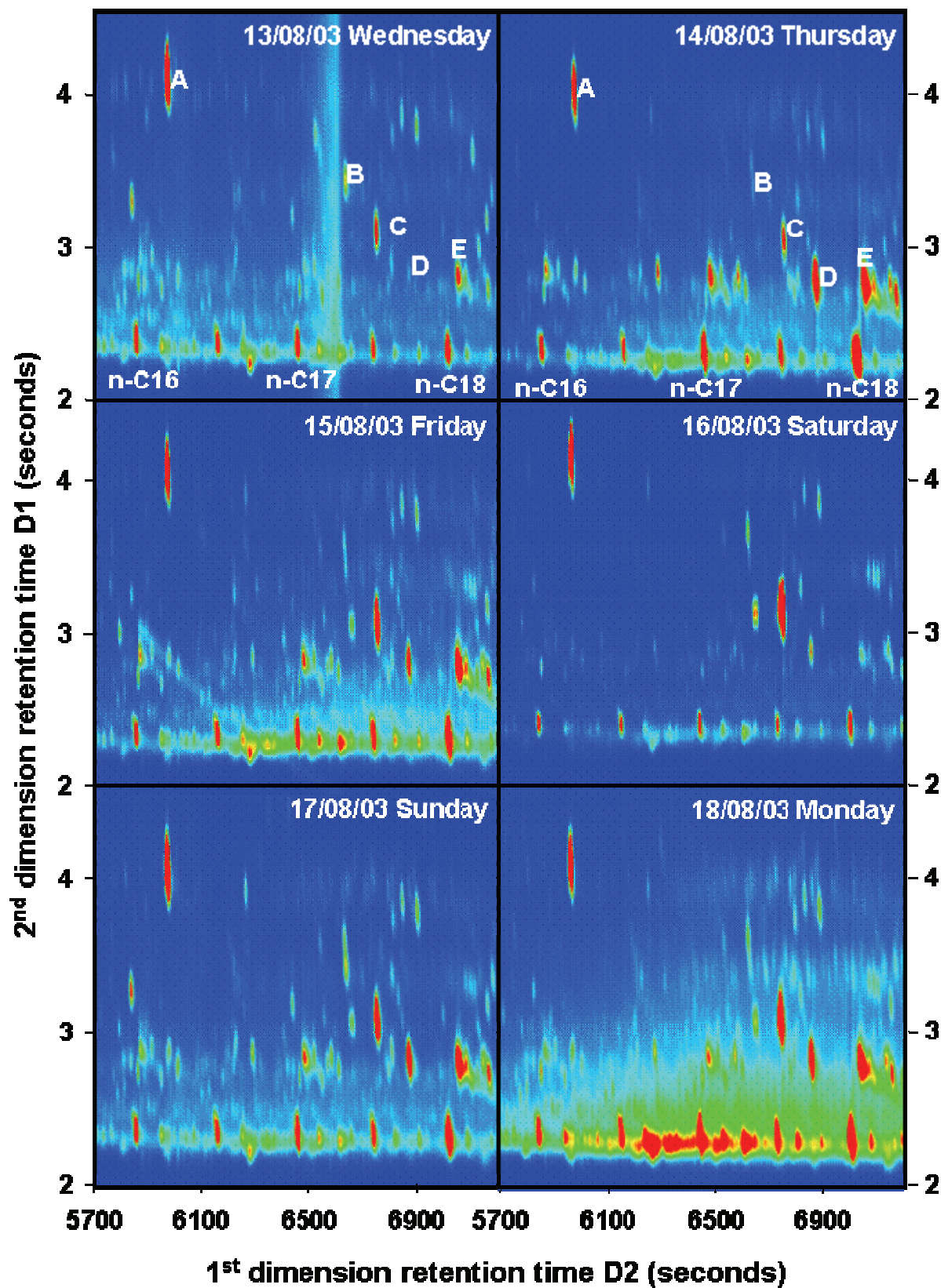


Figure 3.15 Extracted sections from Figure 3.10, indicating compositional differences in the samples

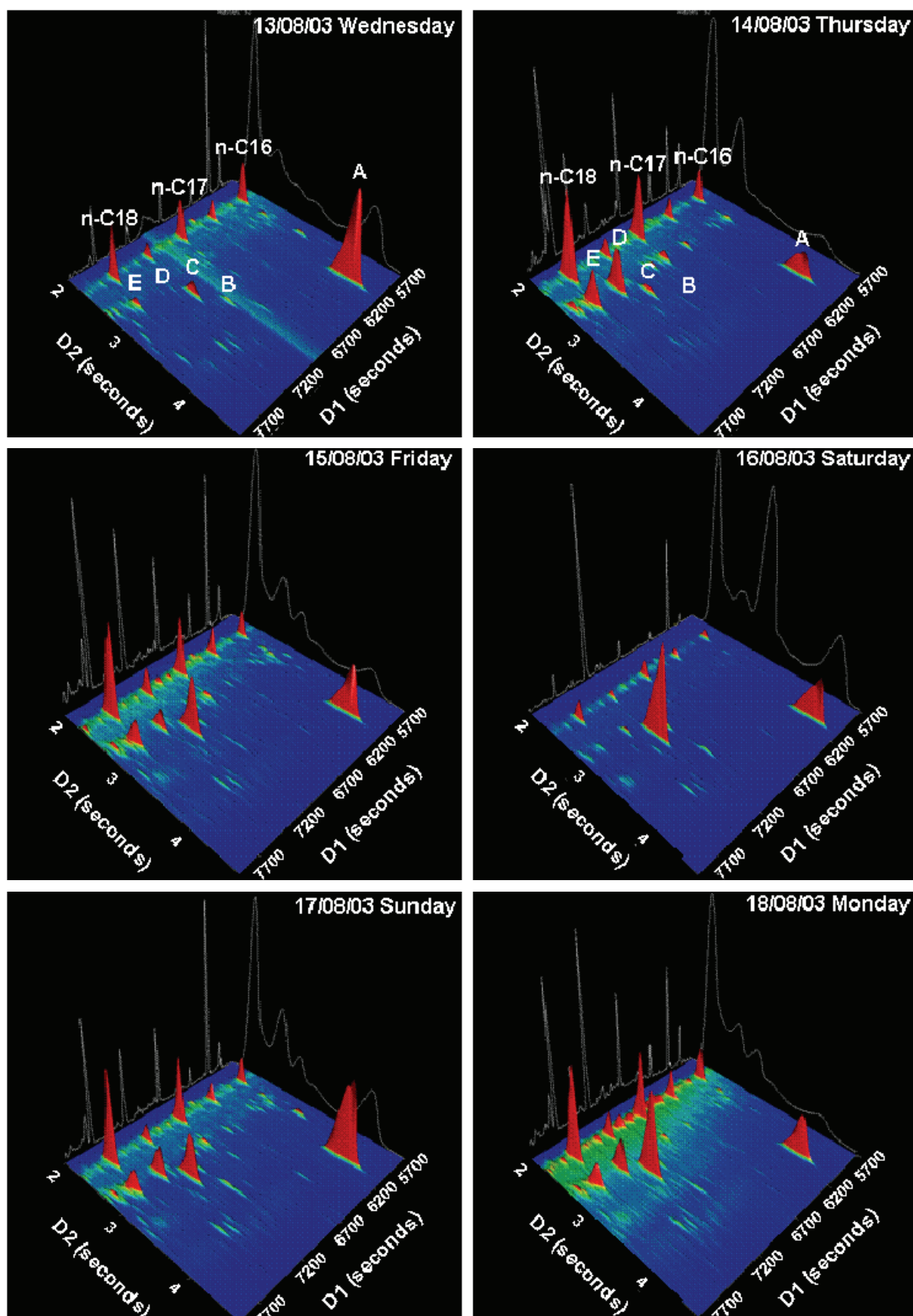


Figure 3.16 3D plots of the extracted section depicted in Figure 3.11, for the evaluation of concentration differences.

Direct thermal desorption – two-dimensional comprehensive gas chromatography – time-of-flight mass spectrometry (DTD–GC x GC–TOFMS) [20]

Two ambient aerosol samples were investigated. These two samples represent a sample with a high and low poly aromatic hydrocarbon (PAH) content, as observed in their *DTD–GC–TOFMS* analysis. Several thousand peaks were found in the two-dimensional chromatogram, using the automated peak identification routine based on deconvolution methods. Among various other compound classes, alkanes, alkenes, cycloalkanes, long chain carboxylic acids and esters, aldehydes, ketones, substituted aromatics, PAH, oxygenated-PAH and heterocyclic aromatic compounds were identified by library search routines (NIST). However, large numbers of unknown and probably mismatched compounds still occur.

The mass spectra of compounds co-eluting in one-dimensional GC show much cleaner spectra when analyzed with GC x GC, although some of these compounds still overlap to a small degree. To demonstrate this a small section from a autumn aerosol sample is analyzed by both GC-TOFMS and GC x GC-TOFMS. Figure 3.17 shows the one dimensional chromatogram of the analyzed sample in total ion current with Figure 3.18 the extracted section to be compared using single ion currents ($234 m/z$, $219 m/z$ and $230 m/z$).

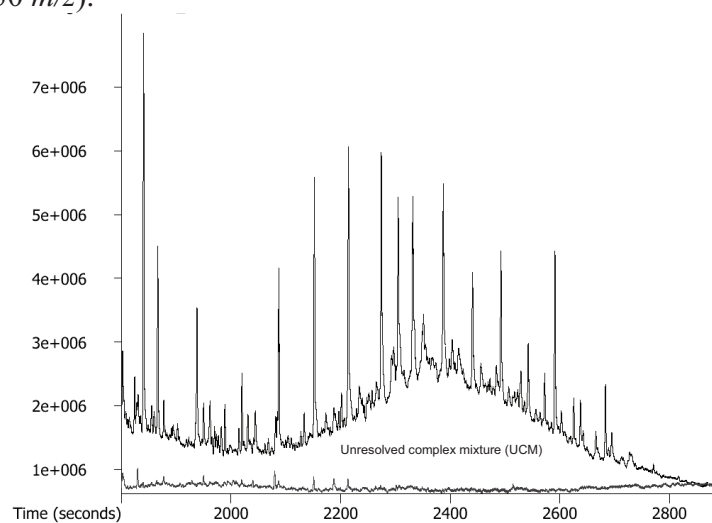


Figure 3.17: Total ion chromatograms of an autumn PM_{2.5} sample (black) and a field blank sample (grey) [20].

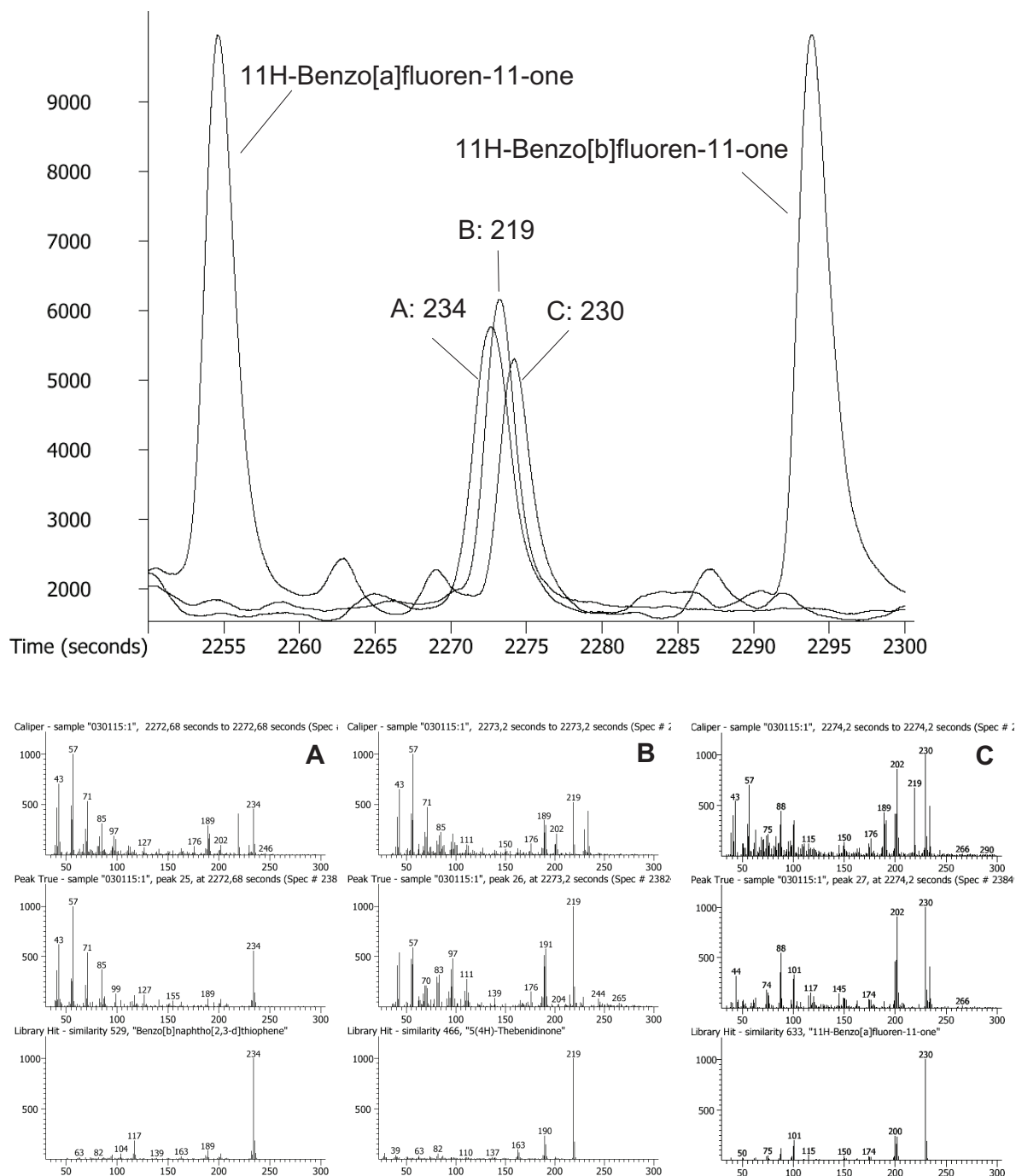


Figure 3.18: Top: Extracted ion chromatograms of characteristic ions for benzofluorenones ($m/z = 230$), benzonaphthothiophene ($m/z = 234$) and an unknown compound ($m/z = 219$ and 234). Bottom: mass spectra of the three peaks in the peak apex (top, caliper), deconvoluted spectra (middle, peak true) and reference library hits (bottom) [20].

In the one-dimensional chromatograms (Figure 3.17) of the $PM_{2.5}$ samples about 1500 compounds could be separated. The data acquisition rate of 25 scan s^{-1} facilitates automated peak finding and spectral deconvolution of co-eluting compounds and therefore enhances the information which could be drawn from the chromatograms. Figure 3.18 depicts the advantages and limitations of spectral deconvolution. In the

sample shown, the peak finding algorithm detected 30 peaks in the retention time window between 11H-benzo[a]-fluoren-11-one and 11H-benzo[b]fluoren-11-one. Several minor peaks were detected with these mass traces but for most of them no good library matches were achieved. In the middle between the two benzofluorenones an example of co-eluting peaks with similar intensities are shown. The peak maxima are at 2272.68 s, 2273.20 s and 2274.20 s for the characteristic ion traces 234 m/z , 219 m/z and 230 m/z respectively. In Figure 3.18 bottom (A) the analytical mass spectrum in the peak apex (calliper), the deconvoluted mass spectrum (peak true) and the library hit for the first peak (characteristic ion 234 m/z) are shown. In the analytical mass spectrum the masses of the co-eluting peaks which are discussed above and the background masses of the unresolved complex mixture (UCM), which is present in all ambient particulate mater samples are present. In the peak true spectrum the masses of the peaks discussed above are subtracted, whereas the masses of the UCM background are still present. After spectral deconvolution it was possible to identify this peak as benzonaphthothiophene and the third peak as either 11H-benzo[a]fluoren-11-one or pyrenecarboxaldehyde. It was not possible to identify the peak in the middle. In the deconvoluted (peak true) spectrum of this peak e.g. the mass 234 is missing (spectrum in Figure 3.14, bottom, B) although examination of the peak shape of the mass trace m/z 234 showed, that this mass is present in the first and the second peak.

In conclusion spectral deconvolution often fails, when co-eluting peaks have common masses, or when a “constant” background is present. This drawback can be greatly reduced with the use GCxGC where the compounds of interest often are completely separated from one another and from other overlapping peaks like the aliphatic compounds in the UCM band in the same volatility range.

In the GCxGC analysis of the same autumn sample more than 10 000 compounds were detected by the LECO Chromatof® software. This indicates an estimated separation increase of about 10 times over the one-dimensional results. A two-dimensional chromatogram of the autumn sample discussed above is shown in Figure 3.19. The indicated lines represent compound classes with similar properties. Compound classes which have similar chemical polarities like the PAH, oxi-PAH and the alkanes forms straight bands and can thus be easily grouped in their respective classes, the n-alkanoic acids and methyl-esters can also be easily detected, but shows a non-linear relationship as the polarity of the compounds decreases with increasing carbon chain length.

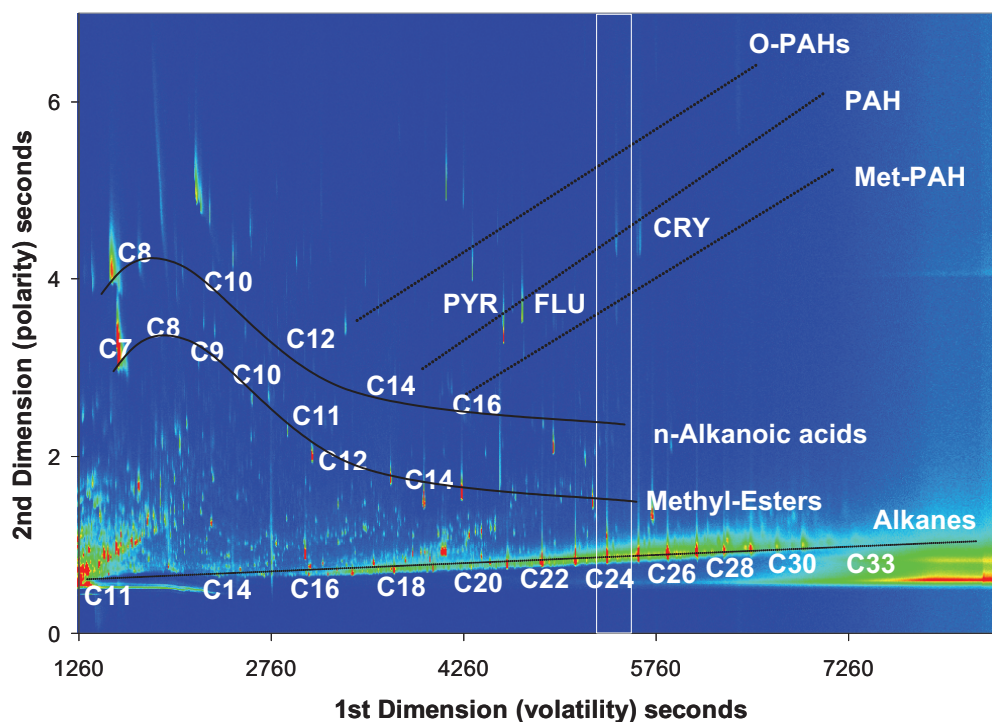


Figure 3.19 Two-dimensional chromatogram (TIC) of an autumn aerosol sample. Homologous rows of compounds or compound classes are indicated by black lines. The white lines are indicating the retention time region displayed in detail in Figure 3.16.

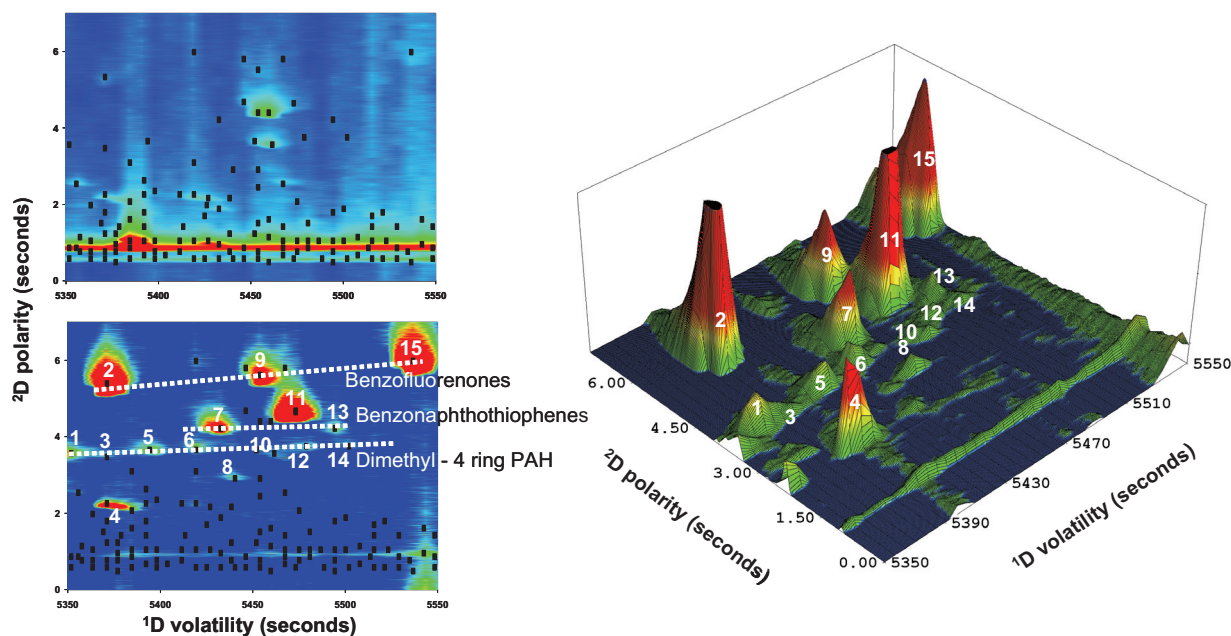


Figure 3.20: Retention time region indicated in Figure 3.19. Left two-dimensional chromatograms. The detected peaks are indicated in the TIC-chromatogram (top) and the chromatogram constructed from the masses 219, 230 and 234 (bottom). The identified peaks with base masses 219, 230 or 234 (ref. Table 3.3) are numbered two dimensional chromatogram and the three dimensional plot constructed from this three masses [20].

Figure 3.20 shows the same chromatographic section between 11H-benz[a]fluoren-11-one and 11H-benz[b]fluoren-11-one as used in Figure 3.18. In this section alone about 150 peaks were detected through the deconvolution process. For demonstration of the enhanced resolution power only the masses 219, 230 and 234 m/z are used to construct 3D plot (Figure 3.20, right) of the GCxGC chromatogram. Compounds containing the masses 219, 230 or 234 that can be observed by simple inspection in the chromatographic region of Figure 3.20 are given in Table 3.3. From this figure it can immediately be seen, that the compounds previously co-eluting on the one-dimensional chromatogram are now base-line separated. The mass spectra of these peaks now have much less interfering masses from background peaks and can be better deconvoluted and thus are identified with improved library matches.

Another advantage of GCxGC regarding the two-dimensional retention times of the compounds are demonstrated by the lines indicated on Figure 3.19 left. Since compounds of the same chemical class have similar polarities, bands of compounds of the same chemical class can be seen on the two-dimensional separation plane. This can be used in our advantage to distinguish compounds that have similar mass spectra but belonging to different compound classes. An example of this feature is the peak 9 (peak C that co-eluted in the one-dimensional chromatogram). The NIST library results identifies this compound as either 11H-benzo[b]fluoren-11-one or pyrenecarboxaldehyde but as we now can see the relationship of this peak to the other benzofluorenones in the same line we are assuming the compound to be 7H-benzo[c]fluoren-7-one, the last remaining possible benzofluorenone.

Table 3.3: Identified compounds with mass traces 219, 230 or 234 in the two dimensional chromatograms in the time window 5340 to 5537 seconds [20].

Peak	¹ D Ret time [s]	² D Ret time [s]	Base [m/z]	Compound
1	5348	3.603	230	Dimethyl(4-Ring)PAH I
2	5369	5.192	230	11H-Benzo[a]fluoren-11-one*
3	5369	3.480	230	Dimethyl(4-Ring)PAH II
4	5369	2.200	233	Unknown
5	5397	3.616	230	Dimethyl(4-Ring)PAH III
6	5418	3.704	230	Dimethyl(4-Ring)PAH IV
7	5432	4.168	234	Benzo[x]naphthothiophene I
8	5439	3,105	215	Unknown
9	5453	5.464	230	Benzo[c]fluorenone
10	5453	3.608	228	Benzo[c]phenanthrene
11	5474	4.536	219	1-(10-Methylanthracene-9-yl)ethanone
12	5481	3.728	230	Dimethyl(4-Ring)PAH V
13	5495	4.220	234	Benzo[x]naphthothiophene II
14	5502	3.760	230	Dimethyl(4-Ring)PAH VI
15	5537	5.776	230	11H-Benzo[b]fluoren-11-one*

*: identification certified by authentic standard

Comparing the mass spectra of peak 11 shown in Figure 3.21 with the spectra from the one dimensional GC analysis, it can be seen that a clearer spectra was obtained for the same compounds than the spectra previously obtained from one-dimensional GC (Figure 3.18 C). In the one-dimensional run interferences of the two overlapping peaks were observed in the mass spectra as well as masses from alkanes, in two-dimensional separation the peaks are resolved and thus no additional masses are observed.

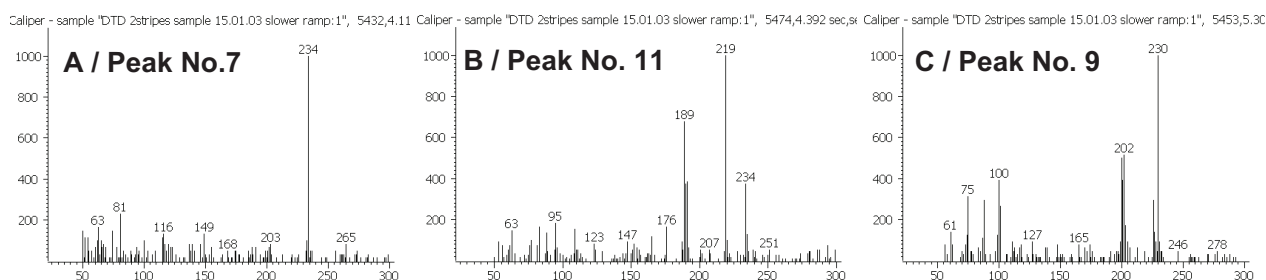
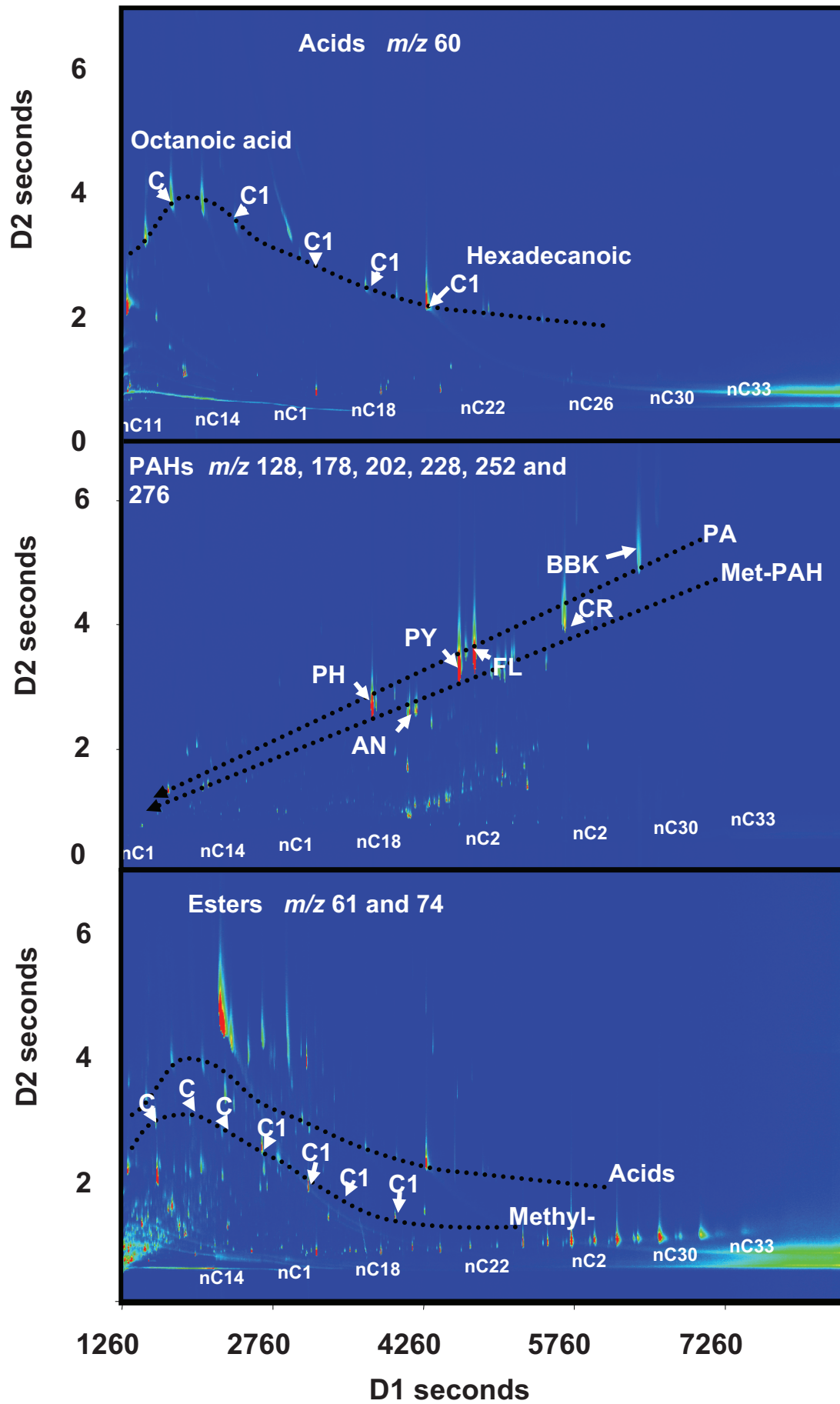


Figure 3.21: Mass spectra from GC x GC of the three compounds co eluting in one dimensional GC as shown in Figure 3.14 [20].

An important feature is the ordered appearance of chemically related compounds in the 2D GC x GC chromatogram. This is due to the physico-chemical similarities within compounds classes and the gradual changes of these properties with increasing molecular sizes/chain length. The ordered appearance helps to classify unknown substances.



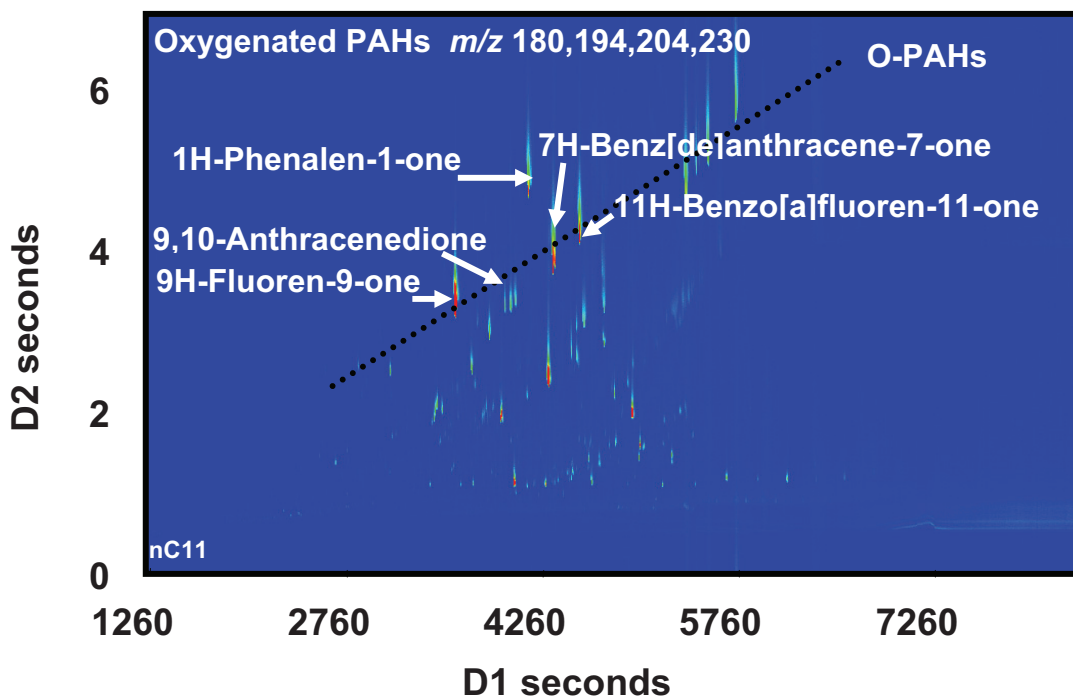


Figure 3.22 Two-dimensional GC x GC-TOFMS chromatograms of an Augsburg PM 2.5 sample: selected ion (SI) representation for n-alkanopic acid masses (60 m/z), Ester masses (61 and 74 m/z), PAH masses (128, 178, 202, 228, 252, 276 m/z), Methyl-PAH masses (142, 192, 216, 242 and 266 m/z) and oxy-PAH masses (180, 194, 204, 230 m/z).

The 2D-chromatogram based on the total ion current (Figure 3.19) is totally dominated by non-polar hydrocarbons, which are weakly separated by the chosen column parameters. However, many compounds that are suspect to be health relevant are occurring in rather low concentrations and are more polar than the alkanes. In order to visualise these compounds, characteristic selected ions are chosen (SI) for generating the contour plots that are depicted in Figure 3.22. The contour plots represent the selected ion for n-alkanoic acids (60 m/z), and for n-alkanoic acid esters (61 and 74 m/z). Some selected ion signals for PAHs methyl-PAHs and oxygenated-PAHs are also depicted (PAH, e.g. phenanthrene and anthracene, 178 m/z; pyrene and fluoranthene, 202 m/z; chrysene, triphenylene and benz[a]anthracene, 228 m/z; benzofluoranthenes, benzpyrenes and perylene, 252 m/z) (Met-PAH, e.g. methyl-phenanthrene and -anthracene, 142 m/z; methyl-pyrene and -fluoranthene, 192 m/z) and (Oxy-PAH e.g. 9H-fluoren-9-one, 180 m/z, 9,10-anthracenedione 180, 204 m/z). The simple “selected ion” approach to view the PAHs and oxy-PAHs, however, relies on the high stability of the aromatic, polycyclic species. Under electron impact (EI) ionization, the aromatic compounds are relatively stable against reactions that would destroy the highly stable aromatic moieties. The high stability of aromatic compounds could be explained by electron delocalization due to resonance effects [24]. This leads to few dominant peaks in the mass spectrum such as the molecular ions for the PAH. However, many other chemical compounds are much less stable than PAH or oxy-

PAH. For these less stable compounds, identification routines based just on a “selected ion” representation are not sufficient. The use of the fragmentation patterns obtained from these compounds could, however provide useful identification.

Pattern recognition techniques may be applied to find chemical differences in PM_{2.5} samples. Furthermore, the ordered appearance of the chemically related peaks in GC x GC is clearly visible. Unknown compounds and mismatched compounds could be classified (i.e. assigned to belong to a substance class or sub-class) utilizing the mass spectrometric fragmentation pattern information as well as 2D-chromatographic information.

It is thus possible by using the proposed classification rules to analyze the two samples and compare differences in their composition. The classification rules proposed earlier are adapted for two PM 2.5 samples from the collected samples for DTD-GC-TOFMS analysis representing a low PAH (Figure 3.23A, 13/09/02) and a high PAH (Figure 3.23B, 15/01/03) content sample. The classification rules are extended by adding the some PAH, Oxy-PAH and Phthalate unique ions (Table 3.4).

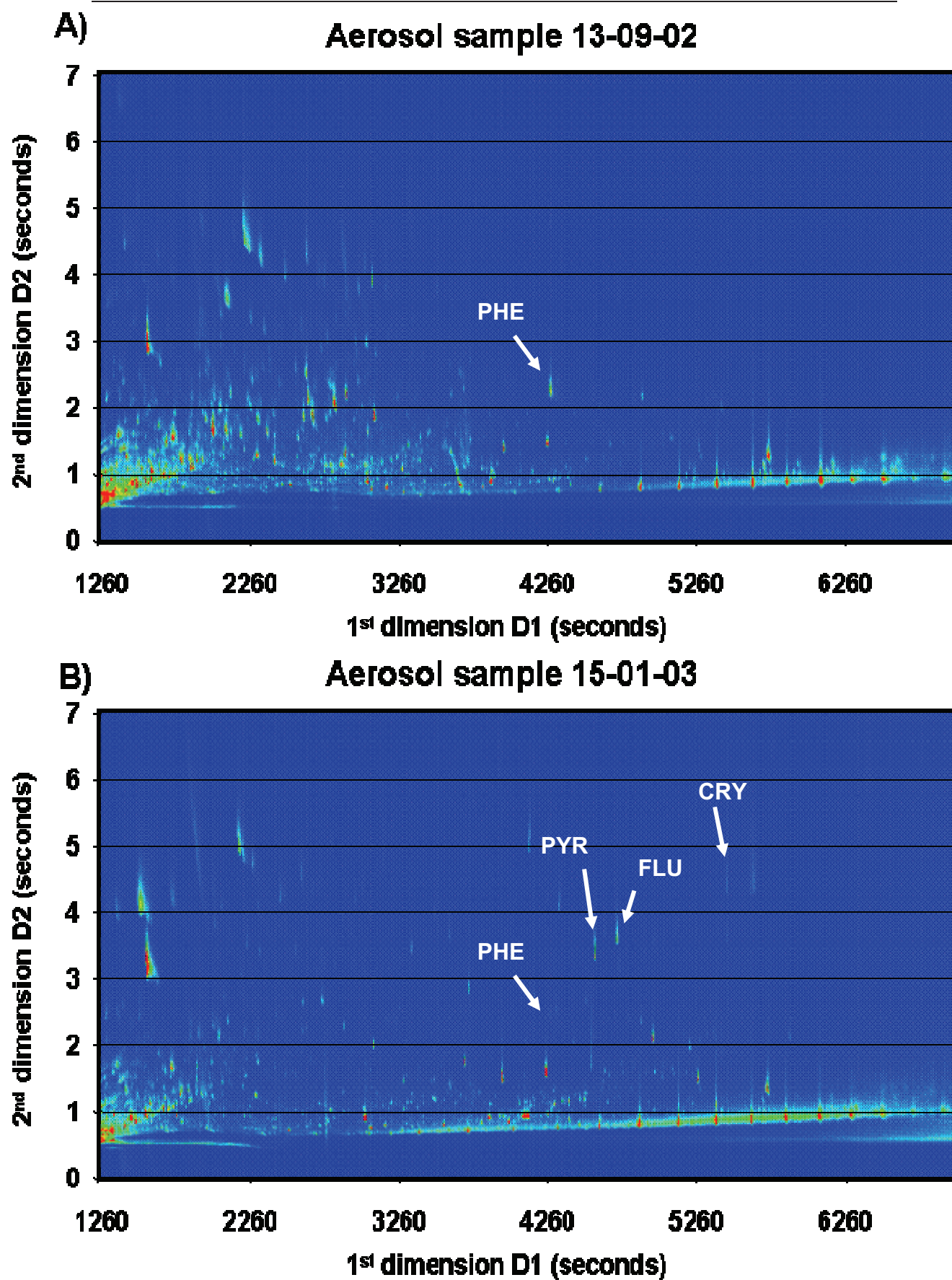


Figure 3.23 Two GC x GC-TOFMS chromatograms of a winter and summer sample. The winter sample contains a significantly higher of combustion related compounds such as PAH

Table 3.4 Extended classification rules for the analysis of a high and low PAH content sample

Compound class/group	Compound class/group identification rules	
	Mass pattern selection rules	Retention time selection rules
Alkanes	Base Peak 57 or 71 m/z with second largest peak 71 or 57 m/z	<u>No time Rule needed</u> (Must be within 0.8s and 1.2s of second dimension)
Alkenes and Cycloalkanes	Base peak 55 or 69 m/z with both present and with three of following peak in more than 15% relative intensity 97,83,70,57,56 m/z	Must be within 0.8s and 1.5s of second dimension
n-Alkane acids	Peaks with base mass 60 m/z and second highest mass 73 m/z	<u>No time Rule</u>
PAHs	Peaks with masses 178, 202, 228, 252 or 276 m/z with relative intensity above 80% or as base peak	<u>No time Rule needed</u> 1. Generally above 2s second dimension time
Oxy-PAHs	Peaks with masses 180, 194, 204 or 230 m/z above 80% relative intensity or as base peak	Above 2s second dimension time
Phthalates	Peaks with mass 149 as base peak. (note only applicable to this sample where phthalates are in much higher concentrations than other 149 m/z base peak compounds)	<u>No time Rule needed</u>

With small changes to the classification rules used in the initial introduction, the rules could be directly applied to these samples. These changes are mostly in regards to the retention time obtained in the two experiments due to changes in column parameters. However, the mass selection rules are still applicable to the new samples. New ion abundance rules are also introduced for compounds of particular interest in aerosol PM, these include the PAH compounds and Oxygenated PAH compounds. The PAH and Oxy-PAH compounds have very stable molecular ions which make it easy to identify them. Phthalate compounds can also be classified through using the unique mass of 149 *m/z*.

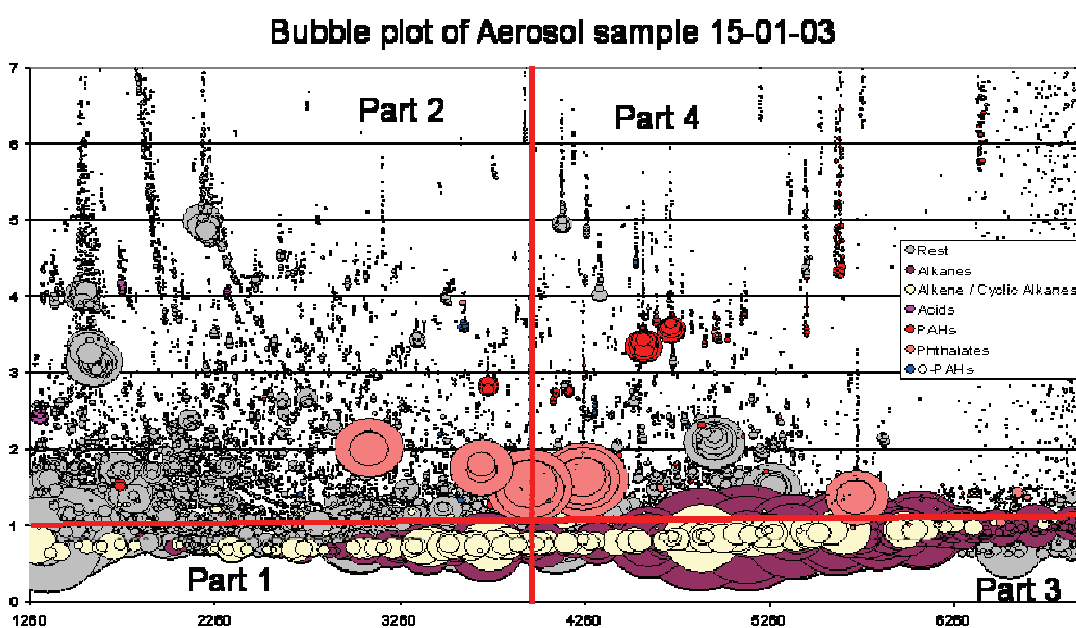
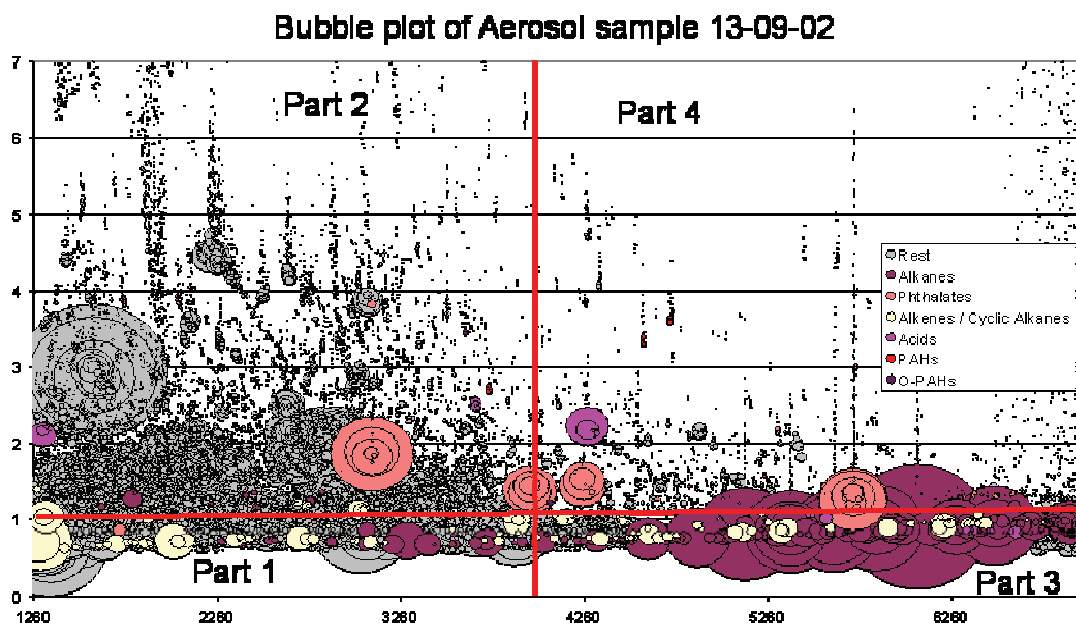


Figure 3.24 Bubble plot representation of the identified peaks from Table 3.5 shown in color.

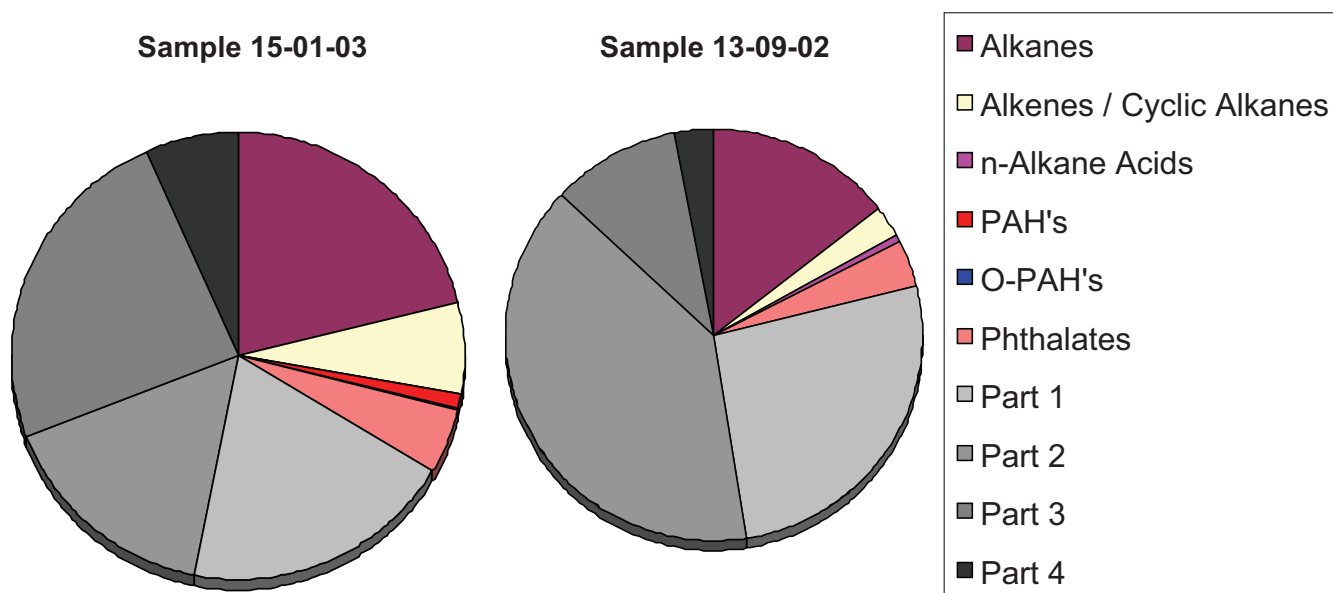


Figure 3.25 Pie-graph representations of the two PM 2.5 samples

The resulting pie plots (Figure 3.25) of the two aerosol samples (Figure 3.24A and B) show an increase in compound total area (compounds were not quantified in this experiment thus only quantitative data available is the relative areas of the chromatographic peaks) in the winter sample when compared to the autumn sample. The winter sample also show a particular high amount of PAH compounds. The increased amounts could possibly be ascribed to the usual wood and oil burning for domestic heating.

3.2.4 Conclusions

The rule based approach developed in this study shows significant improvement for the use of complex two-dimensional gas chromatography data to group compounds in distinct chemical classes. Even though a lot of refinement of the technique is still required it has been accepted in the chromatographic community and is developed further by the two main instrument suppliers of GC x GC TOFMS (Leco and Zoex). The application of the technique for the analysis of ambient particular matter in epidemiological studies is in particular helpful to aid in the development of statistical models for the chemical variability in aerosols. The technique is also not limited to aerosol analysis as demonstrated through the analysis of a diesel sample. Through user defined criteria of different chemical groups can be assigned with unlimited possibilities.

3.3 Methods for comparison of sample classes and the application on metabolomic profiles

For the comparison of samples of different classes and to statistically evaluate those, new methods need to be developed and tested. The data obtained from GC x GC analyses provide a detailed graphical representation when plotted in a two-dimensional chromatogram. This type of two-dimensional plot is quite similar to the two-dimensional gel plots familiar to biological analysis (Figure 3.26). Two dimensional electrophoresis (2D gel) is used commonly in the separation of proteins [24]. Molecules are typically separated in one dimension using for example the isoelectric point the plate is then turn 90 and molecules is then separated using for example protein mass to obtain a two-dimensional separation plane of proteins. These two-dimensional chromatograms provide ideal fingerprints for sample classes and differences can be observed quite easily between different sample classes. However, when complex samples are compared it is possible to have variations within the same sample class. This is in particular true for biological profiles where biological diversity within same sample sets is quite common. Averaging methods and statistical methods to reduce these variations in the same sets thus need to be implemented. In this section metabolomic profiles from mouse tissue extracts are being examined.

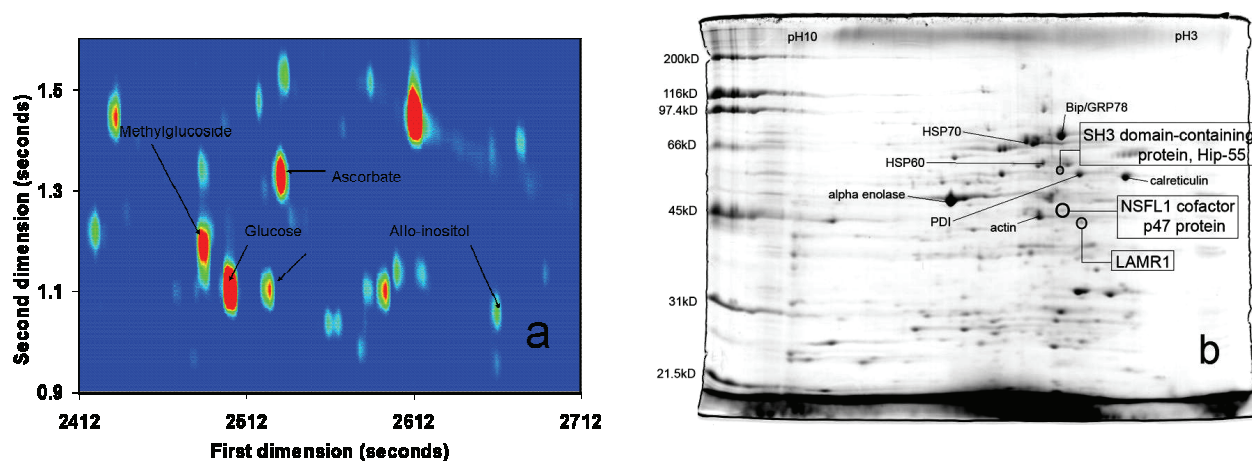


Figure 3.26 The similarity of the possible separation between two-dimensional separation obtained through GC x GC and 2D gel electrophoresis. a) A GC x GC extraction obtained from mouse spleen extracts, compounds are identified through TOF MS connected with the GC x GC. b) A 2D gel electrophoresis image of detergent extracts from PS Clone D cell monolayer. The first dimension was run on linear 7 cm IPG strip, pH 3-10. The second dimension was 10 % SDS PAGE. The gel was stained with coomassie brilliant blue and spots were picked and subjected to in-gel trypsin digestion. The major spots can be identified offline through MALDI TOFMS. [24]

The function of genes in producing products such as mRNA and proteins have been covered by genomic and proteomic research, but the change this have in the biological function of organisms is still relatively unknown. One way of investigating these

biological changes is by metabolomic analysis. Metabolomic analyses reveal the unique chemical fingerprints of the living processes on cellular, organ or organism level. Such analysis would compliment genome analysis and provide a direct link to gene function and metabolic networks by allowing a phenotyping on molecular level. In this section the first application of GC x GC-TOFMS on mammalian tissue samples is presented. The aim of the study is to distinguish between two mice strains by their metabolomic fingerprint.

3.3.1 Biomarker identification in mouse spleen extracts [25]

A comprehensive and individual characterization of the majority of the metabolites present in a given biological situation (metabolomics) is a challenging task for instrumental analysis. In the past 5 years, metabolomic strategies [26] have been developed mainly in the field of plant biology, with various applications being published [27]. These applications range from unraveling plant gene functions in physiological contexts [27], to unbiased detection of unexpected metabolic responses under environmental stress conditions [28] or co-regulation of biochemical pathways that are commonly mapped far apart from each other [26]. Protocols are adapted, tested and validated also for other organisms like bacteria [29]. Furthermore, alternative strategies have been applied to characterize global metabolic fingerprints in mammalian samples mainly by nuclear magnetic resonance spectroscopy (NMR) [30]. NMR metabolic fingerprinting offers the advantage of truly quantitative measurements compared to mass spectrometry (MS), which relies on calibration or relative quantitations. However, NMR analyses lack the resolution and sensitivity required to individually quantify and identify the whole suite of metabolites present in typical biological samples. Typically, less than 30 signals can be referred to specific metabolites in NMR metabolic fingerprints [31, 32]. The chemical diversity of metabolites can better be covered if at least two different physicochemical properties are exploited, like in gas chromatography– mass spectrometry (GC–MS: volatility and mass) [33] or high performance liquid chromatography– mass spectrometry (LC–MS: hydrophobicity and mass) [34].

The combination of data from GC–MS and monolithic-LC–MS runs with the application of appropriate data deconvolution and extraction techniques enables the detection of some 1400 individual (and genuine) metabolites. The overlap between LC–MS and GC–MS with respect to the range of detectable compounds is limited due to the differences in separation and ionization mechanisms. An alternative global approach that applied three different methods based on capillary electrophoresis (CE) coupled to mass spectrometry was elaborated, in which more than 1600 metabolites from *B. subtilis* cultures were detected [35]. Although CE/MS is definitely stronger than GC–MS, NMR or LC–MS with respect to phosphorylated or sulfated small molecules, it seems to be less suitable for secondary metabolites and lipophilic

compounds. Difficulties with scaling up injection volumes and capillary diameters further render CE/MS a less suitable choice with respect to elucidating unknown structures by fractionation and subsequent MSⁿ and NMR analysis. Researchers have recently tried to utilize the high resolution of electrospray-ion cyclotron resonance-FT/MS for annotating individual changes in metabolome composition [28]. Although direct infusion-MS may be easily applied for sample classification [36], relative quantitation of individual metabolites is problematic, due to severe physical limitations such as ion suppression [37] and adduct formation. These fundamental constraints are hardly solvable by current instrumentation, and lead to major analytical errors in the comparison of samples from different matrices, or in situations where largely altered metabolite abundances occur, such as in comparisons of plant mutants or stress conditions.

A combination of GC-MS and LC-MS may be regarded as benchmark technique; however, with respect to metabolome coverage, further improvements are needed. Demonstrated for the first time in metabolomic analysis, the use of a technique which significantly enhances metabolite resolution: comprehensive two-dimensional gas chromatography–time-of-flight mass spectrometry (GC x GC-TOF). For proof of concept an application in mammalian biology: a comparison of two well-characterized mice strains, namely New Zealand Obese (NZO) mice and C57BL/6 control strains was selected (Figure 3.27). Spleen tissue was selected as target for two reasons: (a) no report on metabolic profiles or NMR-based metabolic fingerprints from spleen extracts has been published up to date of the research, and (b) obesity and overfeeding have been demonstrated to negatively affect immune response in humans as well as rodents [38]. The NZO mouse was studied as a potential model for autoimmune diabetes. NZO mice develop obesity, glucose intolerance, and insulin resistance, and have low-titer IgM antibodies to the insulin receptor. It is proposed that metabolomics might help in elucidating the underlying mechanisms.



Source: German Institute of Human Nutrition (DIfE)

Figure 3.27 New Zealand obese (NZO) mouse (model for autoimmune diabetes) and a C57BL6 control mouse

GC x GC-TOFMS is directly applicable to differential metabolomic analysis, but owing to the expected large biological variability there is a requirement to perform a sufficient number of biological replicates in order to ensure that statistically significant findings are presented. Fiehn showed that quantitative differences, in metabolite levels in plants caused by extraction, chemical modification (derivatization) and analysis by GC-MS, are small when compared to the biological variability within samples [39]. Indeed biological variation (in plants) generally exceeds instrumental error by an order of magnitude [40]. In general for metabolomics demands several replicate analyses are required for each diverse system.

In addition to a general need to minimize the analysis time, such high throughput GC x GC-TOFMS studies should be supported by an approach for comparing the resulting chromatograms. The use of automated statistical procedures is of utmost importance in high sample throughput GC x GC studies and up to now research has been lagging in this regard. In this investigation we propose some different statistical methods for the evaluation of the differences in GC x GC chromatograms.

3.3.2 Experimental

Instrumentation

GC x GC-TOFMS analysis was performed using a 30 m x 0.25 mm x 0.25 μm d_f dimethyl polysiloxane (Rtx-1MS, Restek Corp., USA) first-dimension column, coupled to a 1.5 m x 0.10 mm x 0.10 μm d_f 50% phenyl polysilphenylene-siloxane (BPX-50, SGE, Australia) second dimension column. The primary GC oven (which housed the first-dimension column) was temperature programmed from 50 °C (held for 8 min) to 310 °C at 5 °C/min. The secondary oven (second dimension column) was temperature programmed from 56 °C (held for 10 min) to 300 °C at 5 °C/min. A modulation period of 3.0 s was used. Constant flow rate was used calculated from a linear flow rate of 20 cm/s at 25 °C. All injections (1 μl) were performed in split mode (1:2) at a constant injector temperature of 250 °C. The MS transfer line temperature was kept at 280 °C, the ion-source temperature was held constant at 250 °C, and the detector voltage was 1.8 kV. Data were acquired at 100 spectra/s (40–400 m/z). One-dimensional GC-TOF separation was performed on a 30 m x 0.250 mm x 0.25 μm d_f dimethyl polysiloxane (Rtx-1MS Restek) column under otherwise same conditions as the two-dimensional separations except a 10-fold higher sample injection due to lower sensitivity in GC-TOF compared to GC x GC-TOF

Samples

Mice were housed in standard barrier facilities, according to the Federation of European Laboratory Animal Science Associations (FELASA) regulations, and were fed standard chow (Altromin, Lage, Germany). Tissues were collected from five individual 10 months old non-fasted female, lean C57BL/6 control strain mice, and five separate 10 months old fasted female lean C57BL/6 mice. Tissues were also collected from five separate 10 months old non-fasted female obese NZO strain mice, as well as from four individual 10 months old male non-fasted NZO strain mice. 5 mg fresh weight samples were extracted at -15 °C with 1ml of a mixture of degassed $\text{H}_2\text{O}:\text{MeOH}:\text{CHCl}_3$ (2:5:2, v/v/v) and shaken for 5 min at 4 °C according to the procedure described by Weckwerth et al. [15]. A 500 μl aliquot was concentrated to complete dryness.

Derivatization

Methyl oxime derivatives were produced by dissolving the dry extracts in 20 μl of freshly prepared methylhydroxylamine HCl (40 mg/mL in pyridine) and incubated at 30 °C for 90 min with continuous shaking. Subsequent trimethyl silylation was

achieved by the addition of 80 μl of *N*-methyl-*N*-trimethylsilyltrifluoroacetamide, followed by continuous shaking for 30 min at 37 °C.

Data analysis

The raw GC x GC-TOFMS chromatograms were firstly processed through the Chromatof software (Leco corporation, St. Josephs, USA), where chromatographic peaks are deconvoluted, integrated and tentatively identified through library mass spectrum matching (NIST). The obtained peak lists with integrated areas were then exported into a spread sheet (Excel, Microsoft Office) for bubble plot representations and simple processing/ statistical calculations including, averaging or addition comparison, subtraction routines of peak areas and a t-test evaluation. Further statistical operations were done with Matlab (Mathworks), including fisher-value calculation and a principle component analysis (PCA). The resulting PCA score plots and loading plots was presented with Origin (Microcal Software inc.).

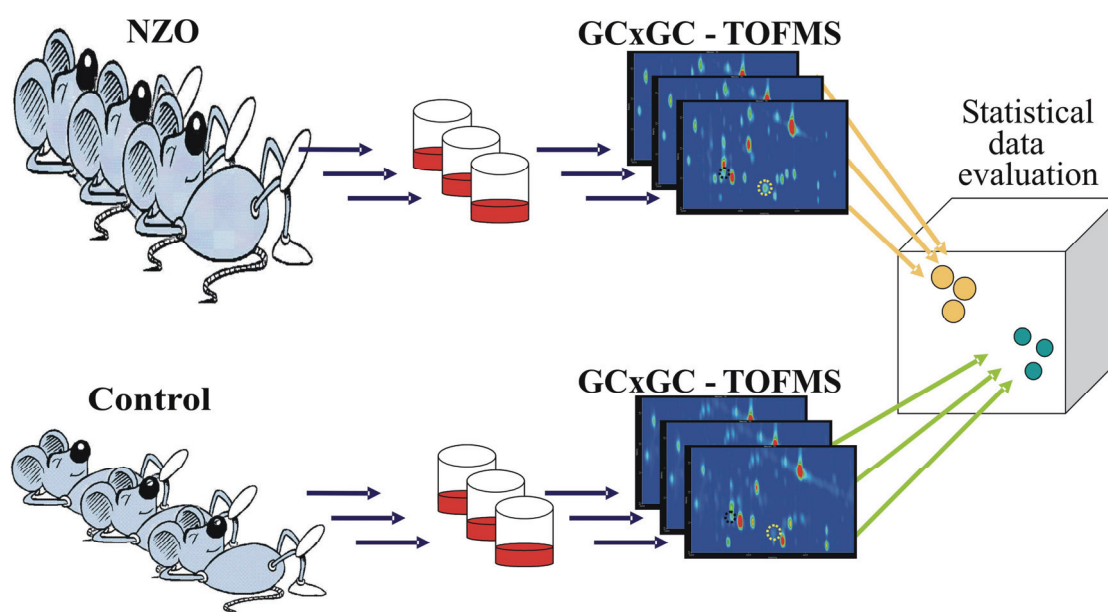


Figure 3.28 Graphical representation of experimental procedure of extraction to statistical evaluation

3.3.3 Results and discussion

Chromatograms of mouse spleen extracts (polar fraction) exhibit a medium complexity when compared to other specimen such as plant leaf samples. In Figure 3.29, one- and two-dimensional separations of a spleen extract are compared as total ion current (TIC) based chromatograms.

In one-dimensional GC-TOF chromatograms (Figure 3.29a), 538 peaks were detected after deconvolution and artifact removal. There were many amino- and hydroxy acids among these detected peaks. Compared to early results from plant metabolite profiling by GC-quadrupole MS and manual chromatogram inspection [33], the use of GC-TOF and mass spectral deconvolution increases the number of detectable peaks by a factor of three [25, 27]. Mass spectral deconvolution is based upon slight differences in the time evolution of ions belonging specifically to different near co-eluting compounds. Not all of the detected peaks are immediately visible in the TIC chromatogram because a high proportion of them are present as minor and/or poorly resolved components. The apparent difference between the number of detectable peaks and the number of visibly plotted peaks in TIC chromatograms (peak heights in Figure 3.29) highlights the importance of the data treatment by mass spectral deconvolution. The majority of low abundance peaks can only be observed by plotting a series of unique ion chromatograms, using the unique ions that the software automatically finds and reports for each detected peak.

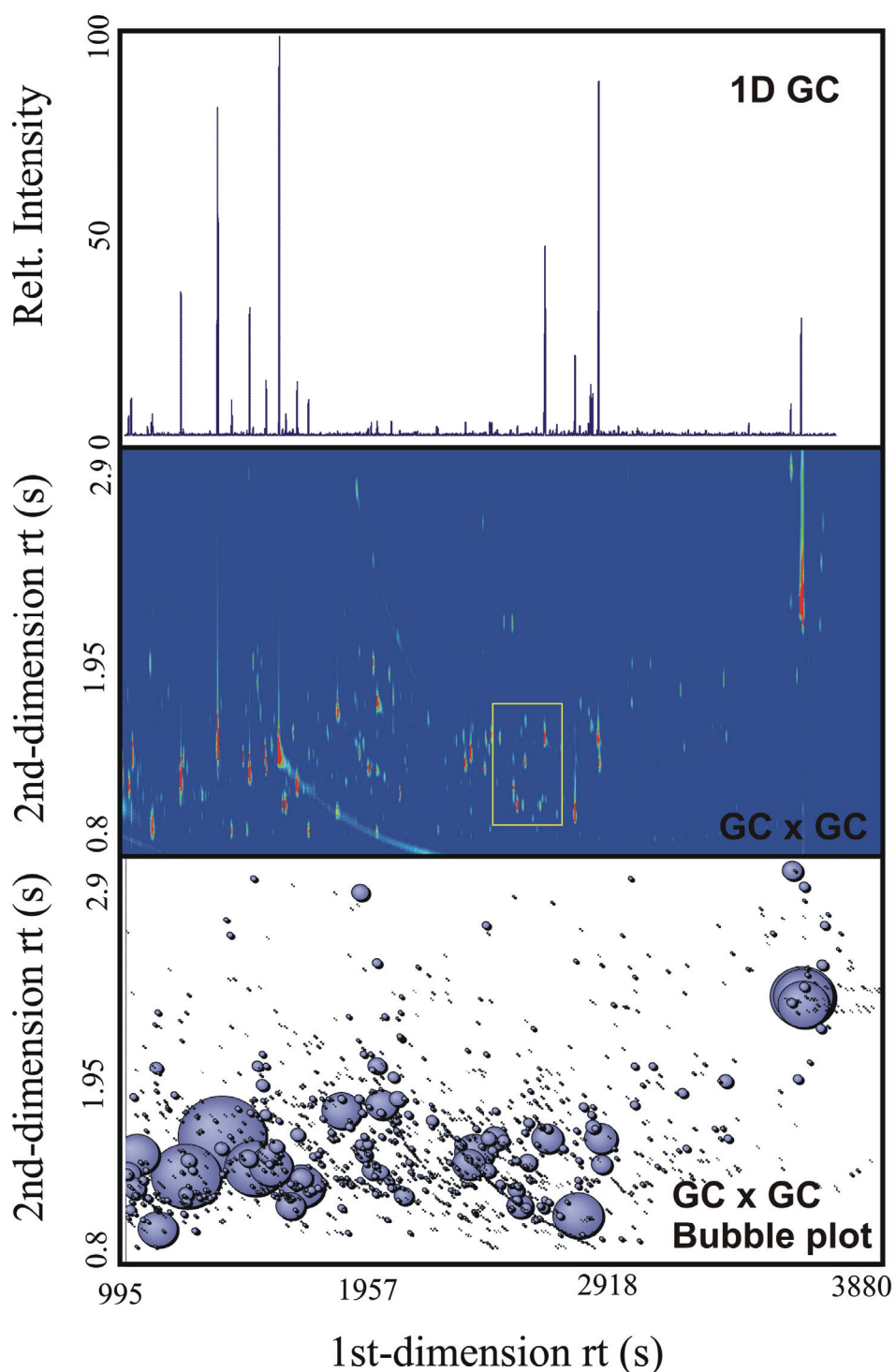


Figure 3.29 A comparison of a GC-TOF chromatogram analyzed independently (a, top panel) with a GC x GC-TOF two-dimensional chromatogram (b, middle panel) of a NZO female mouse spleen extract. The lower panel (c) is a bubble plot representation of the identified peaks in the GC x GC chromatogram after the removal of known artifacts, with the bubble radius indicating the TIC intensity. [25]

Despite these improvements, the deconvolution approach fails for fully co-eluting peaks or near co-elution of minor species with intense main compounds. This is specifically problematic when multiple chromatograms are to be compared: in such

cases, subtle chromatographic shifts will cause overlapping of previously separated peaks, causing false negative peak detections and hence missing values. GC x GC-TOFMS enhances resolution and thus reduces the problem of co-eluting peaks [19]. Following the conventions of the majority of published GC x GC applications [19, 41], the first-dimension separation was performed on a relatively non-polar column, in which the separation approximates a boiling point separation, while the second separation was performed on a fast isothermal moderately polar coated column for compound class separation based on the components' relative polarity. The total run time from GC-TOF analysis of 65 min was pulsed into 1000 individual 3s modulation slices for GC x GC-TOFMS with an acquisition rate of 100 spectra/s, resulting in a total file size of 700 MB. Peak detection and deconvolution of GC x GC-TOFMS chromatograms was performed as described above and was complemented by combination of thermally modulated peaks using the Chromatof software (Leco corporation, St. Josephs, USA). With a personal computer of 768 MB RAM and 2.0 GHz speed raw data processing took less than 30 min per sample. Surprisingly, even for medium-complex samples like mouse spleen polar extracts, GC x GC-TOFMS revealed a considerably higher number of separated peaks (Figure 3.29b, peak intensity is given in color code from light blue to red). In excess of 1220 peaks were counted following data treatment by deconvolution and removal of known artifacts such as polysiloxanes, phthalates or column bleed. Figure panel 3.29c gives a bubble plot representation of the same GC x GC-TOF chromatogram as in Figure 3.29b, in which the size of the bubbles represents the TIC area of the respective chromatographic peaks. In comparison to Figure 3.29b, this type of bubble plot presentation allows an improved overview of the peak distribution in the two-dimensional plane (Chapter 3.2, [3]).

	GC-TOFMS	GC x GC-TOFMS
# Compounds	538	1227
# With S/N > 50, Purity < 1	79	563
# With S/N > 100	202	342
Median purity	1.9	0.2
Mean purity	2.2	0.4
Median S/N	63	47
Mean S/N	411	310

Note: Threshold for peak detection was a signal/noise (S/N) ratio > 10.

Table 3.5 gives a comparison of GC-TOFMS to GC x GC-TOFMS with respect to the resulting number and mass spectral quality of peaks. It becomes clear that overall, not only was the number of detectable metabolic peaks again increased by more than 2-fold, but also that analytical purity was greatly improved. Analytical purity refers to the combination of chromatographic resolving power and mass spectra deconvolution

power. Therefore a compound may co-elute with other compounds yet still be pure if its spectrum contains unique features relative to the co-eluting compounds. Obviously, it is more likely to achieve good purity if the chromatographic resolution is enhanced as in the case of GC x GC-TOFMS. Purity approaches zero in the optimal case and can theoretically reach infinitum in problematic cases. We have found that spectra with purity <1.0 are often the most trustworthy. Specifically for high throughput and unsupervised operation it is highly mandatory that only large and pure peaks are compiled in the list of target compounds. It is a clear advantage of GC x GC-TOFMS analysis that there are about 7-fold more abundant and high quality peaks compared to one-dimensional GC-TOFMS, as defined by the threshold combination of $S/N > 50$ and purity <1 . This finding was observed despite the total number of high abundance peaks being comparable and despite the roughly 10-fold lower sample injection into GC x GC-TOFMS. This enhanced mass spectral quality is also reflected by the comparison of mean and median purity: most peaks in GC x GC-TOFMS match the required quality thresholds. Correspondingly, such peaks are more easily identifiable by matching to external spectral libraries and result in higher reliability in comparative quantifications between chromatograms.

A more detailed investigation of Figure 3.29 leads to further insights to the advantages of GC x GC applications. For example, some problems with injection of silylated compounds are more clearly highlighted in GC x GC than with one-dimensional GC-MS: thermolabile compounds may partially decompose in the hot injector leading to characteristic sickle shaped extended peak tailing [4]. An example of this is seen for tris-trimethylsilylated phosphoric acid (which partially also stems from decomposition of organic phosphates), visibly tailing in Figure 3.17b from about 1500–2100 s. This peak tail was therefore regarded as artifact and removed from the data set (as seen in Figure 3.29c) applying classification rules based on its mass spectrum. It should be noted that this unusual peak shape is not a result of GC x GC, it is simply more noticeable in GC x GC than in one-dimensional GC, where the low intensity peak tail would disappear below the chemical baseline [42]. Despite the number of detectable peaks, only 126 peaks were positively identified based on first-dimension retention index and mass spectral similarity when compared to a user library of 500 reference compounds (Figure 3.30 and Appendix B). Apart from classical biomedical targets such as glucose, fatty acids, amino acids and cholesterol, a range of other compounds were identified, among them dicarboxylic acids, aromatics and phosphorylated sugars.

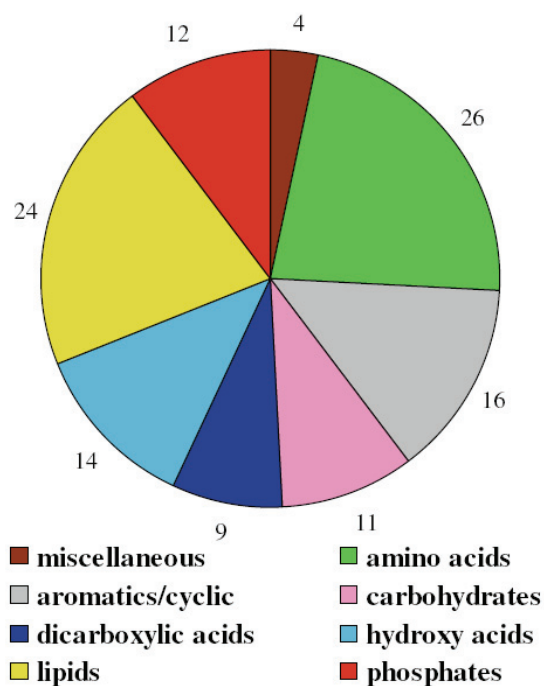


Figure 3.30 Compilation of identified peaks in GC-TOF based on first-dimension retention index and mass spectral similarity.[25]

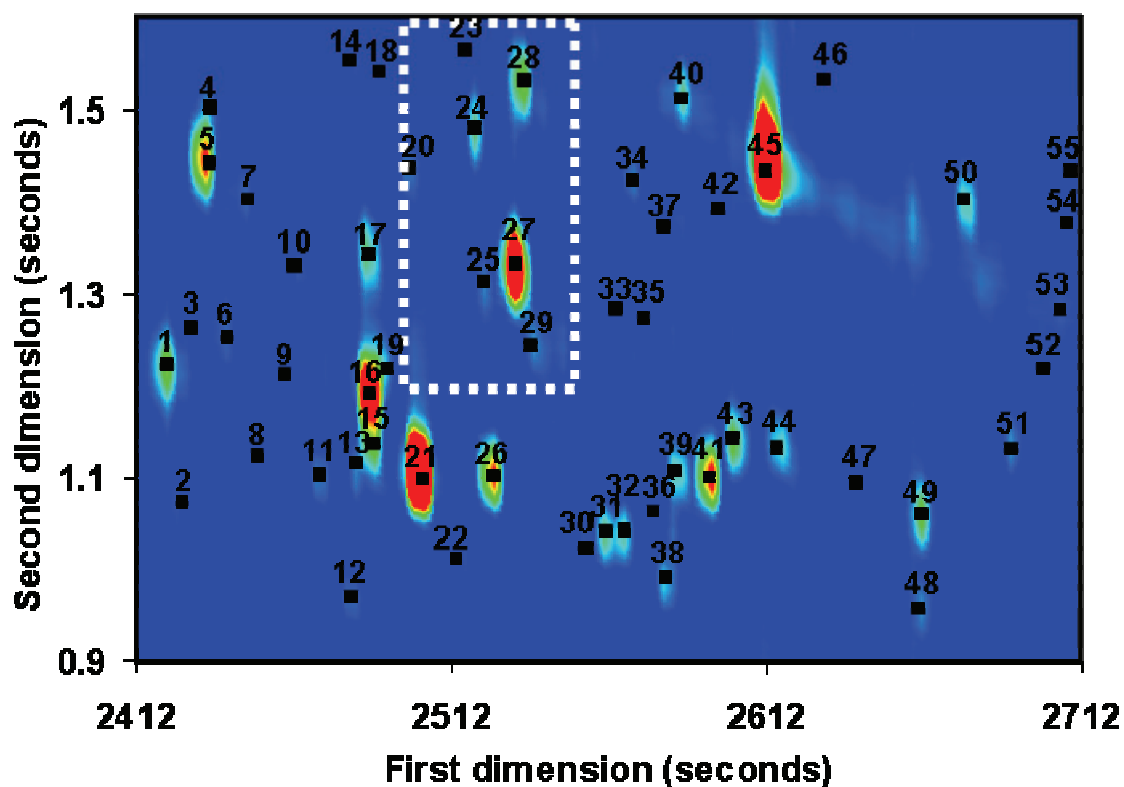


Figure 3.31 An extracted section from Figure 3.29, showing the number of peaks detected (peak markers, black dots). Exemplary characterization of compounds is listed in Table 3.6 (Appendix A). The indicated marked region is enlarged in Figure 3.29 [25]

Number	Peak assignment according to NIST best hit	Similarity hit
1	d-Erythrotetrofuranose, tris-O-(trimethylsilyl)-	795
2	α -D-Glucopyranosiduronic acid, 3-(5-ethylhexahydro-2,4,6-trioxo-5-pyrimidinyl)-1,1-dimethylpropyl 2,3,4-tris-O-(trimethylsilyl)-, methyl ester	647
3	Benzene, 1-[1,1-dimethylethyl]-4-[2-propenyloxy]-	391
4	α -D-Glucopyranoside, methyl 2-(acetylamino)-2-deoxy-3-O-(trimethylsilyl)-, cyclic methylboronate	555
5	2,2-Dimethyl-5-[2-(2-trimethylsilylethoxymethoxy)-propyl]-[1,3]dioxolane-4-carboxaldehyde	639
6	α -D-Glucopyranoside, methyl 2-(acetylamino)-2-deoxy-3-O-(trimethylsilyl)-, cyclic methylboronate	616
7	4-Ketoglucose, methoxy, silyl	594
8	α -D-Glucopyranosiduronic acid, 3-(5-ethylhexahydro-2,4,6-trioxo-5-pyrimidinyl)-1,1-dimethylpropyl 2,3,4-tris-O-(trimethylsilyl)-, methyl ester	568
9	Heptadecane, 9-hexyl-	543
10	Inosose, 2-desoxy-, O-methyloxime, tetrakis-O-(trimethylsilyl)-	602
11	D-Fructose, 1,3,4,5,6-pentakis-O-(trimethylsilyl)-, O-methyloxime	727
12	Octasiloxane, 1,1,3,3,5,5,7,7,9,9,11,11,13,13,15,15-hexadecamethyl-	616
13	Pregn-4-ene-3,11,20-trione, 17,21-dihydroxy-, bis(O-methyloxime), mono(trimethylsilyl) ether	537
14	α -D-Glucopyranoside, methyl 2-(acetylamino)-2-deoxy-3-O-(trimethylsilyl)-, cyclic methylboronate	587
15	D-Glucose, 2,3,4,5,6-pentakis-O-(trimethylsilyl)-	808
16	Glycoside, α -methyl-tetrakis-O-(trimethylsilyl)-	884
17	4-Ketoglucose, methoxy, silyl	668
18	2,4-Imidazolidinedione, 5-[3,4-bis[(trimethylsilyloxy)phenyl]-3-methyl-5-phenyl-1-(trimethylsilyl)-	558
19	Heptadecane, 9-hexyl-	646
20	α -D-Glucopyranoside, methyl 2-(acetylamino)-2-deoxy-3-O-(trimethylsilyl)-, cyclic methylboronate	605
21	D-Glucitol, 6-deoxy-1,2,3,4,5-pentakis-O-(trimethylsilyl)-	730
22	α -D-Glucopyranosiduronic acid, 3-(5-ethylhexahydro-2,4,6-trioxo-5-pyrimidinyl)-1,1-dimethylpropyl 2,3,4-tris-O-(trimethylsilyl)-, methyl ester	625
23	α -N-Acetylneuraminic acid, methyl ester-2-methyl-7,9-methyl-boronate-3,8-di(trimethylsilyl)-	518
24	4-Ketoglucose, methoxy, silyl	668
25	1-Dimethyl(chloromethyl)silyloxyhexadecane	619
26	Ribitol, 1,2,3,4,5-pentakis-O-(trimethylsilyl)-	732
27	L-Ascorbic acid, 2,3,5,6-tetrakis-O-(trimethylsilyl)-	793
28	4-Ketoglucose, methoxy, silyl	702
29	Heneicosane, 11-(1-ethylpropyl)-	698
30	N-Acetyl glucosamine, methoxy silyl	635
31	D-Glucitol, 6-deoxy-1,2,3,4,5-pentakis-O-(trimethylsilyl)-	794
32	Xylitol, 1,2,3,4,5-pentakis-O-(trimethylsilyl)-	787
33	α -D-Glucopyranosiduronic acid, 3-(5-ethylhexahydro-2,4,6-trioxo-5-pyrimidinyl)-1,1-dimethylpropyl 2,3,4-tris-O-(trimethylsilyl)-, methyl ester	601
34	α -Alanine, N-[3,3-dimethyl-1-oxo-2,4-bis[(trimethylsilyloxy)butyl]-, methyl ester, (R)-	596
35	α -D-Glucopyranosiduronic acid, 3-(5-ethylhexahydro-2,4,6-trioxo-5-pyrimidinyl)-1,1-dimethylpropyl 2,3,4-tris-O-(trimethylsilyl)-, methyl ester	611
36	α -D-Glucopyranosiduronic acid, 3-(5-ethylhexahydro-2,4,6-trioxo-5-pyrimidinyl)-1,1-dimethylpropyl 2,3,4-tris-O-(trimethylsilyl)-, methyl ester	507
37	α -N-Acetylneuraminic acid, methyl ester-2-methyl-7,9-methyl-boronate-3,8-di(trimethylsilyl)-	578
38	Octasiloxane, 1,1,3,3,5,5,7,7,9,9,11,11,13,13,15,15-hexadecamethyl-	709
39	D-Ribofuranose, 1,2,3,5-tetrakis-O-(trimethylsilyl)-	741

40	Palmitelaidic acid, trimethylsilyl ester	803
41	Glucose, pentakis-O-trimethylsilyl-	881
42	α -D-Glucopyranosiduronic acid, 3-(5-ethylhexahydro-2,4,6-trioxo-5-pyrimidinyl)-1,1-dimethylpropyl 2,3,4-tris-O-(trimethylsilyl)-, methyl ester	553
43	Myo-Inositol, 1,2,3,4,5,6-hexakis-O-(trimethylsilyl)-	711
44	D-Ribofuranose, 1,2,3,5-tetrakis-O-(trimethylsilyl)-	722
45	Hexadecanoic acid, trimethylsilyl ester	832
46	Cholan-24-oic acid, 3,7-dioxo-, (5 α)-	577
47	α -D-Glucopyranosiduronic acid, 3-(5-ethylhexahydro-2,4,6-trioxo-5-pyrimidinyl)-1,1-dimethylpropyl 2,3,4-tris-O-(trimethylsilyl)-, methyl ester	652
48	Heptasiloxane, hexadecamethyl-	684
49	Myo-Inositol, 1,2,3,4,5,6-hexakis-O-(trimethylsilyl)-	835
50	2-Desoxy-2-N-acetylamido-arabino-hexodialdose, methoxy, silyl	568
51	α -DL-Arabinopyranose, 1,2,3,4-tetrakis-O-(trimethylsilyl)-	671
52	Carda-16,20(22)-dienolide, 3-[(6-deoxy-3,4-O-methylenehexopyranos-2-ulos-1-yl)oxy]-5,11,14-trihydroxy-12-oxo-, (3 α ,5 α ,11 α)-	502
53	α -D-Glucopyranoside, methyl 2-(acetylamino)-2-deoxy-3-O-(trimethylsilyl)-, cyclic methylboronate	599
54	2,4(1H)-Cyclo-3,4-secoakumamilan-16-carboxylic acid, 17-hydroxy-10-methoxy-, methyl ester, (16R)-	609
55	Heptadecanoic acid, trimethylsilyl ester	654

In Figure 3.29b, a small area is marked (box) which is analyzed and discussed in more detail in the following section. An enlarged representation of this area is shown in Figure 3.31. The peak apex of each deconvoluted chromatographic peak is represented by the peak markers (black dots). In total 69 separated peaks are found in this small section, from which 22 of the more abundant components are labeled by numbers and annotated in Table 3.6. Furthermore their deconvoluted mass spectra are available as supplementary material Appendix B. Most mass spectra show the characteristics of sugar alcohols such as inositol-like species, based on mass spectral similarity and retention indices of allo-inositol or methylinositol (ononitol). For a further identification, however, authentic references compounds are needed. Nevertheless, the sheer complexity of detected sugar alcohol analogues might add potential hypotheses to the well known involvement of inositol-phosphates in signaling cascades, which have been associated with diseases like diabetes and cancer [43, 44] both known to be caused and/or promoted by elevated body weight [45]. Within the section marked by the indicated box in Figure 3.31, two peaks (#27 and #28) are present which completely co-elute in the first-dimension and thus can be taken as an example to demonstrate the enhancement of resolving power gained by the GC x GC approach (Figure 3.32).

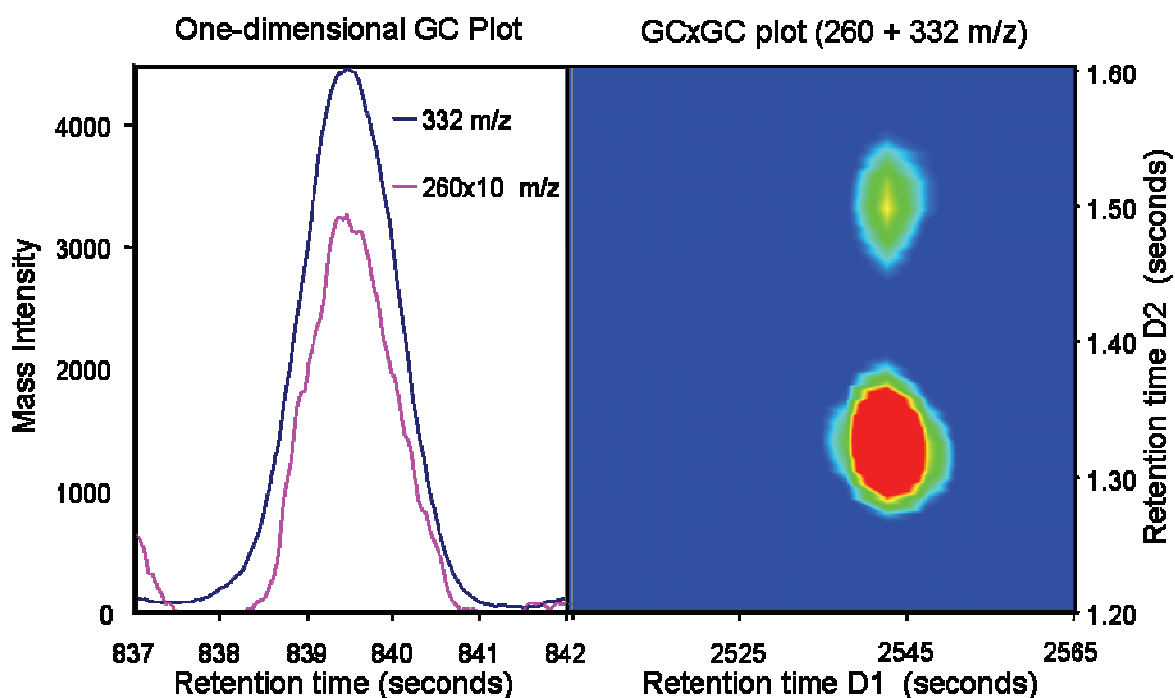


Figure 3.32 Extraction section from Figure 3.31, the co-elution of two peaks is indistinguishable in 1D GC-TOFMS (left panel), but clearly separated in GC x GC-TOFMS (right panel). The more abundant peak is identified as ascorbate with a unique ion signal at 332 m/z , whereas and the unknown compound has a unique ion of 260 m/z . The intensity of ion m/z 260 is given with a 10-fold enlargement in the one-dimensional GC-TOFMS ion chromatogram. [25]

One of the two peaks (#27) is identified as ascorbate with a unique ion signal at 332 m/z , while the second peak (#28) indicates an unclassified and low abundant compound with a unique ion trace at 260 m/z . In Figure 3.32 the corresponding section of the one-dimensional GC-TOFMS chromatogram is shown at the selected ion traces of 260 and 332 m/z (left panel). Complete co-elution of these two compounds hampers the spectral quality of the more abundant compound (#8, ascorbate) and renders the minor compound (#28) undetectable (false negative). In comparison, these two compounds can be nicely separated by GC x GC-TOFMS (Figure 3.32, right panel) with baseline separation in the second chromatographic dimension. This serves as an example of why (a) considerably more compounds are detected in GC x GC-TOFMS than in one-dimensional GC-TOFMS, and equally important, why (b) the mean spectral purity in two-dimensional analysis was largely improved. One could argue that these peaks would have been separable in a one-dimensional GC-TOFMS run using a column of different polarity. However, although this is certainly true for a specific peak pair, this would only be achievable at the price of creating new co-elutions among the 1200 detectable compounds. With a lack of a universally applicable procedure for stationary phase selection, one may initiate a

process of trial-and-error in the hope of identifying a specific stationary phase column that produces a globally optimized separation. However this still might not resolve key biomarker compounds. Conversely, GC x GC has the capacity to resolve many more peaks in a single one-shot analysis than any one-dimensional GC separation (of equivalent time). The three main benefits of the GC x GC-TOFMS approach are therefore

- (1) the maximum comprehensive separation obtainable within a single chromatographic run,
- (2) the increased average mass spectral purities and
- (3) the increased sensitivity obtained by the zone compression property of the cryogenic modulation [46].

This is specifically important in studies that go beyond manual interpretation of chromatograms, but focus at high-throughput and high-quality routine operation in metabolomics, specifically with respect to an enhanced quality of database entries in automated sample identification routines. Apart from an in-depth method validation for high-throughput operation with respect to ruggedness, accuracy and reproducibility of quantitation, it is foreseeable that long-term data storage and handling may get problematic with respect to the large size of the raw data files.

To demonstrate the usefulness of GC x GC-TOFMS for differential metabolomic biomarker identifications, four non-fasted female NZO obese mice (#5–8) were compared to four non-fasted female C57BL6 controls (#1–4). Extracts of the corresponding 8 GC x GC chromatograms are depicted in Figure 3.33, using the same retention selection as indicated in Figure 3.31 for the extractions.

On the one hand, the chromatograms demonstrate the method reproducibility (i.e. stability of the separation pattern). For larger series of runs, potential shifts in first-dimension retention times can easily be corrected for by using retention index markers. For shifts in the second dimension, absolute peak shifts are regularly less than the total peak widths which therefore gives an estimate for peak finding windows in differential analyses of series of chromatograms. On the other hand, in Figure 3.33 the biological variability between the individual mice becomes visually clear by the relative intensity differences among the metabolites of either the control strain samples (left panel) or the NZO mice spleen extracts (right panel). Such biological variability largely exceeds the analytical error measured by repeated injections of identical extracts (~5–10% relative standard deviation). Although the individuals belong to isogenic lines held under controlled environmental conditions, such a biological variability is the expected result of metabolic snapshots [47].

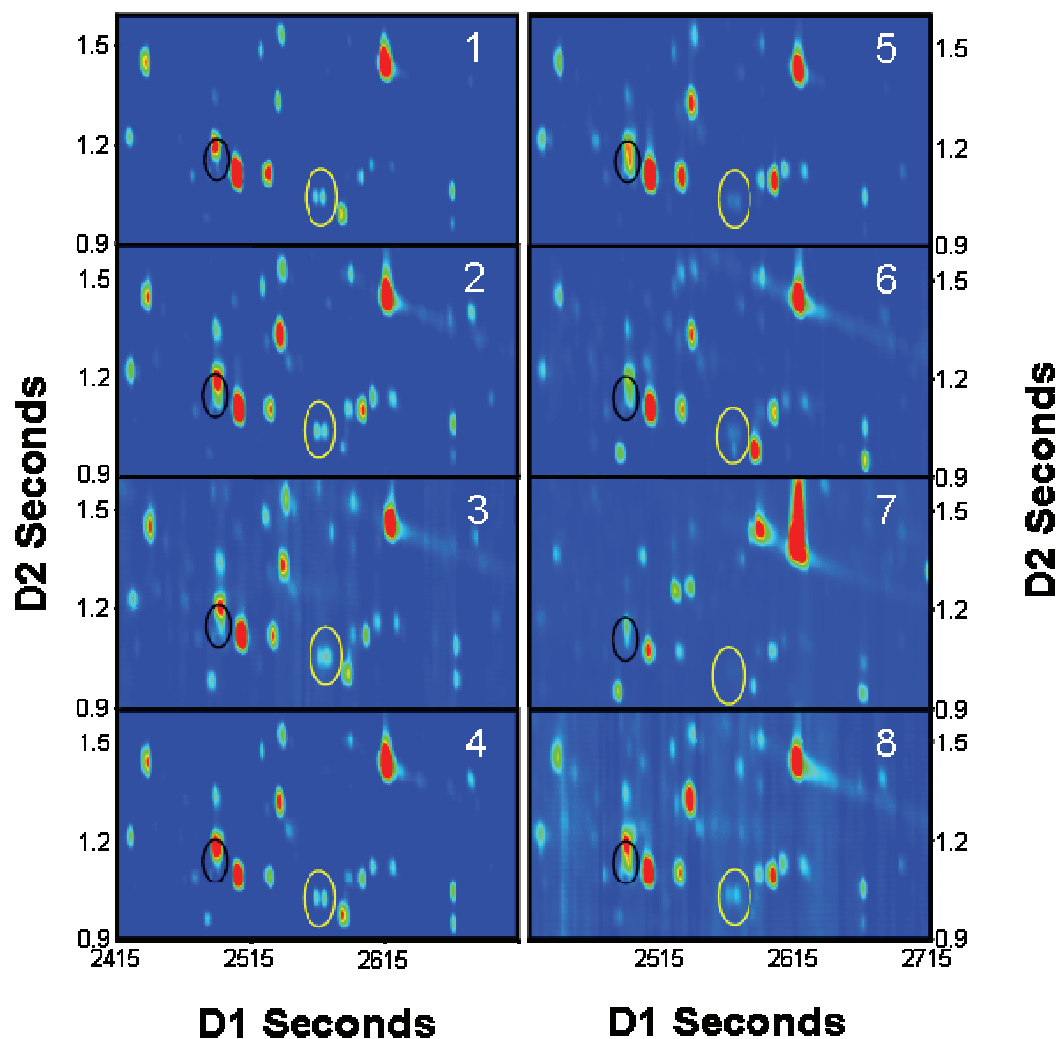


Figure 3.33 A direct comparison between the analyzed C57BL/6 female mouse spleen samples (left panel, samples 1–4) with the NZO female mouse samples (right panel, samples 5–8). The encircled compounds were used for exemplary statistical evaluation (table 3.6) of biomarker efficiency. [25]

3.3.3.1 Comparison of the chromatograms of the two classes

Through direct comparison of the chromatograms (Figure 3.33) systematic differences can be observed which might give potential biomarkers for obesity and obesity driven illnesses like diabetes type 2. Two sugar alcohols (peaks #31 and #32, indicated by yellow circles, numbering according to Figure 3.31) are relatively less abundant in NZO spleen tissues compared to C57BL/6 samples. For a more conclusive comparison some strategies need to be developed based on a more logical or statistical approach.

Chemometric analysis of comprehensive two-dimensional separations (Ref [48], and references therein) has the potential to extend the information gained from GC x GC separations. However, there is still work required for such approaches to be fully utilized, especially in the development of algorithms for retention time alignment of

two-dimensional chromatographic data. In comparing different metabolic profiles with one another we have proposed a number of possible strategies.

3.3.3.2 Averaging or addition of the chromatograms from the two classes [49]

Similar to the direct comparison of chromatograms, if the samples are analyzed in a reproducible fashion the chromatograms can be added up (same amount of samples in both sets) or averaged. Averaging or summation of the chromatogram would smooth out subtle differences in the chromatograms of a same set and potentially enhance the characteristic peaks of the set to be compared with the other set.

A summation of the TIC chromatograms was performed in this case. The, same extraction selection that was used in direct comparison was chosen (indicated with two box in Figure 3.29). Some differences can be seen in the extracted sections even by means of visual inspection (Figure 3.34). These differences are primarily based on concentration differences in the two samples, which result in a change in color intensities of the two samples compared. Some of the areas where differences can be spotted are encircled. It is important that the color scaling on both samples corresponds to the same relative peak heights, for future work it would be advised to use internal standards to normalize the data sets.

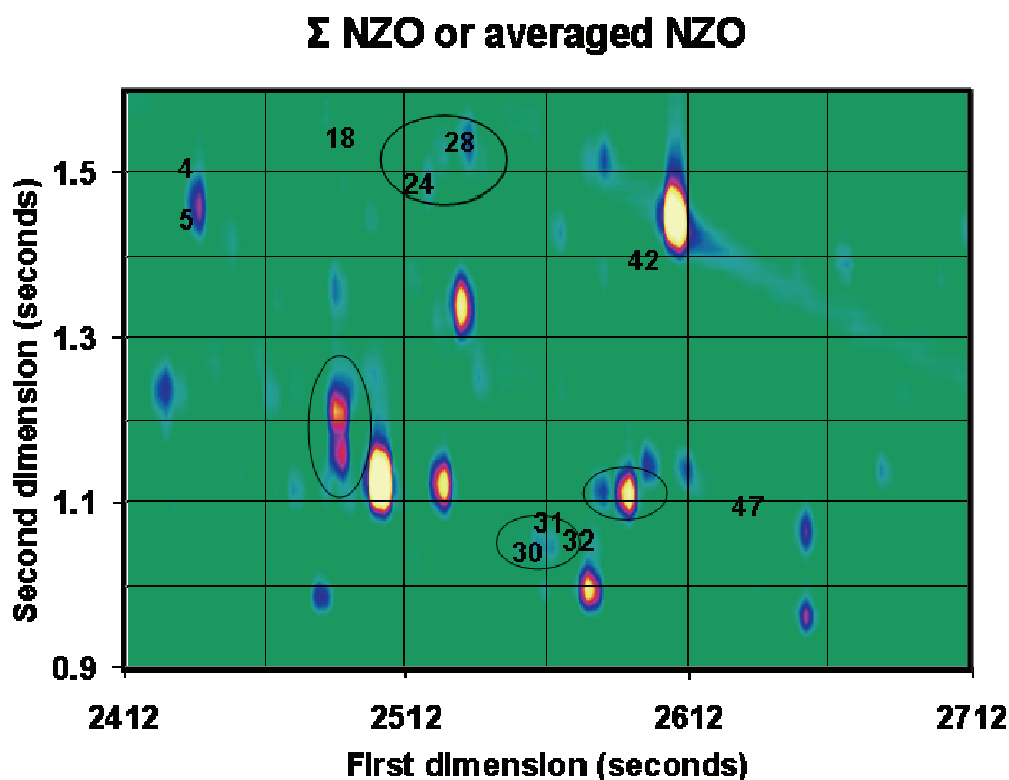
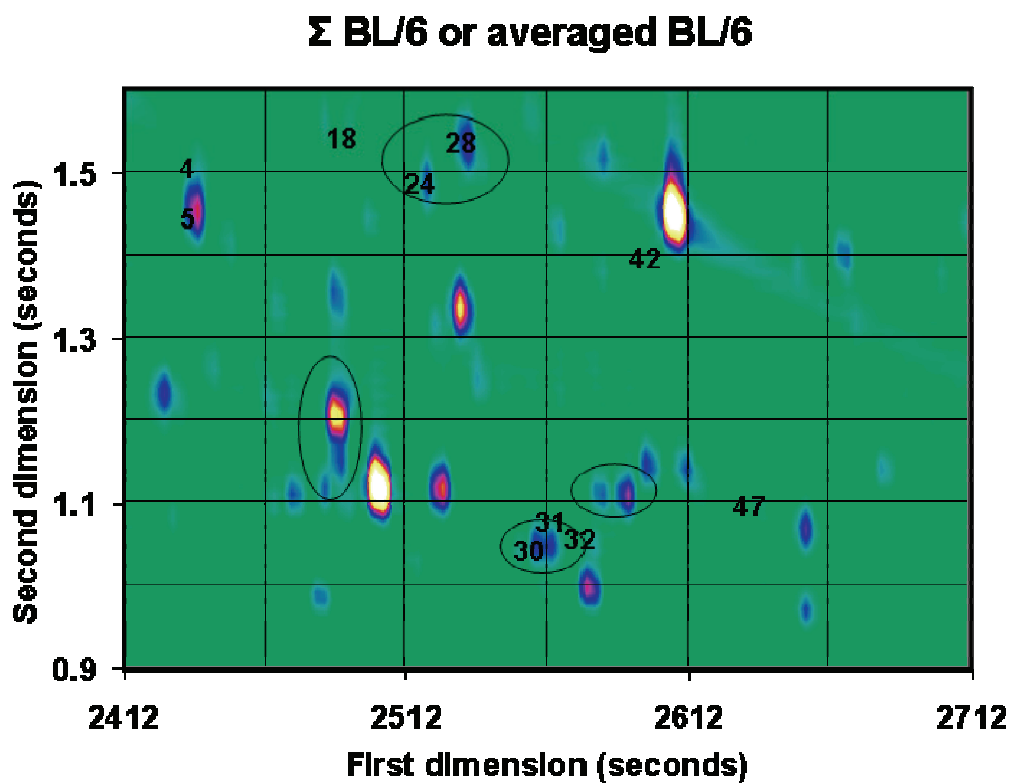


Figure 3.34 Expanded sections from the summed GC x GC-TOFMS (TIC) chromatograms with encircled areas where differences in the color intensity (i.e. peak concentration differences) occur. The numbered peaks correspond to peaks identified with the *t*-test method to show differences (see Figure 3.39). [49]

3.3.3.3 Difference chromatograms of the sample classes [49]

The approach of directly subtracting chromatograms from one another also reveals differences of the different classes. We stress however that reproducible results (retention times) are critical for this approach. The two summed chromatograms illustrated earlier were used to investigate this approach. When subtracting two ideally identical samples from one another only the base line (i.e. the empty 2D chromatographic surface) should remain. However, if there are any peaks concentration differences in the two subtracted samples both negative and positive peaks should result upon the subtraction procedure.

Figure 3.35a shows a subtracted chromatogram ($\sum\text{BL}/6 - \sum\text{NZO}$). The positive peaks are visible (i.e. the compounds with higher peak intensity in the summed BL/6 chromatogram) while Figure 3.35b shows the resulting negative peaks (i.e. corresponding to higher peak intensities in the NZO chromatograms). Medium to high relative peak intensity differences between the NZO and BL/6 chromatograms can easily be spotted for the major compounds in the subtracted chromatograms. Differences in minor peaks are of course more difficult to detect. The differences in concentration of minor compounds could of course be as significant as the differences in the major peaks in the detection of biomarkers. Thus more improved statistical methods need to be introduced for the evaluation of both major and minor compounds.

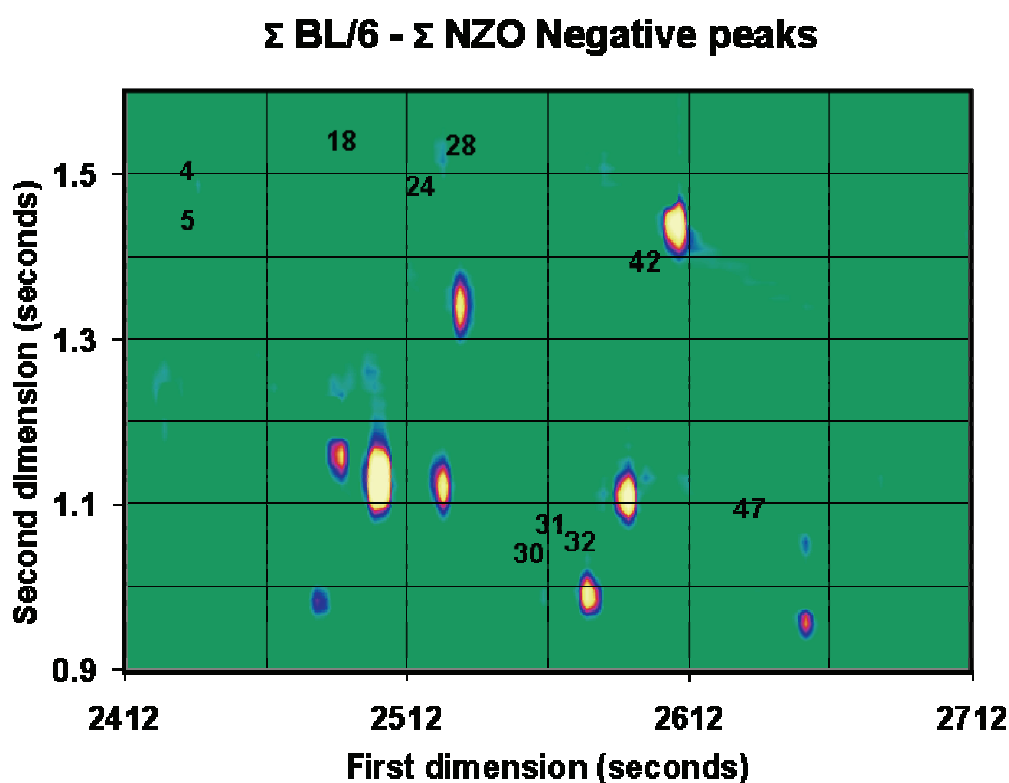
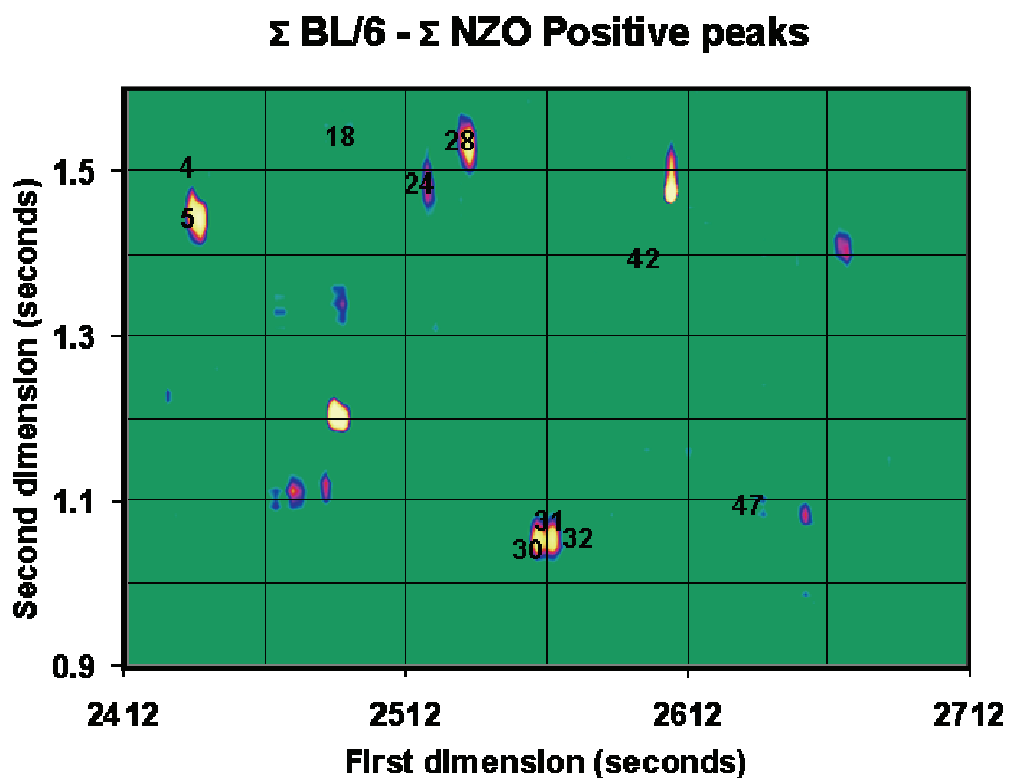


Figure 3.35 Direct subtraction of the summed NZO obese mice GC x GC-TOFMS (TIC) chromatogram from the summed BL/6 control mice GC x GC-TOFMS (TIC) chromatogram showing the resulting positive peaks in (a) and the negative peaks in (b). [49]

3.3.3.4 Bubble plot representation of GC x GC-TOFMS data [49]

Although the method of direct comparison could be performed quite easily, a lot of information generated by GC x GC-TOFMS is lost. In GC x GC-TOFMS compounds are not only separated chromatographically, but also separated by deconvolution of the mass spectra generated by TOFMS detection. The use of the deconvoluted peaks could thus reveal many more underlying differences in the two samples. The introduction of bubble plots in the analysis of GC x GC-TOFMS data [7] makes use of the peak tables generated by the Leco Chromatof software (after peak deconvolution) and presents them in a visual perspective where bubbles represent the individual peaks and bubble sizes correspond to the integrated peak areas. The peaks identified in four BL/6 mice and four NZO mice were firstly normalized and then added together to create two bubble plots (Figure 3.36).

This was achieved on a basis of normalizing the peaks in the extracted area to the total area of all the peaks (excluding artifact peaks). Normalization is necessary to eliminate possible changes in sample volume or any other factors that could influence the detection and quantification. Internal standards could be used instead of using the total peak area as a reference for the normalization. Arrows are used to highlight differences between the two summed bubble plots. These also correspond with the t -test values that are discussed later. Some of the differences corresponding to those encircled in Figure 3.34 are now more obvious. This is already a big improvement, but changes occurring in compounds of low concentration cannot be seen unless the bubble sizes are scaled appropriately.

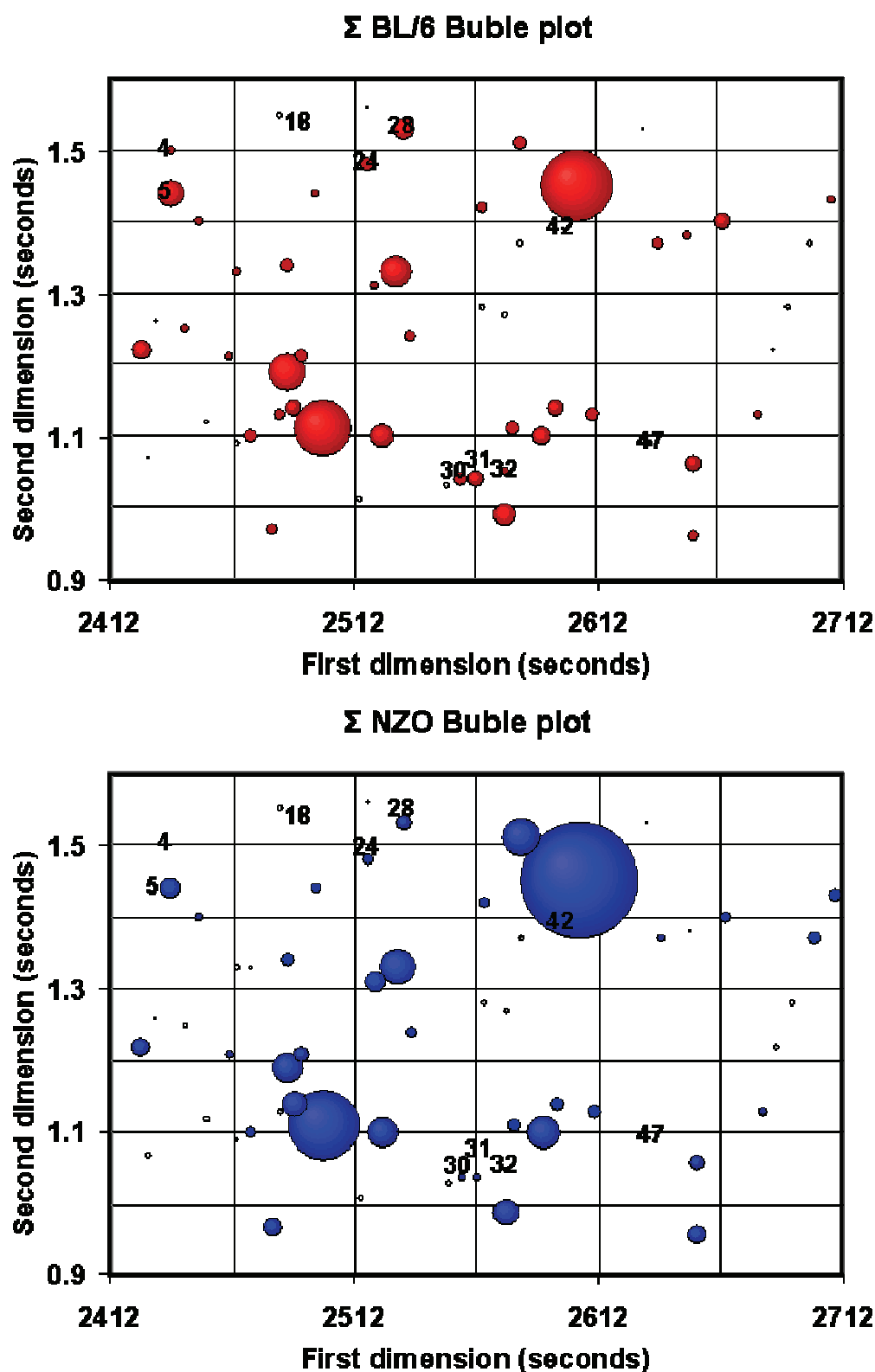


Figure 3.36 Bubble plot representation of the deconvoluted peak tables generated by summation of the areas of the compounds in the two samples groups examined. Assigned peaks corresponding with *t*-test identified values (see Figure 3.39). [49]

3.3.3.5 Normalizing peak surfaces for generation of difference chromatograms [49]

A higher significance can be obtained if the method of direct subtraction is used for the deconvoluted peak data set. In Figure 3.37, the bubble plot representation of the data set resulting from the subtraction of the NZO peak surfaces from the respective BL/6 peak surfaces is given (BL/6–NZO).

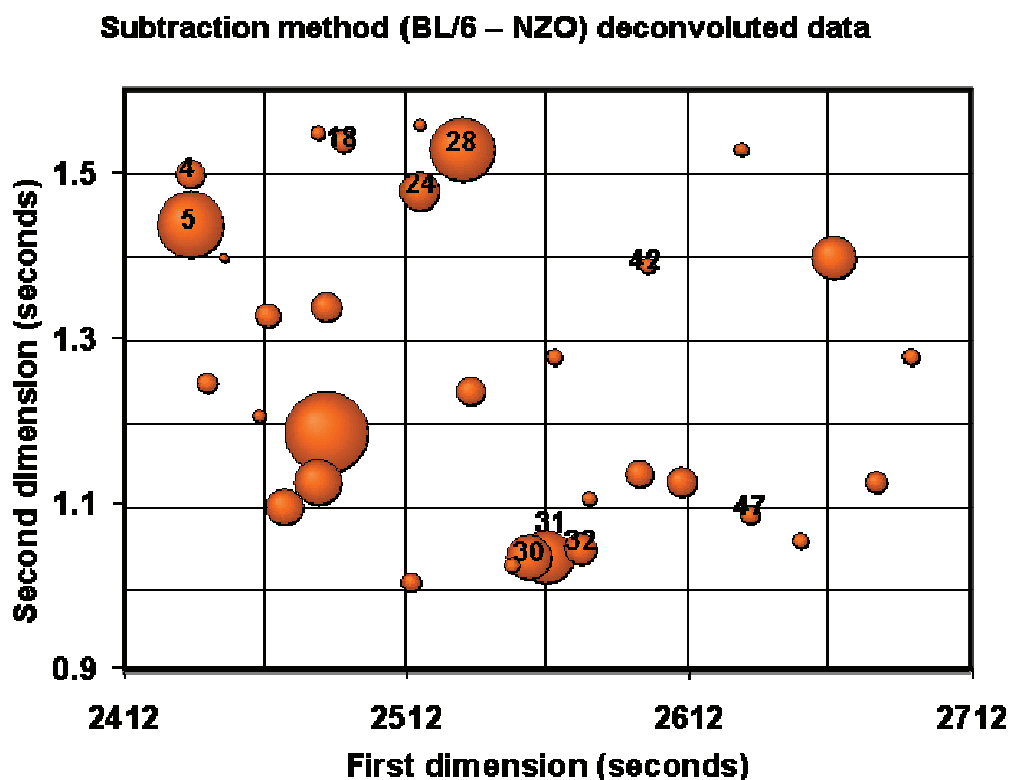


Figure 3.37 The direct subtraction of the normalized bubbles (peaks) of the averaged NZO sample from the bubbles of the averaged BL/6 mice sample. Numbered peaks correspond with *t*-test bubbles (Figure 3.39) [49]

Figure 3.37 shows good comparison with Figure 3.36, but, it is still problematic to identify differences in low concentration compounds (i.e. small bubbles in Figure 3.36). In other words, it would be desirable to see solely the relative peak surface changes but not the absolute ones. This drawback of direct subtraction can be overcome by using a peak surface normalized subtraction approach, which is shown in the following example on the BL/6–NZO case.

We are starting from the averaged BL/6 and NZO samples ($n = 4$ in both cases) with i peaks (in the section of the chromatogram under consideration $i =$ number of peaks). Firstly, i normalization factors $N_{i\text{BL/6}}$ are calculated which transform the peak surface $S_{i\text{BL/6}}$ of the i th peak in the BL/6 sample to the unity value c according to the formula

$$S_{i\text{BL}/6}N_{i\text{BL}/6} = c$$

with $N_{i\text{BL}/6} = c(S_{i\text{BL}/6})^{-1}$ and c being a constant (i.e. $c = 1$). Subsequently the normalization factors $N_{i\text{BL}/6}$ are applied on the respective i th peak surface values $S_{i\text{NZO}}$ of the NZO sample:

$$S_{i\text{NZO}}N_{i\text{BL}/6} = S_{i\text{NZO norm}}$$

By subtraction of the obtained $S_{i\text{NZO norm}}$ from c one gets the relative peak surface difference $S_{i\text{BL}/6\text{-NZOrel}}$ of the i th peak:

$$S_{i\text{BL}/6\text{-NZOrel}} = c - S_{i\text{NZO norm}}$$

A common phenomenon in biological samples, however, is bio-diversity. The concentration of the same compound in a target tissue can differ from specimen to specimen and even from day to day within the same specimen. By the abovementioned peak surface normalized subtraction approach, the relative differences between small peaks have the same impact as the relative differences between larger peaks. However, as the number n of the respective averaged chromatographic NZO and BL/6 samples is rather low) it is appropriate to consider the standard deviation σ_i of the i th peak surface with $\sigma_i = (\sigma_{i\text{NZO}} + \sigma_{i\text{BL}/6})/2$. By dividing the relative peak surface difference $S_{i\text{BL}/6\text{-NZOrel}}$ by the standard deviation σ_i the relative weighted peak surface difference $S_{i\text{BL}/6\text{-NZOwigrel}}$ are obtained which are a good measure for significant peak surface differences between the two averaged samples:

$$S_{i\text{BL}/6\text{-NZOwigrel}} = \frac{S_{i\text{BL}/6\text{-NZOrel}}}{\sigma_i}$$

In Figure 3.38, the resulting relative weighted peak surface difference ($S_{i\text{BL}/6\text{-NZOwigrel}}$) values are depicted in a bubble plot representation (i.e. the division by the standard deviation factors σ_i reduces the bubble size of compounds prone to bigger deviations). The output bubble sizes indicate the metabolites in the control BL/6 mice samples that are of higher concentration compared to the NZO mice, weighted according to the intra-sample variability. The comparison of Figure 3.37 and Figure 3.38 depicts that the normalization method puts emphasis on some compounds which only exhibit a minor absolute peak size difference (i.e. small sizes in Figure 3.37). The 15 highest $S_{i\text{BL}/6\text{-NZOwigrel}}$ values are considered as potential biomarker candidates and are indicated in Figure 3.38 by filled printing (green color).

Subtraction method (BL/6 – NZO) normalized deconvoluted data

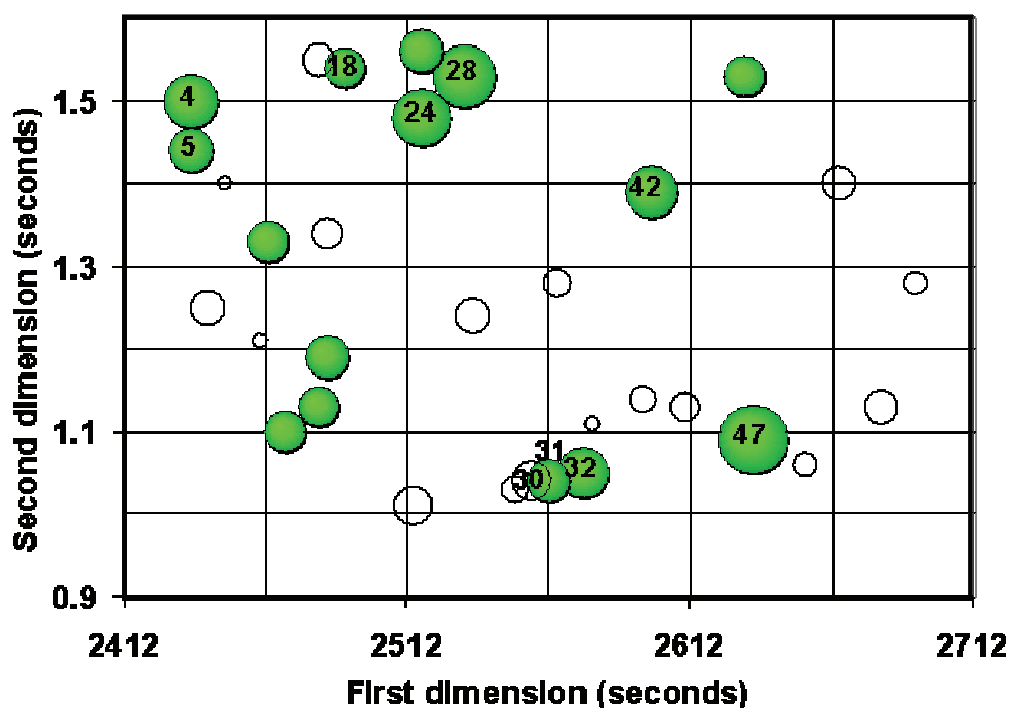


Figure 3.38 The direct subtraction of the normalized bubbles (peaks) of the averages NZO sample from the bubbles of the averages BL/6 mice sample divided by the standard deviation factor (for details see text). The 15 highest peaks are indicated in green color. Numbered peaks correspond with *t*-test bubbles (Figure 3.39) [49]

3.3.3.6 *t*-Test comparison [49]

The *t*-test is the most commonly used statistical method to evaluate the differences in means between two normally distributed groups. The groups to be evaluated can be either independent or dependent. A *t*-test can be used on small sample sizes if the variables in the groups are normally distributed and the variation of scores in the two groups is not reliably different. The *t*-test for dependent samples can be used to analyze designs in which the within-group variation can be easily identified and excluded from the analysis. The independent group *t*-test (used here) is designed to compare means between two groups where there are different subjects in each group. When the number of samples in each group is equal, the following equation can be used.

$$t = \frac{\bar{X}_1 - \bar{X}_2}{s}$$

With s the grand standard deviation, and with \bar{X}_1 and \bar{X}_2 the mean of the two sets. Alternatively, the control group standard deviation can be used for a more conservative estimate.

The t -value calculated in this way has the probability to show whether the mean in the one group is 'different' or 'different by chance' than the mean in the other group.

The Student's t -test is thus applied to potentially identify peaks showing differences in the two mice groups (although it should be noted that the number of biological replicates n was too small to achieve actual statistical significance levels). All the peaks identified and deconvoluted in the extracted chromatographic area were subjected to a t -test comparison, for the possible detection of bio-markers. Figure 3.39 shows the bubble plot of the inverse of the t -test value. Thus, a larger bubble corresponds to a larger probability of being a biomarker. The peaks are numbered according to their bubble size, with 1 being the largest. Table 3.7 shows these indicated bubbles along with the corresponding results from the normalized bubble subtraction method.

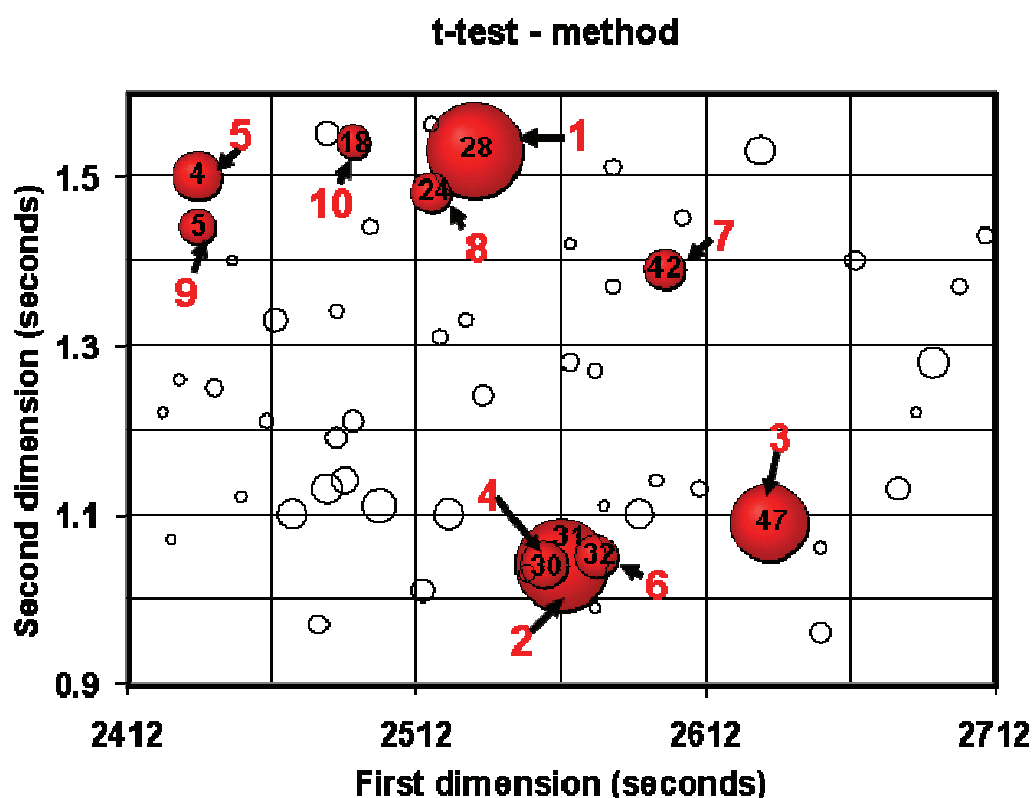


Figure 3.39. Bubble plot of the inverse of the t -test values obtained by comparing the BL/6 control mice with the NZO obese peak tables. The 10 peaks that show the highest degree of difference are indicated in red and ranked according to their t -test value. [49]

Based on the final *t*-test results the 10 highest peaks are compared in each of the above methods. From the direct comparison of the summed chromatograms only 4 of the 10 peaks correspond, while 6 of the 10 *t*-test peaks correspond in the bubble plot of the summed peak tables.

The subtraction method using the summed chromatograms also shows six corresponding peaks. All three of these methods however also show other peaks that exhibit changes in concentration, but due to the variability of these peaks in the same sample set they do not show up in the *t*-test plot.

Table 3.7 The *t*-test values of the compounds that show the highest probability of being biomarkers and their corresponding relatively weighted peak surface obtained from the normalized subtraction method.

[49]

Rank number of <i>t</i> -test (Figure 3.39)	<i>t</i> -test value	Compound Name	Relative weighted peak surface difference values (rank) (Figure 3.38)
1	0.0068	4-Ketoglucose, methoxy, silyl	231.8 (2)
2	0.0072	Sugar Alcohol	109.5 (8)
3	0.0106	Unknown	267.0 (1)
4	0.0257	Unknown	173.9 (4)
5	0.0265	Sugar Alcohol	91.6 (16)
6	0.0329	Unknown	146.6 (6)
7	0.0381	Sugar Alcohol	153.1 (5)
8	0.0392	Unknown	107.9 (3)
9	0.0490	Unknown	113.3 (4)
10	0.0515	Unknown	95.5 (14)

The bubble plot subtraction method, with the correction factor for variations, contains 9 out of the 10 peaks highlighted as being significant by *t*-tests. Furthermore, the 20 largest bubbles using this approach correspond to 17 of the most significant components (as determined by *t*-test). This indicates that these two approaches are essentially equivalent (in terms of efficacy) for use in biomarker identification. These bubble plot interpretations are, however, not done automatically yet and require considerable effort to arrange the peak tables in spreadsheets to obtain a suitable (and consistent) order.

3.3.3.7 Fisher values

Another method to effectively differentiate between different data sets using the single data is through the use of Fisher-values (or Fisher-Ratios). The pair wise Fisher-Ratio between any two classes is defined as the ratio of between-class scatter and within-class scatter. The obtained Fisher-Ratios can then be selected for

differentiating between data sets. Higher Fisher-values indicate a higher probability that the data point can be used to differentiate between the samples.

The corresponding mean value μ_k and standard deviation σ_k for a compound k is calculated from the individual measurement values y_k for each data set. The Fisher-Ratios were then calculated for the two mice groups according to:

$$F_{ijk} = \frac{(\mu_{ik} - \mu_{jk})^2}{(\sigma_{ik}^2 + \sigma_{jk}^2)}$$

Where μ_{ik} and μ_{jk} the mean-value for the k^{th} compound and σ_{ik} and σ_{jk} the corresponding variances of the two sets i and j represent. From the equation it can be derived that the Fisher-value becomes largest when inter-class separation is high and intra-class variability is minimized.

The metabolites relevant for discriminating between NZO and BL/6 mice could thus be calculated with the Fisher-value approach. Figure 3.40 show the obtained Fisher-values plotted on the two-dimensional chromatographic plane in a bubble plot representation. The bigger bubbles corresponding with higher Fisher-values and thus more likely discriminate between the two groups.

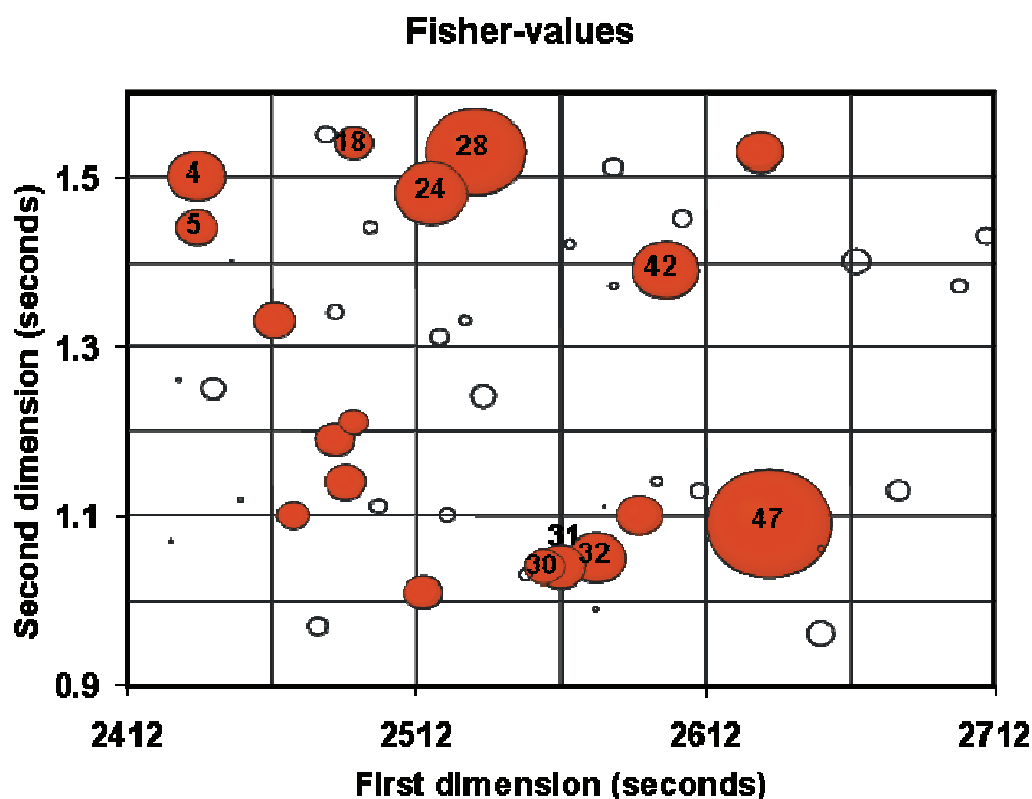


Figure 3.40 Fisher-values plotted in a bubble plot with numbered peaks corresponding with the t -test assigned peaks.

3.3.3.8 Principle component analysis

Principal components analysis (PCA) is a technique for simplifying a dataset by reducing multidimensional datasets to lower dimensions for analysis. This is achieved by transformation of the existing data variables to a new set of variables (Principal Components (PCs)), which are uncorrelated and ordered so that the first few components contain most of the variation of the entire original data set. The PCA is based on the covariance matrix of the entire data set. The eigenvectors of the covariance matrix are the so-called loading vectors (which project the original data to the new space spanned by the Principal Components) and the respective eigenvalues representing the fraction of the variance explained by the Principal Components. Often a projection of the original data spanned by the first two PCs is sufficient. The outcome of PCA is mostly depicted by two, two-dimensional plots, the loading-plot and the score-plot. The loading-plot visualises the influence of the original variables on the respective Principal Components, the scores are the projected data in the lower dimensional subspace defined by the PCs.

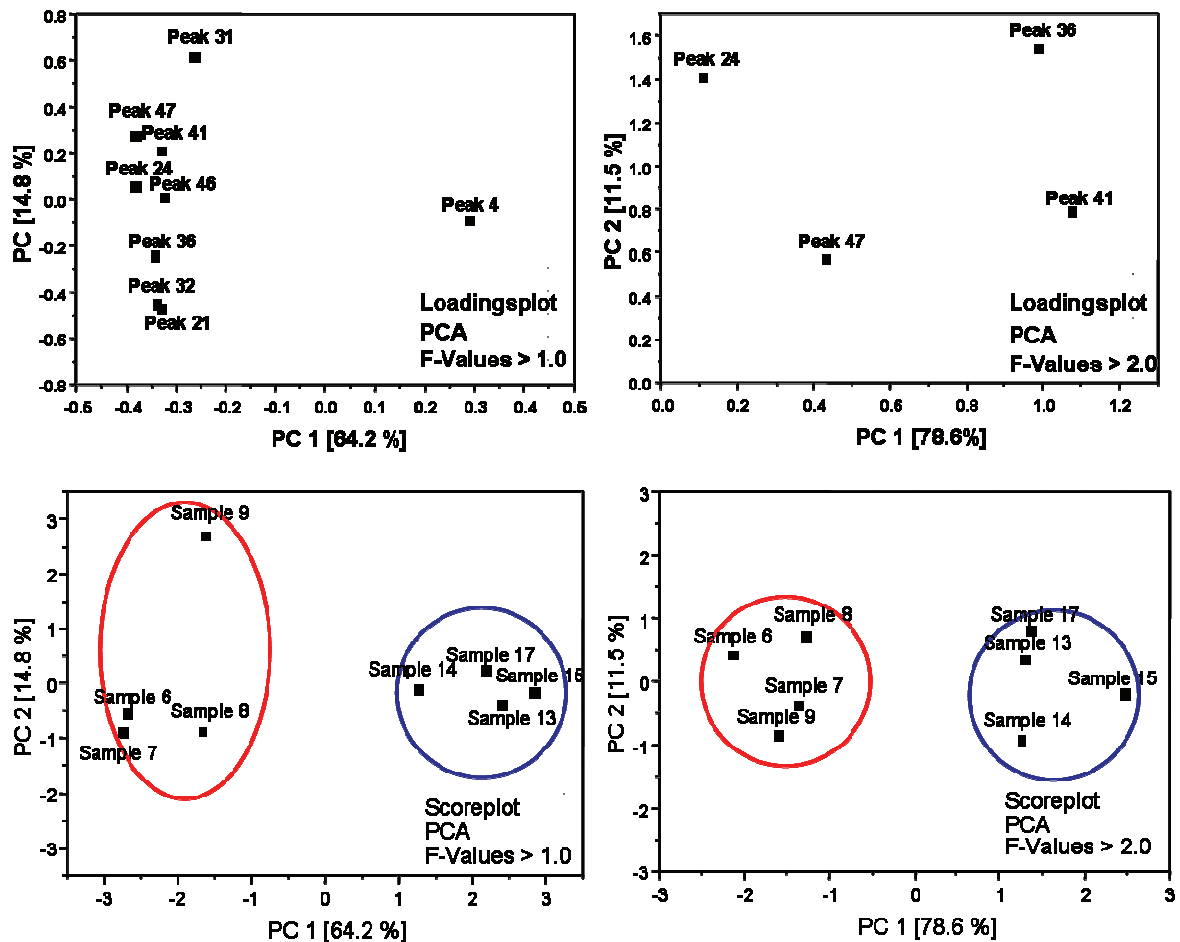


Figure 3.41 Loading plot and score plot for the F-values with a value higher than 1.0 and 2.0

For the two mice groups the Fisher-values with a value higher than 1 and 2 were analyzed through the PCA approach. Through the PCA analysis it is possible to differentiate between the two mice groups (Figure 3.41). Both the PCA plot using Fisher values above 1 or 2 are relevant. The data peaks used in the PCA correspond well with those obtained earlier from the t-test method.

It is interesting to note that the only classical analytical target in obese mice observed in this experiment was glucose. The other prominent changes such as free fatty acids or cholesterol were not present in significantly different concentrations in the two groups. Other contributing compounds were mostly sugar alcohols and some unidentified substances. This finding indicates the prospects as well as the problems of this technique for biomarker discovery: the technique is mature and can directly be applied for biomedical research; however, the diversity of the metabolome and the difficulties in *de novo* identifications of GC-MS peaks [33] disable a direct and easy route to mapping differences in biochemical pathways.

3.3.4 Conclusions

It was demonstrated that extending GC-MS to the level of comprehensive GC x GC-TOFMS analysis is directly applicable to differential metabolomic analysis of mammalian tissues. Apart from the increased number of safely detectable peaks, the most important feature is the enhanced spectral purity, which improves mass spectral deconvolution and similarity matches. This will certainly improve the data quality in biomedical data bases, if this technique is employed in larger research projects.

In a proof-of-concept study on spleen extracts from lean versus obese mice strains, it was shown that data extraction and normalization tools are ready to be used for tentative biomarker detection. Tissue extracts from obese NZO mice and lean BL/6 mice were compared using direct chromatogram comparisons, and by employing chromatogram subtraction and averaging routines. An additional method for generating relative weighted peak surface difference chromatograms compared favorably with a more conventional Student's *t*-test statistical approach for determining differences in the samples, indicating that the latter two approaches are essentially equivalent (in terms of efficacy) for use in biomarker identification. A more comprehensive Fisher-value and Principle Component Analysis also proved that it is possible to differentiate between the two sets. The comparison routines presented here were performed on TIC chromatogram data and as a consequence they are equally transferable for use with GC x GC-FID data (although the benefit of peak deconvolution will be lost). It is important to note that the number of replicates performed throughout these studies may be insufficient to produce statistical significant results, nonetheless, as a proof-of-concept it can be shown that GC x GC-TOFMS is useful for differentiating NZO and BL/6 mice based upon their individual metabolomes.

3.4 References

- [1] Dallüge J, Van Stee LLP, Williams J, Beens J, Vreuls RJJ, Brinkman UAT (2002) *J. Chromatogr. A* 974:169-184
- [2] Dallüge J, Beens J, Brinkman UAT (2003) *J. Chromatogr. A* 1000:69
- [3] Welthagen W, Schnelle-Kreis J, Zimmermann R (2003) *J. Chromatogr. A* 1019:233-249
- [4] Beens J, Tijssen R, Blomberg J (1998) *J. Chromatogr. A* 822:233-251
- [5] Welthagen W (2004) The optimisation of GC x GC and the analysis of diesel petrochemical samples. In: Chemistry Department University of Pretoria, Pretoria
- [6] Giddings JC (1984) *Anal. Chem.* 56:1258-1270
- [7] Giddings JC (1995) *J. Chromatogr. A* 703:3-15
- [8] McLafferty FW, Turecek F (1993) Interpretation of Mass Spectra. In: Interpretation of Mass Spectra University Science Books, Sausalito, pp. 139-141,238-241
- [9] Brown DM, Wilson MR, MacNee W, Stone V, Donaldson K (2001) *Toxicol. Appl. Pharm.* 175:191-199
- [10] van Vliet P, Knape M, de Hartong J (1997) *Environmental Research Environ. Res.* 74:122-132
- [11] Janssen NN, Schwartz J, Zanobetti A, Suh HH (2002) *Environ. Health Perspect.* 110:43-49
- [12] Wichmann HE, Spix C, Tuch T, Wölke G, Peters A, Heinrich J, Kreyling WG, Heyder J (2000) Daily Mortality and Fine and Ultrafine Particles in Erfurt, Germany, Part I: Role of Particle Number and Particle Mass. Health Effects Institute, Cambridge, MA, pp. 1-96
- [13] Tolbert PE, Klein M, Metzger KB, Peel J, Flanders WD, Todd K, Mulholland JA, Ryan PB, Frumkin H (2000) *J. Expo. Anal. Environ. Epidemiol.* 10:446-460
- [14] Cass GR (1998) *Trends anal. chem.* 17:356-366
- [15] Simoneit BRT, Rushdi AI, Bin Abas MR, Didyk BM (2003) *Environ. Sci. Technol.* 37:16-21
- [16] Falkowich AH, Dudich Y (2001) *Environ. Sci. Technol.* 35:2326-2333
- [17] Waterman D, Horsfield B, Leistner F, Hall K, Smith S (2000) *Anal. Chem.* 72:3563-3567
- [18] Phillips JB, Beens J (1999) *J. Chromatogr. A* 856:331-347
- [19] Marriott PJ, Shellie R (2002) *Trends Anal. Chem.* 21:573-581
- [20] Schnelle-Kreis J, Welthagen W, Sklorz M, Zimmermann R (2005) *J. Sep. Sci.* 28:1648-1657
- [21] Waterman D, Horsfield B, Hall K, Smith S (2001) *J. Chromatogr. A* 912:143-150
- [22] Simoneit BRT (2002) *Applied Geochemistry Applied Geochemistry* 17:129-162
- [23] Rogge WF, Hildemann LM, Mazurek MA, Cass GR (1993) *Environ. Sci. Technol.* 27:636-651
- [24] Tio PH, Jong WW, Cardosa MJ (2005) *Virology Journal* 2:25
- [25] Welthagen W, Shellie R, Spranger J, Ristow M, Zimmermann R, Fiehn O (2005) *Metabolomics* 1:65-73

- [26] Fiehn O (2003) *Phytochemistry* 62:875-886
- [27] Weckwerth W (2003) *Annual Review of Plant Biology* 54:669-689
- [28] Hirai MY, Yano M, Goodenowe DB, Kanaya S, Kimura T, Awazuhara M, Arita M, Fujiwara T, Saito K (2004) *Proceedings of the National Academy of Sciences of the United States of America* 101:10205-10210
- [29] Wittmann C, Krömer JO, Kiefer P, Binz T, Heinzle E (2004) *Analytical Biochemistry* 327:135-139
- [30] Nicholson JK, Foxall PJD, Spraul M, Farrant RD, Lindon JC (1995) *Anal. Chem.* 67:793-811
- [31] Keun HC, Beckonert O, Griffin JL, Richter C, Moskau D, Lindon JC, Nicholson JK (2002) *Anal. Chem.* 74:4588-4593
- [32] Wang Y, Bollard ME, Keun H, Antti H, Beckonert O, Ebbels TM, Lindon JC, Holmes E, Tang H, Nicholson JK (2003) *Analytical Biochemistry* 323:26-32
- [33] Fiehn O, Kopka J, Trethewey RN, Willmitzer L (2000) *Anal. Chem.* 72:3573-3580
- [34] Tolstikov VV, Lommen A, Nakanishi K, Tanaka N, Fiehn O (2003) *Anal. Chem.* 75:6737-6740
- [35] Soga T, Ohashi Y, Ueno Y, Naraoka H, Tomita M, Nishioka T (2003) *Journal of Proteome Research* 2:488-494
- [36] Vaidyanathan S, Rowland JJ, Kell DB, Goodacre R (2001) *Anal. Chem.* 73:4134-4144
- [37] Schmidt A, Karas M, Dülcks T (2003) *J Am Soc Mass Spectrom.* 14:492-500
- [38] Lamas O, Martínez J, Marti A (2004) *J. Nutr. Biochem.* 15:418-425
- [39] Fiehn O, Kopka J, D'ormann P, Altmann T, Trethewey RN, Willmitzer L (2000) *Nat. Biotechnol.* 18:1157
- [40] Roessner U, Willmitzer L, Fernie AR (2002) *Plant Cell Rep.* 21:189
- [41] Beens J, Tijssen R (1997) *J. High. Resol. Chromatogr.* 21:63-64
- [42] Shellie R, Xie L-L, Marriott P (2002) *J. Chromatogr. A* 968:161-170
- [43] Cantley LC (2002) *Science* 296:1655-1657
- [44] Pendaries C, Tronchère H, Plantavid M, Payrastré B (2003) *FEBS Letters* 546:25-31
- [45] Adami H-O, Trichopoulos D (2003) *The New England Journal of Medicine* 348: 1623-1624
- [46] Lee AL, Bartle KD, Lewis AC (2001) *Anal. Chem.* 73:1330-1335
- [47] Steuer R, Kurths J, Fiehn O, Weckwerth W (2003) *Bioinformatics* 19:1019-1026
- [48] Sinha AE, Prazen BJ, Synovec RE (2004) *Anal. Bioanal. Chem.* 378:1948
- [49] Shellie R, Welthagen W, Zrostlikova J, Spranger J, Ristow M, Fiehn O, Zimmermann R (2005) *J. Chromatogr. A* 1086:83-90

Chapter 4

**PHOTO IONIZATION MASS SPECTROMETRY
COUPLED TO GC AND GC x GC**

4.1	Introduction	118
4.1.1	<i>Comprehensive coupling of GC and MS: Separation enhancement</i>	118
4.1.2	<i>Coupling of GC with selective detectors: Selectivity enhancement</i>	120
4.2	Laser photo ionization (REMPI / SPI) for GC x MS	122
4.2.2	<i>Experimental</i>	122
4.2.3	<i>Results and discussion</i>	124
4.3	Laser photo ionization (SPI) for GC x GC x MS	146
4.3.2	<i>Experimental</i>	146
4.3.3	<i>Results and discussion</i>	147
4.4	VUV-lamp photo ionization (SPI) for GC x MS	152
4.4.1	<i>Experimental</i>	152
4.4.2	<i>Results and discussion</i>	154
4.5	VUV-lamp photo ionization (SPI) for GC x GC x MS	162
4.5.1	<i>Experimental</i>	162
4.5.2	<i>Results and discussion</i>	163
4.6	Conclusions	173
4.7	References	173

Chapter 4

PHOTO IONIZATION MASS SPECTROMETRY COUPLED TO GC AND GC x GC

4.1 Introduction

The analysis of complex samples requires analytical methods with a high degree of separation or selectivity in order to identify closely related compounds. Hyphenation of different techniques is currently the preferred method for analyzing these complex mixtures. These analytical methods typically include spectroscopic techniques (UV spectroscopy, mass spectroscopy, etc.) and separation techniques (chromatography, etc.). Analytical techniques can be combined (hyphenated) to improve the detectability of individual compounds or for the analysis of complex samples. In general, the coupling of a chromatographic separation step with a spectrometric detector is the most common setup. Examples include gas chromatography coupled to mass spectrometry (GC-MS) [2] as well as gas chromatography coupled to Fourier transformation infra red spectrometry (GC-FTIR) [3].

For very complex mixtures, however, the selectivity or separation capability of the current hyphenation techniques is not sufficient. Two approaches are proposed to improve the analysis of these mixtures: the first approach is to enhance the separation power of the analytical technique (multidimensional separation of complex mixtures) and the second is the introduction of more selective spectrometric detectors (highly specific target analysis).

4.1.1 Comprehensive coupling of GC and MS: Separation enhancement

Separation enhancement can be achieved by the hyphenation of different separation techniques, as is the case with heart-cut two-dimensional gas chromatography (GC-GC) [4, 5]. In GC-GC the separation efficiency of the analytical technique is improved in an additive manner where the separation efficiency of the first-dimension is added to the separation efficiency for individual second-dimension fractions. In an improved separation method where second-dimension separations are repetitively generated, an orthogonal as possible second-dimension separation is used to maintain

any separation gained on the first-dimension. This kind of separation is known as a comprehensive two-dimensional separation [6]. A typical example of a comprehensive two-dimensional separation is GC x GC [7-10] (discussed in Chapter 3) in this approach, the separation efficiency of the first-dimension is enhanced by the separation efficiency of the second-dimension. In other words the possible peak capacity of the first-dimension is multiplied by the possible peak capacity of the second-dimension, increasing the separation efficiency of the combined system (Chapter 2.2).

In contrast to comprehensively coupled separation techniques (e.g. GC x GC), the second-dimension in hyphenated two-dimensional technologies (e.g. GC-MS) often represents a spectroscopic identification technology. As separation in this dimension is only possible through deconvolution of the spectral information, two-dimensional data representation does not result in ordered groups of signals representing different compounds with similar chemical/physical properties. In this context MS exhibits interesting properties. On the one hand MS can be applied as a spectrometric technique, whereby the fragmentation fingerprint pattern of a molecule is used to determine its identity. On the other hand MS separates molecular ions and fragments according to their mass, thus representing literally a separation technique. The separation aspect of MS is, however, in the most typical case (i.e. electron impact ionization, EI with 70eV kinetic energy) dominated by the spectrometric aspect due to the fragmentation of the molecules. Venkatramani *et al.*[11] proposed that systems such as coupled gas chromatography and mass spectrometry can also be regarded as comprehensive two-dimensional systems (GC x MS). This is particularly true, however, if soft ionization methods such as photo ionization (PI), chemical ionization (CI) [12] or field ionization (FI) [13] are used for the ion generation in MS. Soft ionization avoids the formation of fragments and therefore fully reveals the “separation character” of mass spectrometry (i.e. molecular ions are separated by their mass). Thus, in principle, the comprehensive coupling of chromatographic and mass spectrometric separation is possible (GC x MS). Wang *et al.* [14] have recently demonstrated that with appropriate gas chromatography separation parameters, i.e. a polarity separation (column), coupled to mass spectrometry with soft ionization, the hyphenated system is independent enough to allow a comprehensive GC x MS approach [1, 11, 14]. However, even with the use of a column which separates compounds due to selective interaction such as polarity or polarizability, the effect of the volatility of compounds cannot be eliminated since gas chromatographic separations are usually also driven by a temperature program. The resulting plot of chromatographic retention time against molecular mass thus results in inefficient use of the two-dimensional separation plane. In classical GC x GC (i.e. with polar second column) this effect does not occur to this extent, as the second column is operated at quasi-isothermal conditions, emphasizing the orthogonal polarity aspect of the separation. In GC x MS, however, a more efficient use of the two-dimensional plane can be obtained by adjusting the retention time axis to a relative axis where the retention time of the two-dimensional plot is normalized to the n-alkanes[14]. Using

this procedure the volatility aspect of the chromatographic separation is eliminated. The retention time transformation is a Kovats Index like adjustment [15] as it refers to the n-alkanes as reference point. Relative chromatographic retention times are now used as the first separation dimension and the mass of the molecular ion is used as the second dimension. These two dimensions are highly orthogonal; the criteria for a comprehensive gas chromatography mass spectrometry coupling (GC x MS) are met.

4.1.2 Coupling of GC with selective detectors: Selectivity enhancement

The second approach for improving the analytical performance for the analysis of complex mixtures is to increase the spectrometric selectivity. With increased selectivity compounds masked by other compounds in the sample matrix can be selectively detected and analyzed. The coupling of a more selective spectrometric detector to a separation technique, such as gas chromatography, thus enables the compounds of similar physical and chemical properties to be separated and identified. In conventional GC-MS, electron impact ionization (EI, 70 eV) is a universal ionization method since all organic compounds are ionized and fragmented [16]. With the obtained fragmentation spectra, compounds can be identified using fragmentation libraries, or even be distinguished from one another through deconvolution. Fragmentation, however, can not be used to distinguish between isomers in most cases, as for example alkanes. By use of deconvolution methods with mass spectral data, the separation efficiency of the hyphenated technique can be increased. Another possibility to increase the selectivity of mass spectrometry is high resolution mass spectrometry or tandem mass spectrometry. With the high resolution MS it is possible to assign the elemental composition of the compounds analyzed, which supports in the identification of compounds [17, 18]. With tandem mass spectrometry (GC-MS/MS) target molecules are selected in the first MS step and further fragmented to obtain secondary fragmentation spectra in the second MS step [17, 18].

A particularly interesting approach for increasing selectivity in MS is the use of selective ionization methods. In selective ionization methods, only compounds of specific chemical or physical criteria are ionized; this followed by MS can provide more information on the identity of the compound being analyzed. Chemical ionization [19] is such a selective ionization method where the analyte is ionized by chemical ion-molecule reactions during collisions in the source. Different ion-molecule reactions can thus be achieved by introducing different ionization molecules and ultimately selectively ionize different analytes for selective detection. Photo ionization (PI) is the selective ionization method of choice in this presented work. In photo ionization systems, selectivity is obtained by using different light wavelengths, i.e. photon energies. Photo ionization using different wavelengths combined with mass spectrometry thus provides a two-dimensional detector with selectivity as first dimension (wavelength) and molecular mass (using soft ionization)

as second dimension [20-24]. The use of photons to ionize compounds is an inherently highly selective mechanism, as photons will only ionize a target molecule if the energy transferred by the photon can be sustained by the target molecule (ionized state or transition state). The two PI methods as discussed in this thesis are the very selective resonance enhanced multi photon ionization (REMPI) [20-24] and single photon ionization (SPI) [25, 26].

4.2 Laser photo ionization (REMPI / SPI) for GC x MS

Both laser pulse based ionization methods, REMPI and SPI are preferably used together with Time-of-Flight mass spectrometry (TOFMS) [21, 23, 27], as the total mass spectra of each laser pulse can be recorded. Mass spectrometric techniques based on the soft photo ionization methods SPI and REMPI are typically well suited for online analytical applications [28-30]. This is due to the high sensitivity, selectivity and inherent softness of the laser based ionization methods.

Photo ionization mass spectrometry also represents an interesting option for the coupling with chromatographic methods. In particular since the online applications mentioned before uses gas inlet systems the coupling to gas chromatography is a logical step. The use of REMPI-TOFMS coupled to gas chromatography have been often described in the literature [31-34]. REMPI-TOFMS allows for a very selective ionization and is applied as such to differentiate between isomers and other compounds that would otherwise be co-eluting in gas chromatographic separation. In this section we will look at REMPI-TOFMS as well as SPI-TOFMS coupled to gas chromatography.

4.2.1 Experimental

Instrumentation

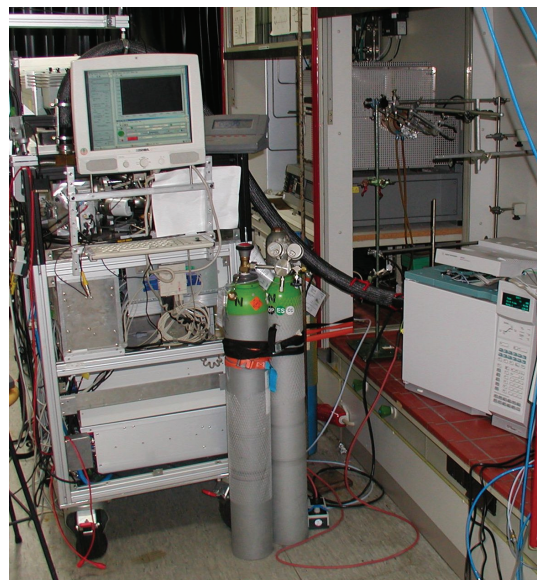
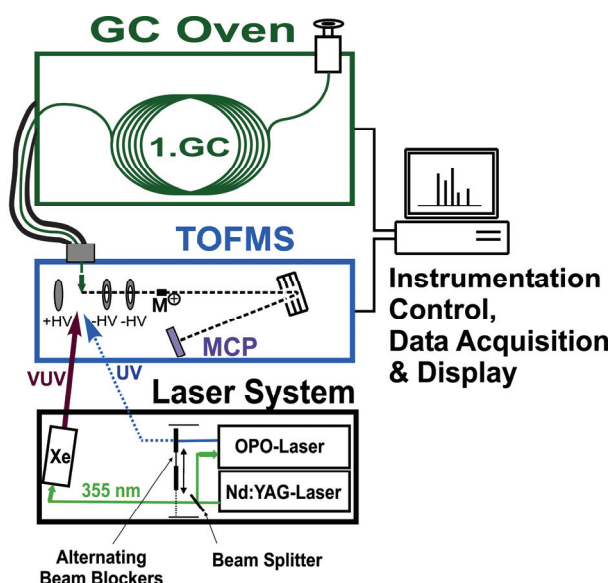


Figure 4.1 Laser based ionization system with both SPI and REMPI [1]

A normal GC system (Agilent 6890, Agilent Technology, Unites States) are used for the first dimension. Interfacing the GC with the MS is a gas inlet system based on a

completely heated 1 m long quartz glass capillary with an inner diameter of 0.2 mm, providing at 250 °C roughly a flow of 2.5 ml/min into the ion source [30, 35-37]. The end of the capillary was modified into a capillary jet [30]. The capillary jet is created in a 0.53 mm ID deactivated silica column where the end of the column is carefully melted closed and the abraded open using fine sandpaper. The gas flow through the exit of the jet is controlled by measuring the flow through the column in a flow meter using a constant back pressure (desired gas flow rate of ~10 mL/min). Additional heating sources in the form of heating lamps were build into the inlet chamber to improve chromatographic peak shapes.

The MS are a combination of electron impact ionization (EI), single photon ionization (SPI), and resonance enhanced multiphoton ionization (REMPI) is used (Figure 2.x). The REMPI/SPI-TOFMS setup is described in detail by Mülberger et al [38]. Fundamental Nd:YAG laser pulses with a wavelength of 1064 nm and a repetition rate of 10 Hz are frequency tripled to a wavelength of 355 nm and used for simultaneous generation of UV and VUV laser pulses for REMPI and SPI ionization, respectively. In doing so, 87 % of the energy is guided into a β -BBO (β -barium borate) crystal of an optic parametric oscillator (OPO) laser (GWU, Germany) to generate laser pulses in a range from 205 to 2500 nm.

A minor fraction (13 %) of the laser-beam is used for frequency-tripling in a rare-gas-cell (Xenon) to generate 118 nm laser pulses. The VUV beam with a wavelength of 118 nm is separated from the fundamental beam to avoid post-fragmentation of ions through multiphoton absorption and is directed into the ion-source for the single photon ionization of the organic molecules in the gas sample.

Two computer-controlled beam blockers are used to select between the REMPI and SPI beams, allowing alternating application of REMPI and SPI with a corresponding frequency of 5 Hz [38]. Both beams are focused underneath the inlet needle in the ion source. The molecular ions generated are extracted into the flight tube of the reflectron time-of-flight mass spectrometer (Kaesdorf Instruments, Germany).

A 30 m x 0.25 mm ID x 0.25 μ m d_f , BPX50 (SGE, Australia) gas chromatographic column was used with temperature program of 5 °C/min from 40 °C to 360 °C. 0.1 μ l diesel sample was injected splitless at 300 °C with helium carrier gas at 30 cm/s linear flow rate (200 kPa constant pressure mode). Chromatograms were recorded using REMPI at 250 nm, 275 nm and 300 nm, SPI at 118 nm. Spectra from the REMPI and SPI were acquired at 10 Hz and averaged to record 5 spectra per second. For comparison reasons the same sample was analyzed with conventional EI at 70 eV, 50 Hz data acquisition.

Samples

A Fischer-Tropsch diesel sample (source: SASOL Ltd., Sasolburg, RSA) with an alkane range from C4 to C28 was used as test sample for demonstration. A diesel-

sample is the matrix of choice since it is a well-studied mixture containing a variety of compounds of different polarity (mono-, di-, and tri-aromatics) and a boiling point range ideal for most GC-separations. Furthermore an n-alkane standard containing C6 to C22 was used for the evaluation of fragmentation in the ion source and as reference for shifting the retention times as described later. The diesel sample has also been analyzed using GC x GC-FID for comparison with the GCxMS results.

4.2.2 Results and discussion [1]

Three modes of GC – photo-ionization MS interfaces are described in the literature[34]: effusive gas inlets, pulsed-supersonic beams and continuous supersonic beams. In an effusive inlet the end of the heated capillary column is typically introduced directly into the ion source[23, 32]. With this technique some of the selectivity potential of the REMPI photo-ionization method is reduced. This is due to the thermal excitation of vibrational and rotational intra-molecular motions of the molecules in the hot eluent. This results in strong overlapping of the UV absorption bands. Effusive inlets are, however, simplistic and have small gas flows into the vacuum as well as a high sensitivity. In supersonic beam couplings, the eluent is mixed with an expansion gas (e.g. He or Ar) and expanded through a restriction nozzle into the vacuum of the ion source. The molecules are cooled to very low temperatures in this process and thermal excitation of the vibrational and rotational intra-molecular motions is reduced [34, 39-41]. The UV spectra of these cooled molecules often feature very sharp absorption bands which could be compared to those obtained in IR spectroscopy fingerprinting and allow selective ionization of target compounds[34, 41]. Usually supersonic jets are pulsed in order to reduce the gas load of the vacuum. For continuous jet expansions differential pumping steps need to be implemented in order to handle the high gas flow into the vacuum system. Supersonic jets are also used to reduce fragmentation in electron impact ionization[42].

In this work, besides a conventional effusive inlet, a novel continuous micro capillary jet system [37] was used for the first time as a GC x MS interface. This device combines the cooling power of conventional jet systems with the low gas flow of the effusive inlet system. A detailed description of micro capillary jet inlet systems can be found in Hafner *et al.* [37]. The cooling efficiency of the used nozzle was measured by scanning the A-X absorption band of nitric oxide, at 226.1 nm with a backpressure of 2 bar, by UV-wavelength scans measured with the previously described REMPI/SPI-TOFMS instrument. The resulting spectra are compared with simulated spectra (LIFBase-software[43]) to evaluate the cooling efficiency (rotational temperature) of the supersonic jet.

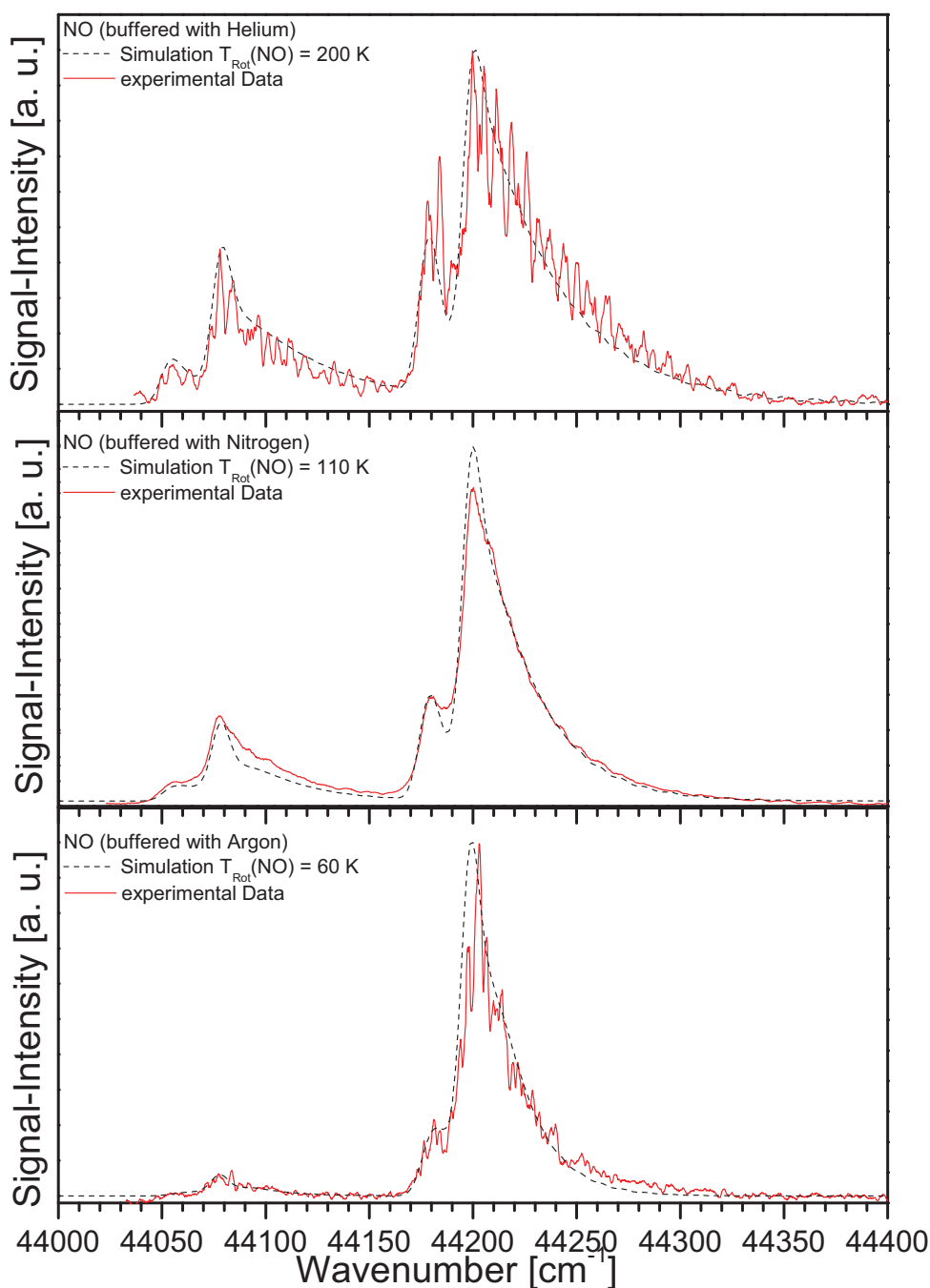


Figure 4.2 Measurement of the cooling efficiency of the continuous micro nozzle supersonic jet interface. The measured REMPI spectrum (ion yield versus photon energy) of the rotational contour of the XY-band of NO is shown with the respective overlain best fitting simulated contour. With Argon a rotational temperature of 60 K is reached, while with nitrogen and helium 110 and 200 K are achieved, respectively [1].

The respective REMPI-spectra of NO obtained by the installed jet with selected buffer-gases are shown in Figure 4.2. For the GC-carrier gas, helium, the resulting rotational temperature was determined to be 200 K. For further investigation of the jet

performance, similar measurements were carried out using the improved cooling efficiency of argon and nitrogen. The data and related simulation are shown in Figure 4.2 indicate a rotational temperature of 60 and 110 K for argon and nitrogen, respectively. The jet capillary inlet into the ion source was heated throughout to 523 K.

First studies with an effusive system exhibited that some thermally induced fragmentation of fragile compounds such as alkanes occurs (Figure 4.3b). When the capillary jet was installed practically no residual fragmentation was detectable. The resulting fragmentation-reduced spectrum of the alkane nonane is shown in Figure 4.3c. Note that the gas-flow into the instrument with the supersonic micro nozzle is not reduced with respect to the effusive inlet. (i.e. no decrease in sensitivity). In Figure 4.3a the 70 eV EI spectrum of nonane is shown for comparison (data source: NIST [44]).

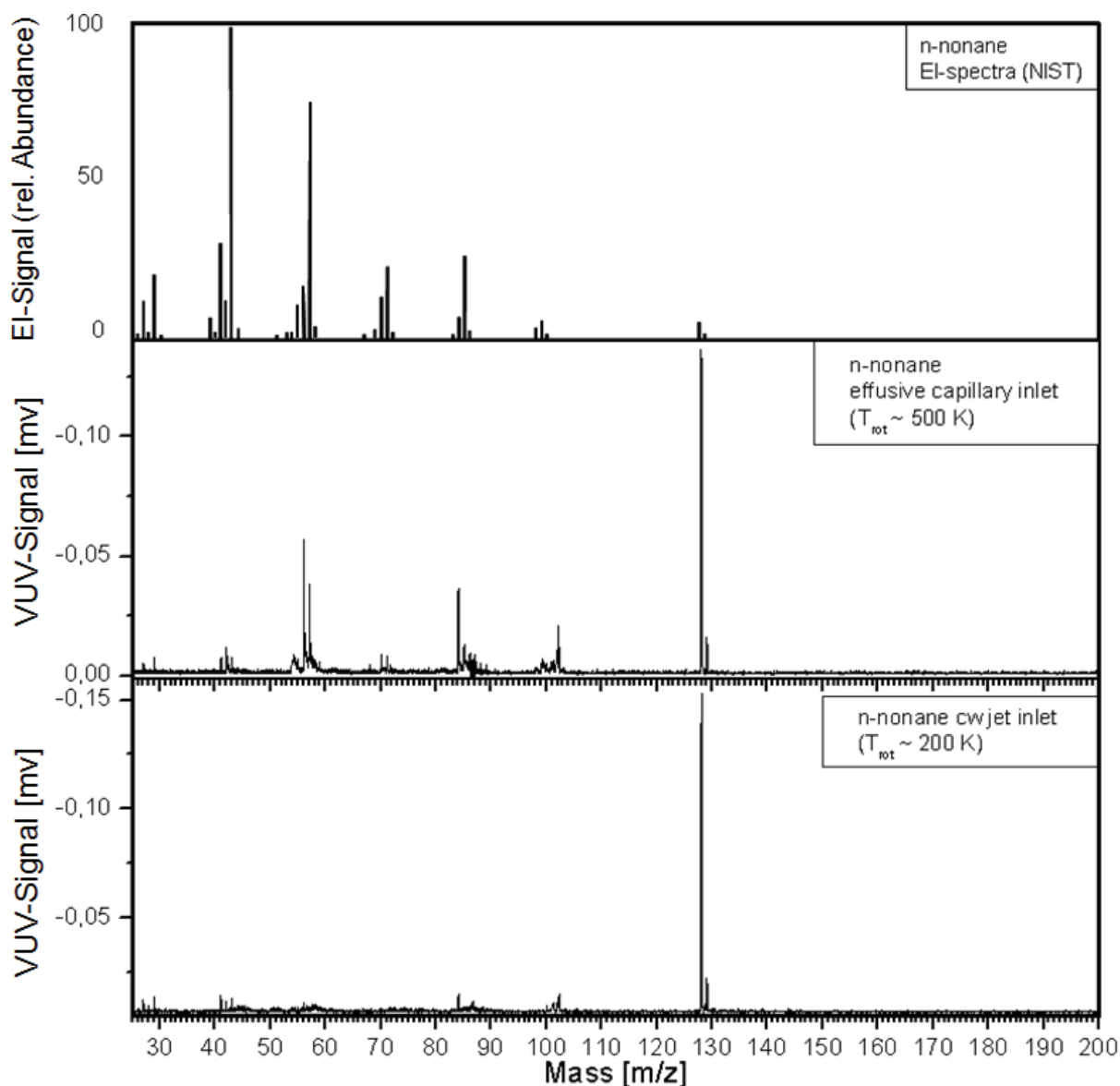


Figure 4.3 Effect of the supersonic jet cooling on the fragmentation of alkanes in the SPI process. Two SPI mass spectra of nonane (b, c) are shown and compared to the EI spectrum obtained from NIST (a). The upper SPI-spectrum (b) is recorded with a conventional effusive inlet. The temperature of the gas molecules is ~ 525 K. Some thermally induced fragmentation is observed. The lower mass spectrum (c) is recorded with the micro supersonic jet nozzle.

The molecules are cooled to ~ 200 K (rotational temp.), the thermal fragmentation has vanished.

The striking advantage of photo ionization methods is their capability to efficiently ionize organic molecules without fragmentation (soft ionization). As the ionization efficiency depends on the photon flux and advanced high flux light sources such as lasers or novel lamps [45] are readily available, high sensitivities can be achieved in photo ionization mass spectrometry (PIMS). Furthermore, PI methods, such as REMPI, can be highly selective, i.e. can be used to selectively address specific

compounds or compound classes. This results in an additional optical dimension for the GC-MS making it possible to further simplify the mass spectra.

In order to demonstrate the properties of the different ionization schemes the summed mass spectral patterns from the whole gas chromatographic run of the diesel samples were recorded. The summed mass spectra in principle shows the mass spectrum that one would obtain if the sample is directly inserted and fully vaporized in the ionization region (e.g. as in an on-line measurement application[28-30]). The summed mass spectra using EI (70 eV), SPI (118 nm) and REMPI (at different wavelengths: 250, 275 and 300 nm), are shown in Figures 4.4 a) -e).

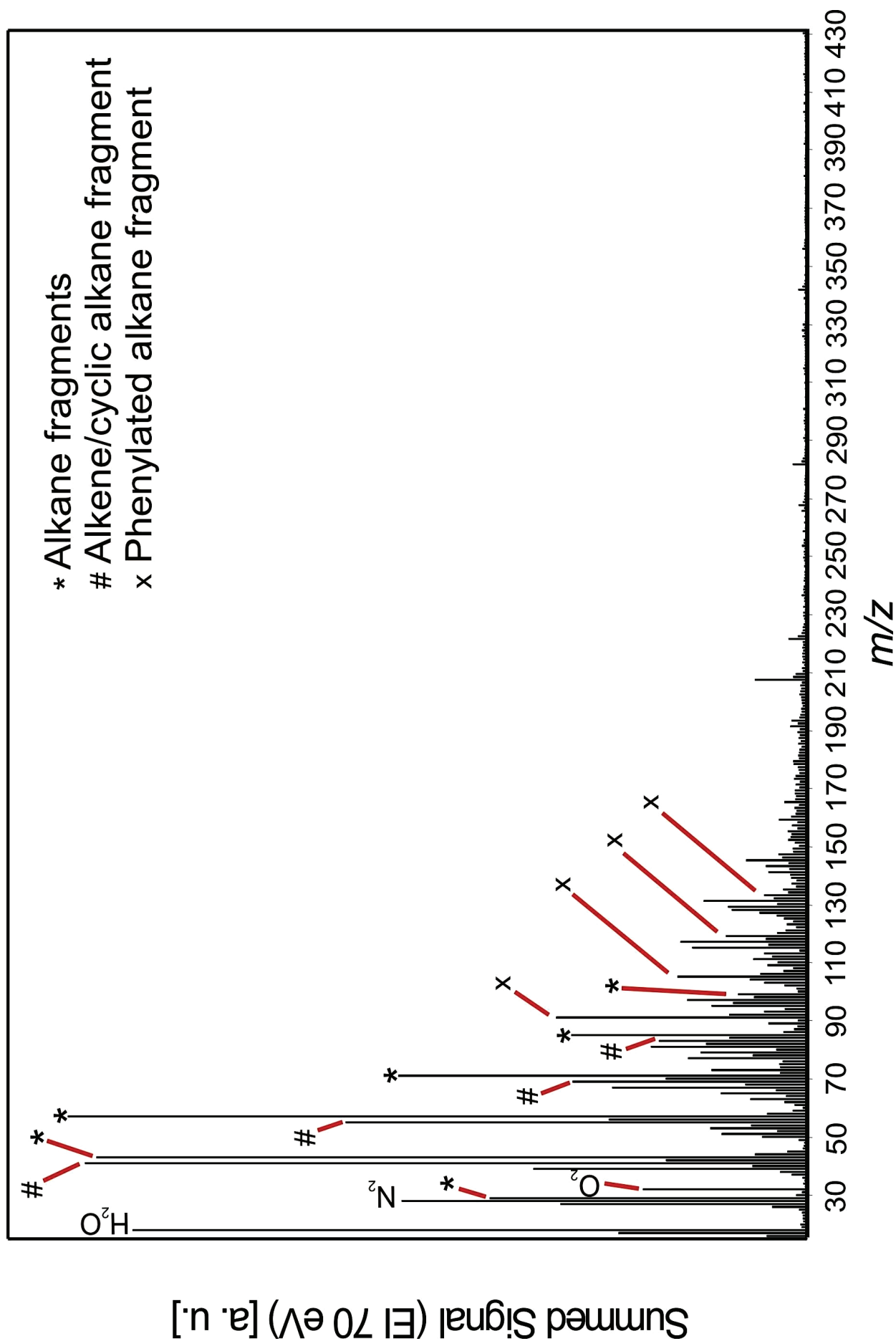


Figure 4.4a Mass spectra summed up over the total gas chromatographic run of the diesel sample recorded with conventional 70 eV electron impact ionization (EI). The mass spectrum is dominated by fragments of aliphatic compounds [1]

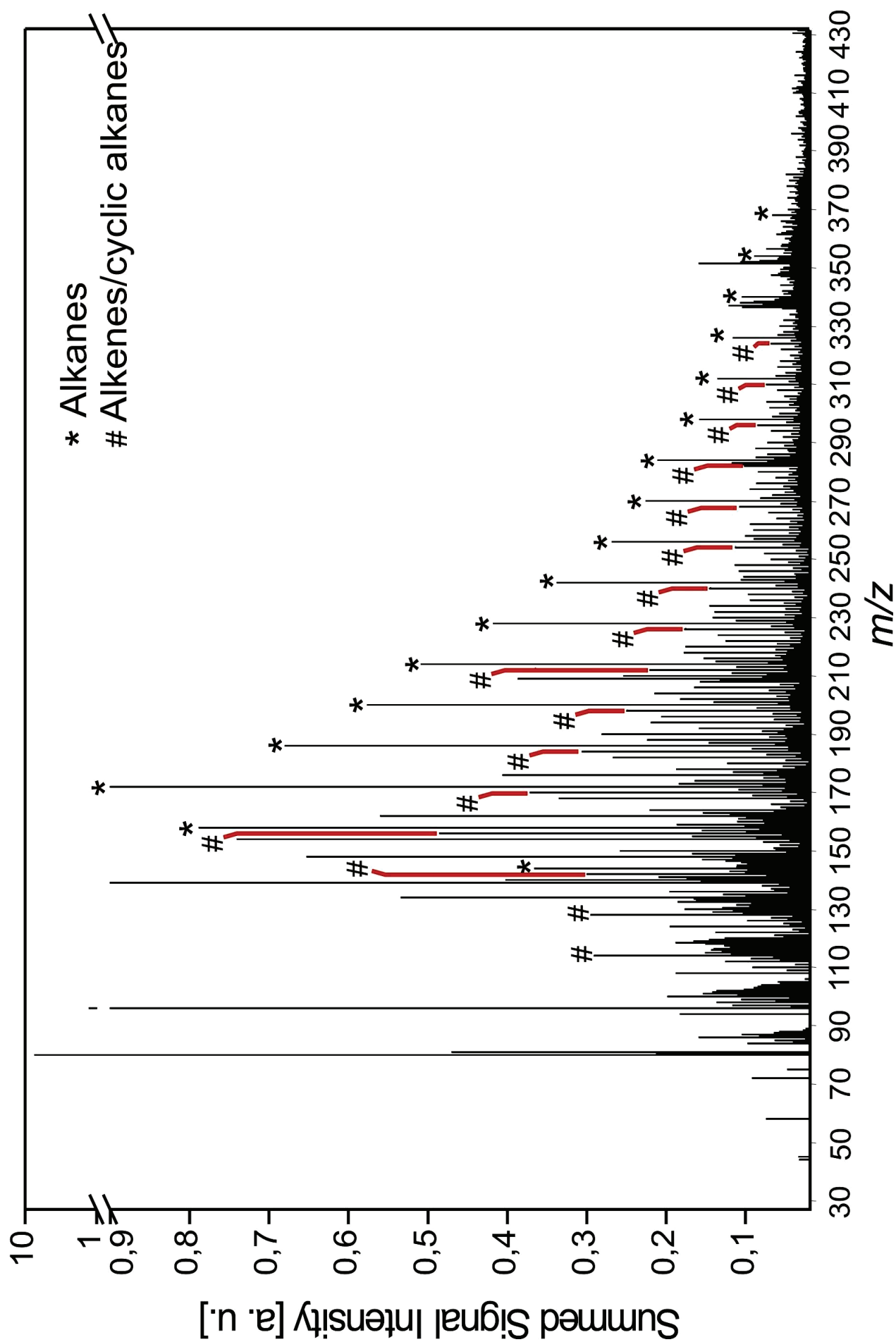


Figure 4.4b Mass spectra summed up over the total gas chromatographic run of the diesel sample recorded with soft SPI ionization (118 nm /10.5 eV). The mass spectrum is dominated by the homologous aliphatic series, most prominent the alkanes [1]

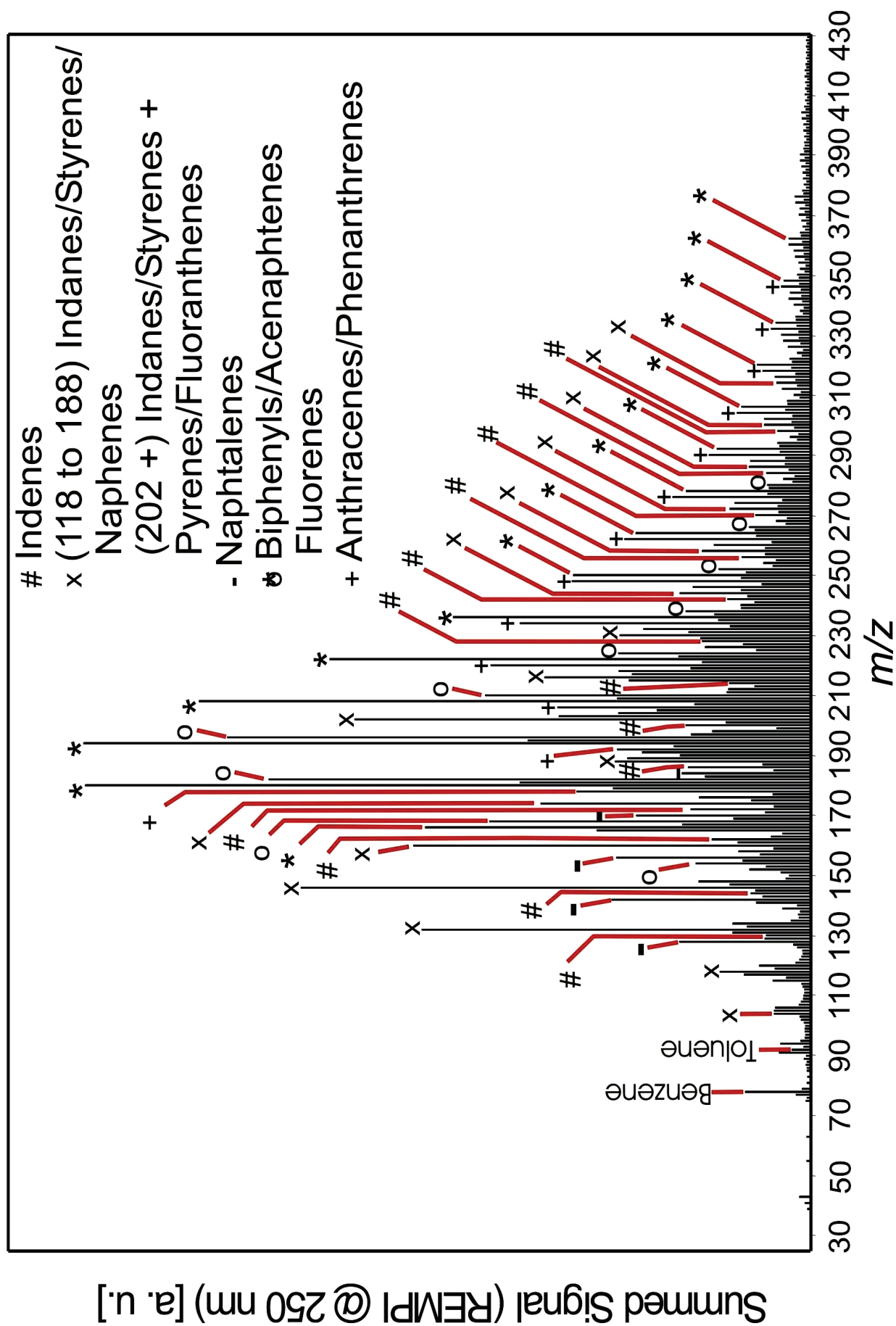


Figure 4.4c Mass spectra summed up over the total gas chromatographic run of the diesel sample recorded with soft REMPI ionization (250 nm /4.95 eV). The mass spectrum shows nearly all aromatic compounds, including benzene and toluene. Aliphatics are suppressed [1]

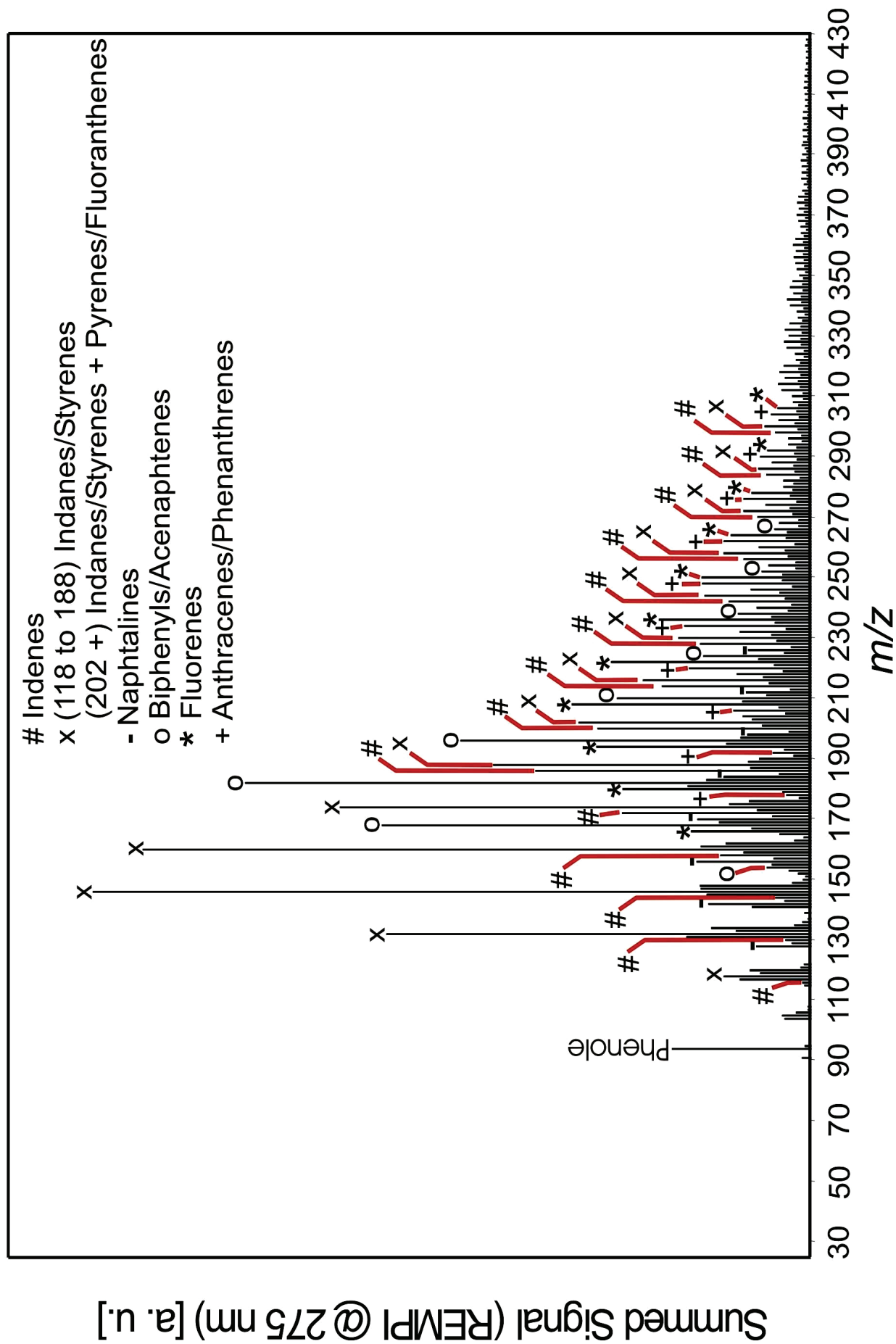


Figure 4.4d Mass spectra summed up over the total gas chromatographic run of the diesel sample recorded with soft REMPI ionization (275 nm /4.5 eV). The mass spectrum shows nearly all aromatic compounds with slightly changes intensity profiles. Toluene and benzene are not visible at this wavelength and phenol is enhanced. Aliphatics are suppressed [1]

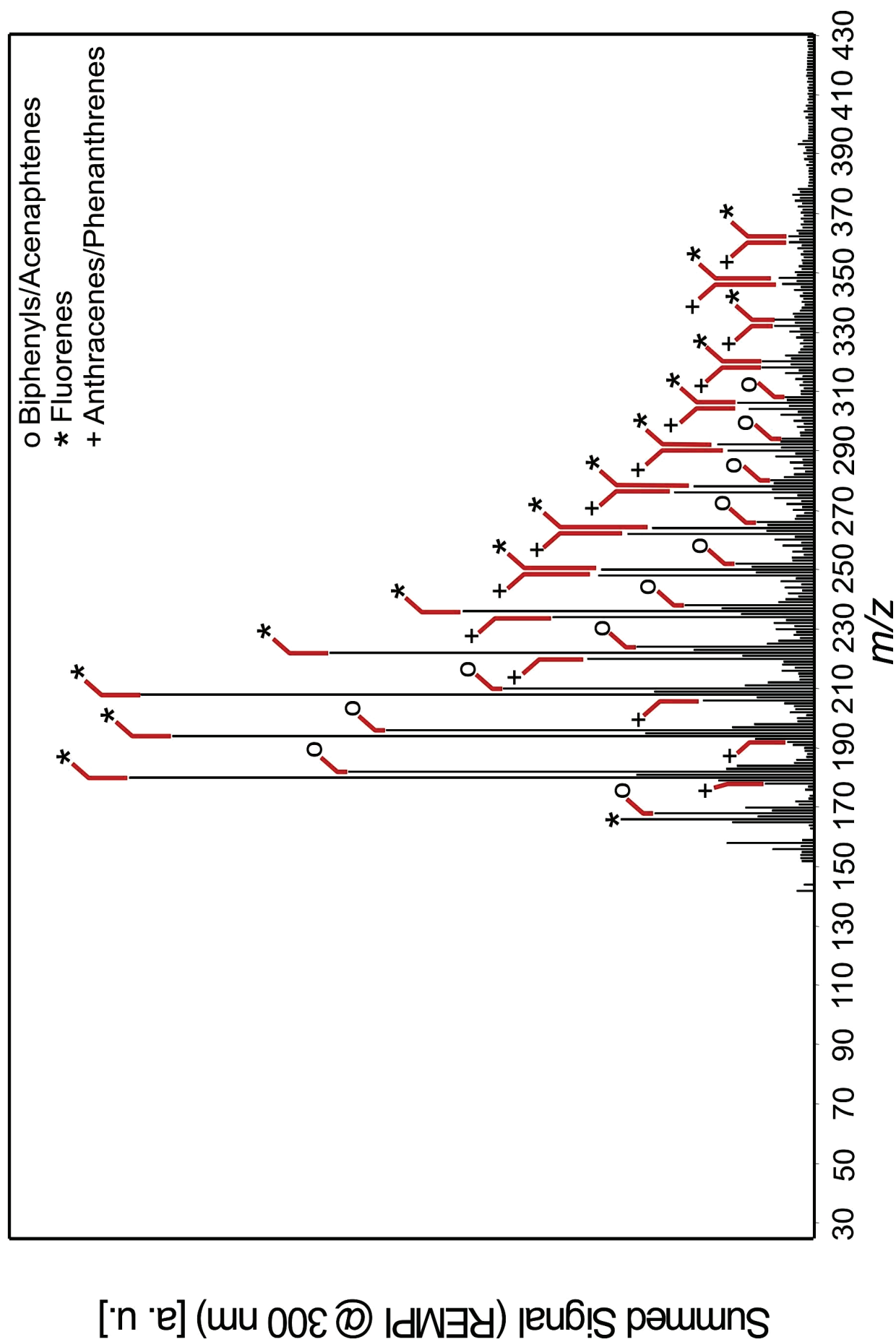


Figure 4.4e Mass spectra summed up over the total gas chromatographic run of the diesel sample recorded with Soft REMPI ionization (300 nm /4.13 eV). The mass spectrum shows only compounds aromatic compounds with three or more rings. Naphthalenes and benzene derivatives are excluded from ionization as well as the aliphatics [1]

The EI mass spectrum (Figure 4.4a) shows solely hydrocarbon fragmentation peaks, subsequently no definite molecular information can be extracted. Thus only the information that the samples predominately consist of aliphatic hydrocarbons can be extracted from the EI mass spectrum. In contrast the mass spectra obtained by soft photo ionization methods show clear molecular information. The summed SPI (118 nm) mass spectrum clearly depicts the homologue row of the alkanes (marked by * in Figure 4.4b). Other homologue rows can also be assigned. Note that each peak may consist of several isomeric compounds. As aliphatic compounds are in higher concentration in the diesel mixture, the respective aliphatic homologue rows are dominating the visible peaks on the spectrum.

The REMPI method does not address aliphatic compounds as they do not have suited absorption bands in the applied UV-range. Moreover, aromatic compounds can be ionized in the used UV-wavelength range. In the Figure 4.4c, d and e the summed REMPI mass spectra of the Fischer-Tropsch Diesel sample, recorded with different laser wavelength (250, 275 and 300 nm) are presented. A large number of homologue rows of alkylated aromatic species are observable.

The differences in the three summed REMPI mass spectra visualize the wavelength-dependent differences in the REMPI efficiency for different aromatic compound classes. While with a laser wavelength of 250 nm the vast majority of the aromatic compounds are ionized (a more or less “universal aromatic ionization”), the number of accessible aromatic homologue rows decreases towards longer wavelengths. This is mainly due to the decrease of the two-photon energy with increasing wavelengths. Compounds with ionization potentials higher than the two-photon energy are excluded from ionization. Furthermore there is an influence of the UV spectroscopy as some compound classes do not have suited UV absorption bands at all used wavelengths. The homologue rows of e.g. the isobaric compounds anthracene and phenanthrene (starting at $m/z = 178$) as well as the homologue rows of fluorenes (starting at $m/z = 166$) and the isobaric compounds biphenyl and acenaphthene (starting at $m/z = 154$) are detectable with all applied REMPI laser wavelengths.

With a laser wavelength of 250 nm (two-photon energy: 9.91 eV) for REMPI most polyaromatic compounds including the naphthalenes are ionized efficiently. Furthermore, homologue rows of compounds with a single aromatic ring such as benzenes, naphthenes, styrenes, indanes are ionized. With 275 nm (two-photon energy: 9.01 eV) some of the polycyclic compounds are less prominent. Benzene (IP: 9.2 eV) and toluene (IP: 8.8 eV) are not detectable anymore while phenol is now accessible.

With a REMPI laser wavelength of 300 nm (two-photon energy: 8.26 eV) the picture has changed more drastically. All compounds with a single aromatic ring (naphthenes, benzenes etc.) are now excluded from ionization. The two-ring aromatic naphthalenes still are ionized but are comparably weak due to very weak UV transition at this wavelength. Therefore, the spectrum is largely simplified, showing predominately three-ring aromatics.

If the whole complexity of a sample should be revealed, however, the mass spectral information is not sufficient. The gas chromatographic separation is required to distinguish isobaric and isomeric compounds such as e. g. the different branched and linear alkanes, the alkenes and cycloalkanes or the homologues row of isobaric carbon skeletons such as phenanthrene and anthracene (starting at $m/z = 178$), biphenyl and acenaphthene (starting at $m/z = 154$) or indane (starting at $m/z = 118$) and styrene (starting at $m/z = 104$).

As discussed above, the data of a GC-MS data can be represented as a two-dimensional contour plot when the retention time is plotted against the m/z values. This is shown in the exemplarily for the GC-SPI-TOFMS data set (Figure 4.5a and 4.5b). Due to the soft ionization capability of SPI only molecular ion signals are present, thus resembling a boiling point type separation obtained with a non-polar gas chromatographic column. A retention time shift was applied to eliminate the influence of the temperature program and increase the orthogonality of the two separation axes in analogy to the work of Wang *et al.* [14] (Figure 4.5a). The retention time axis is adjusted so that the n-alkanes in the final GC x MS plot a straight line form. The adjustment is achieved by doing a 10 point polynomial fit on the retention times of the n-alkanes and then shifting the retention times so that the n-alkanes align with one another.

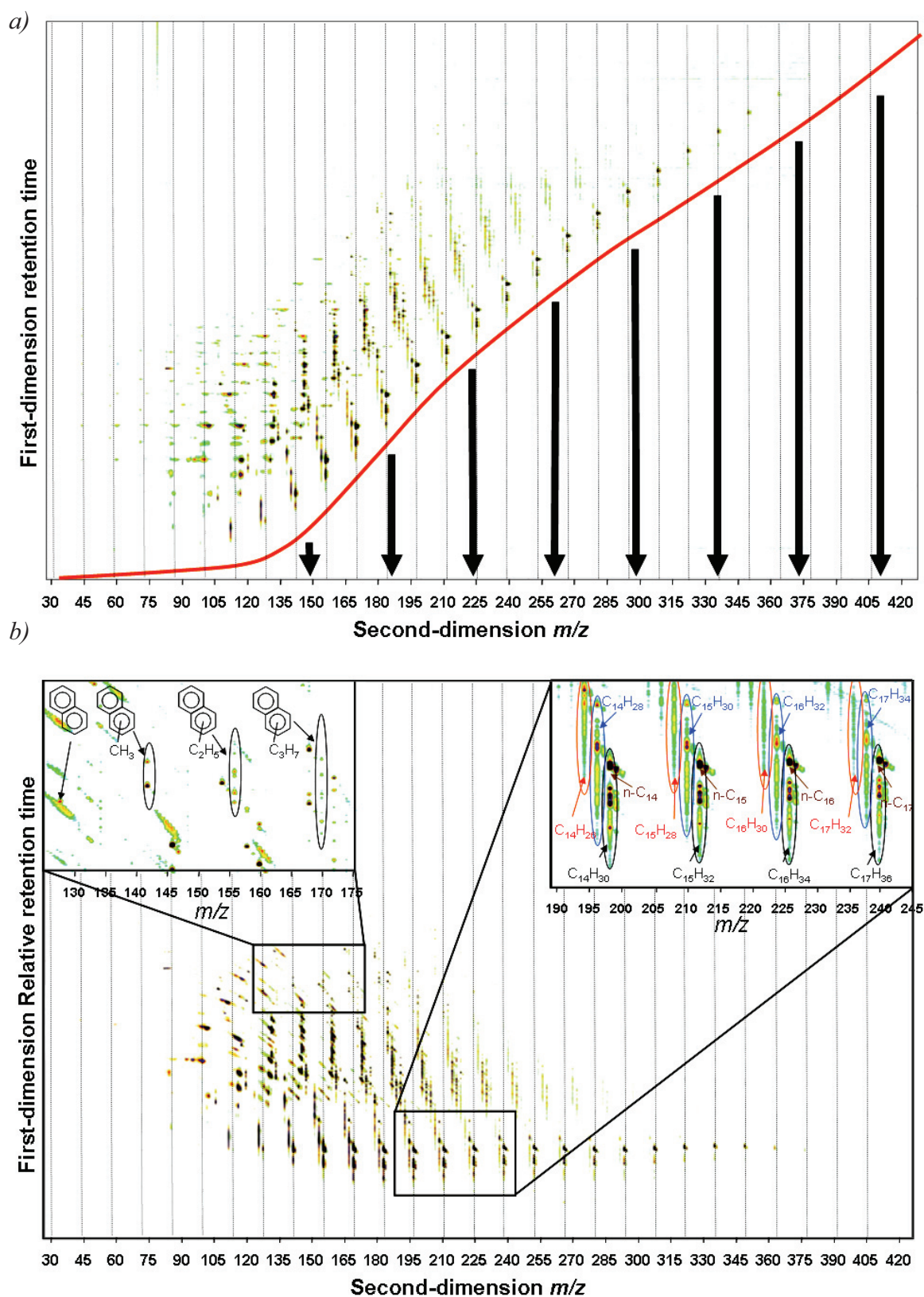
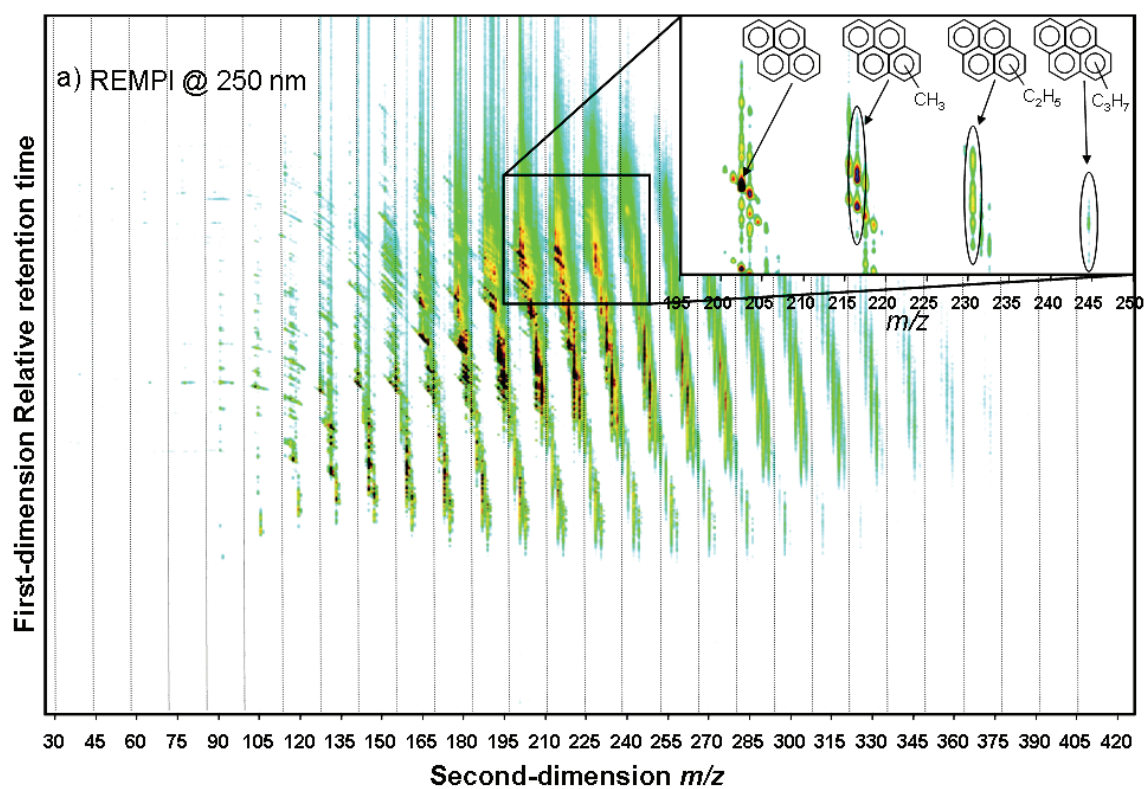


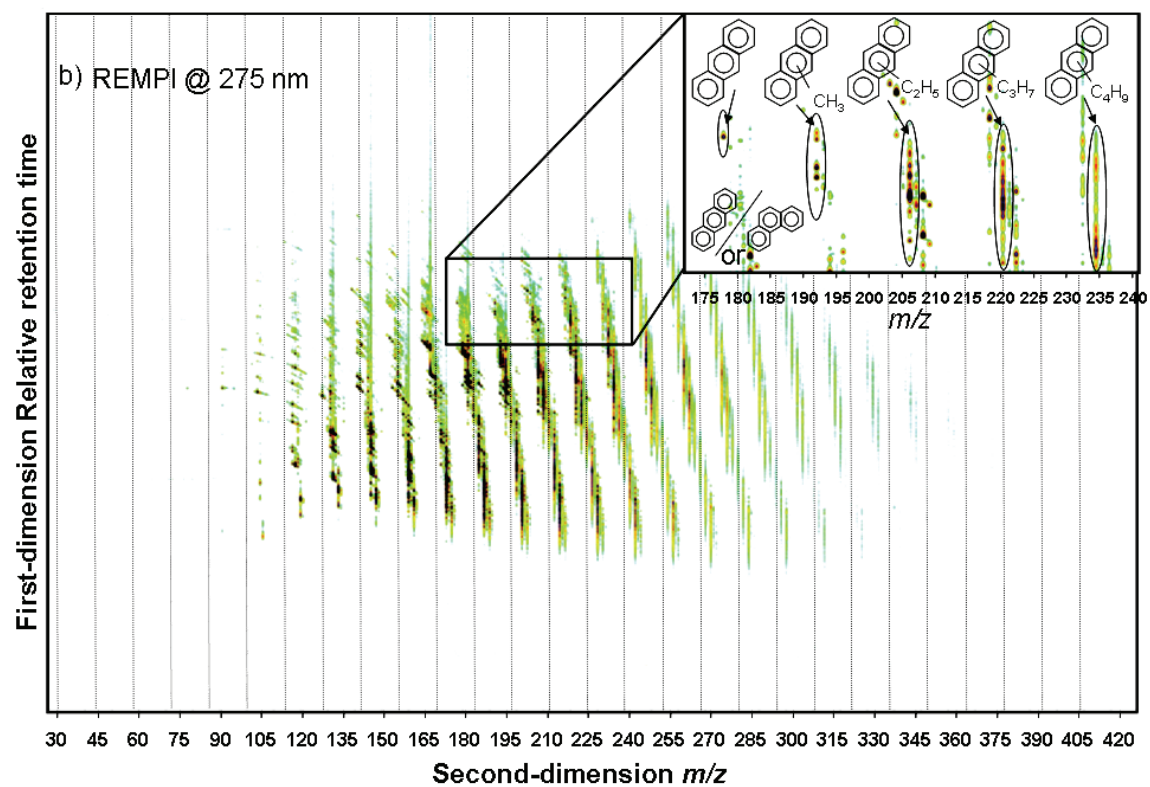
Figure 4.5 Comprehensive gas chromatography coupled to soft ionization mass spectrometry (GC x MS) representation, using SPI-mass spectrometry. With a) the GC x MS chromatogram before transformation and b) the chromatogram after doing the 'Kovats Index' like transformation of the retention time axes [1].

With the retention time adjustment, the temperature program influence of the chromatographic separation is “eliminated”. Thus the relative time scale now only represents the polar separation component of the gas chromatographic separation (GC x MS plot). In the GC x SPI-TOFMS plot (Figure 4.5b) compounds with an ionization potential below 10.5 eV (~118 nm) are appearing. The enlarged section depicts the aliphatic compounds from C₁₄ to C₁₇ with the alkanes C_nH_{2n+2}, the cyclic alkanes or alkenes C_nH_{2n}, and the dienes, cyclic alkenes or alkynes C_nH_{n-2} and demonstrate the type of separation achieved through the comprehensive combination of GC and SPI-TOFMS. The aliphatic compounds in the sample dominate the GC x MS plot, as is expected from diesel samples. Aromatic compounds also are well detectable, but, according to their lower abundance, appear at considerably smaller signal intensities. Note that by changing of the wavelength of the SPI process some compounds classes can be excluded from ionization. For example SPI-TOFMS systems based on newly developed highly efficient VUV-lamps are available at various wavelengths[25, 45] and can be used as a selective GC detector. With a wavelength of 126 nm (9.86 eV), for example, most aliphatic compounds would be excluded and the GC x SPI-TOFMS plot would be dominated by aromatic species and conjugated unsaturated species. A similar effect, i.e. the selective detection of aromatic species, but at a tremendously increased sensitivity can be obtained by application of the laser based resonance enhanced multiphoton ionization (REMPI) method. With ion yields of up to the 10 % range in the laser focus, REMPI is one of the most efficient ionization methods for aromatic compounds[46].

a)



b)



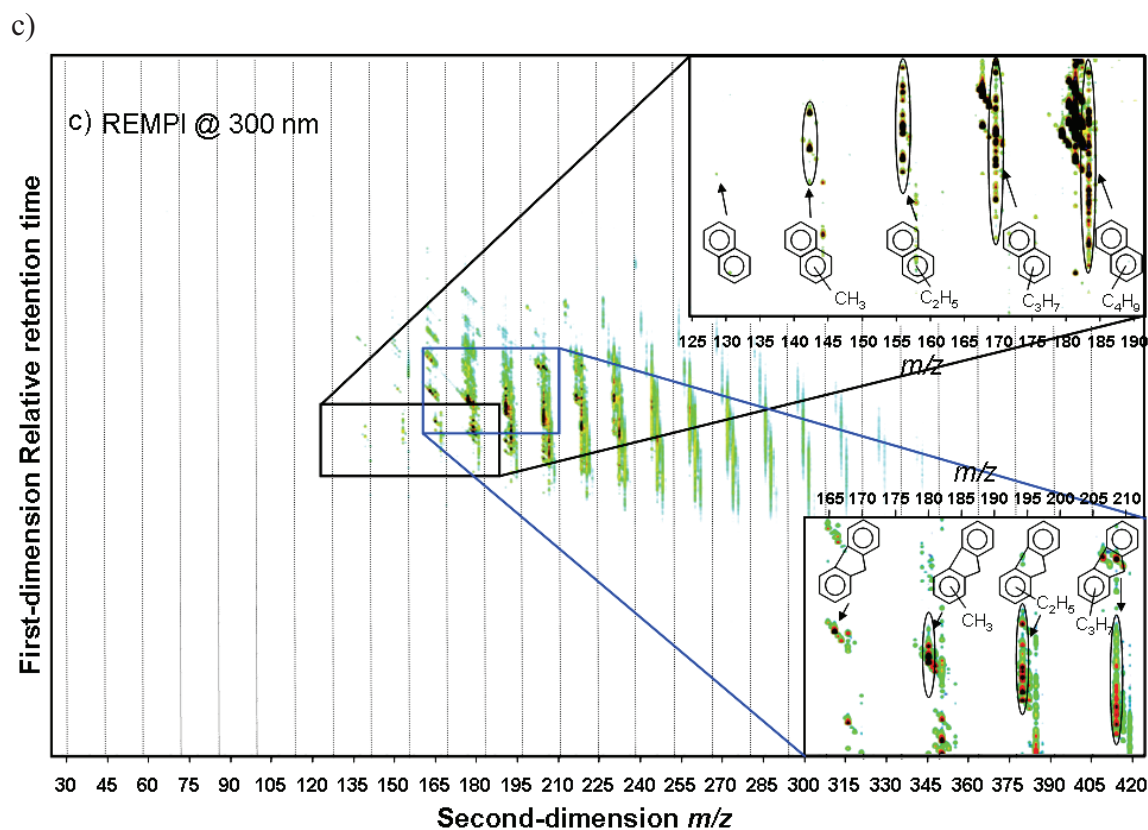


Figure 4.6 Transformed GC x MS representation of the REMPI-mass spectrometry coupled to gas chromatography. The retention times being adjusted to the same polynomial function used in the GC x SPI TOFMS retention shift. Three different REMPI wavelengths were used a) 250 nm, b) 275 nm and c) 300 nm [1].

In the Figures 4.6a-c three GC x MS plots obtained by the REMPI ionization method at the wavelength 250, 275 and 300 nm are shown. As REMPI only addresses aromatic compounds at the applied laser wavelength, this is an example of highly chemical structure selective ionization. From the GC x REMPI-TOFMS contour plots similar trends in compound class selectivity can be seen as in the summed mass spectra at these wavelengths (Figure 4.4). With longer wavelengths the accessible compound classes are reduced. On each of the GC x REMPI-TOFMS plots a small section is enlarged to demonstrate the separation possibilities of the comprehensively coupled gas chromatography and soft REMPI ionization MS technique. In Figure 4.6a the GC x REMPI-TOFMS plot obtained with as laser wavelength of 250 nm is depicted. Here, most aromatic compounds are addressed. The inset shows the enlarged origin area of the homologue row of the four-cyclic aromatic pyrene system (starting at 202 m/z). According to the increasing non-polar character the relative retention time tends to decrease with increased alkylation demonstrating the chemical logics behind the obtained comprehensive GC x MS separation. Increased alkylation (or alkylation degree) refers to the increased amount of alkyl groups vs. functional groups in the molecule. In the GC x REMPI-TOFMS plot obtained from the data with 275 nm laser ionization wavelength (Figure 4.6b) some of the di- and tri-aromatic systems are particularly efficiently ionized. This is seen in the extracted sections

showing the origin region of the three-ring aromatic homologous series of the isobaric anthracene and phenanthrene (starting at 178 m/z). The GC x REMPI-TOFMS plot obtained from the 300 nm laser wavelength (Figure 4.6c) shows the least compounds ionized, as e.g. all compounds with only a single aromatic ring are now excluded from ionization. Due to weak UV absorption also the naphthalenes as well as some larger PAH are considerably weaker at 300 nm. The inset shows the region of the homologue rows of the relatively weaker ionized naphthalene series (starting at 128 m/z) as well as the more intense fluorine series (starting at 166 m/z).

A particularly interesting representation of chemical information in the GC x MS plot can be obtained if the combined SPI-TOFMS and the REMPI-TOFMS (250 nm) data is displayed (Figure 4.7). Peaks obtained by SPI are depicted in red, while the REMPI data is displayed in blue. In this representation the blue peaks are thus originating from the aromatic systems while the predominant part of the red colored peaks are belonging to aliphatic structures. Note that the intensity of the aromatic systems is exaggerated due to the higher ionization efficiency of REMPI. However, in principle it is possible to apply suitable scale factors in order to adjust the sensitivities of REMPI and SPI. The additional chemical classification allows the ad-hoc differentiation of overlapping peaks e.g. in the naphthene region of the GC x MS chromatogram. The combination of the GC x MS separation is very comparable to the separation achieved by the conventional two-dimensional comprehensive gas chromatography approach (GC x GC). In Figure 4.8 a GC x GC separation of the same diesel samples is shown. Similar groupings of different compound classes can be made in both GC x GC and GC x MS like the differentiation between aliphatics, mono-aromatics, di-aromatics, tri-aromatics and even higher aromatics as indicated on the GC x MS plot.

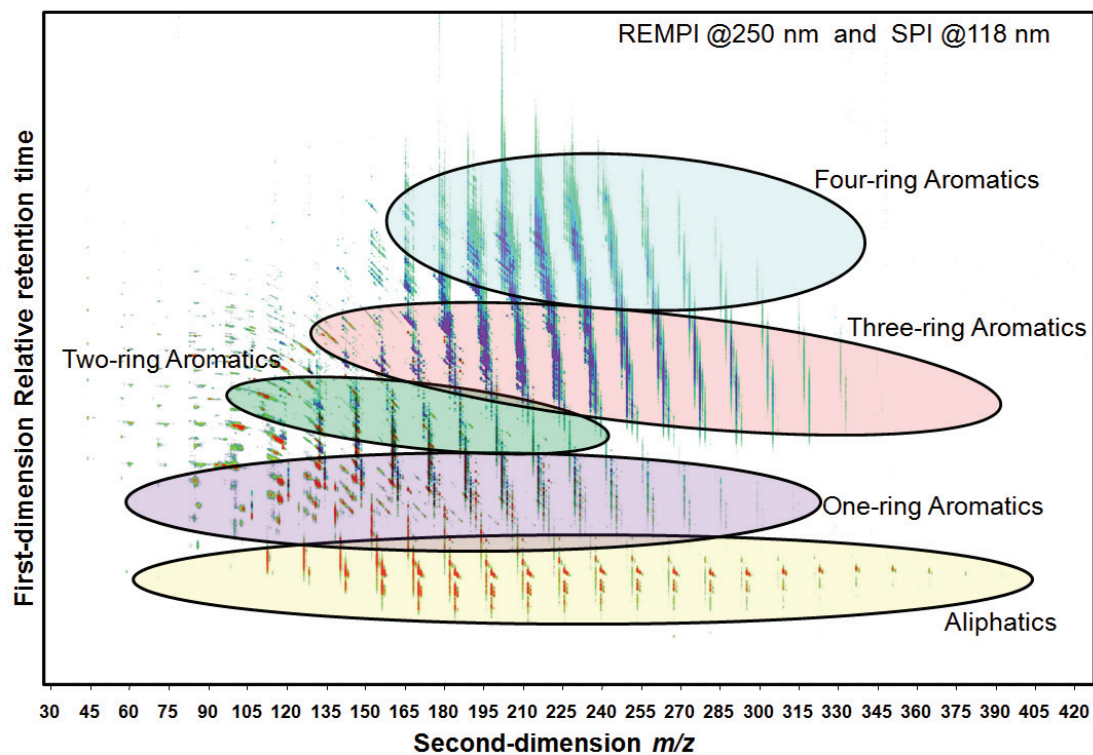


Figure 4.7 GC x SPI TOFMS and GC x REMPI TOFMS (250 nm) plotted on the same two-dimensional contour plot for an overview of the total ionized molecules. The SPI peaks are color coded from green to blue (blue highest intensity) and the REMPI from green to red (red highest intensity). The aliphatics and the different aromatic species are encircled for comparison with GC x GC results (Figure 4.8) [1]

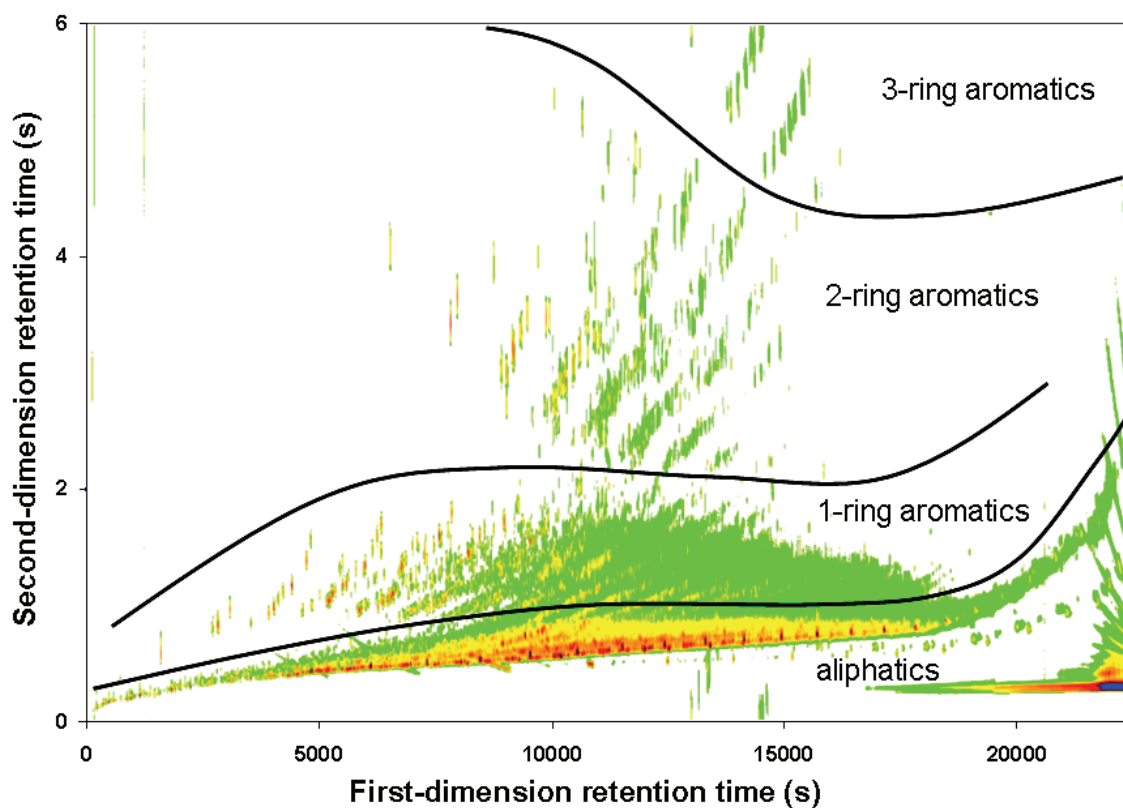


Figure 4.8 Comprehensive two-dimensional gas chromatography plot of the same diesel sample, indicating similar compound class groupings as obtained through the GC x MS analysis (Figure 4.7) [1, 47]

Note that the GC x REMPI-TOFMS and GC x SPI-TOFMS data was obtained in separated runs in the presented work. However, the used homebuilt TOFMS system has the ability to record simultaneously REMPI- and SPI-TOFMS data (at 5 Hz respectively) as well as the electron impact data (EI). Thus within a single chromatographic run the above mentioned aromatic/aliphatic selective GC x MS plot can be obtained as well as the conventional GC-EI-MS data. The EI-MS data allows the use of the conventional fragmentation libraries for identification of sufficiently separated peaks. This, however, is not relevant for the discrimination of branched hydrocarbons, since the distinction of isomers in most cases is not possible. The combination of comprehensive separation (i.e. the position of a peak in the GC x MS plane) and the chemical selectivity introduced by the application of different photo-ionization methods (here: REMPI and SPI for discrimination of aromatic and aliphatic structures) represents a novel separation/classification concept.

The photo-ionization selectivity can be further changed by using different ionization wavelengths for REMPI or SPI. With e.g. different wavelengths for the REMPI ionization process specific aromatic compound classes can be either emphasized or suppressed. Therefore, the selectivity of the comprehensive separation can be adjusted to the separation/analysis problem. An additional possibility to further increase the

separation power of the analysis system is to use a high resolution TOFMS system for determination of the elemental composition. The sensitivity of the REMPI process is extremely high for aromatic compounds[46], so that despite of the relatively low duty cycle MS detection sensitivities equal or better as with EI are obtained. The sensitivity of laser based SPI method is lower than the REMPI process. This is due to the rather inefficient conversion of UV laser photons to VUV photons in the third harmonic generation process[28]. The sensitivity of the SPI method is proportional to the applied VUV photon flux therefore it can be increased by using more intense VUV light sources. This is advantageous in comparison to some other soft ionization methods such as field ionization (FI) [Wang] which are rather insensitive without much potential for further optimization.

It is however needed to evaluate the separation efficiency of GC x MS and compare that with the already established comprehensive two-dimensional techniques such as GC x GC. In GC separation efficiency is evaluated through the determination of chromatographic plates or through the calculation of the chromatographic peak capacity. The peak capacity in a comprehensive two-dimensional GC is given by the multiplication of the peak capacities obtained in both chromatographic dimensions [37]. In GC x MS, however, the peak capacity of the first-dimension has to be multiplied by the mass resolution of the second-dimension to obtain the separation efficiency of the two-dimensional technique.

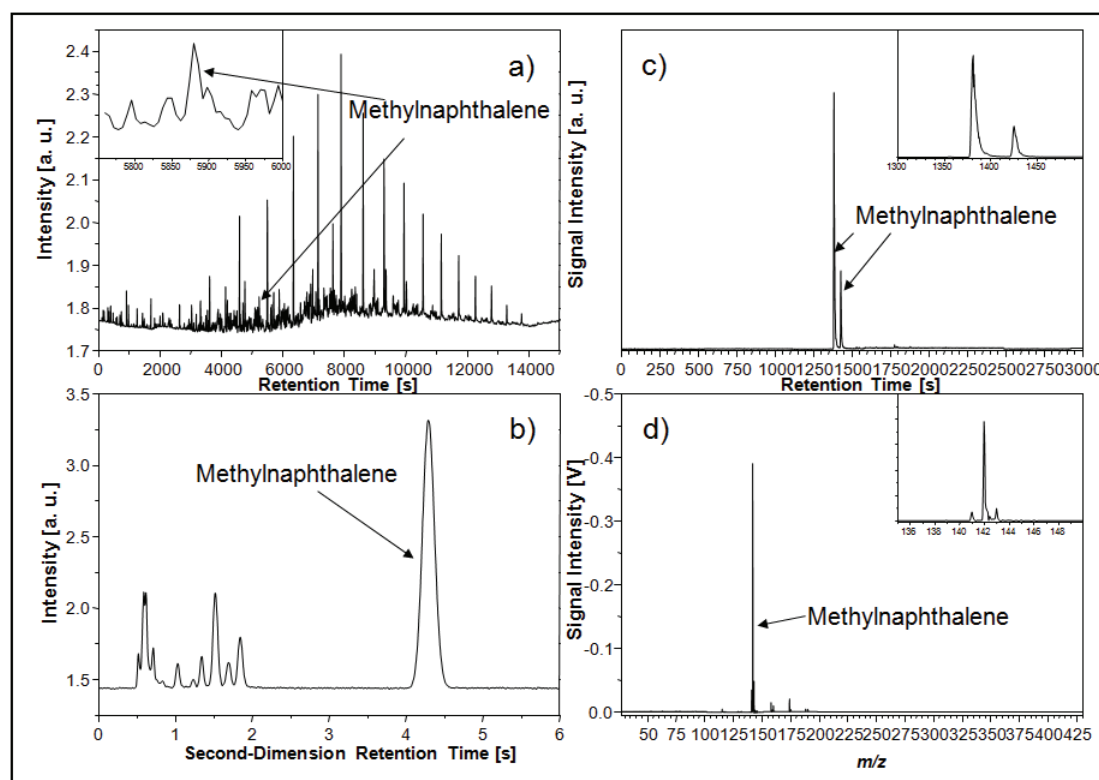


Figure 4.9 The comparison of the separation obtained through GC x GC and GC x MS. The first-dimension chromatogram of a diesel sample is shown in (a) with an extracted section of methyl-naphthalene peak. The second-dimension chromatogram is shown in (b). A single ion chromatogram (142 m/z) of the GC x SPI-TOFMS is shown in (c) with the mass spectra (d) of the methyl-naphthalene [48].

Figure 4.9 shows a two-dimensional chromatographic peak of a methyl-naphthalene in the first chromatographic dimension as well as in the second chromatographic dimension. The GC x GC results not further discussed in this thesis is from an optimized GC x GC run of the same diesel sample using a non-polar first-dimension column (0.25mm ID, RTX1, Restek) and a polar second-dimension column (0.1mm ID, RTX-Wax, Restek) with a 6 second modulation period. Using the formula for calculating peak capacity:

$$n = 1 + \frac{\sqrt{N}}{4} \ln \frac{t_n}{t_1}$$

n = peak capacity,

N = theoretical plate height,

t^n = retention time of last peak,

t_1 = retention time of first peak

It is thus possible to calculate the peak capacities in both the first and second dimension column. For a 30 m first-dimension column where for example $N = 100\,000$ plates, $t_1 = 90$ s, $t_n = 15\,000$ s and $H = 0.3$ mm, the peak capacity can be calculated

to 452 peaks. Similarly for a 1 m second-dimension column where $N = 3\,333$ plates, $t_1 = 0.5$ s, $t_n = 5.5$ s and $H = 0.3$ mm the peak capacity can be calculated as 35 peaks. The combined peak capacity of the comprehensive two-dimensional system is thus approximately 15 820 peaks. For the multiplication rule to apply for the combined two dimensions it has to be assumed that no separation is lost in either dimension.

For the GC x MS the peak capacity of 452 peaks in the first-dimension can also be assumed, but to calculate the overall separation capacity of the two-dimensional system the resolution of the mass spectrometer need to be used. The TOFMS used in this work has a mass resolution of 1800. However, in the mass range used (50-300 m/z) integration usually is done over full masses. Thus the “peak capacity” of the mass spectra used could thus be seen as 250 mass peaks. The overall peak capacity of the GC x MS system can finally be calculated as 452 chromatographic peaks multiplied by 250 mass peaks results to 113 000 peaks. Note, that if the physical mass resolution is high enough to solve the elemental composition, much higher separation efficiency is obtainable.

4.3 Laser photo ionization (SPI) for GC x GC x MS

The resolving power of GC x MS can be even further improved by the addition of another separation dimension. Since comprehensive two-dimensional gas chromatography GC x GC is easily implemented in the place of one-dimensional GC it presents an interesting option to increase the separation dimensions. When SPI-TOFMS is coupled to a two-dimensional gas chromatographic system (GC x GC), the resulting system can be viewed as a comprehensive three-dimensional separation method. Prerequisite for the combined technique to be a three-dimensional separation method is to have the three dimensions as orthogonal as possible to each other. This would imply that the different stationary phases used in the GC x GC separation should be as orthogonal as possible to the molecular mass obtained through the soft ionization and used as the third-dimension. Potential GC x GC stationary phases [49] would include polar separation (hydrogen bonding on a poly-ethylene glycol column), polarizability (pi-pi interactions on a 50% phenyl polysilphenylene-siloxane column) and possibly molecular size or structure through the use of liquid crystal phases. GC x GC however have some high requirements for the detector in especially the detection frequency. In this section laser-SPI-TOFMS will thus be evaluated as a potential detector for GC x GC.

4.3.1 Experimental

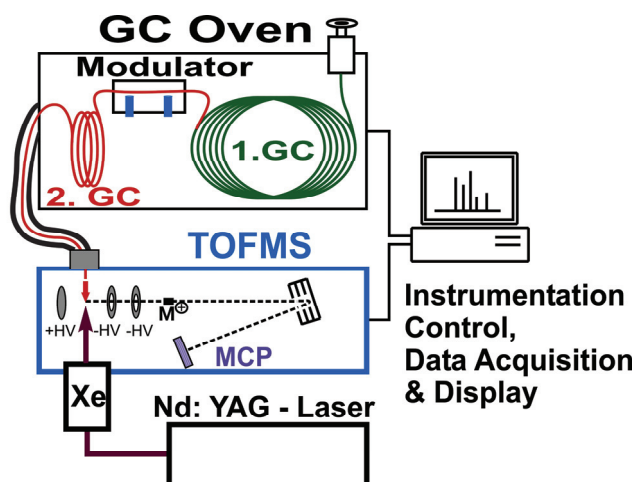


Figure 4.10 Instrumental setup of the three dimensional GC x GC x SPI TOFMS

The TOFMS system (described in detail by Mulberger *et al* [50]) designed originally for online applications were modified for fast GC conditions by reducing the typical transfer line used in online application from 1.5 m to about 30 cm. The ionization chamber was also installed with more heating elements to reduce gas chromatographic tailing.

The GCxGC-SPI TOFMS was done with a CO₂ duel jet modulator (Thermo trace GCxGC, Thermo, Italy). The first-dimension column was a 30 m x 0.25 mm ID x 0.25 μm d_f , Solgel-wax (SGE, Australia) and a 2 m x 0.1 mm ID x 0.1 μm d_f , BPX50 (SGE, Australia) as second-dimension. A temperature program of 1 °C/min from 50 °C to 250 °C was applied together with a modulation period of 20 s. The mass spectra corresponding to the interval from 100 °C to 150 °C were recorded at 5 Hz (10 Hz acquisition 2 point average). 0.1 μl of a diesel sample was injected at a 50:1 split ratio with helium as carrier gas at 30 cm/s linear flow rate.

4.3.2 Results and discussion [48]

The choice of chromatographic columns in this three-dimensional separation approach demands that the common view of polar and un-polar chromatographic columns be revisited. This of particular importance since the commonly revered to un-polar columns also implicates columns separating compounds on a “volatility” basis. The third-dimension applied in this work also uses molecular mass as a separating dimension which is in most cases directly related to the compound’s “volatility”. Two chromatographic dimensions thus have to be chosen such that they are unique to one another and to the mass spectrometric dimension. As first-dimension separation were based on Hydrogen bonding between compounds and the stationary phase while the second-dimension were more based on π -bonding between the compounds and the stationary phase. The resulting two-dimensional chromatograms using either single photon ionization or electron impact ionization can be seen in Figure 4.11. As was expected from using a 10 Hz laser system for the SPI, the required data points of at least 5 per chromatographic was difficult to reach. This is mostly due to the extreme sharp chromatographic peaks generated through GC x GC. The second separation column is operated under fast GC conditions such that the dimensions of the column (short length and small inner diameter) produce chromatographic peaks with base width is between 50 and 500 ms. The use of laser ionization with a maximum repetition of 10 Hz would thus not be sufficient for conventional GC x GC conditions. To obtain sufficient data points per chromatographic peak so that resolution is not lost at least 4 data points per chromatographic peak is required. For this experiment the second column dimension and conditions were thus altered from the conventional GC x GC column dimensions. The length of the column was doubled to provide double the peak widths and a longer modulation period (20 s) was used to allow all the peaks to elute. The temperature program rate for the first dimension was also lowered down to 1 °C per minute not to loose resolution obtained in the first dimensions due to the longer modulation period. The required minimum amount of data points (5 points per peak) could however still not be achieved for the low retained species. However, the experiment demonstrates for the first time the feasibility for a three-dimensional separation using GC x GC x MS.

Figure 4.11 shows the resulting two-dimensional plot of the GC x GC with the mass spectra summed up to give a total ion chromatogram (TIC). The resulting chromatogram, although not optimized for comprehensive two-dimensional separation, shows that separation with high orthogonality can still be achieved using the selected stationary phases. For each two-dimensional data point a mass spectra can be obtained, displaying the molecular ions of the analyzed data point.

Combining the three-dimensional data of first-dimension retention time, second-dimension retention time and mass spectrometry the graphic displayed on a two-dimensional piece of paper becomes considerably complex.

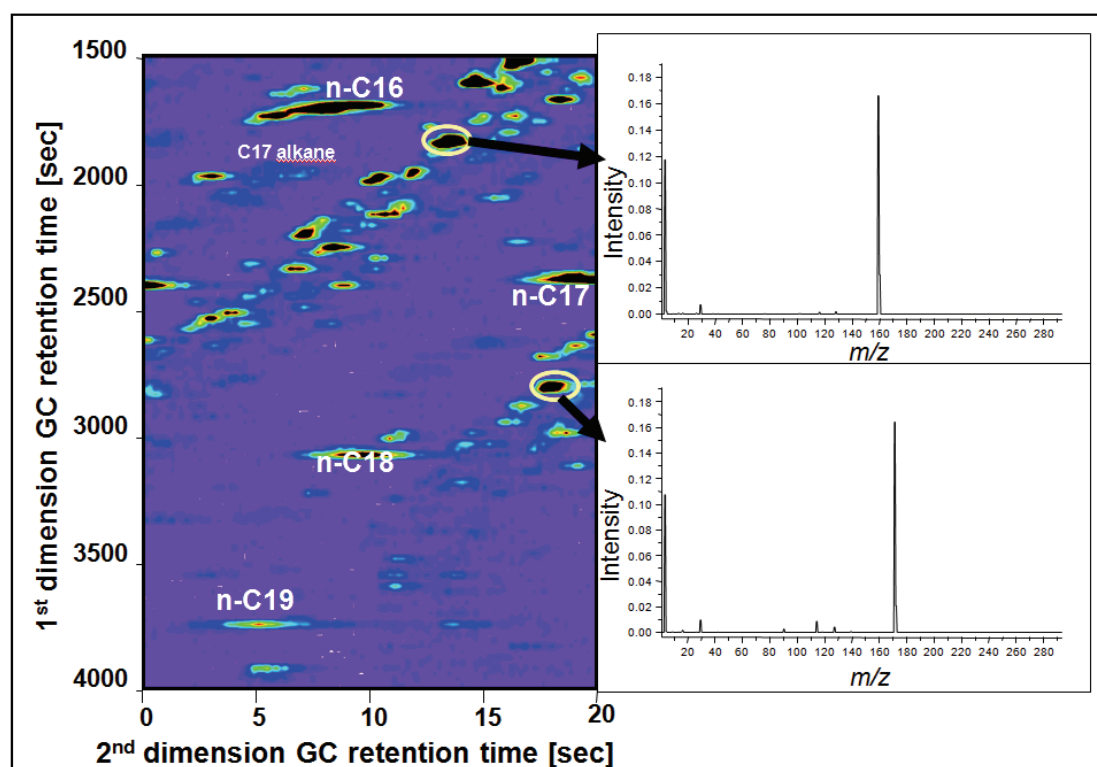
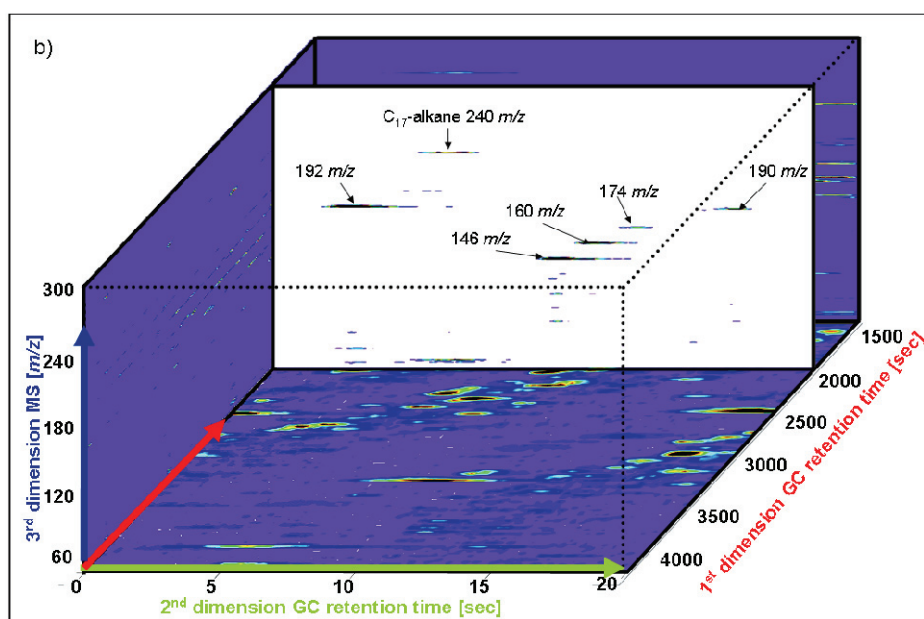
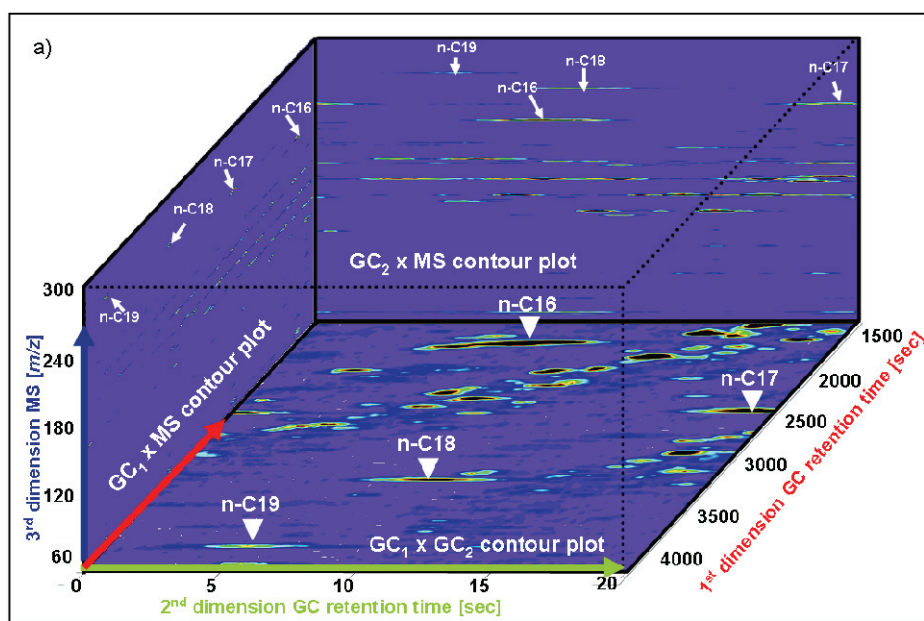


Figure 4.11 A GC x GC contour plot, of the total ion signal from the mass spectrometric dimension. Each data point on the GC x GC contour plot has a full mass spectrum containing mostly molecular ions [48].

It is however still possible to draw contour plots of two-dimensions at a time. In figure 4.12a three contour plots is combined in one figure to give the representation of the combined dimension. The bottom rectangle of the box is a summation of the mass spectra and is thus presenting a typical two-dimensional GC x GC chromatogram. The left rectangle of the box is a summation of the chromatographic peaks obtained in the second dimension to give a contour plot of the first-chromatographic dimension and the mass spectrometric-dimension. The back rectangle in turn represents the summation of the obtained first-dimension chromatograms to create a contour plot of

the second chromatographic-dimension and the mass spectrometric-dimension. From the triple contour plot it are however still difficult to locate or to identify any specific compounds. The simplest way is to look at individual second-dimension chromatograms plotted in a GC x MS contour plot. Figure 4.12b and 4.12c shows two individual GC x MS contour plots that can be extracted from the three-dimensional separation data. In Figure 4.12b a C_{17} alkane can be identified from its molecular mass 240 m/z , and the n - C_{17} alkane can be seen in the extract from Figure 4.12c. Molecular masses of the other compounds in the chromatogram can also be obtained, but no identification of peaks has been done in this preliminary study.



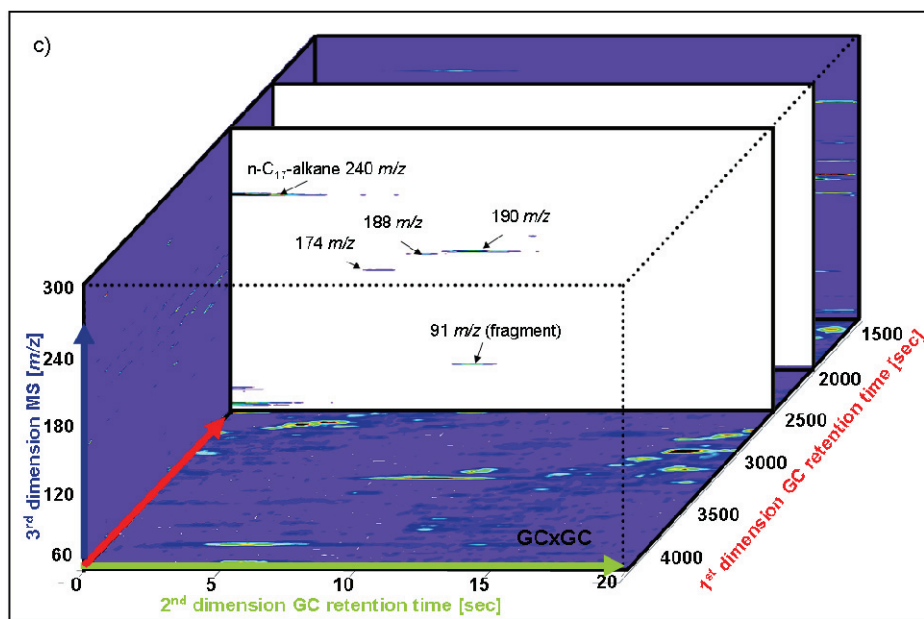


Figure 4.12 a) Three-dimensional representation using three contour plots to present the GC x GC x MS data. b,c) Individual contour plots of second-dimension GC vs MS can be extracted to identify compounds easier [48].

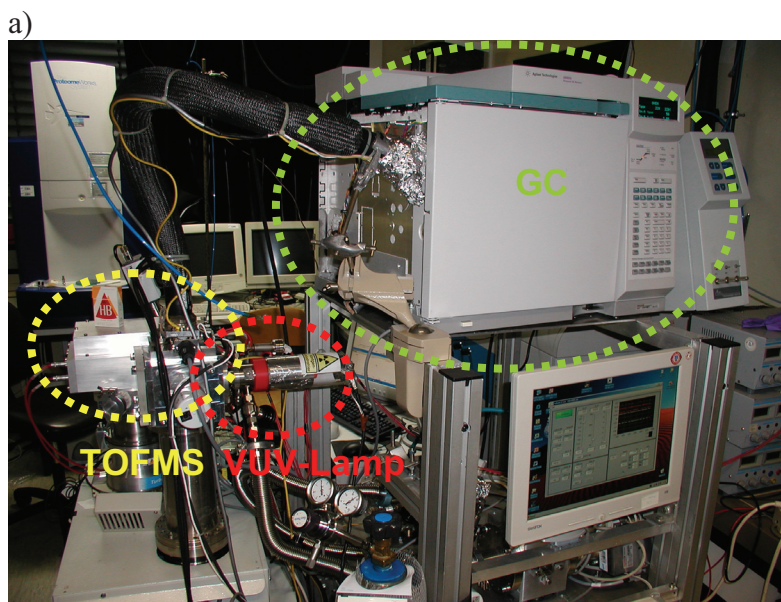
The petroleum diesel fraction analyzed in this work is not the most challenging example for the three-dimensional separation possibilities of GC x GC x MS, however, samples like environmental aerosol particles consist of an even more complex mixture of different chemical classes which can not be separated by using only two-dimensional separation parameters. For these types of samples it would be beneficial to further increase separation dimension to identify still unresolved compounds.

Similar to GC x MS the n-alkanes in both dimensions can be adjusted to improve the orthogonality of the two dimensions. The data acquired in this proof of concept were insufficient to do a proper adjustment. The short falls of the laser technique is, however, addressed in the following sections and the orthogonality adjustment is discussed in detail.

4.4 VUV-lamp photo ionization (SPI) for GC x MS

Up to now only laser photon sources were used for ionization. The laser sources are limited by their repetition rates and subsequently the cost for faster repetition rates is increasingly more expensive. A continuous source of photons for ionization is possible through the use of a vacuum ultra violet lamp. With the use of the introduced vacuum ultra violet (VUV) lamp, it is thus possible to eliminate some of the limitations of the laser system. The VUV-lamp provides a continuous source of photons and ionization could thus also be achieved on a continuous basis. This would allow photo ionization to be operated under the same conditions as electron impact ionization. The repetition rate of the laser system used before in the GC x MS (maximum of 10 laser shots per second), could now be dramatically improved. The number of spectra to be collected per second is mostly now limited to the acquisition rate of the mass spectrometer and the subsequent recording of the obtained spectra. The orthogonal accelerated time-of-flight mass spectrometer (oa-TOFMS) used here have an acquisition rate of 100 000 Hz coupled to a data acquisition card capable of averaging up to 5000 spectra and recording the data on the acquisition computer at a rate of 10-200 Hz. The data acquisition rate of 10 – 200 Hz is adequate for GC and GC x GC applications where in normal GC acquisition rates of 10-50 Hz are used and 75-200 Hz in GC x GC applications.

4.4.1 Experimental



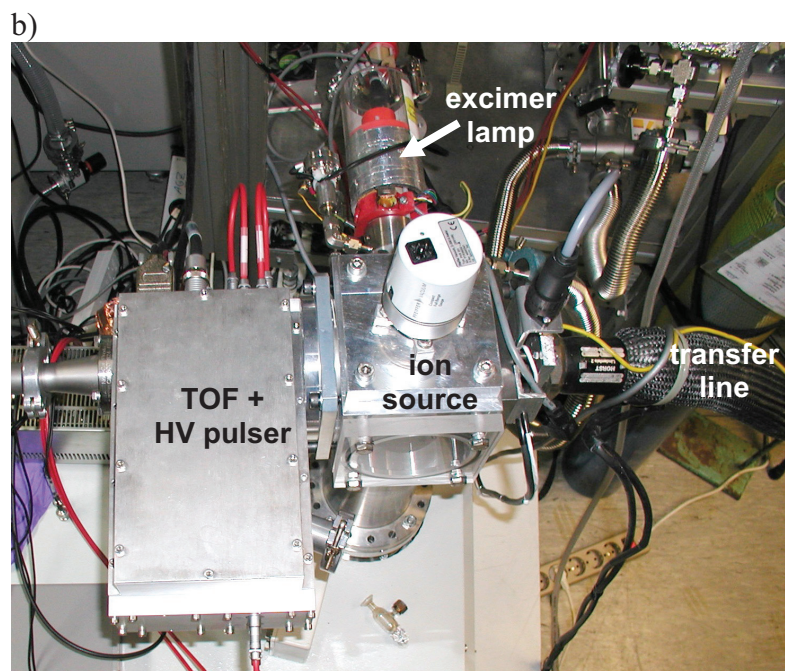


Figure 4.13a GC system coupled to a VUV-lamp SPI oa-TOFMS system b) oa-TOFMS fitted with a VUV-lamp ion source

The lamp source is described in more detail in Chapter 2.3.4 and by Mühlberger et al) [45]. The ion source was only heated by the filament in EI mode and was not heated at all in SPI mode. The MCP output signal is detected simultaneously in two channels of a high-speed (1 Gs/s) analog-to-digital conversion data acquisition card (model DP 240, Acqiris, Geneva, Switzerland). The two channels can record the detector signal with different amplification in order to extend the dynamic range of the 8-bit analog to digital converter (ADC). Data collected by the data acquisition card are transferred to a personal computer and stored to disc. For the applied high duty cycle rates, mass spectra raw data were collected and averaged on the ADC board in real time before transfer to the PC.

In this approach a GC (Agilent 6890N, Agilent, US) with a 30 m x 0.25 mm ID x 0.25 μm d_f , BPX50 (SGE, Australia) was used. A temperature program of 20 °C/min from 50 °C to 360 °C was applied. Splitless injection was used with a 0.1 μl diesel sample and helium carrier gas at 30 cm/s linear flow rate (200 kPa constant pressure mode). Chromatograms were recorded using VUV lamp filled with argon to produce photons of 126 nm wavelength or 9.8 eV equivalent. Data acquisition of 20 Hz. For comparison reasons the same Fischer-Tropsch diesel sample (source: SASOL Ltd., Sasolburg, RSA) was analyzed with conventional EI at 70 eV, 20 Hz data acquisition.

4.4.2 *Results and discussion*

In this first application of VUV-lamp coupled to GC an effusive inlet was used instead of the capillary jet used in the laser approach. The use of the effusive inlet potentially would result in more fragmentation. The different ionization energy from lamp (9.8 eV at 126 nm) to laser (10.49 eV at 118 nm) would reduce the fragmentation in the lamp ionization. The lower ionization energy of the lamp would also result in a lower ionization of the smaller alkanes as can be seen in Figure 4.14.

The lamp ionization show much less mass signals below mass 150 compared to the laser ionization. Although the fewer ions below mass 150 can be ascribed to the lower ionization energy of the lamp it can also imply that there is potentially less fragmentation occurring with the lower ionization energy and potentially less electron impact ions being produced through the laser hitting the metal parts inside the ion source. Through using the gas chromatographic retention together with the mass information it would possibly be easier to examine the ionization differences.

Plotting the GC-MS (EI 70eV) chromatogram of the diesel sample in a two-dimensional plane shows the fragmentation patterns expected from hard ionization, and thus it remain difficult to identify any specific compound in this type of presentation.

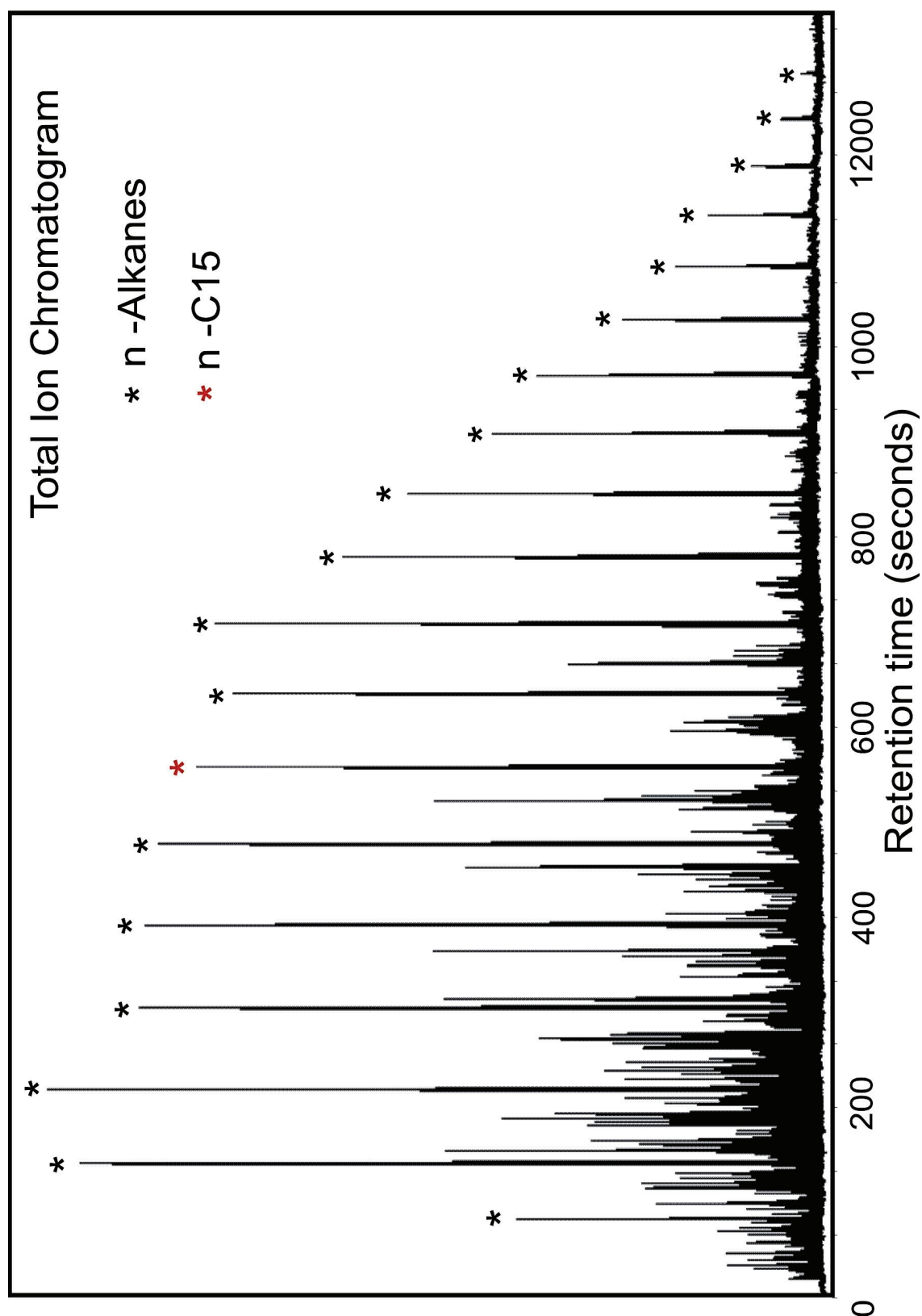


Figure 4.14a Total ion chromatogram of a diesel sample obtained through GC – TOFMS with EI at 70 eV. The n-alkane peaks are indicated on the chromatogram.

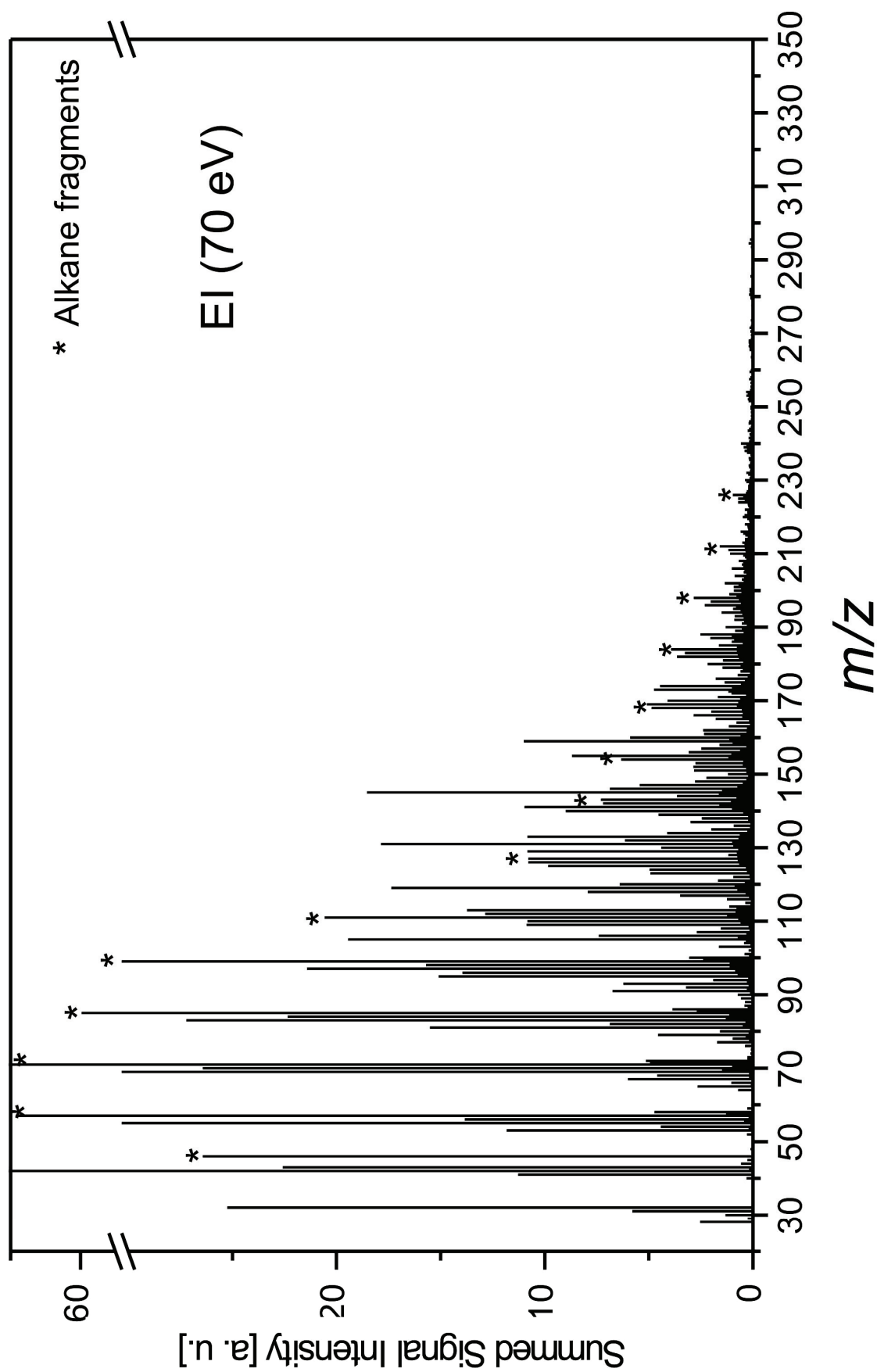


Figure 4.14b Mass spectra summed up over the total gas chromatographic run of the diesel sample recorded with electron impact ionization (EI 70 eV). The fragments of the alkanes are indicated on the spectrum.

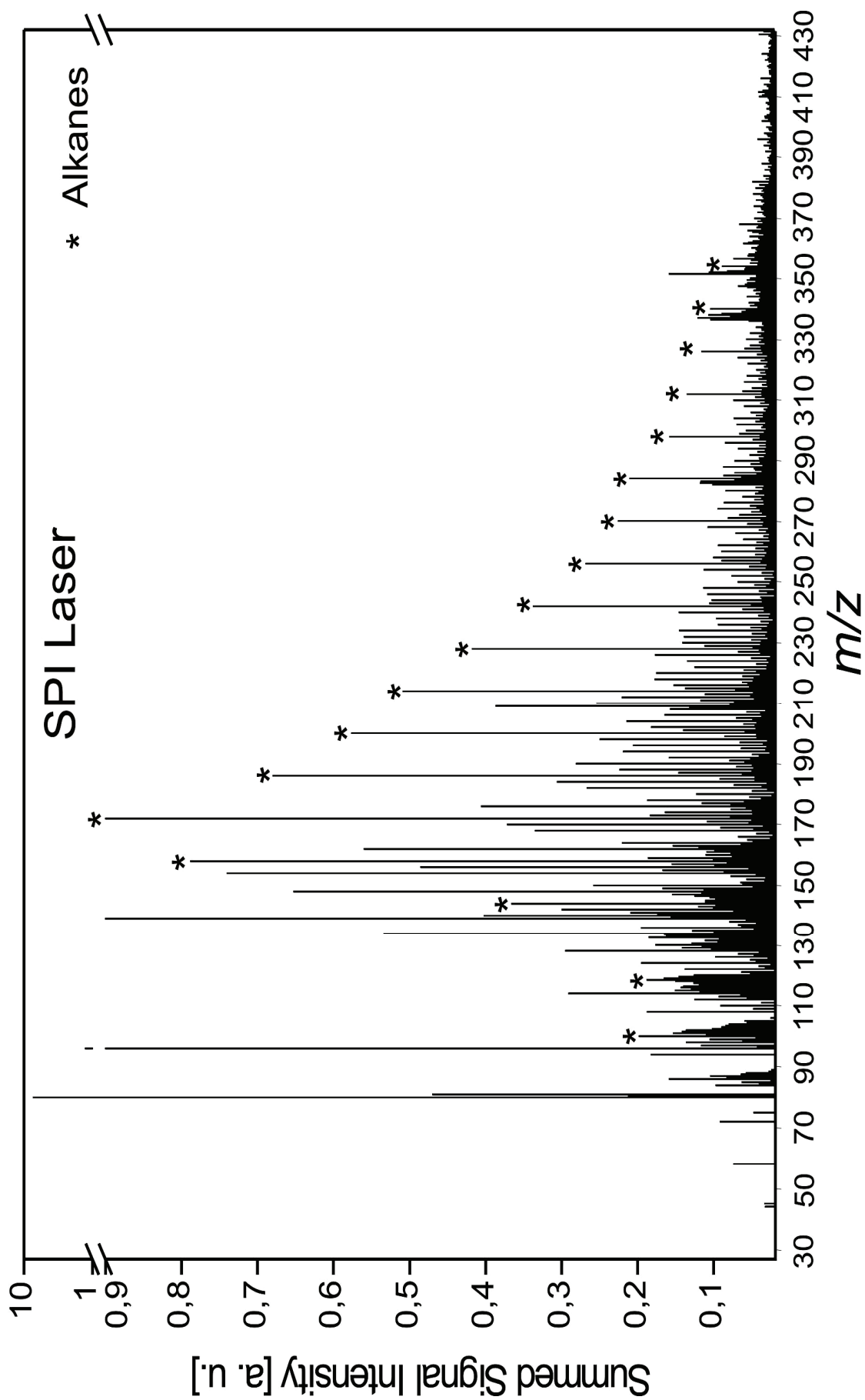


Figure 4.14c Mass spectra summed up over the total gas chromatographic run of the diesel sample recorded with laser SPI at 118 nm.. The molecular masses of the alkanes are indicated on the spectrum.

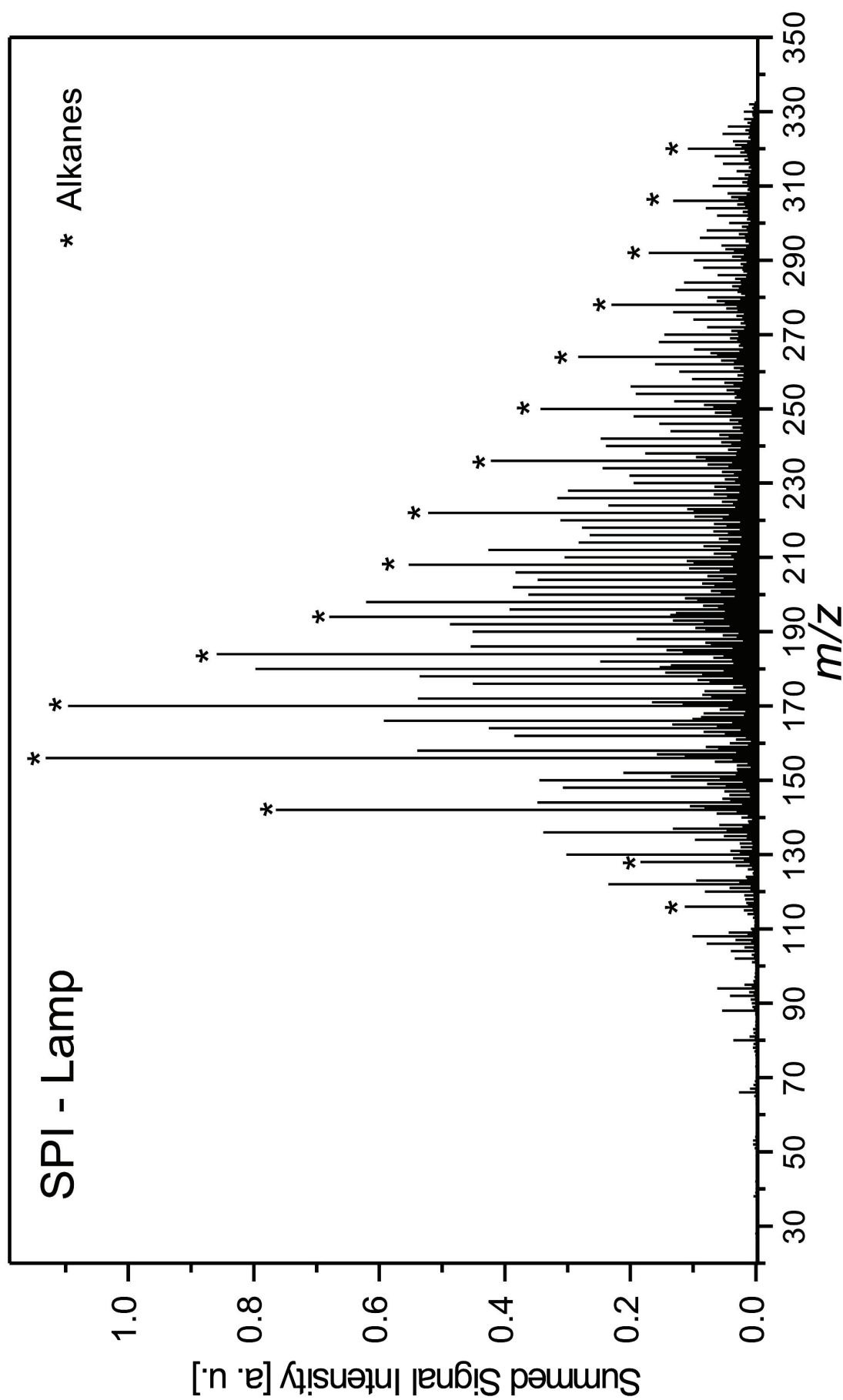


Figure 4.14d Mass spectra summed up over the total gas chromatographic run of the diesel sample recorded with a VUV lamp SPI at 126 nm.. The molecular masses of the alkanes are indicated on the spectrum.

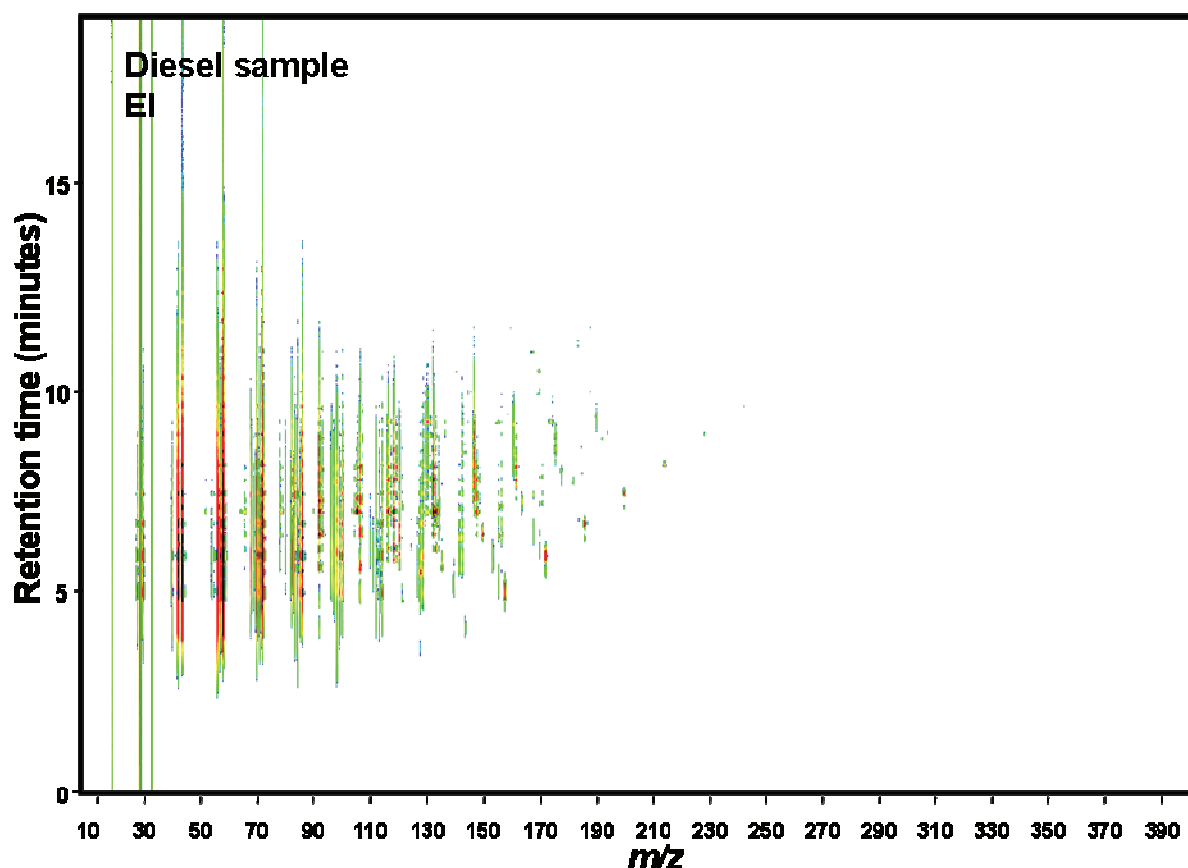


Figure 4.15 Two dimensional contour plot of a diesel sample analyzed by GC-MS (EI 70eV)

Whereas the mass fragments dominate the EI mass spectra, the soft ionization in SPI produce mainly molecular ions. In a two-dimensional contour plot of GC - SPI TOFMS compounds should thus be more easily identified. In Figure 4.16 it is thus possible to spot individual compounds more easily.

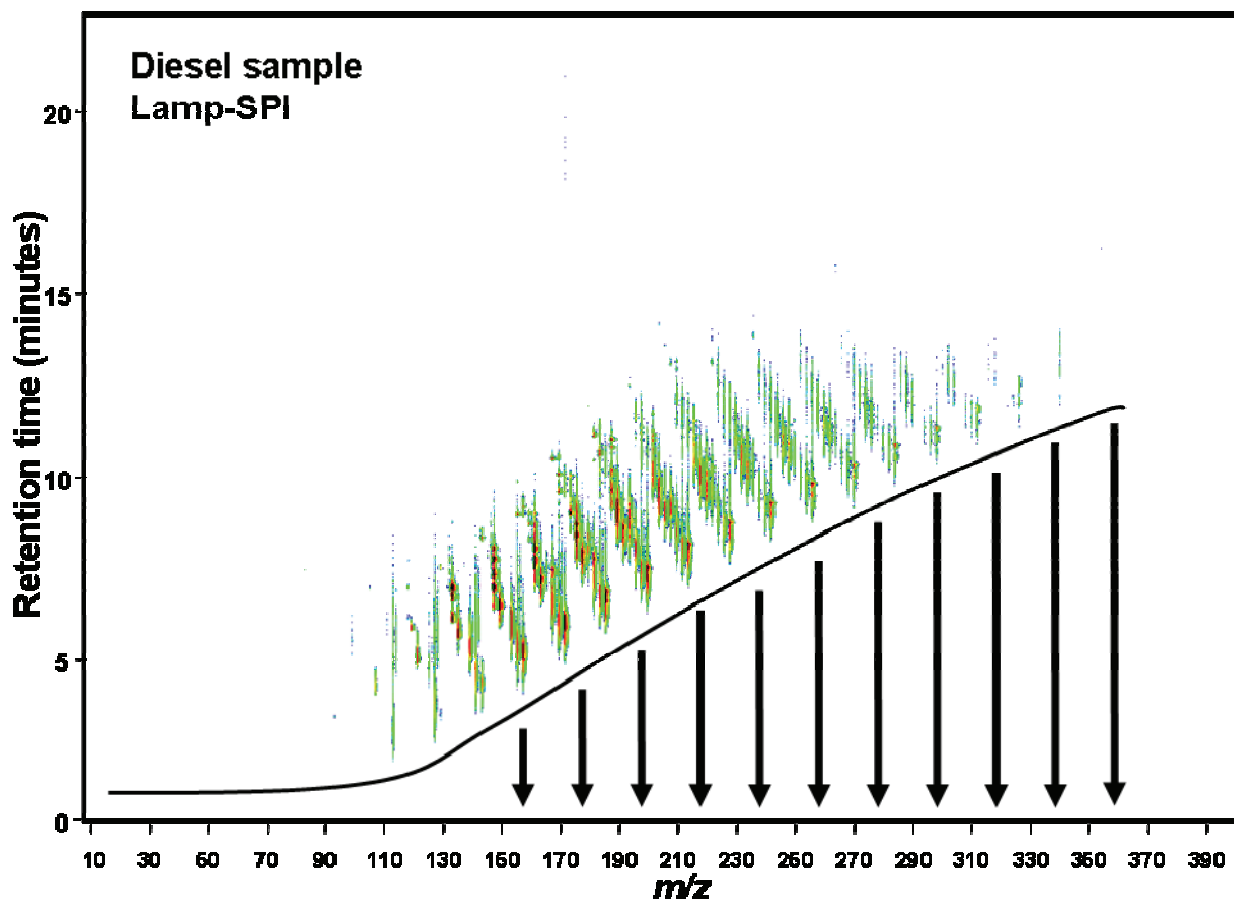


Figure 4.16 Two dimensional contour plot of a diesel sample analyzed with GC coupled to lamp-SPI TOFMS. The line and arrows indicating the polynomial shift in retention time to adjust the n-alkanes into a row.

From the GC x SPI TOFMS chromatogram in Figure 4.16 it also is clear that there are almost no masses below 100 m/z , which would indicate that there is indeed almost no fragmentation occurring. The contour plot has to be adjusted for retention time similar to the procedure applied to the laser ionization, in order to make full use of the chromatographic plane and to effectively eliminate the temperature dependency of the chromatographic dimension. The resulting retention time corrected chromatogram is shown in Figure 4.17. From the obtained GC x MS contour plot it would now be possible to identify compounds and compound class groupings of physical and chemical related compounds. The extraction sections in Figure 4.17 indicate the homologue rows expected from diesel samples, of the aliphatic compounds C_nH_{2n+2} , C_nH_{2n} and C_nH_{2n-2} and also the aromatic homologue rows of alkylated benzenes, alkylated indanes and alkylated naphthalenes.

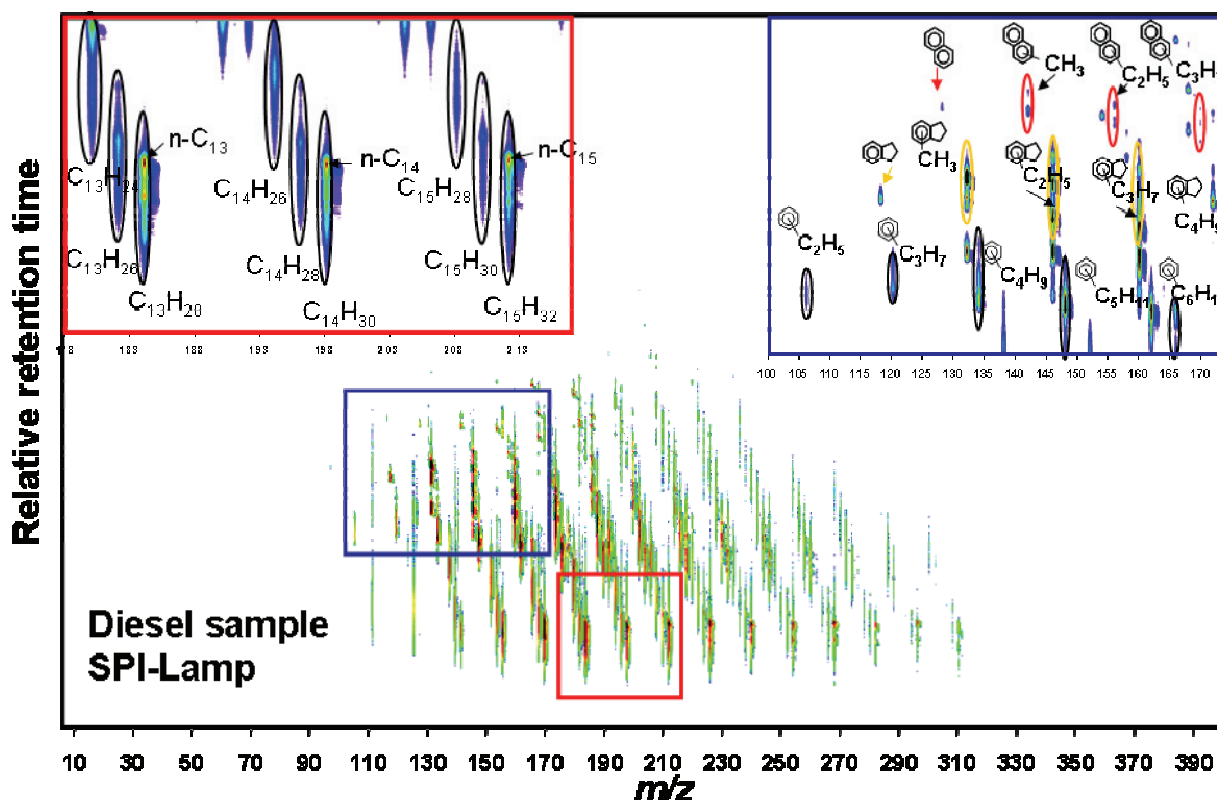


Figure 4.17 GC x SPI-TOFMS contour plot of a diesel sample with two extraction sections for compound identification.

The obtained chromatograms from GC x SPI TOFMS from the VUV-lamp (Figure 4.17) compare very well to the chromatograms obtained from the laser system earlier. Same compound groups are detectable (part from the smaller alkanes) in both SPI methods thus indicating that the VUV-lamp is a viable ion source for GC x SPI TOFMS. In these first experiments it is to be noted that the chromatographic separation in the lamp setup was a lot lower than in the laser setup. This was mainly due to storage constraints in the acquiring of data at the much higher data acquisition rate possible with the lamp setup. The TOF acquired spectra at 80 kHz that was averaged on the data acquisition card (each 4000 spectra) to finally record 20 spectra per second. The huge averaging factor increases the dynamic range at which the compounds can be detected by a huge margin over the 10 Hz sampling from the laser setup. The advantages of the increased dynamic range can be seen in the much cleaner mass spectra obtained in the lamp setup (comparing Figure 4.17 with Figure 4.5). It is however necessary to evaluate the sensitivities that can be obtained through both setups and compare those with what is possible through electron impact ionization.

The lamp SPI could be directly compared to EI as both were obtained using the same TOF system. Thus with the injection of 500 pg of dichlorobenzene standard (1,2-; 1,3 and 1,4- DCBz respectively) it was possible to obtain signal to noise ratio of 25:1 for EI and 5:1 for SPI, resulting to an approximately detection limit of 500 pg for SPI and 100 pg for EI (Figure 4.18).

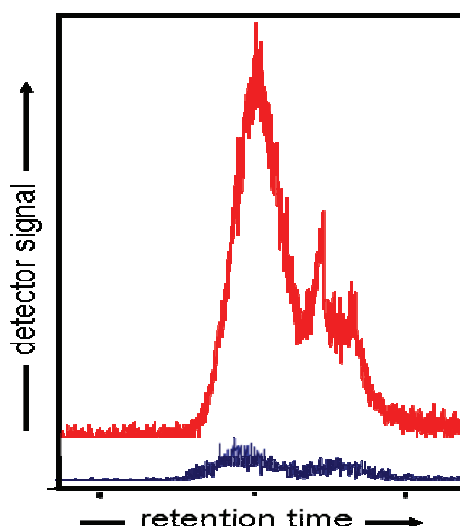


Figure 4.18 Signal to noise ratio of dichlorobenzene analyzed by EI ($s/n = 25$) and SPI lamp ($s/n = 5:1$), Highest peak: co-eluting 1,3- and 1,4-dichlorobenzene

Though the sensitivity in this study is still quite low it is important to note that the intensity of the lamp source can still be increased with optimization and more than one lamp can be introduced.

4.5 VUV-lamp photo ionization (SPI) for GC x GC x MS

The prerequisite of detectors in slow acquisition rate of the The advantage of the lamp source to provide a continuous source of ions (similar to EI) can now be used in applications such as fast GC or even GC x GC without losing any of the separation obtained in those techniques. The lamp coupled to GC x GC is described in the following section. Combining the VUV lamp with GC x GC

Having overcome some of the limitations of the laser based ionization source, it is now possible to investigate the potential of a comprehensive three dimensional separation technique.

4.5.1 Experimental

The experimental setup is similar to the setup used in 4.4 but coupled to a GC x GC instead of a normal GC. A two-dimensional gas chromatogram (Trace GCxGC, Thermo Scientific, Italy) installed with a dual-jet carbon dioxide modulator were used. The chromatographic columns installed were a polyethelene glycol (Solgelwax, 30 m L, 0.25 mm ID, 0.25 μm d.f., SGE, Australia) first-dimension column and a 50% Phenyl Polysilphenylene-siloxane (BPX50, 1 m L, 0.1 mm ID, 0.1 μm d.f., SGE,

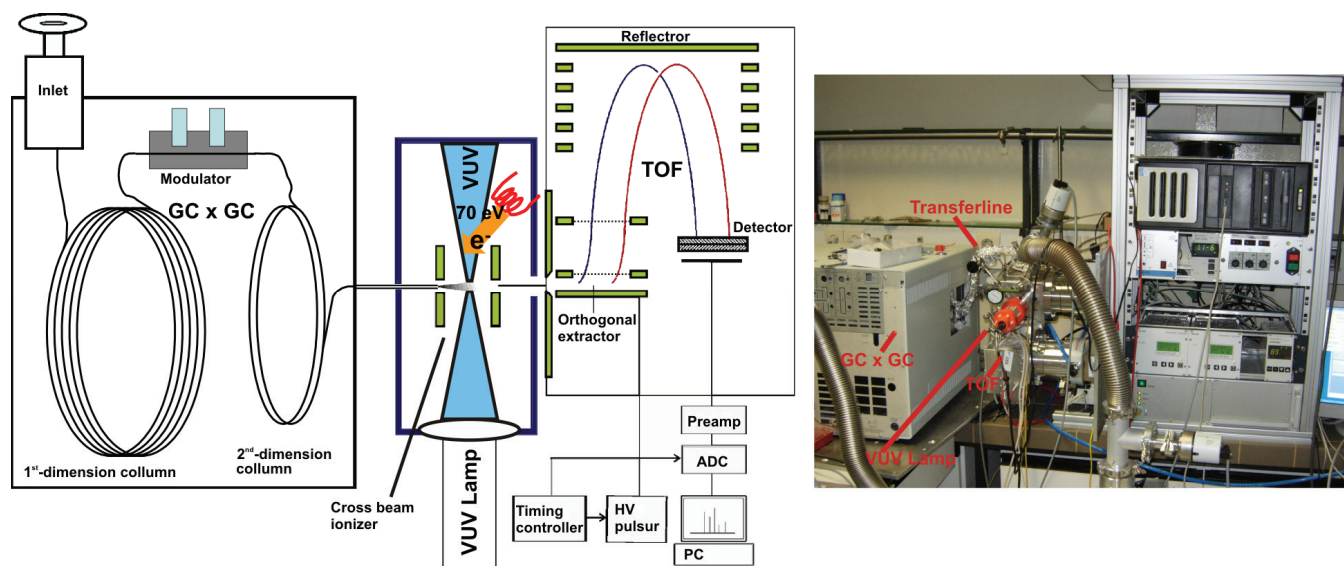


Figure 4.19 Instrumental setup of the three dimensional GC x GC x SPI TOFMS

Australia) second-dimension column. Sample (0.1 μl) was injected at 250 $^{\circ}\text{C}$ with a split of 50:1. Helium was used as carrier gas using constant flow of 1 ml/min. A modulation period of 5 seconds was applied. The chromatographic columns were subjected to the same the temperature program, 40 $^{\circ}\text{C}$ start time with a 20 $^{\circ}\text{C}/\text{min}$ ramp to 100 $^{\circ}\text{C}$ where the temperature were kept constant for 1 minute before a 5 $^{\circ}\text{C}/\text{min}$ ramp to 300 $^{\circ}\text{C}$. The second-dimension column was then connected to the ionization chamber through a short transfer line of 25 cm (15 cm of the end of the chromatographic column and 10 cm of an uncoated 0.1 mm capillary column) heated to 220 $^{\circ}\text{C}$.

4.5.2 Results and discussion

The observations made earlier on GC x GC x Laser MS are still applicable to the GC x GC x VUV-LAMP MS (4.3). However, with the faster data acquisition rates possible with the lamp technique the GC x GC can be run under more optimized conditions. Being able to run the GC x GC under near optimal conditions allows for faster analysis retaining a high peak capacity. The maximum acquisition rates obtained with the current configuration are still limited through the recording rate of the personal computer (~ 20 Hz), but this could be improved through optimizing the software or faster hardware. Enough data points per chromatographic peak can, however, still be obtained and the resulting two-dimensional chromatograms recorded through this setup can be seen in figure 4.20. Data have been recorded using both EI and SPI as ionization with 20 Hz acquisition. The obtained chromatograms does not provide completely resolved peaks due to the chromatographic column choices. Similar as before (4.3) the first-dimension separates compounds based on Hydrogen

bonding between compounds and the stationary phase while separation on the second-dimension were based on π -bonding between the compounds and the stationary phase [49]. Both these separation dimensions are still somewhat dependant on one another and compounds of similar chemical properties tend to still overlap with one another. The mass spectra of some selected peaks on the chromatograms (Figure 4.20) show that when using SPI mostly the molecular ions are observed and it would thus be possible to differentiate between compounds of similar chemical properties but having a different molecular weight.

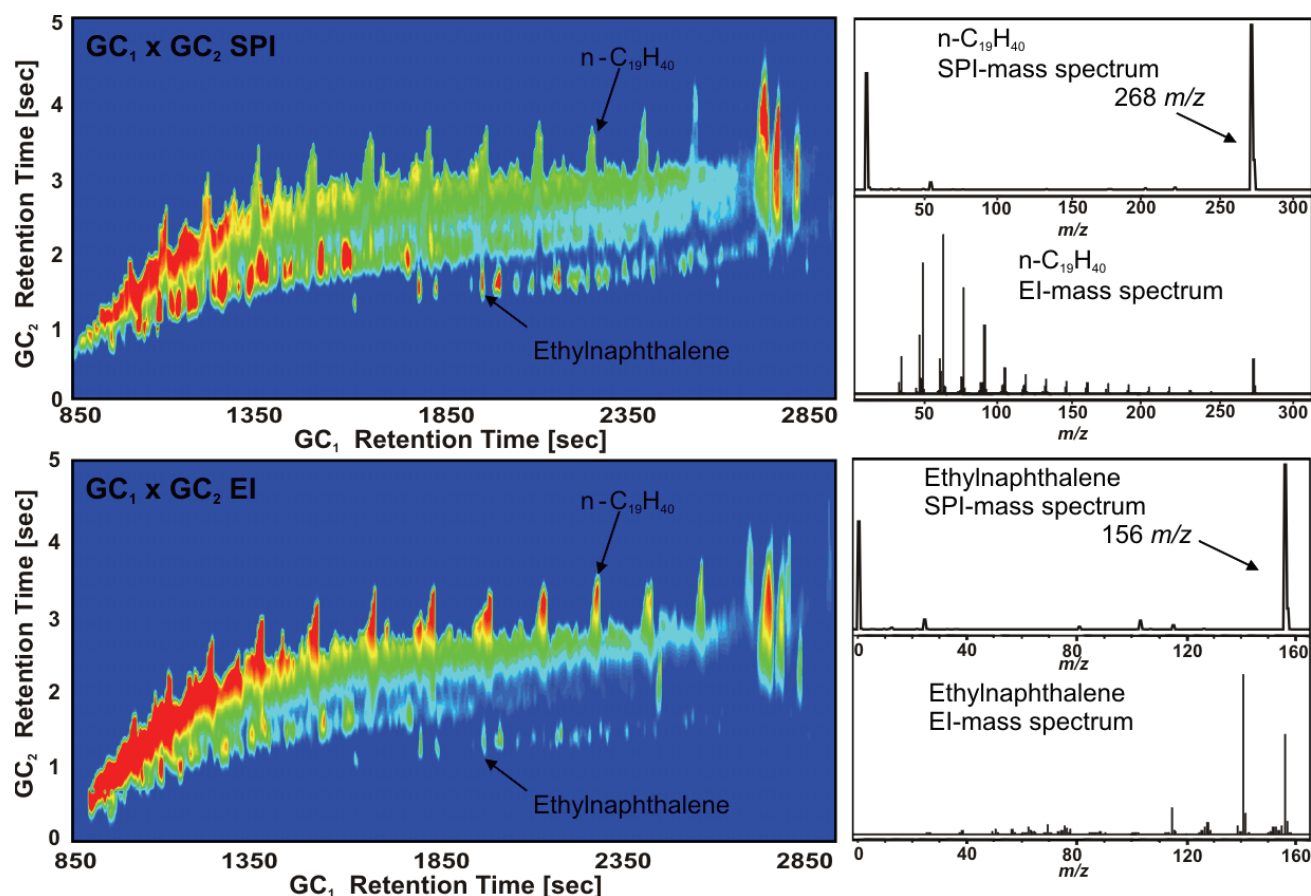


Figure 4.20 GC x GC contour plots, of the total ion signal from the mass spectrometric dimension (both EI and SPI). Each data point on the GC x GC contour plots has a full mass spectrum containing mostly molecular ions.

The overlap of compounds in Figure 4.20 can also possibly be attributed to the dependency of both chromatographic dimensions with temperature. The temperature dependence will be discussed later again in more detail.

From the chromatograms it can also be observed that different compounds have different intensities on SPI compared to EI. The intensity of saturated hydrocarbons ionized with EI appears to be much higher than with SPI while the unsaturated hydrocarbons (aromatic species) appear to be higher with SPI.

The mass spectra obtained can be seen as a third separation dimension and be plotted on a three-dimensional axis (Figure 4.21). From these three-dimensional plots it is difficult to identify different compounds when using electron impact ionization due to the overlap of similar fragments for most hydrocarbon species, but individual compounds can be identified on the plot using the photon ionization.

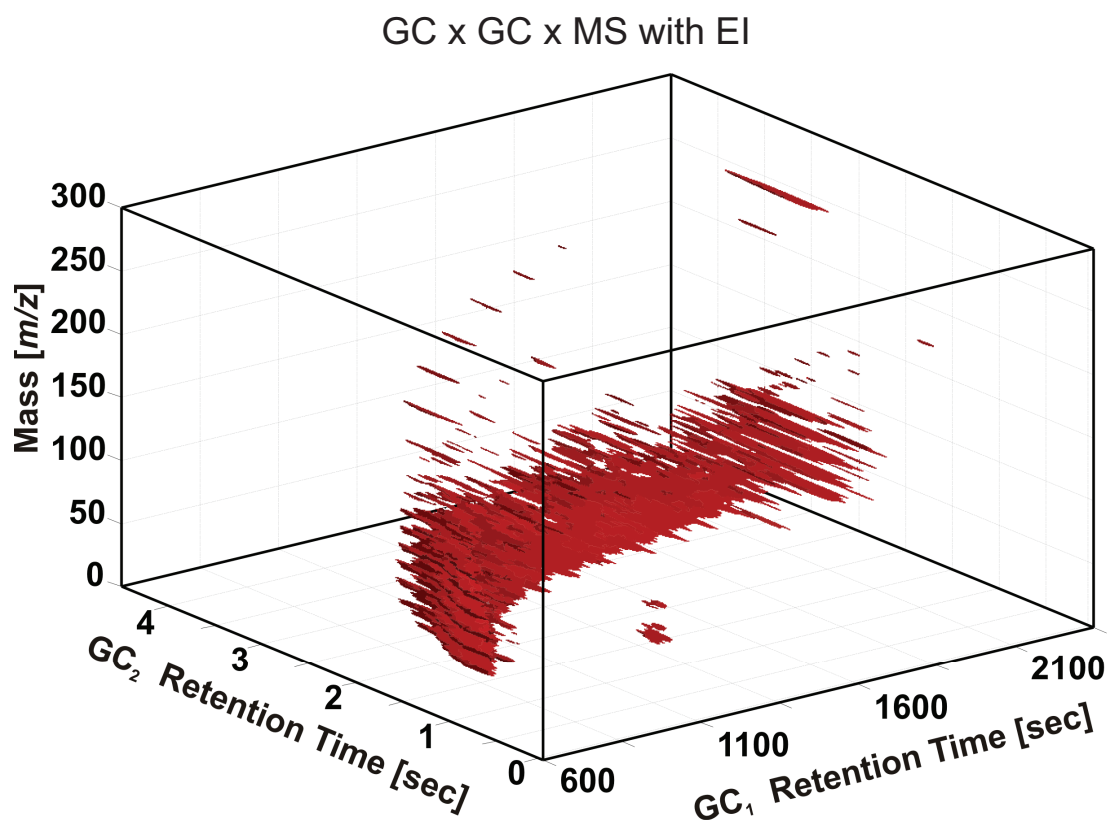


Figure 4.21a Three-dimensional representation of GC x GC x MS with electron impact ionization. Mostly fragmented ions can be observed.

GC x GC x MS with SPI

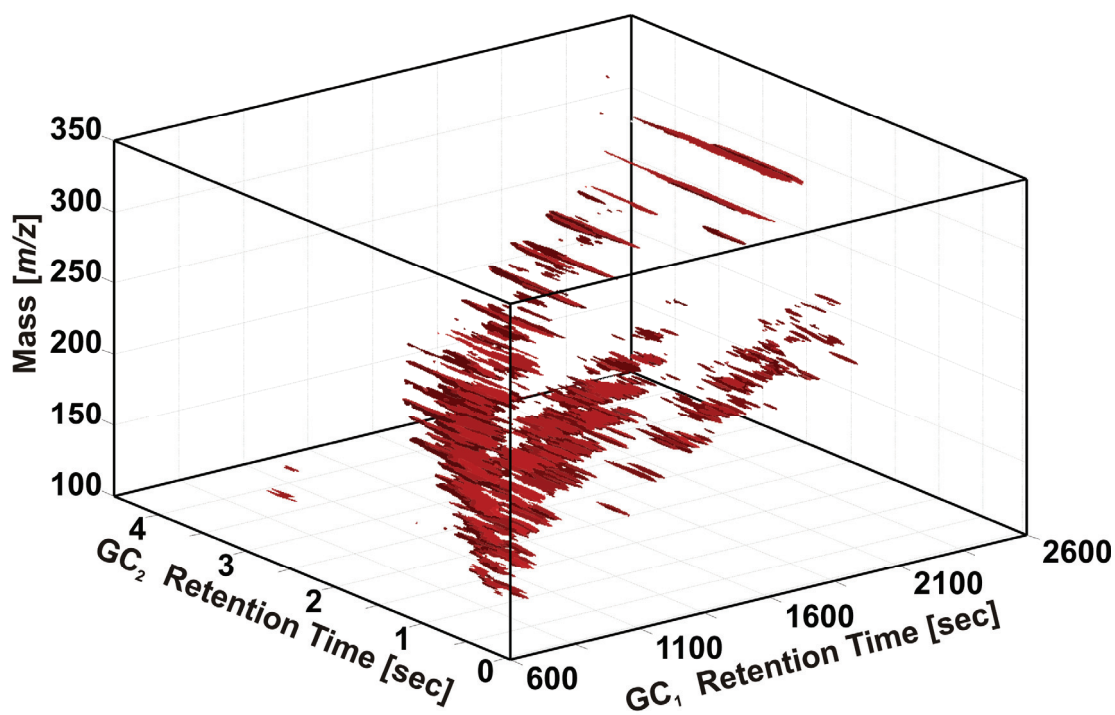


Figure 4.21b Three-dimensional representation of GC x GC x MS with single photon ionization VUV-Lamp. Molecular ions can be observed, or each red peak represent a different compound.

The chromatographic data and the molecular ions of the compounds in the three-dimensional plot from the SPI makes it possible to start identify compounds or group them into different chemical groups. Compounds with different chemical, physical properties or molecular size can be easily distinguished. Some of the different chemical groups that can be easily identified in the analyzed diesel sample are the paraffins, mono-aromatics, indanes, di-aromatics, bi-phenyls, acenaphthenes, benzindanes, tri-aromatics and esters (Figure 4.22). Within any of these identified chemical groups compounds could be easily divided according to their carbon number (molecular mass). It also should be pointed out that though some compounds may seem to still overlap in Figure 4.22, it is more likely to be due to the specific orientation of the three-dimensional plot.

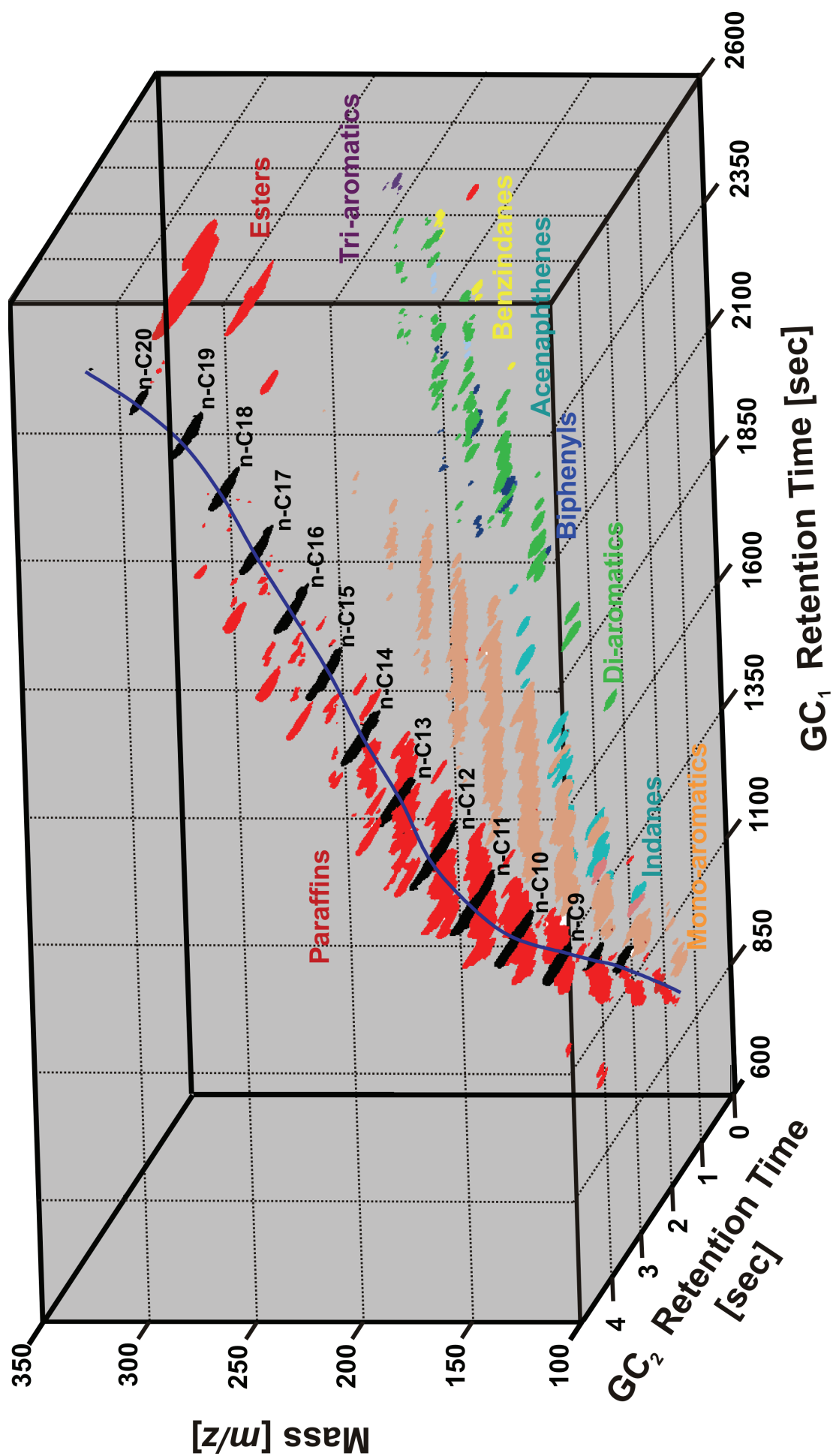


Figure 4.22 Three dimensional separation of a diesel sample using GC x GC x SPIMS. Some chemical groups are identified using different colors.

The potential of this technique to separate mixtures of high complexity is obvious, but the question still remain if all three dimensions are truly independent or orthogonal to one another?

It was already mentioned earlier that the two chromatographic dimensions are not completely independent since both dimensions depend on temperature for separation or in chromatographic terms both dimensions have a strong separation parameter in the “van der Waals”-interaction of compounds with the stationary phase. As noted before this temperature dependency is also closely related to the molecular ion distribution of the compounds.

In previous work done by Wang *et al* [14] on gas chromatography coupled to field ionization mass spectrometry, the orthogonality of the technique were enhanced by normalizing the sample so that the n-alkanes in the chromatographic dimension a straight line form. This normalization effectively minimizes the temperature effect of the chromatographic dimension and increases the orthogonality of the two dimensions. The same principle can be applied to the three-dimensional data set. This is demonstrated in Figure 4.23. For simplicity Figure 4.23a only show the two-dimensional chromatographic slices corresponding to the n-alkanes (n-alkanes indicated with *) in the three-dimensional data set. In Figure 4.23b these two-dimensional slices are now shifted around such that the n-alkanes a straight line forms.

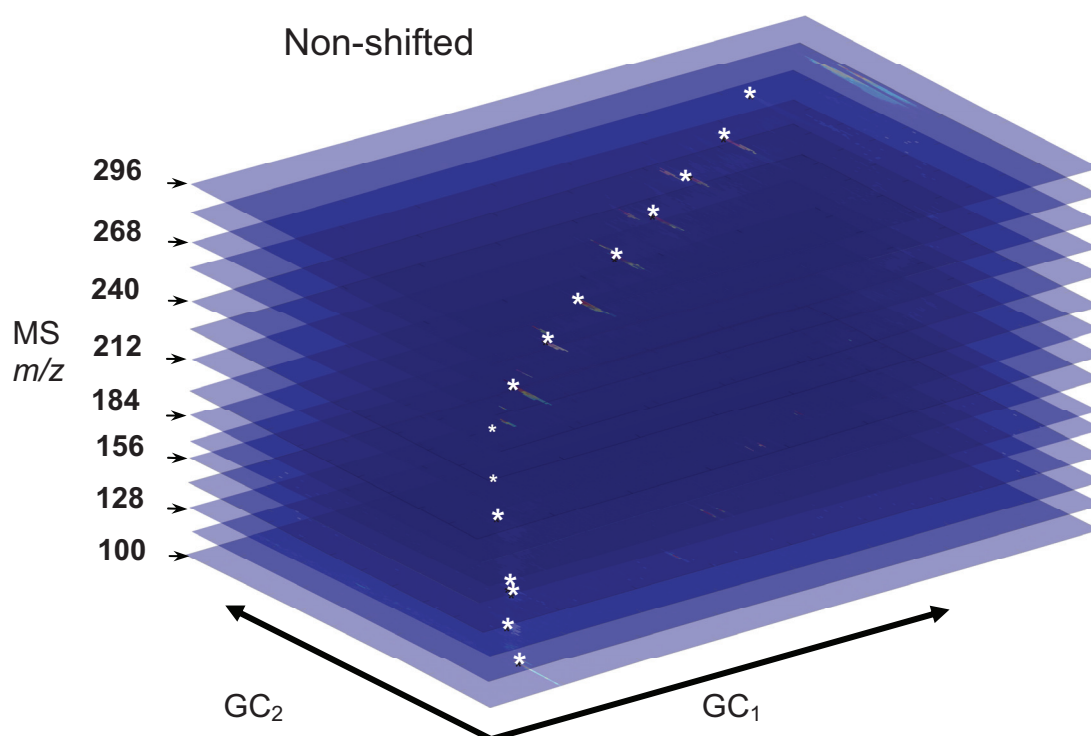


Figure 4.23a Two-dimensional chromatograms containing the n-alkanes.

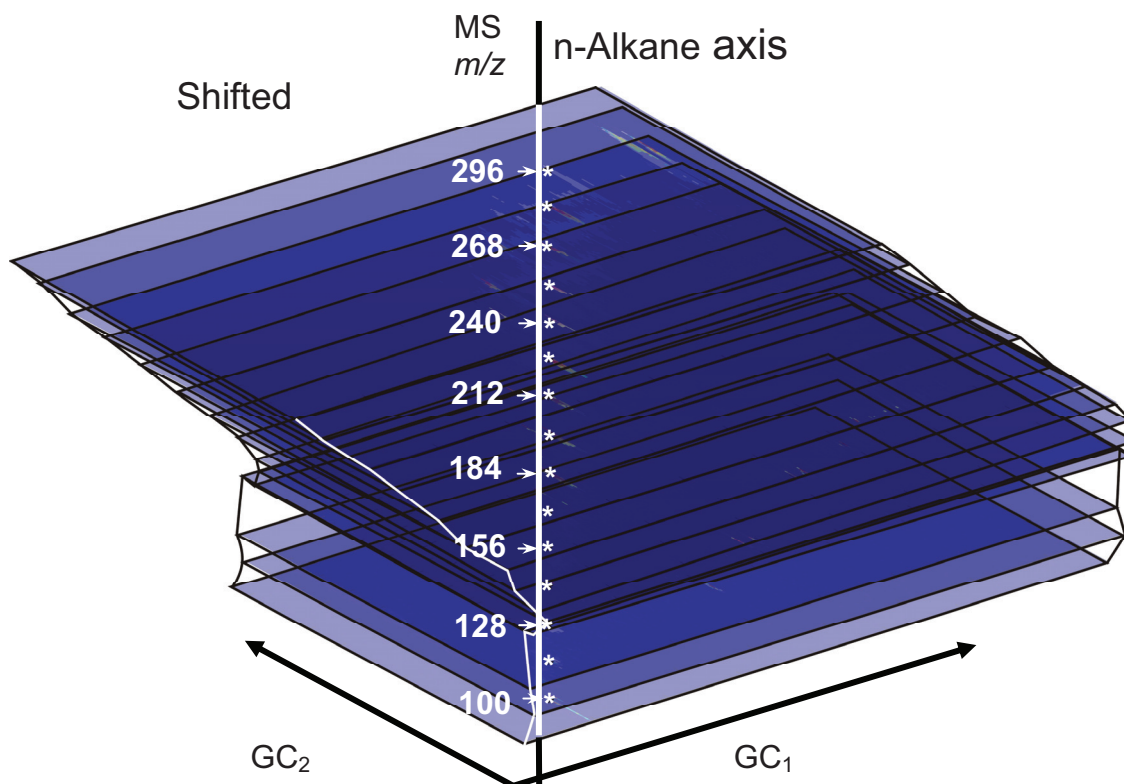


Figure 4.23b Two-dimensional chromatograms containing the *n*-alkanes shifted so that the *n*-alkanes (*) a straight line forms.

Shifting the rest of the three-dimensional data set is increasingly more difficult. Each chromatographic peak occupies a space, stretching into both chromatographic dimensions. Simply moving the peaks as done in Figure 4.23 would distort the peak shapes and create additional complexity. It was therefore decided to only use the apex of each chromatographic peak such that it can be easily moved without distortion. apex plots have been generated by T. Gröger [51].

Figure 4.24a and 4.24bd shows the shift applied to the rest of the data set. The same chemical groups that were identified earlier are once again indicated in the two figures with the same colour code. From Figure 4.24b it can be seen that there are compounds eluting before the *n*-alkanes in the second GC dimension (GC_2). The *n*-alkane axis is thus chosen to be in the middle of the second dimension axis.

From two-dimensional projections (Figure 4.25) of the three-dimensional bubble plots of Figures 4.24a and 4.24b, the effect of the *n*-alkane normalization can be further investigated.

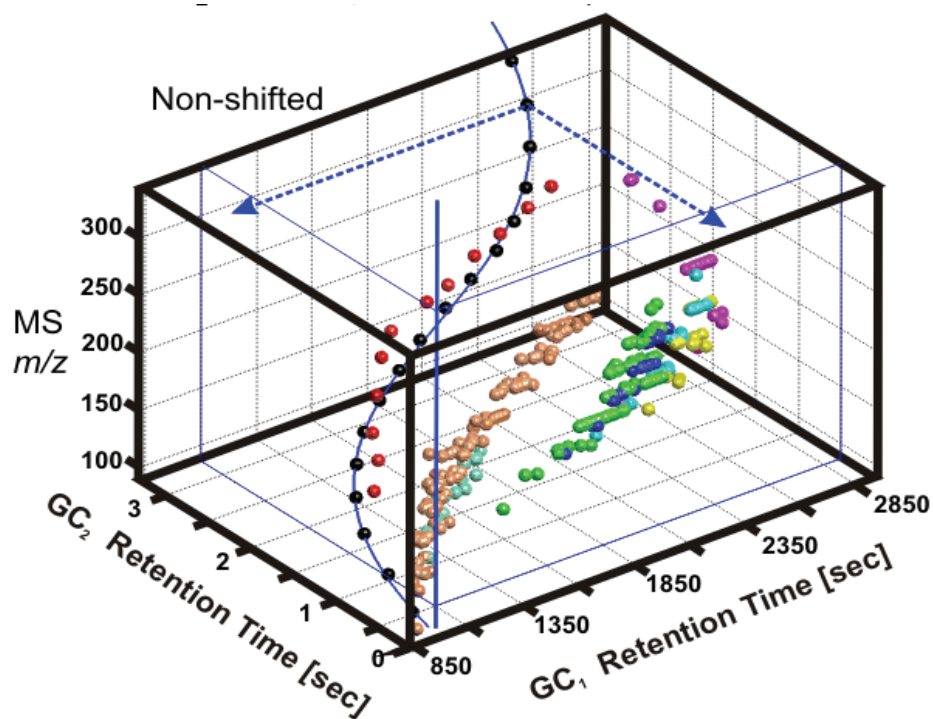


Figure 4.24a Non-shifted apex plot of the three-dimensional data set

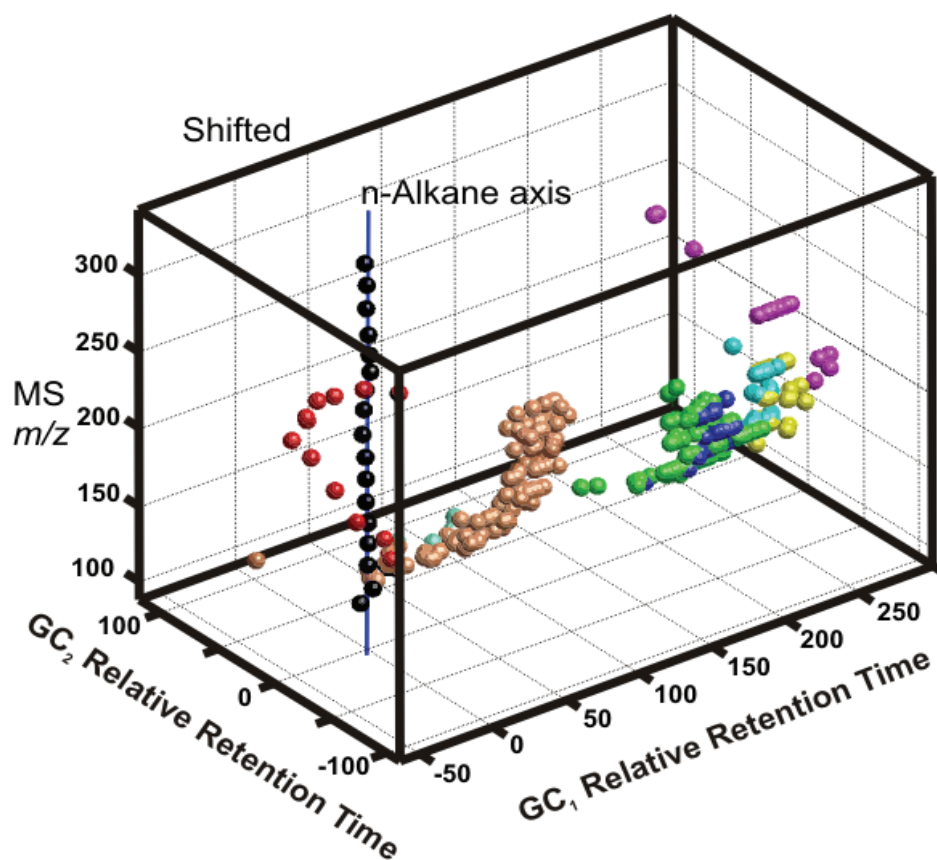


Figure 4.24b Shifted apex plot of the three-dimensional data set. *n*-alkanes are shifted to form a straight line [51]

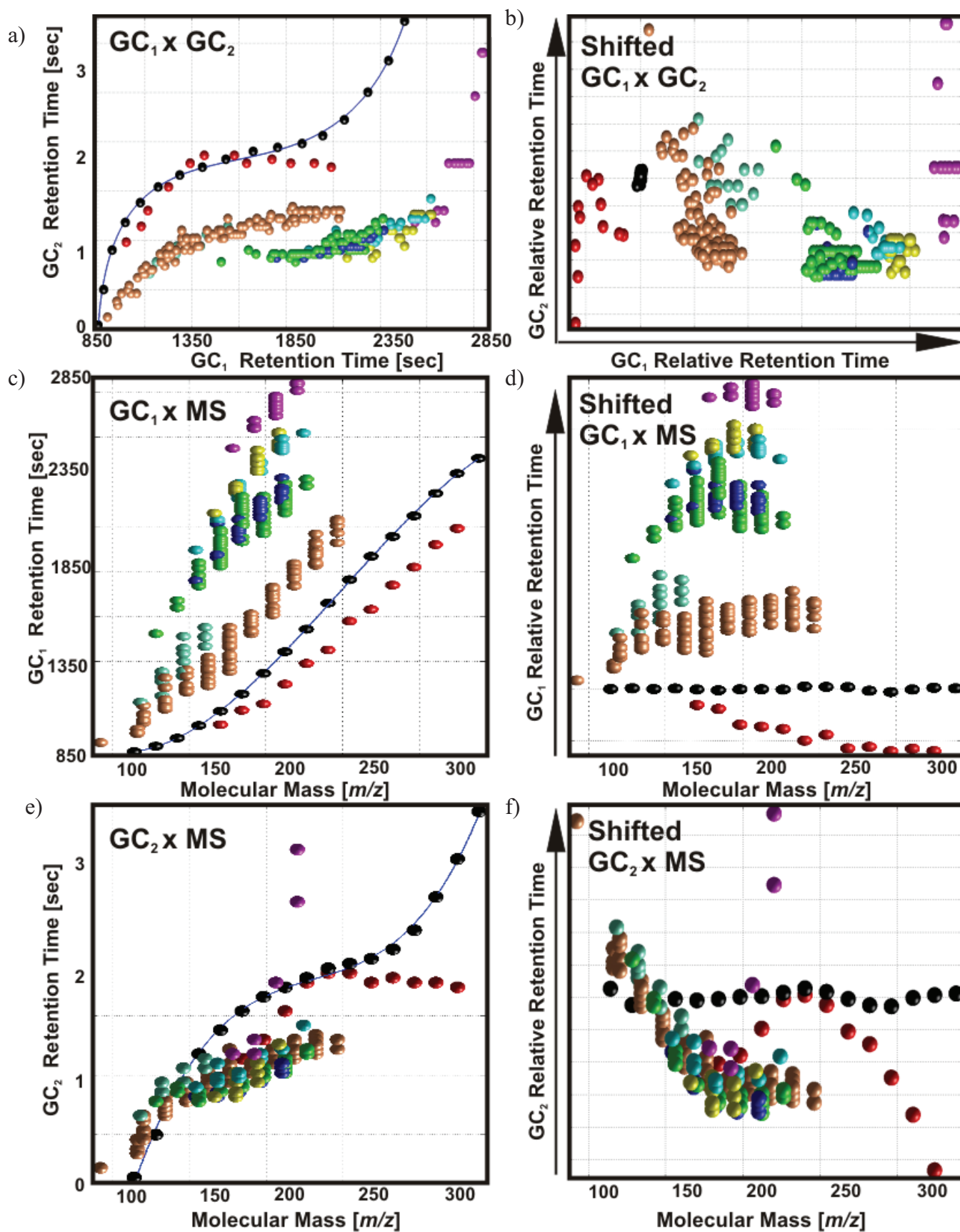


Figure 4.25 Two-dimensional projections from the non-shifted and shifted three dimensional apex plots (Figure 4.24b) [51]

Figure 4.25a represents the unshifted two-dimensional chromatographic plot ($GC_1 \times GC_2$) in a apex plot format. Not only can several groups of compounds be observed similar to the original two-dimensional chromatograms in Figure 4.20, but the added information from the three-dimensional plot made it possible to distinguish compounds in the overlapping parts of the chromatogram. Normalizing the chromatogram according to the n-alkane row can be seen in Figure 4.25b. The n-alkanes now all overlap at a single point which would imply that the temperature dependence have been eliminated and the two chromatographic dimensions now separate the compounds only based on their interaction with the stationary phase. The different groups assigned earlier of compounds of similar compound class also forms more distinct clusters and it would appear as if a larger area of the two-dimensional space are filled with compounds.

The shift in the two-chromatographic dimensions can also be studied individually through the projection of the $GC_1 \times MS$ (Figures 4.25c and 4.25d) and $GC_2 \times MS$ (Figures 4.25e and 4.25f) axis. The $GC_1 \times MS$ projection is similar to the $GC \times MS$ plots discussed in sections 4.1 and 4.3. There is good separation between compounds, but due to the temperature dependence of both the chromatographic dimension and the molecular mass distribution large parts of the two-dimensional space is not being utilized. The n-alkane normalization solves this problem in Figure 4.25d. In the projection of the second chromatographic dimension ($GC_2 \times MS$, Figure 4.25e and 4.25f) it can be seen that poor separation is obtained between the different compound groups. Using a different stationary phase for the second chromatographic dimension is recommended for future work.

4.6 Conclusions

Photo ionization mass spectrometry (PIMS), as a selective detector, can be successfully applied as gas chromatographic detector. The inherently high selectivity of supersonic jet resonance enhanced multiphoton ionization time-of-flight mass spectrometry (jet-REMPI-TOFMS) can be used to selectively ionize different aromatic target molecules in complex samples. The soft-ionization properties of PIMS also allow for the mass spectrometer to be used as a separation dimension in comprehensive two-dimensional gas chromatography mass spectrometry (GC x MS) applications, thus enabling the comprehensive analysis of complex samples. Comprehensive two-dimensional gas chromatography coupled to REMPI-TOFMS (GC x REMPI-TOFMS) can be introduced for very complex samples where compounds of different selectivities can be differentiated. In most applications, the use of a less selective comprehensive two-dimensional gas chromatography coupled to single photon ionization time-of-flight mass spectrometry system (GC x SPI-TOFMS) can be used to comprehensively analyze the complex samples, as compounds should be sufficiently separated in the two-dimensional separation plane. Combining GC x GC with photo ionization mass spectrometry have been demonstrated. Selecting orthogonal or independent separation dimensions for GC x GC x MS is not trivial. Using three separation dimensions, however, provide so much more compositional detail of complex mixtures that it can be utilized as is. The slow repetition rates of pulsed laser based ionization have been overcome by the introduction of VUV-lamps allowing for much faster data acquisition as ions are continuously produced. The lower energy of the lamp is overcome by the very high acquisition rates possible thus increase in dynamic range. It would also be possible to increase the number of VUV-lamps for the ion source to increase the intensity of photons to ionize the molecules.

4.8 References

- [1] Mitschke S, Welthagen W, Zimmermann R (2006) *Anal. Chem.* 78:6364-6375
- [2] Gohlke RS (1959) *Anal. Chem.* 31:535-541
- [3] Fischböck G, Pfannhauser W, Kellner R (1988) *Microchimica Acta* 96:249-257
- [4] Bertsch W (1999) *J. High Resolut. Chromatogr.* 22:647-665
- [5] Bertsch W (2000) *J. High Resolut. Chromatogr.* 23:167-181
- [6] Giddings JC (1984) *Anal. Chem.* 56:1258-1270
- [7] Phillips JB, Beens J (1999) *J. Chromatogr. A* 856:331-347
- [8] Marriott PJ, Shellie R (2002) *Trends Anal. Chem.* 21:573-581
- [9] Beens J, Tijssen R, Blomberg J (1998) *J. Chromatogr. A* 822:233-251

- [10] Dimandja JMD, Stanfill SB, Grainger J, Patterson JDG (1999) *J. High Resol. Chromatogr.* 23:208-214
- [11] Venkatramani CJ, Xu J, J.B. P (1996) *Anal. Chem.* 68:1486-1492
- [12] Munson MSB, Field FH (1966) *J. Am. Chem. Soc.* 88:2621-2630
- [13] Schulten HR, Beckey HD (2005) *Org. Mass Spectrom.* 6:885-895
- [14] Wang FCY, Qian K, Green LA (2005) *Anal. Chem.* 77:2777-2785
- [15] Kovats E (1958) *Helv. Chim. Acta* 41:1915-1932
- [16] de Hoffmann E, Stroobant V (2003) *Mass Spectrometry: Principles and Applications.* Wiley
- [17] De Hoffmann E, Stroobant V (2002) *Mass Spectrometry: Principles and Applications.* Second edition. John Wiley & Sons, LTD, New York
- [18] Schalley CA (2003) *Modern Mass Spectrometry.* Springer, Berlin, Germany
- [19] Harrison AG (1992) *Chemical Ionization Mass Spectrometry.* CRC Press, Boca Raton, Ann Arbor, London, Tokyo
- [20] Lubman DM (1987) *Anal. Chem.* 59:31A-40A
- [21] Lubman DM (ed) (1990) *Lasers and Mass Spectrometry,* Oxford University Press, New York
- [22] Boesl U, Neusser HJ, Schlag EW (1980) *J. Chem. Phys.* 72:4327-4333
- [23] Boesl U, Weinkauff R, Weickhardt C, Schlag EW (1994) *Int. J. Mass Spectrom. Ion Proc.* 131:87-124
- [24] Zimmermann R, Lenoir D, Schramm K-W, Kettrup A, Boesl U (1994) *Organohal. Compd.* 19:155-160
- [25] Mühlberger F, Wieser J, Ulrich A, Zimmermann R (2002) *Anal. Chem.* 74:3790-3801
- [26] Butcher DJ (1999) *Microchem. J.* 62:354-362
- [27] Lubman DM, Kronick MN (1982) *Anal. Chem.* 54:660-665
- [28] Mühlberger F (2003) *Entwicklung von on-line-Analyseverfahren auf Basis der Einphotonenionisations-Massenspektrometrie.* Technische Universität München, München
- [29] Cao L, Mühlberger F, Adam T, Streibel T, Wang HZ, Kettrup A, Zimmermann R (2003) *Anal. Chem.* 75:5639-5645
- [30] Heger HJ, Zimmermann R, Dorfner R, Beckmann M, Griebel H, Kettrup A, Boesl U (1999) *Anal. Chem.* 71:46-57
- [31] Opsal RB, Reilly JP (1988) *Anal. Chem.* 58:1060
- [32] Dobson RLM, D'Silva AP, Weeks SJ, Fassel VA (1986) *Anal. Chem.* 58:2129-2137
- [33] Imasaka T, Okamura T, Ishibashi N (1986) *Anal. Chem.* 58:2152-2155
- [34] Zimmermann R, Lermer C, Schramm K-W, Kettrup A, Boesl U (1995) *Eur. Mass Spectrom.* 1:341-351
- [35] Zimmermann R, Heger HJ, Kettrup A, Boesl U (1997) *Rapid Commun. Mass Sp.* 11:1095-1102
- [36] Mühlberger F, Zimmermann R, Kettrup A (2001) *Anal. Chem.* 73:3590-3604

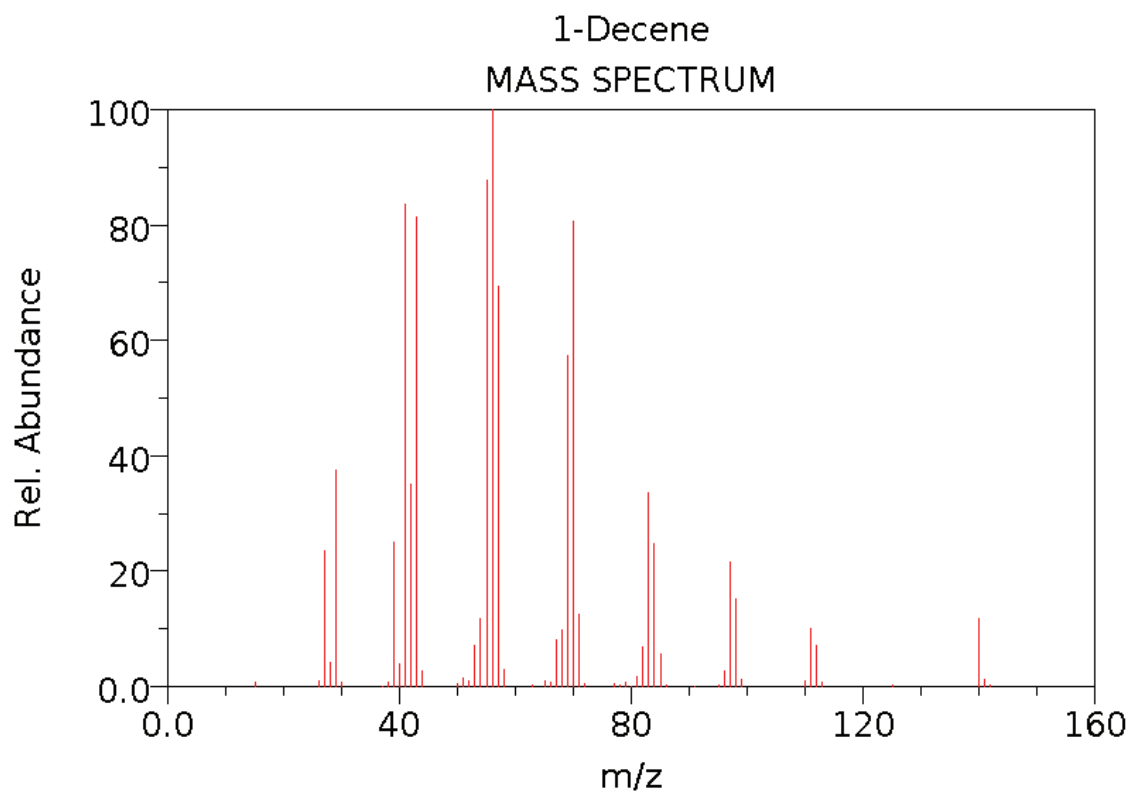
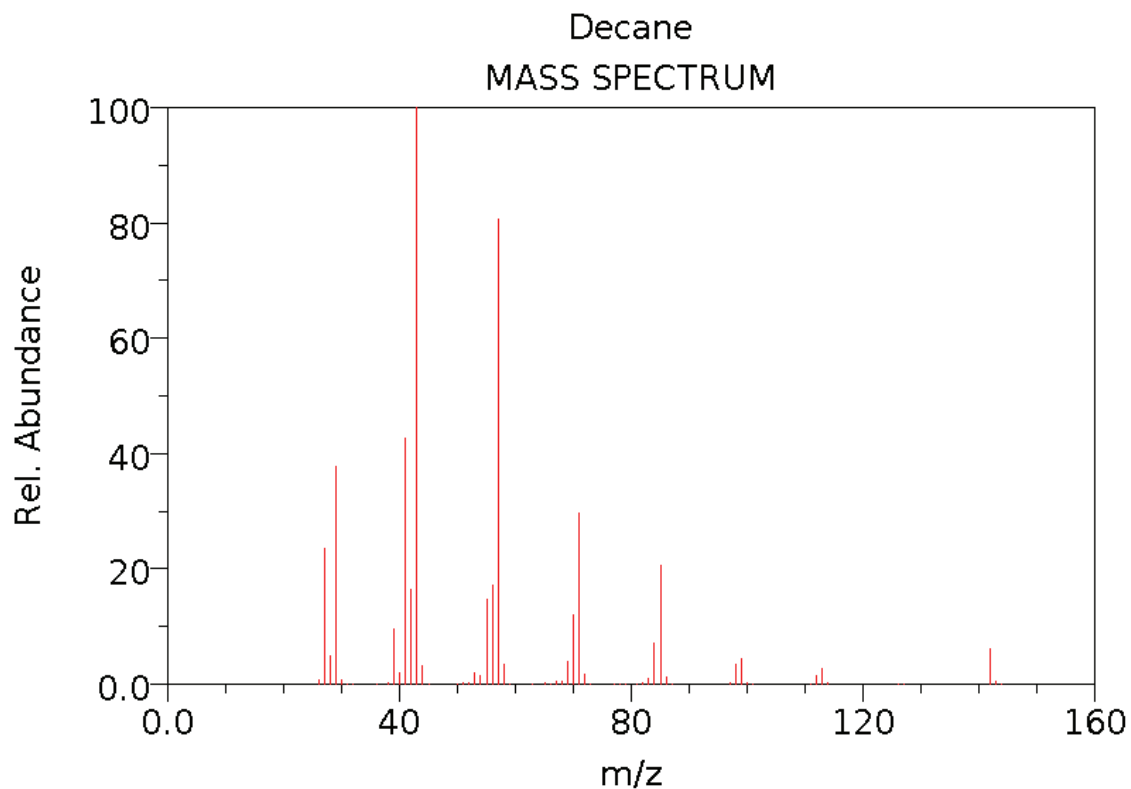
- [37] Hafner K, Zimmermann R, Rohwer ER, Dorfner R, Kettrup A (2001) *Anal. Chem.* 73:4171-4180
- [38] Muhlberger F, Hafner K, Kaesdorf S, Ferge T, Zimmermann R (2004) *Anal. Chem.* 76:6753
- [39] Stiller SW, Johnston MV (1987) *Anal. Chem.* 59:567-572
- [40] Hayes JM (1987) *Chem. Rev.* 87:745
- [41] Zimmermann R, Boesl U, Heger HJ, Rohwer ER, Ortner EK, Schlag EW, Kettrup A (1997) *J. High Resol. Chromatogr.* 20:461-470
- [42] Amirav A, Danon A (1990) *Int. J. Mass Spectrom and Ion Proc* 97:107-113
- [43] Luque J (2005) LIFBASE. <http://www.sri.com/psd/lifbase/>
- [44] <http://webbook.nist.gov/chemistry/> (2005) NIST Chemistry WebBook. NIST
- [45] Mühlberger F, Wieser J, Morozov A, Ulrich A, Zimmermann R (2005) *Anal. Chem.* accepted
- [46] Boesl U, Heger H-J, Zimmermann R, Nagel H, Püffel P (2000) *Laser Mass Spectrometry in Trace Analysis*. In: *Encyclopedia of Analytical Chemistry*, Meyers RA (ed) John Wiley & Sons, Chichester, pp. 2087-2118
- [47] Welthagen W (2004) The optimization of GC x GC and the analysis of diesel petrochemical samples. In: *Chemistry Department University of Pretoria, Pretoria*
- [48] Welthagen W, Mitschke S, Mühlberger F, Zimmermann R (2007) *J. Chromatogr. A* 1150:54-61
- [49] Poole CF, Poole SK (1991) *Chromatography Today*. Elsevier, Amsterdam
- [50] Muhlberger F, Wieser J, Ulrich A, Zimmermann R (2002) *Anal. Chem.* 74:3790-3801
- [51] Gröger T (2007) Apex plot representation of GC x GC x MS data. Welthagen W (ed) Personal comm.

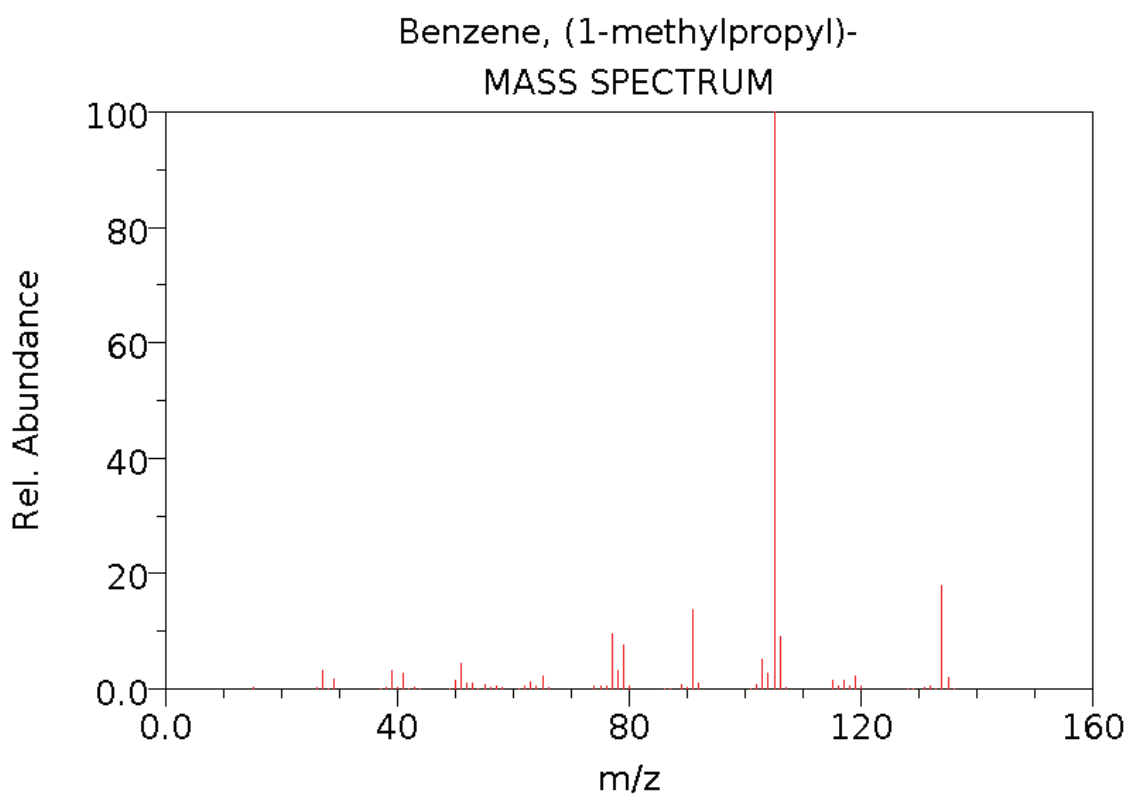
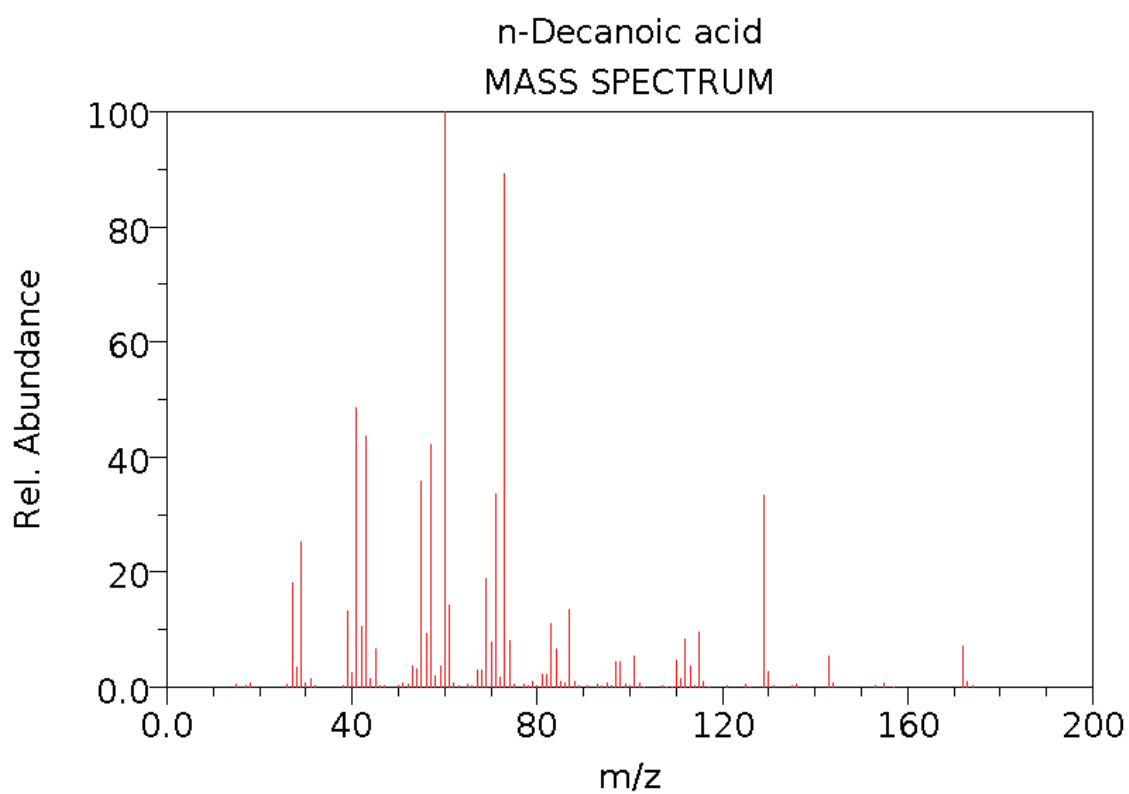
APPENDICES

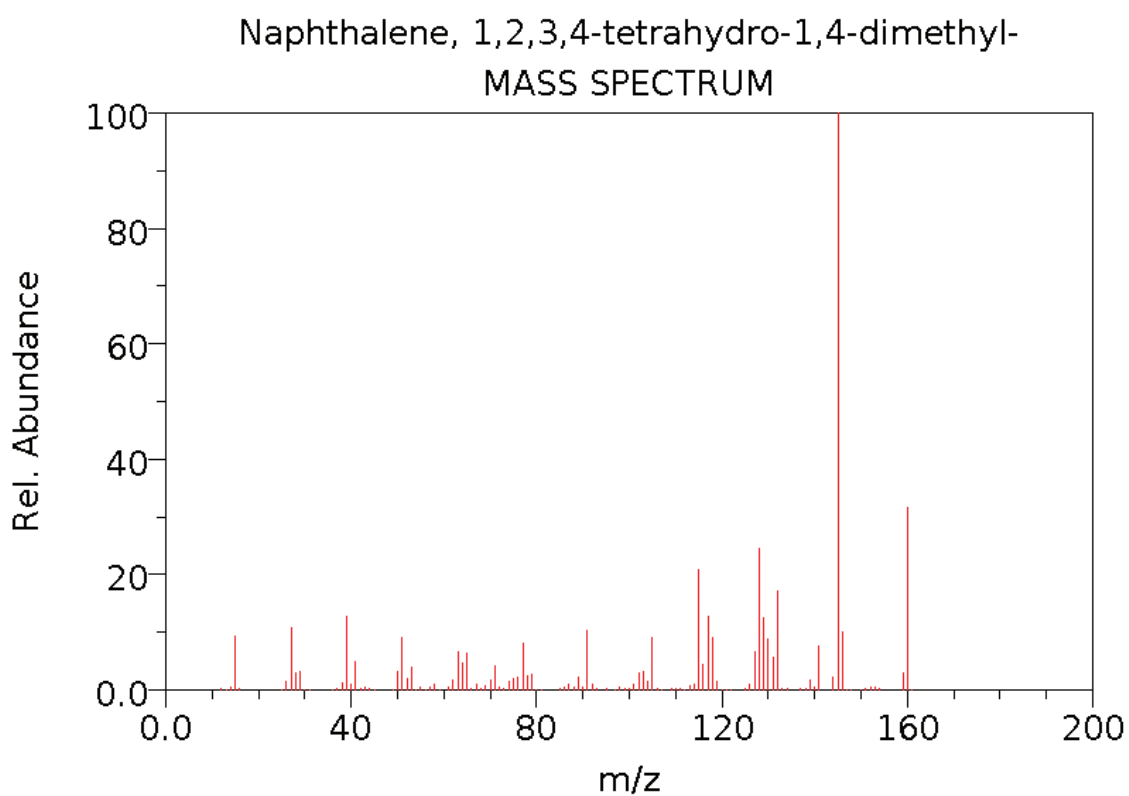
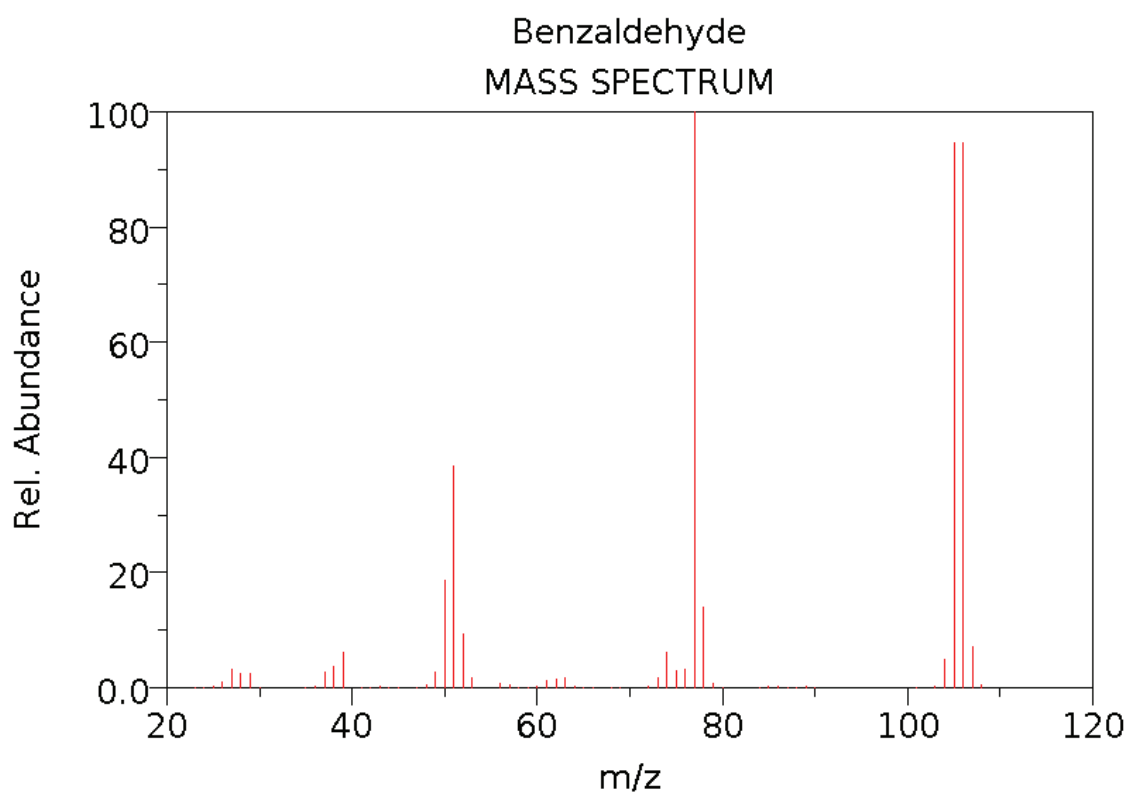
Appendix A	178
Mass spectra for selected compounds used in classification rule approach	
Appendix B	183
Mass spectra of identified peaks in mouse spleen samples	

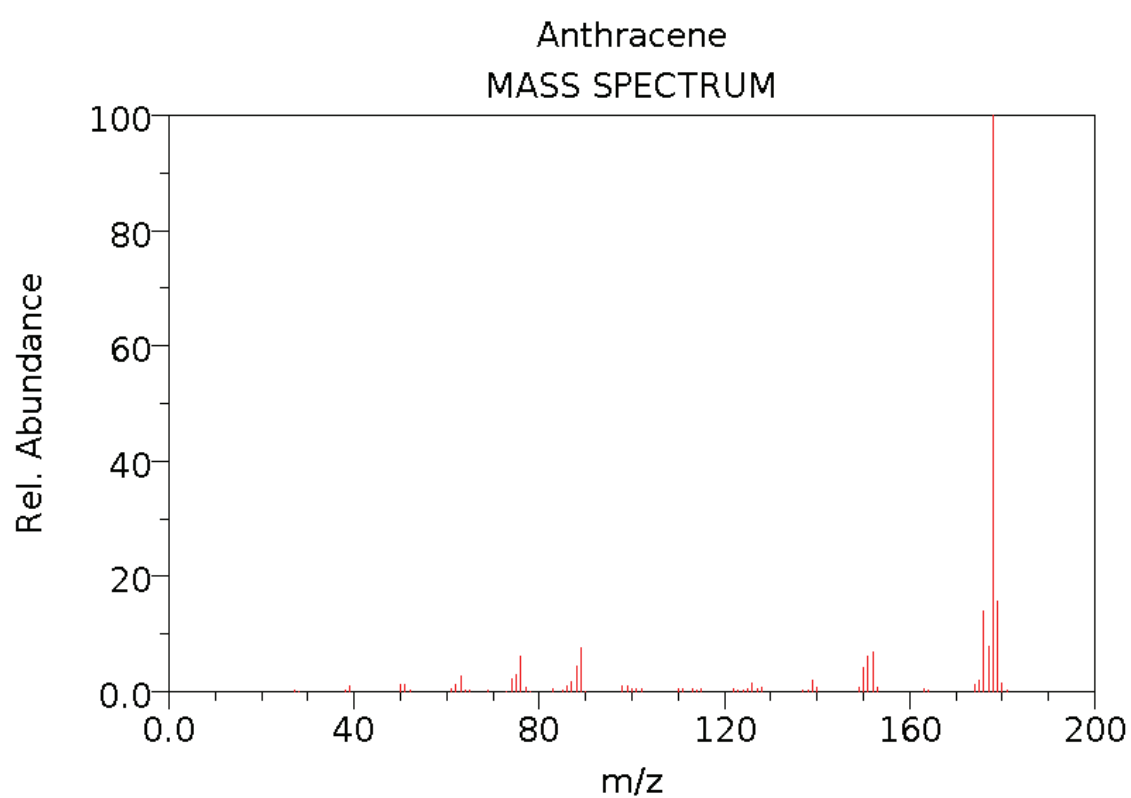
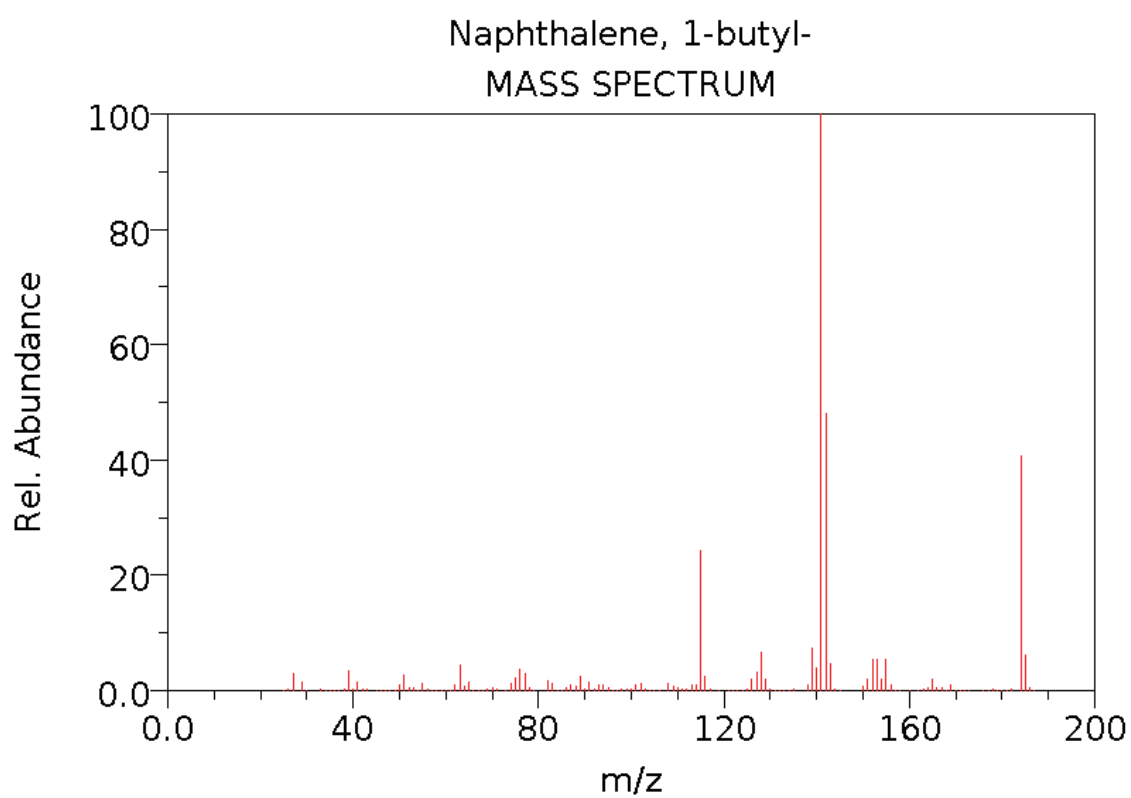
Appendix A

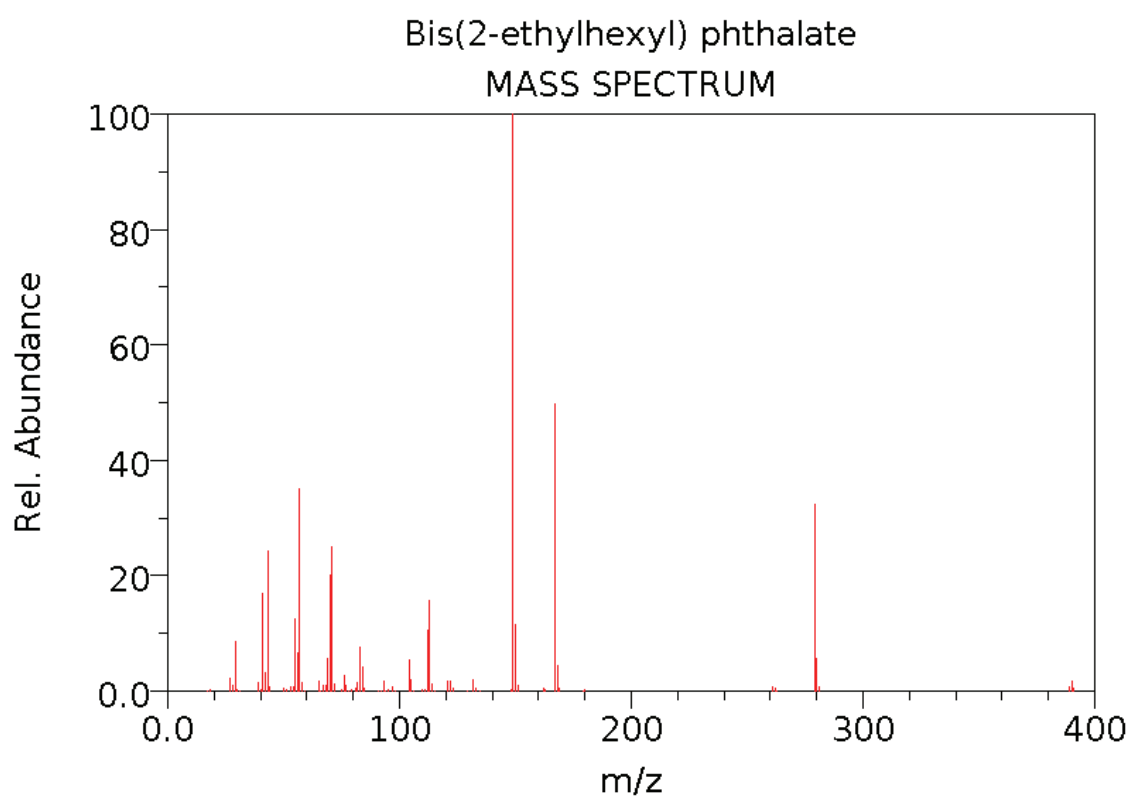
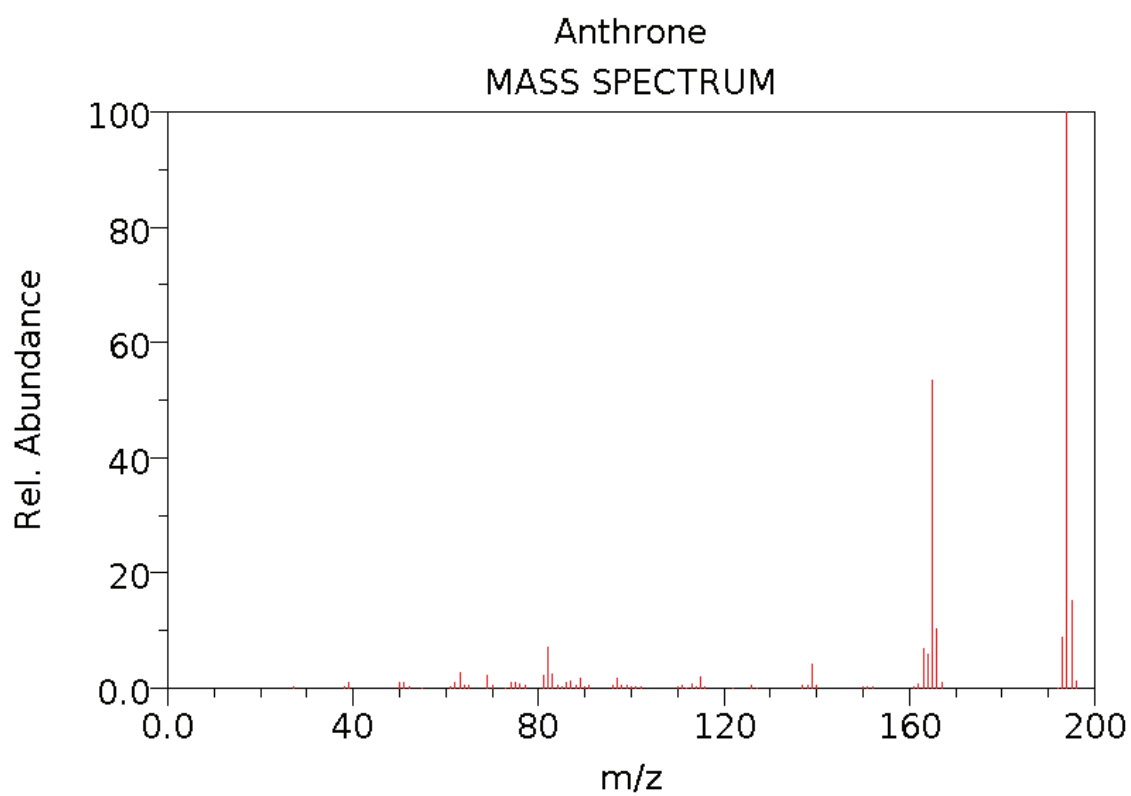
Mass spectra for selected compounds used in classification rule approach Chapter 3 (NIST-library)









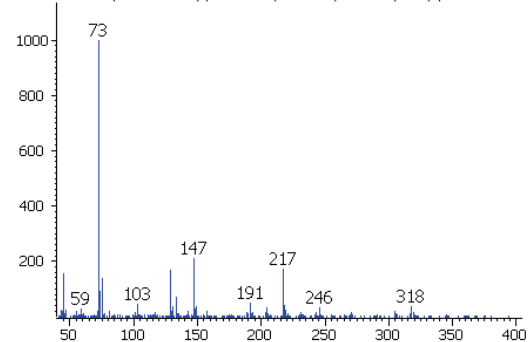


Appendix B

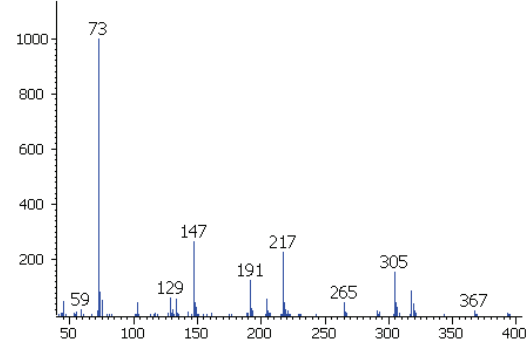
Mass spectra of identified peaks in Figure 3.29 and Table 3.6

Peak #1 Sugar alcohol

Peak True - sample "milt 8:1", peak 1822, at 2595,1.14 sec,sec (Spec # 169614)

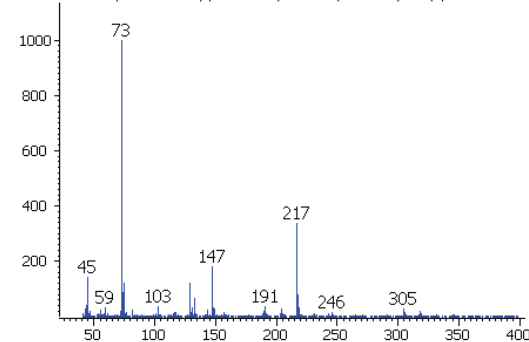


Library Hit - similarity 711, "Myo-Inositol, 1,2,3,4,5,6-hexakis-O-(trimethylsilyl)-"

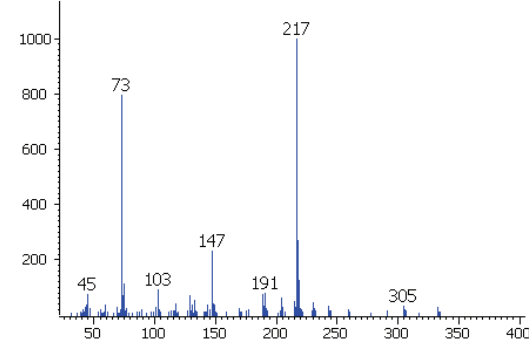


Peak #2 Sugar alcohol

Peak True - sample "milt 8:1", peak 1845, at 2610,1.13 sec,sec (Spec # 171113)

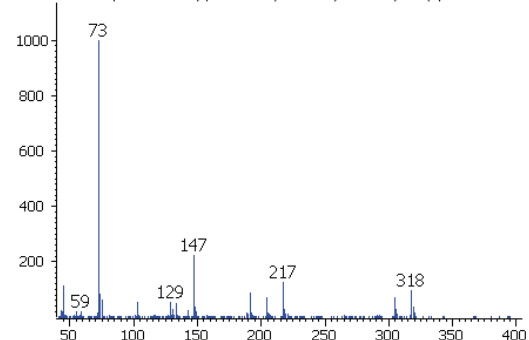


Library Hit - similarity 722, "D-Ribofuranose, 1,2,3,5-tetrakis-O-(trimethylsilyl)-"

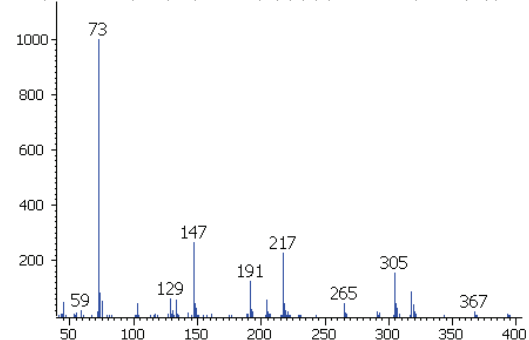


Peak #3 Allo-inositol

Peak True - sample "milt 8:1", peak 1886, at 2652,1.06 sec,sec (Spec # 175306)

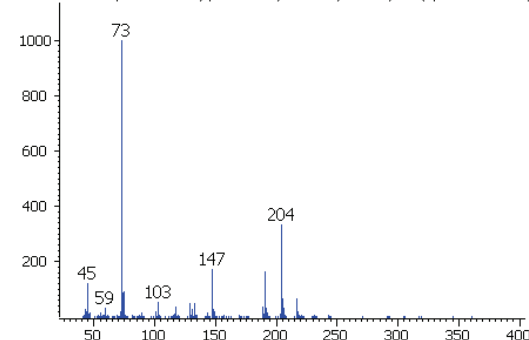


Library Hit - similarity 835, "Myo-Inositol, 1,2,3,4,5,6-hexakis-O-(trimethylsilyl)-"

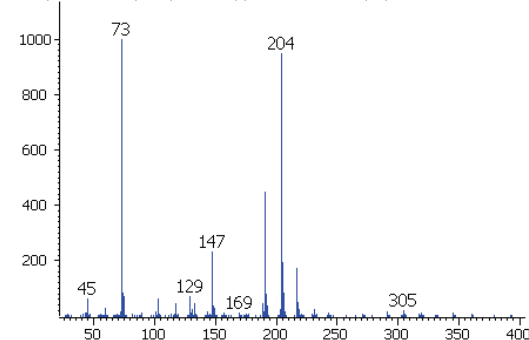


Peak #4 Sugar alcohol

Peak True - sample "milt 8:1", peak 1817, at 2589,1.1 sec,sec (Spec # 169010)

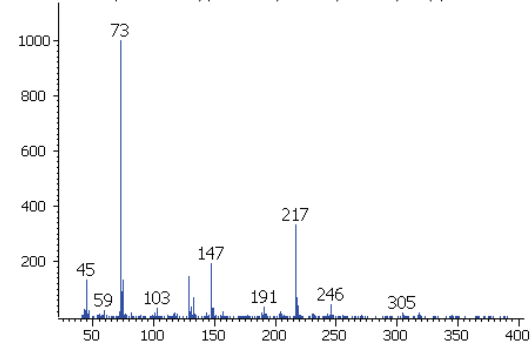


Library Hit - similarity 881, "Glucose, pentakis-O-(trimethylsilyl)-"

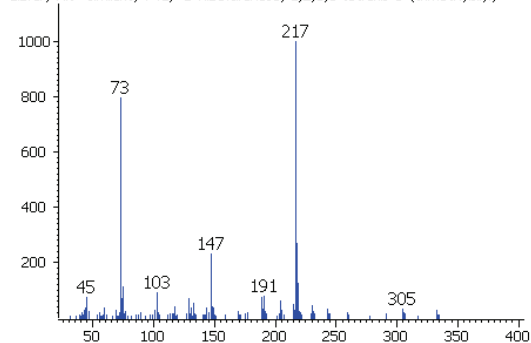


Peak #5 Sugar alcohol

Peak True - sample "milt 8:1", peak 1800, at 2577,1.11 sec,sec (Spec # 167811)

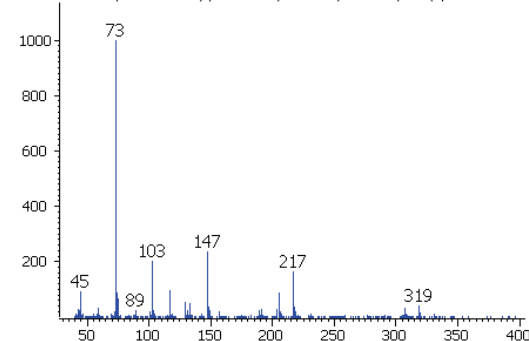


Library Hit - similarity 741, "D-Ribofuranose, 1,2,3,5-tetrakis-O-(trimethylsilyl)-"

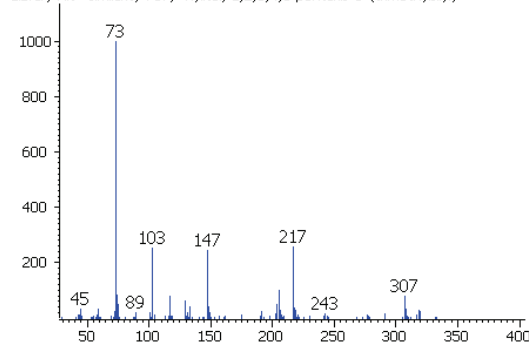


Peak #6 Sugar alcohol

Peak True - sample "milt 8:1", peak 1777, at 2562,1.04 sec,sec (Spec # 166304)

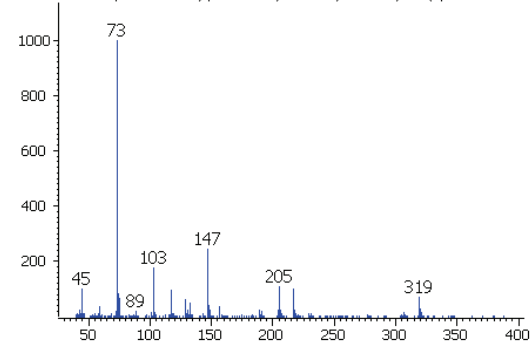


Library Hit - similarity 787, "Xylitol, 1,2,3,4,5-pentakis-O-(trimethylsilyl)-"

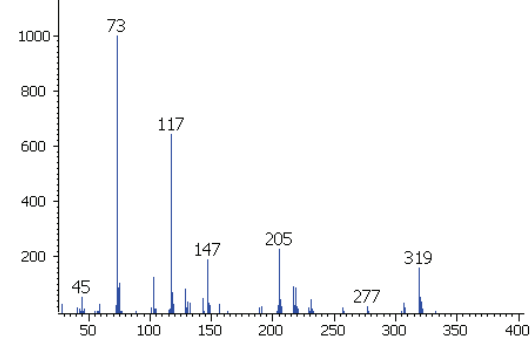


Peak #7 Sugar alcohol

Peak True - sample "milt 8:1", peak 1770, at 2556,1.04 sec,sec (Spec # 165704)

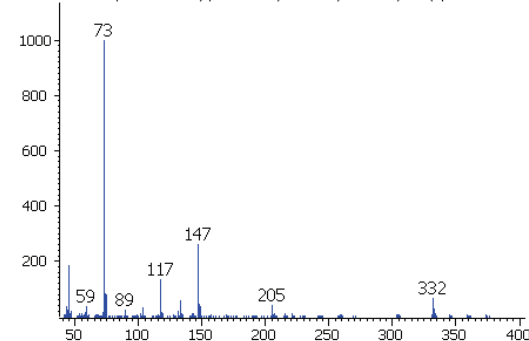


Library Hit - similarity 794, "D-Glucitol, 6-deoxy-1,2,3,4,5-pentakis-O-(trimethylsilyl)-"

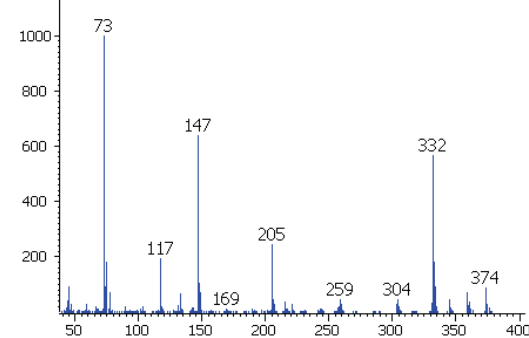


Peak #8 Ascorbate

Peak True - sample "milt 8:1", peak 1736, at 2529,1.33 sec,sec (Spec # 163033)

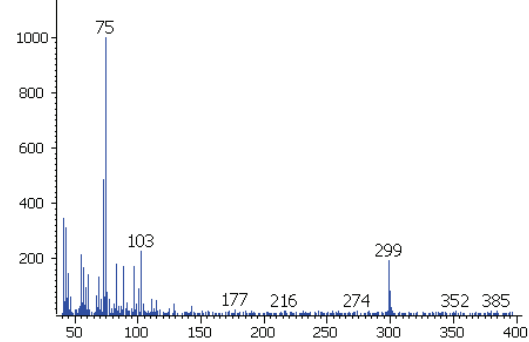


Library Hit - similarity 793, "L-Ascorbic acid, 2,3,5,6-tetrakis-O-(trimethylsilyl)-"

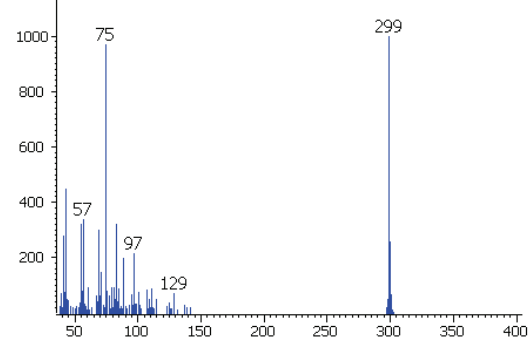


Peak #9 Hexadecanol

Peak True - sample "milt 8:1", peak 1726, at 2520,1.31 sec,sec (Spec # 162131)

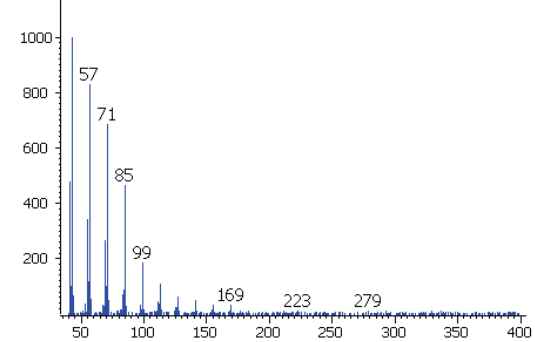


Library Hit - similarity 619, "1-Dimethyl(chloromethyl)silyloxyhexadecane"

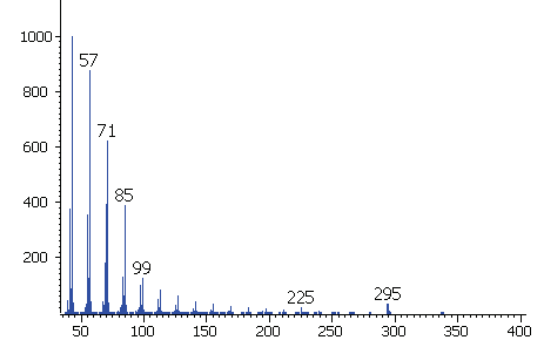


Peak #10 Aliphate

Peak True - sample "milt 8:1", peak 1746, at 2535,1.24 sec,sec (Spec # 163624)

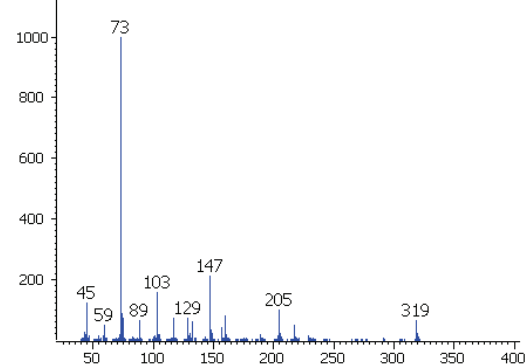


Library Hit - similarity 698, "Heneicosane, 11-(1-ethylpropyl)-"

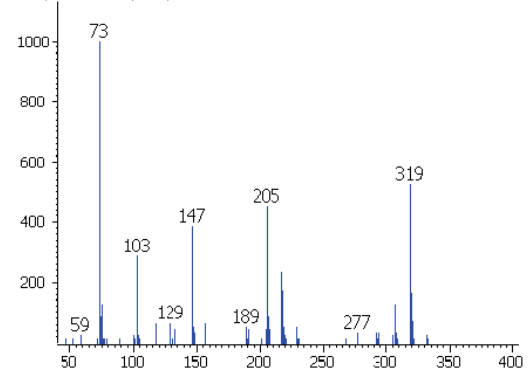


Peak #11 Glucose

Peak True - sample "milt 10:1", peak 1524, at 2526,1.02 sec,sec (Spec # 162702)

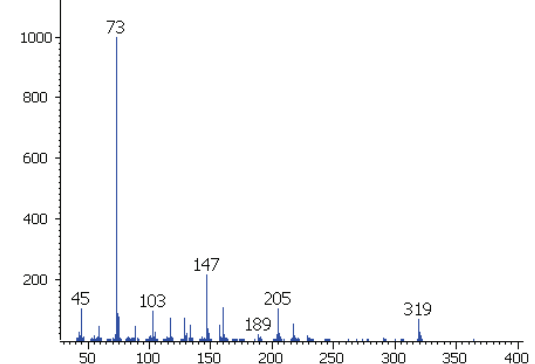


Library Hit - similarity 701, "Glucose oxime hexaTMS"

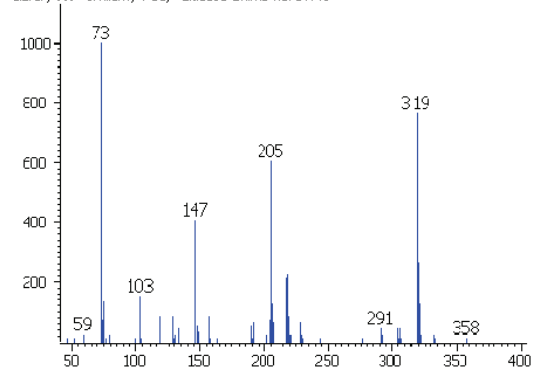


Peak #12 Glucose

Peak True - sample "milt 8:1", peak 1602, at 2499,1.11 sec,sec (Spec # 160011)

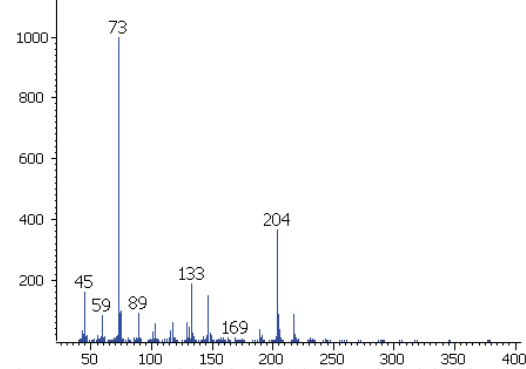


Library Hit - similarity 70., "Glucose oxime hexaTMS"

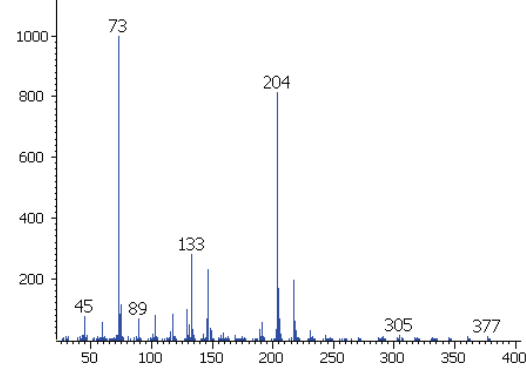


Peak #13 1-methylglucoside

Peak True - sample "milt 8:1", peak 1584, at 2484,1.19 sec,sec (Spec # 158519)

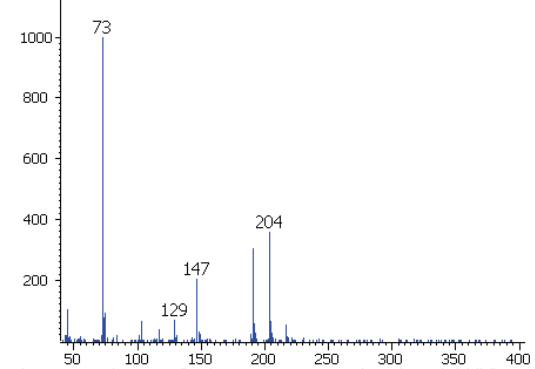


Library Hit - similarity 884, "Glycoside, ð-methyl-trakis-O-(trimethylsilyl)-"

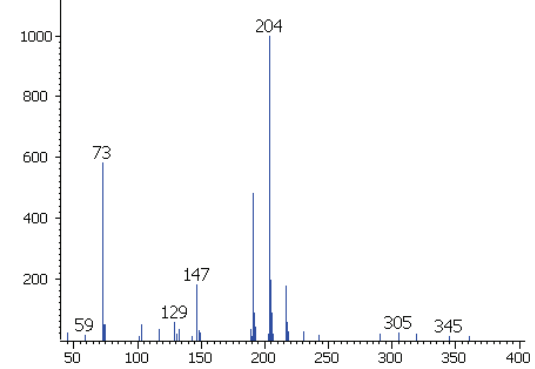


Peak #14 Hexose per TMS

Peak True - sample "milt 8:1", peak 1587, at 2487,1.14 sec,sec (Spec # 158814)

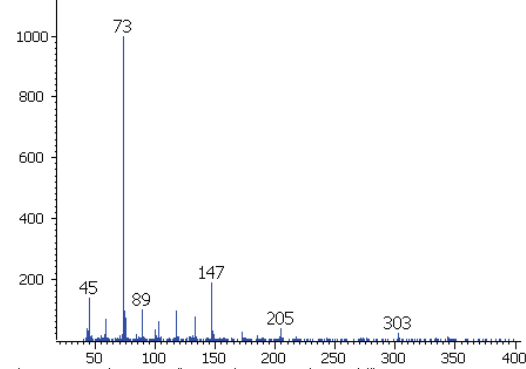


Library Hit - similarity 808, "D-Glucose, 2,3,4,5,6-pentakis-O-(trimethylsilyl)-"

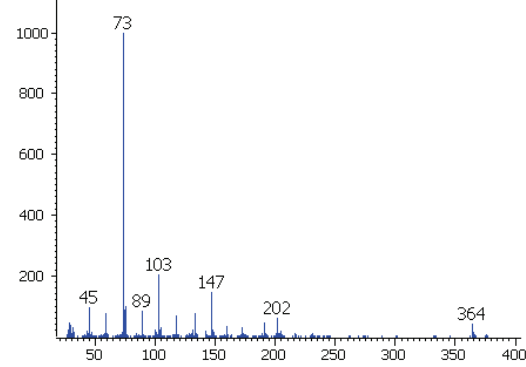


Peak #15 Carbohydrate

Peak True - sample "milt 8:1", peak 1585, at 2484,1.34 sec,sec (Spec # 158534)

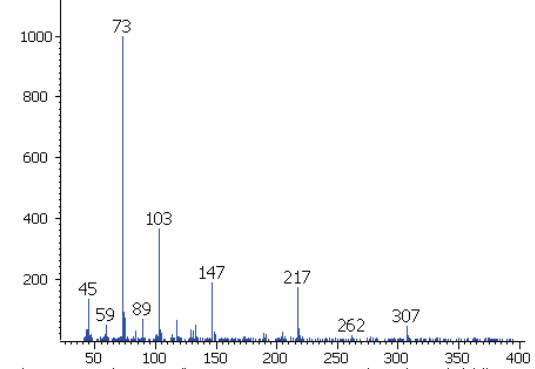


Library Hit - similarity 668, "4-Ketoglucose, methoxy, silyl"

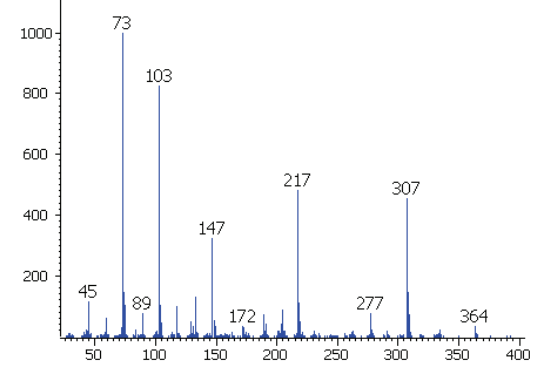


Peak #16 Fructose 1

Peak True - sample "milt 10:1", peak 1480, at 2484,1.02 sec,sec (Spec # 158502)

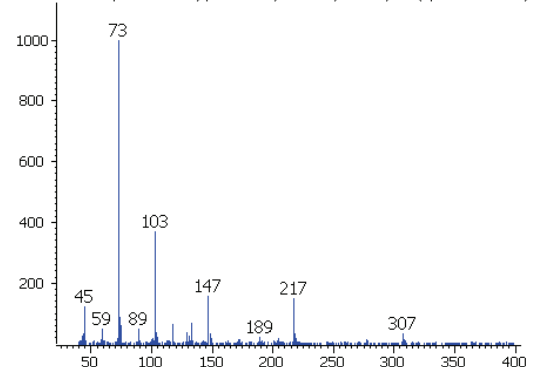


Library Hit - similarity 724, "D-Fructose, 1,3,4,5,6-pentakis-O-(trimethylsilyl), O-met"

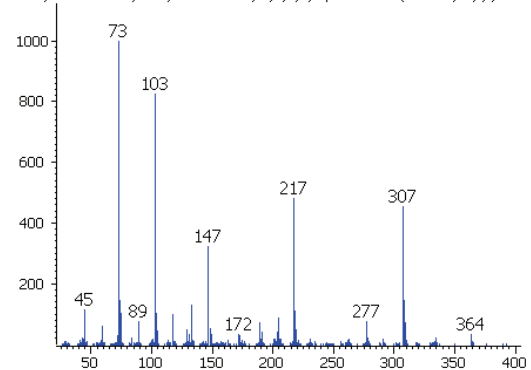


Peak #17 Fructose 2

Peak True - sample "mlt 8:1", peak 1565, at 2469,1.1 sec,sec (Spec # 157010)

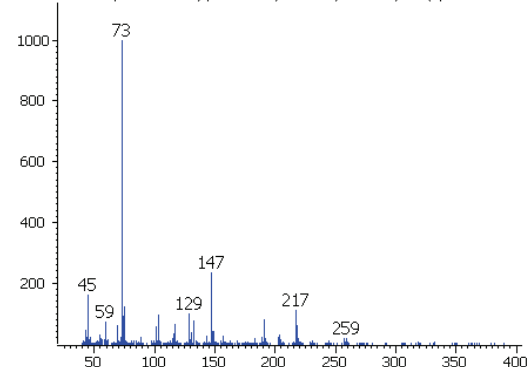


Library Hit - similarity 727, "D-Fructose, 1,3,4,5,6-pentakis-O-(trimethylsilyl)-, O-me

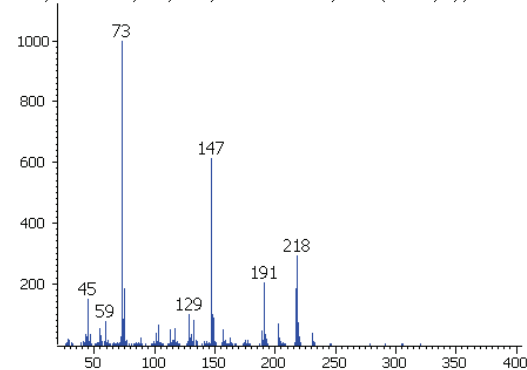


Peak #18 Carbohydrate

Peak True - sample "mlt 8:1", peak 1517, at 2424,1.22 sec,sec (Spec # 152522)

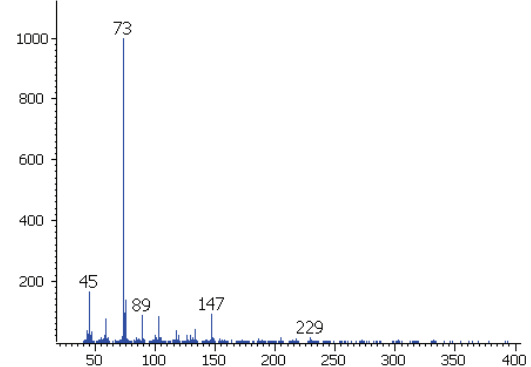


Library Hit - similarity 836, "d-Erythrotetrofuranose, tris-O-(trimethylsilyl)-"

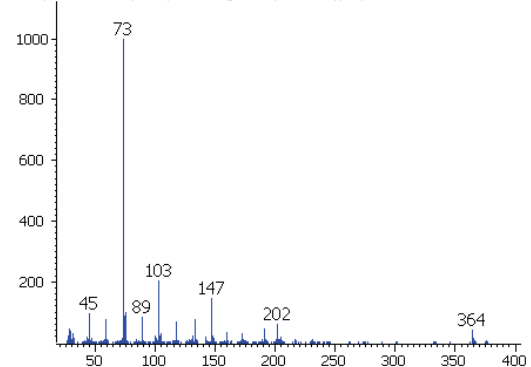


Peak #19 Unknown

Peak True - sample "mlt 8:1", peak 1638, at 2532,1.53 sec,sec (Spec # 163353)

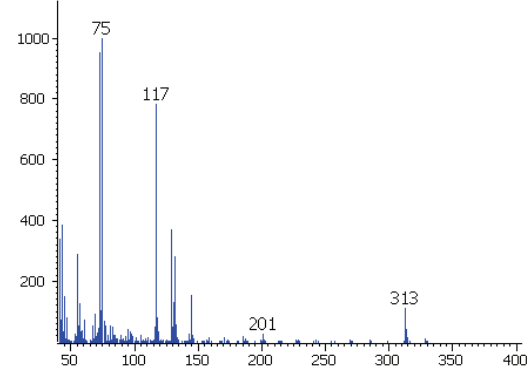


Library Hit - similarity 702, "4-Ketoglucose, methoxy, silyl"

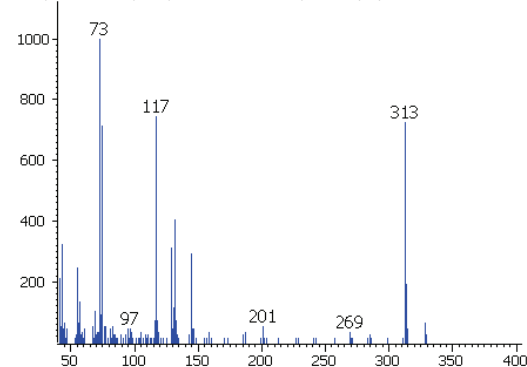


Peak #20 Unknown

Peak True - sample "mlt 8:1", peak 1726, at 2604,1.45 sec,sec (Spec # 170545)

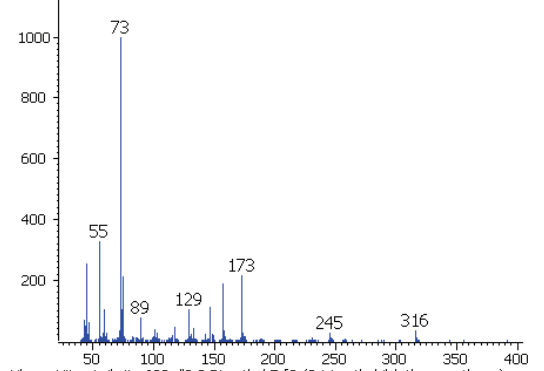


Library Hit - similarity 832, "Hexadecanoic acid, trimethylsilyl ester"

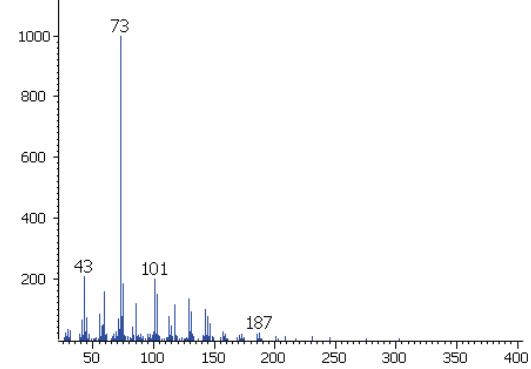


Peak #21 Unknown

Peak True - sample "milt 8:1", peak 1528, at 2436,1.44 sec,sec (Spec # 153744)

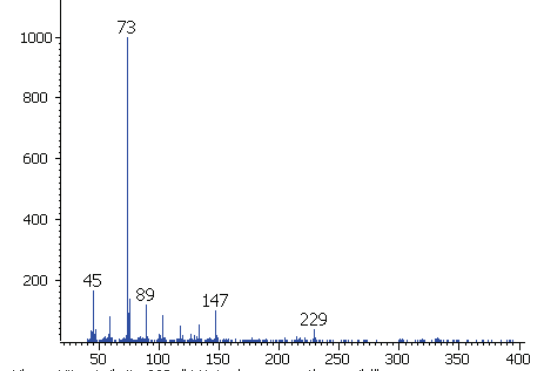


Library Hit - similarity 639, "2,2-Dimethyl-5-[2-(2-trimethylsilyloxyethoxy)-prop-"



Peak #22 Unknown

Peak True - sample "milt 8:1", peak 1620, at 2517,1.48 sec,sec (Spec # 161848)



Library Hit - similarity 668, "4-Ketoglucose, methoxy, silyl"

